NASA TECHNICAL NOTE

NASA TN D-7694

NASA TN D-7694

A WIND-TUNNEL INVESTIGATION OF PARAMETERS AFFECTING HELICOPTER DIRECTIONAL CONTROL AT LOW SPEEDS IN GROUND EFFECT

by William T. Yeager, Jr., Warren H. Young, Jr., and Wayne R. Mantay

Langley Directorate,
U.S. Army Air Mobility R&D Laboratory
Hampton, Va. 23665

NATIONAL AERONAUTICS AND SPACE ADMINISTRATION • WASHINGTON, D. C. • NOVEMBER 1974

1. Report No.	2. Government Accession No.	3. Recipient's Catalog No.
NASA TN D-7694		

4. Title and Subtitle	5. Report Date
A WIND-TUNNEL INVESTIGATION OF PARAMETERS AFFECTING HELICOPTER DIRECTIONAL CONTROL AT LOW SPEEDS IN GROUND EFFECT	November 1974
	6. Performing Organization Code
7. Author(s) William T. Yeager, Jr., Warren H. Young, Jr., and Wayne R. Mantay, Langley Directorate, U.S. Army Air Mobility R&D Laboratory	8. Performing Organization Report No. L-9325
	10. Work Unit No. 760-63-02-06
9. Performing Organization Name and Address NASA Langley Research Center Hampton, Va. 23665	11. Contract or Grant No.
	13. Type of Report and Period Covered Technical Note
12. Sponsoring Agency Name and Address National Aeronautics and Space Administration Washington, D.C. 20546	14. Sponsoring Agency Code

15. Supplementary Notes

16. Abstract

An investigation was conducted in the Langley full-scale tunnel to measure the performance of several helicopter tail-rotor/fin configurations with regard to directional control problems encountered at low speeds in ground effect. Tests were conducted at wind azimuths of 0° to 360° in increments of 30° and 60° and at wind speeds from 0 to 35 knots.

The results indicate that at certain combinations of wind speed and wind azimuth, large increases in adverse fin force require correspondingly large increases in the tail-rotor thrust, collective pitch, and power required to maintain yaw trim. Changing the tail-rotor direction of rotation to top blade aft for either a pusher tail rotor (tail-rotor wake blowing away from fin) or a tractor tail rotor (tail-rotor wake blowing against fin) will alleviate this problem. For a pusher tail rotor at 180° wind azimuth, increases in the fin/tail-rotor gap were not found to have any significant influence on the overall vehicle directional control capability. Changing the tail rotor to a higher position was found to improve tail-rotor performance for a fin-off configuration at a wind azimuth of 180°. A V-tail configuration with a pusher tail rotor with top blade aft direction of rotation was found to be the best configuration with regard to overall directional control capability.

17. Key Words (Suggested by Author(s))		18. Distribution Statement
Rotor aerodynamics	Fins	Unclassified – Unlimited
Helicopter control	Yawing moments	
Directional control	Ground effect	
Tail assemblies	Helicopter wakes	STAR Category 01

19. Security Classif. (of this report)	20. Security Classif. (of this page)	21. No. of Pages	22. Price*
Unclassified	Unclassified	174	$5.00

*For sale by the National Technical Information Service, Springfield, Virginia 22151

A WIND-TUNNEL INVESTIGATION OF PARAMETERS AFFECTING HELICOPTER DIRECTIONAL CONTROL AT LOW SPEEDS IN GROUND EFFECT

By William T. Yeager, Jr., Warren H. Young, Jr.,
and Wayne R. Mantay
Langley Directorate, U.S. Army Air Mobility R&D Laboratory

SUMMARY

An investigation was conducted in the Langley full-scale tunnel to measure the performance of several helicopter tail-rotor/fin configurations with regard to directional control problems encountered at low speeds in ground effect. Tests were conducted at wind azimuths of 0^{o} to 360^{o} in increments of 30^{o} and 60^{o} and at wind speeds from 0 to 35 knots.

The results indicate that at certain combinations of wind speed and wind azimuth, large increases in adverse fin force require correspondingly large increases in the tail-rotor thrust, collective pitch, and power required to maintain yaw trim. Changing the tail-rotor direction of rotation to top blade aft for either a pusher tail rotor (tail-rotor wake blowing away from fin) or a tractor tail rotor (tail-rotor wake blowing against fin) will alleviate this problem. For a pusher tail rotor at 180^{o} wind azimuth, increases in the fin/tail-rotor gap were not found to have any significant influence on the overall vehicle directional control capability. Changing the tail rotor to a higher position was found to improve tail-rotor performance for a fin-off configuration at a wind azimuth of 180^{o}. A V-tail configuration with a pusher tail rotor with top blade aft direction of rotation was found to be the best configuration with regard to overall directional control capability.

INTRODUCTION

The tail rotor and fin of conventionally powered single-rotor helicopters serve two purposes: (1) to counteract main-rotor torque and other adverse torques and (2) to provide directional control in hover and forward flight. Historically, the conventional tail rotor and associated fin assemblies have been the source of low-speed directional control problems. Examples of these problems have been reported in references 1 and 2 where conditions of inadequate directional control have been encountered in low-velocity left-rear-quartering winds in ground effect and during low-speed sideward flight in ground effect.

In the past, efforts to solve these problems have consisted of a series of multiple and frequently random changes in tail-rotor/fin configuration. The random nature of this approach reflects the limited knowledge of the tail-rotor/fin operational environment. Some insight into this environment is provided by reference 3 which identifies a possible source of directional control problems experienced in ground effect at low rearward speeds as a large vortex generated by the interaction of the main-rotor wake and the wind in the presence of the ground. The presence of this ground vortex adjacent to the upwind side of the main rotor suggests that the problem of adverse wake effects on the fin and tail-rotor performance may extend, to some degree, over a wide range of wind azimuths.

In a continuing effort to improve helicopter low-speed directional control, an investigation was conducted in the Langley full-scale tunnel to determine the effects of several tail-rotor and fin parameters on vehicle directional control capability. All tests were conducted in ground effect for a range of wind speeds and wind azimuth angles.

Although not providing detailed design information, the results presented herein indicate factors which will improve helicopter directional control capability and identify other areas where more detailed investigation of helicopter directional control is warranted.

SYMBOLS

The positive senses of forces, moments, and displacements are indicated in figure 1. The measurements and calculations were made in the U.S. Customary Units. The physical quantities used in this paper are given in the International System of Units (SI).

C_F fin force coefficient, $\dfrac{F}{\rho\pi R_{tr}^2(\Omega R)_{tr}^2}$

C_L' main-rotor lift coefficient, $\dfrac{L}{\rho\pi R_{mr}^2(\Omega R)_{mr}^2}$

C_{m_α} rate of change of vehicle pitching-moment coefficient with angle of attack

$C_{m,f}$ vehicle pitching-moment coefficient due to V-tail, $\dfrac{M_f}{\rho\pi R_{tr}^3(\Omega R)_{tr}^2}$

C_{n_β} rate of change of vehicle yawing-moment coefficient with sideslip angle

$C_{Q,mr}$ main-rotor torque coefficient, $\frac{Q_{mr}}{\rho\pi R_{mr}^3(\Omega R)_{mr}^2}$

$C_{Q,tr}$ tail-rotor torque coefficient, $\frac{Q_{tr}}{\rho\pi R_{tr}^3(\Omega R)_{tr}^2}$

$C_{Q,v}$ vehicle torque coefficient, $\frac{Q_v}{\rho\pi R_{mr}^3(\Omega R)_{mr}^2}$

$C_{T,tr}$ tail-rotor thrust coefficient, $\frac{T_{tr}}{\rho\pi R_{tr}^2(\Omega R)_{tr}^2}$

C_σ torque-balance coefficient (value of 1 indicates vehicle is trimmed in yaw), $\frac{l_t T_{tr}}{Q_v}$

F fin force (positive when in opposition to tail-rotor thrust), newtons

L main-rotor lift, newtons

l_t horizontal distance from tail-rotor shaft to main-rotor shaft and assumed longitudinal position of vehicle center of gravity, meters

M_f pitching moment about assumed vehicle center of gravity due to the V-tail, newton-meters

Q_{mr} main-rotor shaft torque, newton-meters

Q_{tr} tail-rotor shaft torque, newton-meters

Q_v vehicle torque (sum of fuselage, main-rotor, and fin assembly torques), newton-meters

R rotor radius, meters

T rotor thrust, newtons

V free-stream velocity, knots

y gap from fin center line to tail-rotor plane of rotation, meters

z tail-rotor height measured from original location as shown in figure 1, positive up, meters

β model azimuth angle (angle between model longitudinal axis and wind-tunnel flow direction), positive nose left, degrees

θ rotor blade collective-pitch angle, degrees

ρ mass density of air, kilograms per meter^3

Ω rotor rotational speed, radians per second

Subscripts:

max maximum

mr main rotor

tr tail rotor

v vehicle (main rotor, body, and fin assembly)

APPARATUS AND TESTS

Model Description

The model used in this investigation is shown in figure 2 and 3. It is the same model described in reference 3 except for new fin configurations and the substitution of an electric motor for the air motor in the tail-rotor drive system. The rotors and tail surfaces are 1/4-scale representations of the attack helicopter of reference 1. The main-rotor disk loading and tail-rotor tip speed are full scale. The entire model, with the exception of the tail-rotor assembly, was mounted on a six-component strain-gage balance attached to the top of a pedestal. The vertical tail was attached to a separate five-component strain-gage balance mounted within the model fuselage aft of the horizontal stabilizer. The two variable-speed electric motors used to drive the main rotor were mounted within the fuselage body. The tail-rotor drive assembly was mounted on a six-component strain-gage balance attached to the end of a horizontal sting which could be

moved to vary the gap between the tail rotor and vertical fin. This sting was mounted on a pedestal attached to the tunnel ground board support structure. The sting could also be moved on the pedestal to change the vertical position of the tail rotor. Figure 4 shows the tail-rotor vertical positions tested relative to the main rotor. In order to change the tail rotor from a pusher to a tractor configuration, the entire tail-rotor, sting, and pedestal assembly was moved from one side of the model to the other.

The main rotor and tail rotor were two-bladed teetering rotors. Both rotors were equipped with remote collective-pitch controls. In addition, the main rotor was provided with longitudinal and lateral cyclic pitch control through a remotely operated, conventional swashplate system. Physical characteristics of the rotors are listed in table I.

The model could be equipped with either of two tail surface configurations. One configuration consisted of a standard vertical fin in conjunction with a horizontal stabilizer (figs. 2(a) and 2(b)). The other tail surface configuration was a V-tail (fig. 2(c)). The standard vertical fin blocked 24 percent of the tail-rotor disk compared with a tail-rotor disk blockage of 20 percent for the V-tail. The area of the V-tail projected onto the horizontal plane was 61 percent of the area of the horizontal stabilizer tested with the standard vertical fin. The V-tail was designed to give the same values of Cm_{α} and Cn_{β} as the standard-vertical-fin/horizontal-tail configuration. In addition, the same horizontal and vertical tail-rotor location was maintained.

The four-letter configuration identification code used during this investigation is given in the following table:

First letter	Second letter	Third letter	Fourth letter
Tail fin	Main rotor	Tail rotor type	Tail-rotor rotation
N No fin installed	N Main rotor not operating	P Pusher	F Top blade forward
S Standard fin	M Main rotor operating	T Tractor	A Top blade aft
V V-tail		N No tail rotor installed	N No tail rotor installed

For example, SMPF denotes the standard fin with the main rotor operating and a pusher tail rotor with top blade forward rotation. This configuration is referred to as the standard configuration throughout this report.

Test Procedure

Data were obtained at wind speeds of 0, 7.5, 10, 12.5, 15, 20, and 25 knots for all configurations at wind azimuths from 0^{o} to 360^{o} in 30^{o} or 60^{o} increments. In addition, data were obtained for the V-tail configuration at 30 and 35 knots at wind azimuths of 0^{o}, 60^{o}, and 300^{o}. Table II shows all model configuration and wind azimuth combinations tested. At each wind azimuth and windspeed, data were obtained for a range of tail-rotor collective-pitch settings which in most cases bracketed the yaw trim flight condition. For the purposes of this report, the yaw trim flight condition is defined as the condition at which the total vehicle yawing moment is balanced by an equal and opposite yawing moment produced by the tail-rotor thrust. At this condition the value of the torque-balance coefficient C_{σ} is equal to 1. The main rotor was operated at a nominal disk loading of 250 N/m^2 and a nominal tip-path-plane angle of attack of 0^{o}.

Data Acquisition

Three independent strain-gage balances and one strain-gage bridge were used for data acquisition. The balance locations are shown in figure 1. The vehicle balance sensed the total aerodynamic forces and moments acting on the main rotor, fuselage, and fin. Within the model fuselage, a separate five-component balance sensed only the fin forces and moments. A third balance was used to measure the tail-rotor forces and moments. A strain-gage bridge on the main-rotor shaft sensed the main-rotor torque.

Two data points were recorded for each test condition on a digital data acquisition system. Data recorded included the forces and moments from the three strain-gage balances, the instantaneous rotational speeds of the two rotors, the main-rotor torque, the main-rotor longitudinal and lateral cyclic pitch, the collective-pitch settings of both rotors, and the tunnel velocity. The signals from the three strain-gage balances and the strain-gage bridge were filtered, and the data recorded were essentially the steady-state values. Time dependent aerodynamic effects at frequencies above 6 Hz have been removed by these filters. However, unsteady effects with frequencies below 6 Hz will appear as scatter in the data. Measurement accuracies have been estimated and are presented in table III.

Tunnel Boundary Conditions

In order to obtain data representative of in-ground-effect flight, the model was installed on the ground board of the Langley full-scale tunnel with the main-rotor shaft 7.5 meters downstream of the leading edge of the ground board. The ground board has a width of 13.0 meters. The Langley full-scale tunnel has an open test section with a nominal width of 18.3 meters and a nominal height of 9.1 meters. The theoretical results of reference 4 indicate that for the conditions of this investigation, the flow in the

tunnel differs little from that of in-ground-effect flight. Therefore, no tunnel boundary corrections were applied to the data.

PRESENTATION OF RESULTS

The figures used for discussion of the results were obtained by interpolating the basic data to achieve, in most cases, a model yaw trim condition for a nominal main-rotor lift coefficient of 0.00470. For configuration NMPF, the tail-rotor thrust required to bracket yaw trim was not obtained, and the results have been extrapolated. These extrapolations have been noted in the figures. In a few instances, aerodynamic effects caused fin force to vary in such a manner that the yaw trim condition could not be accurately determined. These occurrences are denoted in the figures by shaded areas indicating the accuracy of the parameter in question.

The order of presentation of the figures in this report is as follows:

	Figure
Ground vortex	5 to 7
Critical regions of flight	8 to 10
Systematic performance studies	11 to 22
Vehicle pitching moment due to V-tail	23
Basic data	24 to 40

DISCUSSION OF RESULTS

Factors Affecting Tail-Rotor/Fin Aerodynamic Environment

The aerodynamic environment of the tail rotor and fin of the typical single-rotor helicopter may be influenced by factors which are both steady and unsteady (i.e., time dependent) in nature. However, as previously discussed, the data recording technique used herein did not permit an assessment of the time-dependent effects such as may be associated with blade stall or operation of the tail rotor in the vortex ring state. Although the potential contribution of these factors to the helicopter directional control problem is recognized, examination of the steady data taken showed no adverse effects which could be directly attributed to either tail-rotor blade stall or operation of the tail rotor in the vortex ring state.

In addition, reference 3 has identified other factors that can cause a reduction in helicopter directional control capability. The most important of these factors is an adverse effect of the main-rotor wake on tail-rotor performance, that is, the ground vortex phenomenon. Another of these factors is an increased level of main-rotor power

required over a small range of airspeeds while in ground effect. This phenomenon, discussed in reference 5, was not found to be of primary concern as regards helicopter directional control capability during this investigation.

Reference 6 has identified another potential source of helicopter directional control problems in forward flight. This is the rolled-up main-rotor shed vortex (or "wing-tip" vortex). Reference 7 shows that at main-rotor wake skew angles larger than the angle at which the ground vortex is formed, the trailing vortex system from the main rotor is rolling up near the plane of the tail rotor. Intersection of these vortices with the tail rotor could cause directional control problems similar to those caused by the ground vortex.

During this investigation an additional factor was noted which may cause increased difficulty in maintaining yaw trim in hover. For the condition of yaw trim and zero windspeed, the fin force was found to vary as much as 20 to 30 percent for different model azimuth angles for configurations SMPF and SMPA. This variation was reflected in the vehicle yawing moment, but no significant variation in the main-rotor torque occurred. Since no pattern was found in the variation of fin force with model azimuth angle, a low-frequency time-varying aerodynamic phenomenon is suspected as the cause. One possibility is an instability in the main-rotor wake as indicated by reference 8. This wake flow instability was shown to occur at a main-rotor height above the ground board of one-fourth of the main-rotor diameter; however, the instability did not occur when the main rotor was raised to one-half of the main-rotor diameter above the ground board. Motion pictures taken during the studies of reference 9 show the same type of main-rotor wake instabilities for the same main-rotor thrust coefficient and height above the ground board as in the present investigation. Therefore, for zero windspeed, changes in the tail-rotor thrust required to maintain yaw trim could possibly be produced by variations in the main-rotor wake caused by hovering near the ground.

During this investigation the ground vortex was studied as a function of main-rotor disk loading and windspeed at $\beta = 180^{\circ}$. In order to make this study, the tail rotor and fin were replaced by a tuft grid as shown in figure 4. Photographs of this tuft grid were then taken for three different values of main-rotor disk loading at windspeeds up to 25 knots. (See figs. 5 to 7.) The photographs show that the ground vortex exists in the vicinity of the tail-rotor location in rearward flight at windspeeds between 7.5 and 15 knots. The closest approach of the ground vortex to the tail-rotor location and the largest area of vorticity for a nominal disk loading of 250 N/m^2 occur at about 12.5 knots. However, the most well-defined area of vorticity seems to occur at a windspeed of 15 knots for the same disk loading. At windspeeds of 20 and 25 knots, the vorticity has moved from the region of the tail rotor. The photographs show a strong influence of main-rotor disk loading on the position of the ground vortex for windspeeds between 7.5

and 15 knots. The vortex appears to move higher as disk loading is increased. Although this study of the ground vortex was conducted only at $\beta = 180^{o}$, effects of the ground vortex are also in evidence at other wind azimuths as is shown subsequently in this discussion.

Critical Regions of Flight

The maximum values of tail-rotor and fin performance parameters for the yaw trim condition are presented in figure 8 as a function of wind azimuth regardless of windspeed. Since the curves include data over the range of windspeeds investigated and the velocity may vary from point to point on a given curve, the curves cannot be directly compared. These data, however, can be used to indicate the azimuth ranges where potential problems may exist. These problem areas are indicated by high maximum values of tail-rotor torque. In these problem areas research on tail-rotor/fin configuration effects should provide the greatest benefit.

From figure 8 it is immediately obvious that the V-tail configuration has a fundamentally different overall behavior when compared with any configuration using the standard vertical fin. Also, all the standard fin configurations regardless of fin/tail-rotor orientation or direction of tail-rotor rotation exhibit problems, generally within two azimuth ranges. It was found that within each of these azimuth ranges a critical velocity existed, that is, a velocity where each of the directional control parameters reached its maximum value. Figures 12, 13, and 15 to 18 show these azimuths to be between 60^{o} and 90^{o} at a velocity of 25 knots and 240^{o} at approximately 12.5 knots.

Fin and tail-rotor performance in these regions is further illustrated in figures 9 and 10 where the variations of fin and tail-rotor parameters with wind azimuth are given for yaw trim conditions at 25 knots (fig. 9) and at 12.5 knots (fig. 10) for the configurations included in figure 8. At both speeds the variations in total vehicle torque exhibit a closer similarity to the variations in fin force than to variations in any other parameter. Although it is recognized that all the parameters are interactive, this result indicates a predominant influence of fin force on the total vehicle torque.

At 25 knots (fig. 9), the variations of the tail-rotor and fin parameters with β for the V-tail configuration, with the exception of fin force magnitude, are similar to those for the standard fin configurations. In the azimuth range of concern where the maximum values occur ($\beta = 60^{o}$ to 90^{o}), both standard fin and V-tail configurations with the pusher tail rotor with top blade aft direction of rotation produce a reduction in collective pitch and tail-rotor torque when compared with the standard fin configuration with the pusher tail rotor with top blade forward direction of rotation.

At 12.5 knots (fig. 10), marked reductions in the magnitude of all parameters and their gradients with respect to wind azimuth were obtained with the V-tail configuration. In the azimuth range of concern at this speed ($\beta = 150^{\circ}$ to 240°), top blade aft direction of tail-rotor rotation produces less tail-rotor torque and collective pitch required to maintain yaw trim.

In terms of the results given in figures 9 and 10, no significant differences in the merits of pusher as opposed to tractor tail rotors with a standard fin are evident. However, the increased performance gains shown by the V-tail configuration indicate that it should provide the best baseline configuration for any future detailed studies.

Systematic Performance Studies

A systematic documentation of tail-rotor/fin performance is given in figures 11 to 22 where the variations of main-rotor, fin, and tail-rotor parameters with windspeed are given for the various configurations tested at fixed wind azimuths. The results are discussed according to azimuth or azimuth ranges where the results are sufficiently similar.

Performance at $\beta = 0^{\circ}$.- For the configurations tested at $\beta = 0^{\circ}$, no critical windspeeds were found. In addition, using the top blade aft direction of tail-rotor rotation with either the standard fin or the V-tail increases the control margin over the entire range of test windspeeds (fig. 11(d)).

Performance at $\beta = 60^{\circ}$ to 90°.- Figures 12 and 13 show that between $\beta = 60^{\circ}$ and 90° there is a critical region for windspeeds of 25 knots because of the large values of fin force, tail-rotor torque, and collective pitch which are produced. The increase in the adverse fin force as a function of windspeed is to be expected because of the impingement of the free stream on the fin. The top blade aft direction of tail-rotor rotation produces lower values of tail-rotor torque and collective pitch than does the top blade forward direction of rotation. Reference 6 indicates that at the higher windspeeds in this azimuth range the tail rotor may be affected by impingement of the "wing-tip" vortex from the main rotor. It would be possible for such a vortex impingement to produce higher values of tail-rotor torque and collective pitch for a top blade forward direction of tail-rotor rotation than for a top blade aft direction of rotation.

Performance at $\beta = 120^{\circ}$.- Figure 14 shows that significant gains in tail-rotor performance may be realized by use of the V-tail configuration. The top blade aft direction of tail-rotor rotation is also shown to be preferred over the top blade forward direction of rotation.

Performance at $\beta = 150^{\circ}$ to 240°.- The region where the ground vortex is believed to be the predominant cause of low-speed directional control problems for tail-rotor-

type helicopters operating in ground effect is between $\beta = 150^{o}$ and $\beta = 240^{o}$. Reference 3 indicates that this ground vortex causes a critical flight condition near a windspeed of 12.5 knots for the values of main-rotor disk loading and main-rotor height used in the present investigation. Theoretical results from reference 4 indicate the presence of this ground vortex for similar main-rotor test conditions.

The shaded regions in figures 15 to 19 indicate the extent of the uncertainty in the location of the yaw trim condition due to aerodynamic effects of the fin and tail rotor. The data in figures 15 to 18 show that changes with windspeed in the tail-rotor thrust required for yaw trim are due primarily to large changes in the adverse fin force rather than to changes in the main-rotor torque. Also, figures 15 to 18 indicate that the direction of tail-rotor rotation is a more important parameter with respect to the magnitudes of the fin and tail-rotor parameters than is the location of the tail rotor as either a pusher or tractor. This importance of the tail-rotor direction of rotation is an indication of the tail-rotor and ground vortex interaction discussed in reference 3. However, the location of the tail rotor as a pusher or tractor is important with respect to variations of the fin and tail-rotor parameters with windspeed; this is evidenced by the differences in slope of the curves for C_F, $C_{T,tr}$, θ_{tr}, and $C_{Q,tr}$ between windspeeds of 12.5 and 15 knots at $\beta = 150^{o}$, 180^{o}, and 210^{o} (figs. 15 to 17). These figures show that the tractor tail rotor decreases the variations with windspeed of the fin and tail-rotor parameters for the configuration using the standard fin. At $\beta = 240^{o}$ (fig. 18), there appears to be no difference between the pusher and tractor tail rotors concerning variations in the fin and tail-rotor parameters with windspeed. The V-tail configuration tested at $\beta = 180^{o}$ and 240^{o} shows significant decreases in the fin and tail-rotor parameters throughout most of the range of test windspeeds. In addition, this configuration removes the large variations with windspeed in the fin and tail-rotor parameters.

Effect of increased fin/tail-rotor gap at $\beta = 180^{o}$.- The effect of increasing the fin/tail-rotor gap at $\beta = 180^{o}$ for the standard configuration is shown in figure 19. These data show that increasing the fin/tail-rotor gap does not change the basic character of the variation of the fin and tail-rotor parameters with windspeed but does decrease the adverse fin force over most of the range of windspeeds. Although this result is accompanied by a decrease in the tail-rotor thrust required for yaw trim, increases in the tail-rotor collective pitch and torque are shown for the largest fin/tail-rotor gap tested (figs. 19(d) and 19(e)). Thus, no definite advantage is realized by increasing the fin/tail-rotor gap for this particular configuration.

Effect of changes in tail-rotor vertical location at $\beta = 180^{o}$.- Figure 20 shows the results obtained by varying the tail-rotor vertical location for configuration NMPF at $\beta = 180^{o}$. This configuration was used since the intent was to determine the vertical range of the ground vortex effect on the tail rotor without fin interference. The tail-rotor

parameters are plotted as a function of windspeed for a constant value of tail-rotor thrust coefficient regardless of the vehicle yaw trim condition. This method was employed to preclude the use of extrapolated data to obtain the vehicle yaw trim condition. The data show that for windspeeds below 15 knots, the higher tail-rotor positions produce the smallest magnitude and least variations with windspeed in tail-rotor collective pitch and torque for a given value of tail-rotor thrust coefficient. At the highest tail-rotor vertical position ($z/R_{tr} = 0.70$), the tail rotor has apparently been raised above the region of significant influence of the ground vortex as evidenced by the lower magnitudes and variations of θ_{tr} and $C_{Q,tr}$.

Performance at $\beta = 270^{o}$ to 300^{o}. - The variations with windspeed of the fin and tail-rotor parameters at $\beta = 270^{o}$ and 300^{o} are shown in figures 21 and 22, respectively. Tail-rotor direction of rotation is still an important parameter at these azimuths. The top blade aft direction of rotation produces lower values of the fin and tail-rotor parameters except between 15 and 20 knots at $\beta = 270^{o}$. The V-tail configuration tested at $\beta = 300^{o}$ produces the lowest values of adverse fin force and consequently the lowest tail-rotor thrust required for yaw trim. However, the standard fin with the top blade aft direction of rotation produced values of θ_{tr} and $C_{Q,tr}$ about as low as those produced by the V-tail. No tractor tail-rotor configurations were tested at these wind azimuths; therefore, no comparisons between different tail-rotor locations can be made.

Vehicle pitching moment due to V-tail. - At $\beta = 0^{o}$, 60^{o}, and 300^{o}, an effort was made to assess the contribution of the V-tail to the vehicle longitudinal stability at windspeeds up to 35 knots. Figure 23 shows the variation of the vehicle pitching-moment coefficient due to the V-tail with windspeed for these wind azimuths. At $\beta = 60^{o}$ and 300^{o}, rather large excursions in vehicle pitching moment are indicated; whereas, at $\beta = 0^{o}$, the vehicle pitching moment is a steadily increasing nose-up moment. These values do not appear to be too large to be trimmed by the main rotor. However, a control problem could occur for changes in wind azimuth during hover at windspeeds above 15 knots.

CONCLUSIONS

An investigation has been conducted in the Langley full-scale tunnel to study the effects of several fin/tail-rotor parameters on helicopter directional control at low speeds in ground effect. Based on the data obtained, the following conclusions have been reached:

1. The V-tail configuration demonstrated significant advantages with respect to helicopter directional control.

2. The V-tail has a significant effect on vehicle longitudinal pitching moment and could cause control problems during heading changes at windspeeds above 15 knots.

3. At a wind azimuth of 180°, for a fin-off configuration and a constant value of tail-rotor thrust coefficient, moving the tail rotor to a higher than normal position produces significant advantages in tail-rotor performance.

4. Tail-rotor direction of rotation is a primary parameter with respect to helicopter directional control. A top blade aft direction of tail-rotor rotation generally requires less tail-rotor torque and less change of collective pitch with windspeed and wind azimuth to maintain yaw trim.

5. At a wind azimuth of 180°, increases in the fin/tail-rotor gap reduced the adverse fin force but demonstrated negligible advantages in overall directional control capability for a pusher tail rotor with top blade forward direction of rotation in combination with a standard fin.

6. At a constant main-rotor lift coefficient, variations with windspeed of the tail-rotor thrust coefficient required to maintain yaw trim are due to variations in fin force and, to a much less degree, variations in main-rotor torque.

7. Ground vortex effects on the fin/tail-rotor combination appear to extend between wind azimuths of 150° and 240°.

Langley Research Center,
National Aeronautics and Space Administration,
Hampton, Va., July 29, 1974.

REFERENCES

1. Connor, William J.: The Huey Cobra in Vietnam. 1968 Report to the Aerospace Profession, Tech. Rev., vol. 9, no. 2, Soc. Exp. Test Pilots, 1968, pp. 25-32.

2. Lynn, R. R.; Robinson, F. D.; Batra, N. N.; and Duhon, J. M.: Tail Rotor Design. Pt. I: Aerodynamics. J. Amer. Helicopter Soc., vol. 15, no. 4, Oct. 1970, pp. 2-15.

3. Huston, Robert J.; and Morris, Charles E. K., Jr.: A Wind-Tunnel Investigation of Helicopter Directional Control in Rearward Flight in Ground Effect. NASA TN D-6118, 1971.

4. Heyson, Harry H.: Theoretical Study of Conditions Limiting V/STOL Testing in Wind Tunnels With Solid Floor. NASA TN D-5819, 1970.

5. Heyson, Harry H.: Ground Effect for Lifting Rotors in Forward Flight. NASA TN D-234, 1960.

6. Wiesner, Wayne; and Kohler, Gary: Tail Rotor Performance in Presence of Main Rotor, Ground, and Winds. Amer. Helicopter Soc. Preprint No. 764, May 1973.

7. Heyson Harry H.; and Katzoff, S.: Induced Velocities Near a Lifting Rotor With Nonuniform Disk Loading. NACA Rep. 1319, 1957. (Supersedes NACA TN 3690 by Heyson and Katzoff and TN 3691 by Heyson.)

8. Heyson, Harry H.: An Evaluation of Linearized Vortex Theory as Applied to Single and Multiple Rotors Hovering In and Out of Ground Effect. NASA TN D-43, 1959.

9. Lehman, August F.: Model Studies of Helicopter Tail Rotor Flow Patterns In and Out of Ground Effect. USAAVLABS Tech. Rep. 71-12, U.S. Army, Apr. 1971. (Available from DDC as AD 725591.) Motion picture film No. RF-574 taken during these studies is available from Eustis Directorate, U.S. Army Air Mobility R&D Laboratory, Fort Eustis, Virginia 23604.

TABLE I.- ROTOR CHARACTERISTICS

	Main rotor	Tail rotor
Diameter, m	3.35	0.648
Rotor-blade chord, m	0.171	0.053
Solidity	0.065	0.105
Effective cutout, percent	17	20
Blade twist, deg	-10	0
Blade airfoil	(a)	NACA 0015
Nominal tip speed, m/sec	210	224

[a]Coordinates are given in reference 3.

TABLE II.- MODEL CONFIGURATIONS AND TEST RUN SCHEDULE

Fin	Tail-rotor configuration	Configuration designation	Remarks	Wind Azimuth β, deg, of –									
				0	60	90	120	150	180	210	240	270	300
None	None	NMNN	Tuft grid in place						1				
None	Pusher, top blade forward rotation	NMPF	Tuft grid in place						2				
None	Pusher, top blade forward rotation	NNPF	Main rotor tied down			9	8	7	6	14	13	12	
None	Pusher, top blade forward rotation	NMPF				10			[a]3, [b]4, 5			11	
Standard	Pusher, top blade forward rotation	SMPF		19	20	21	22	23	[c]24, [d]25, [e]26	15	16	17	18
Standard	Pusher, top blade aft rotation	SMPA		32	33	34	35	36	27	28	29	30	31
Standard	Tractor, top blade forward rotation	SMTF					44	45	46	47	48		
Standard	Tractor, top blade aft rotation	SMTA						52	51	50	49		
V-tail	Pusher, top blade aft rotation	VMPA	No horizontal tail	[f]41	[f]42		43		38		39		[f]40

[a]Tail rotor at $0.35R_{tr}$ below normal position.

[b]Tail rotor at $0.70R_{tr}$ above normal position.

[c]Fin/tail-rotor gap of $0.2R_{tr}$.

[d]Fin/tail-rotor gap of $0.4R_{tr}$.

[e]Fin/tail-rotor gap of $0.6R_{tr}$.

[f]In addition to standard windspeeds of 0, 7.5, 10, 12.5, 15, 20, and 25 knots, data were taken at 30 and 35 knots.

TABLE III.- ESTIMATED MEASUREMENT ACCURACY

Coefficient	Balance	Accuracy
Vehicle torque, $C_{Q,v}$	Vehicle	±0.000009
Fin force, C_F	Fin	±0.00007
Tail-rotor thrust, $C_{T,tr}$	Tail rotor	±0.0002
Tail-rotor torque, $C_{Q,tr}$	Tail rotor	±0.00003
Vehicle pitching moment contributed by V-tail, $C_{m,f}$	Fin	±0.00007
Main-rotor lift, C_L^*	Vehicle	±0.00005
Main-rotor torque, $C_{Q,mr}$	Mast strain gage	±0.00001

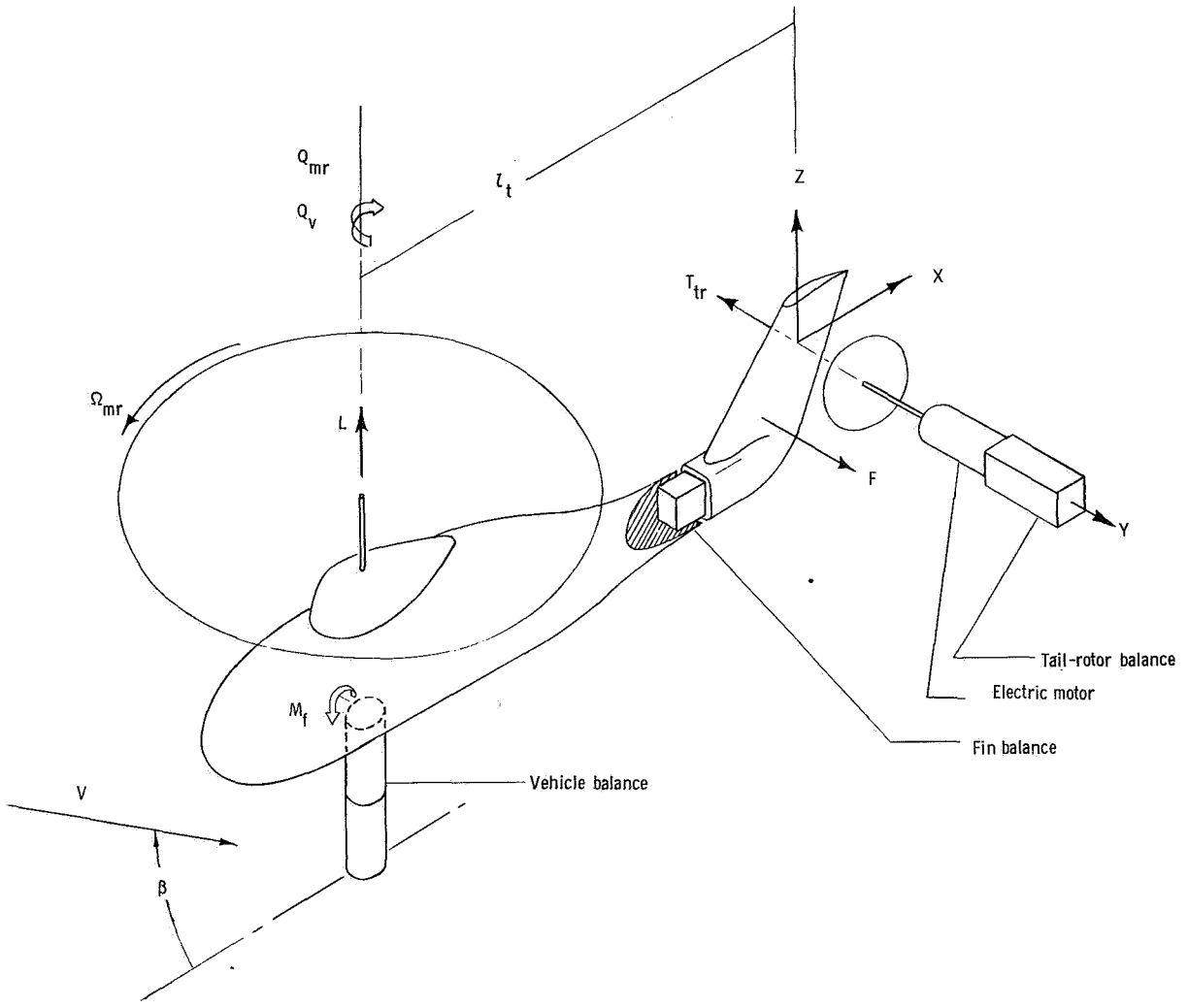

Figure 1.- Model schematic and conventions used to define positive directions.

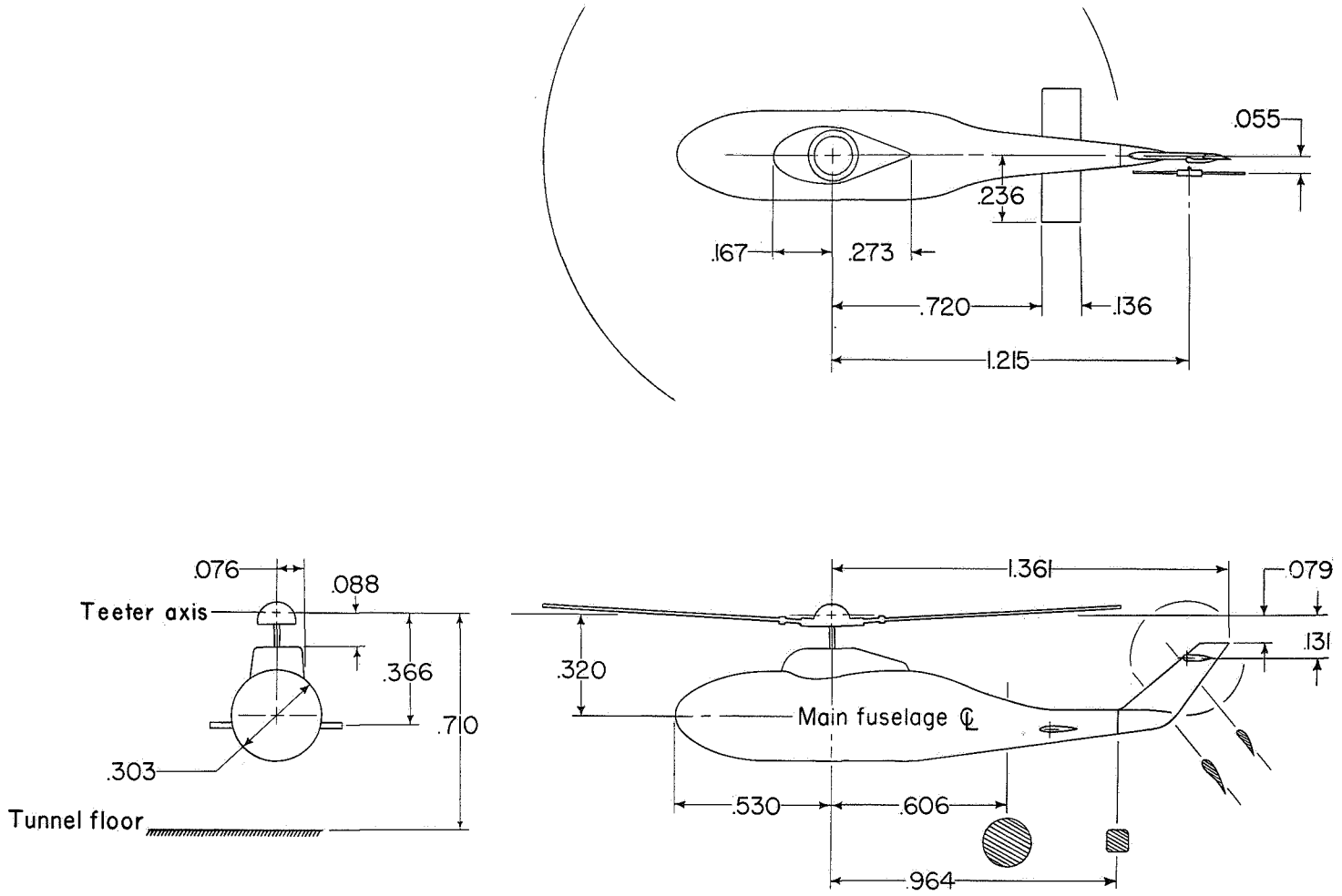

(a) Three-view drawing of complete model.

Figure 2.- Drawings of model and fin assemblies. All dimensions are ratios of main-rotor radius (R_{mr} = 1.68 m).

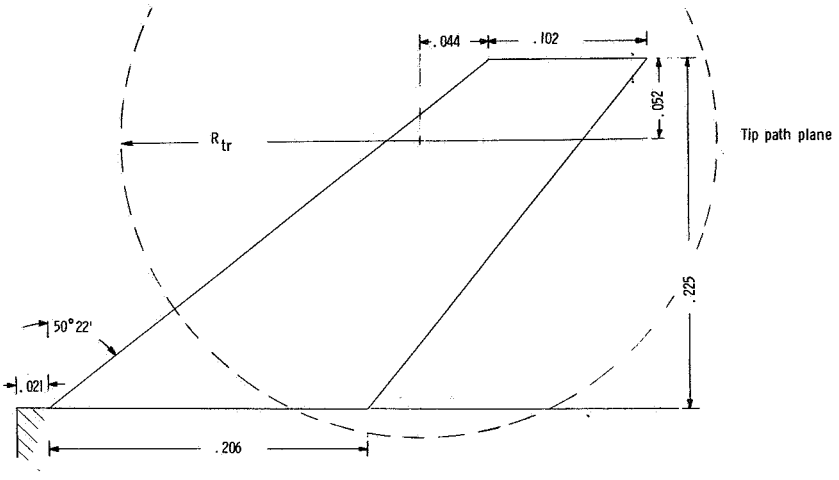

(b) Standard fin.

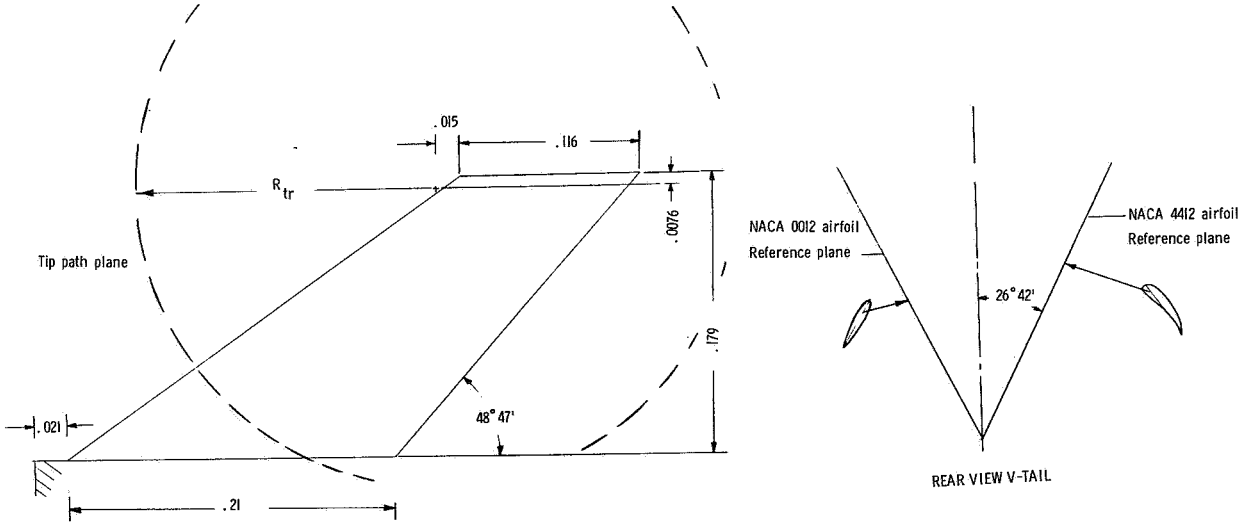

(c) V-tail.

Figure 2.- Concluded.

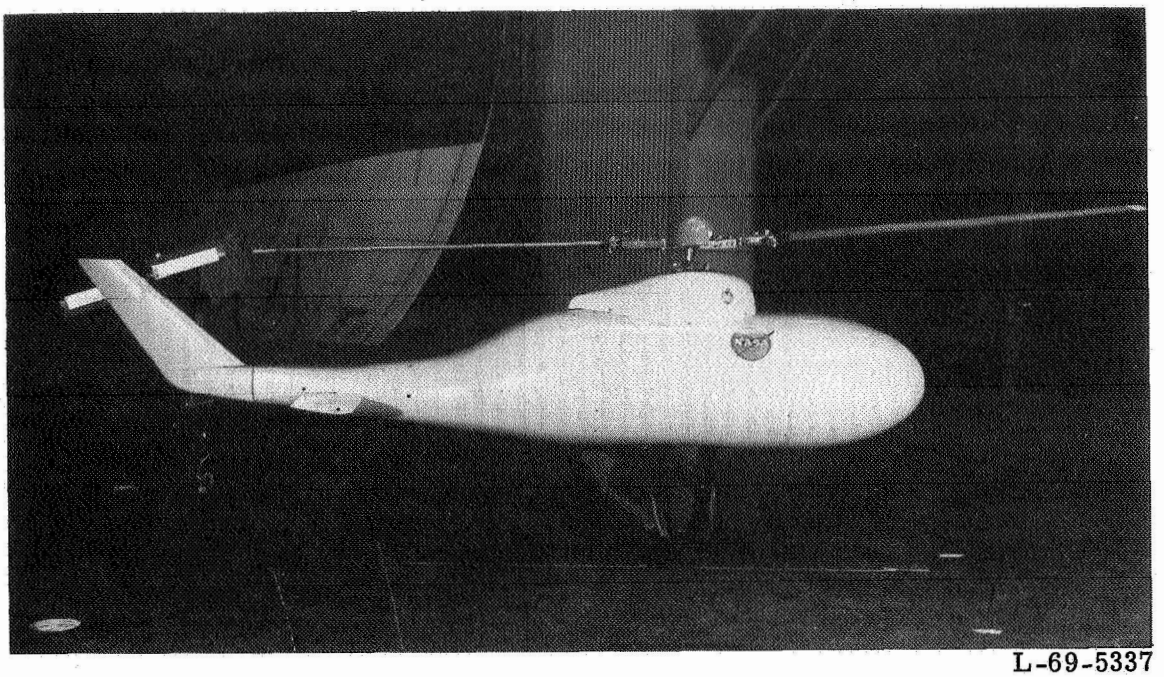

L-69-5337

(a) Side view of model.

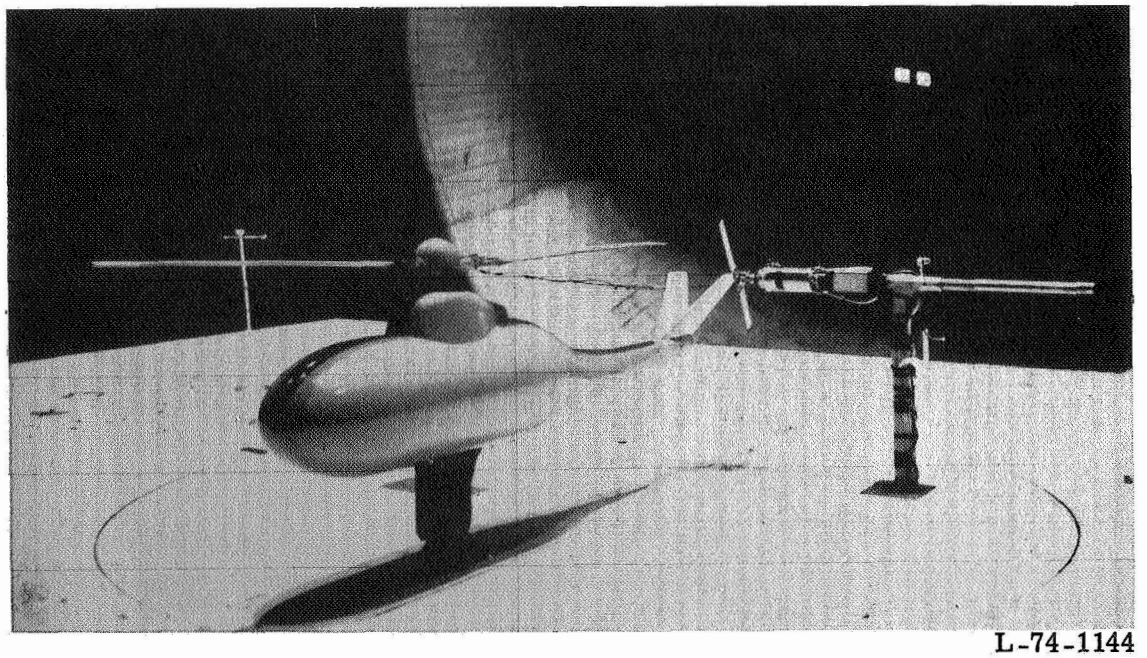

L-74-1144

(b) Model with V-tail installed.

Figure 3.- Model installed in Langley full-scale tunnel.

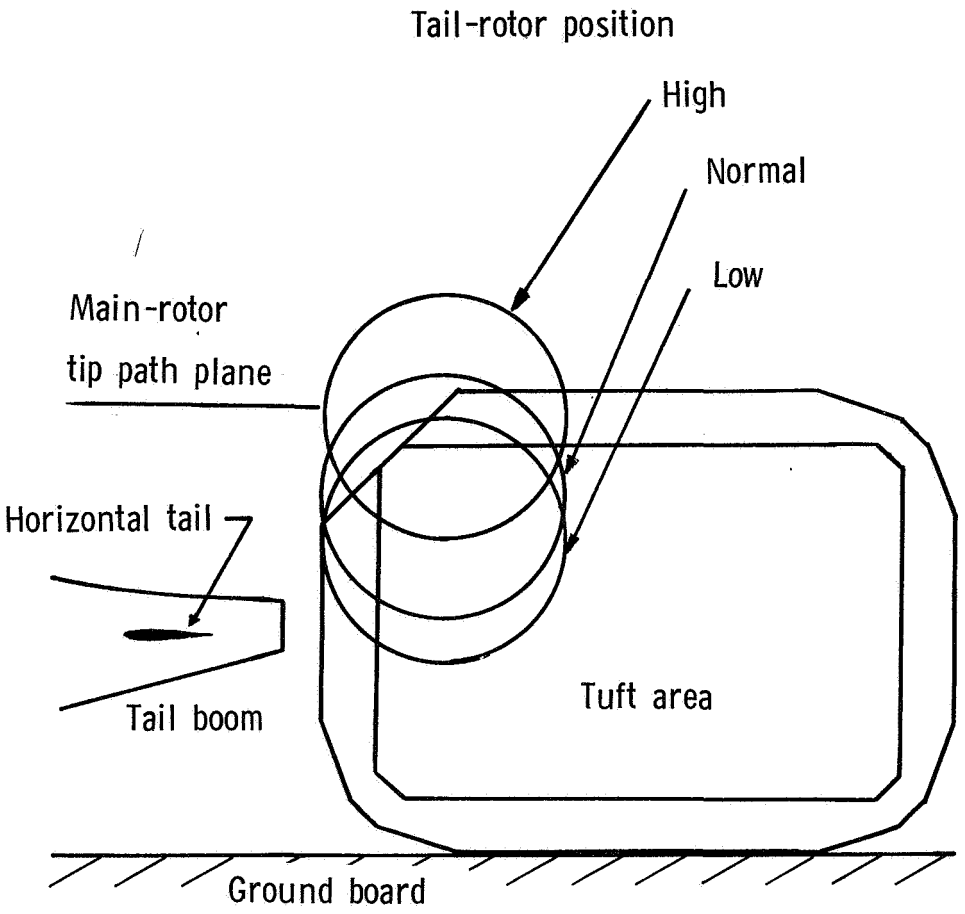

Figure 4.- Tail-rotor vertical position relative to the tuft grid.

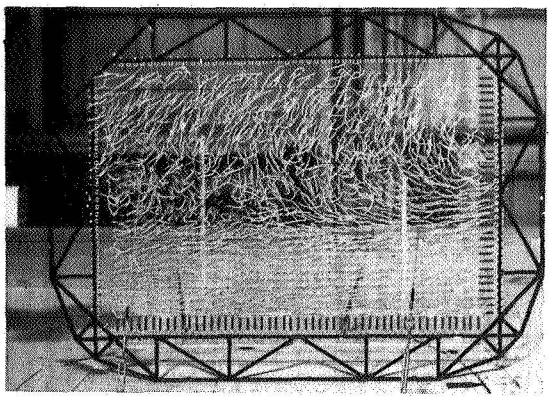

(a) V = 7.5 knots.

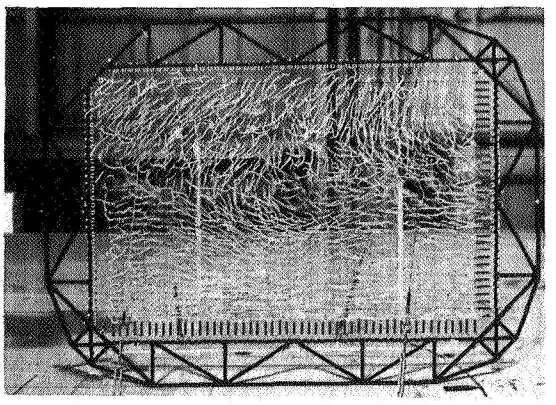

(b) V = 10 knots.

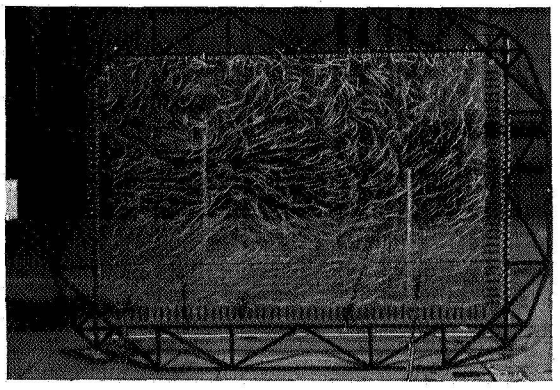

(c) V = 12.5 knots.

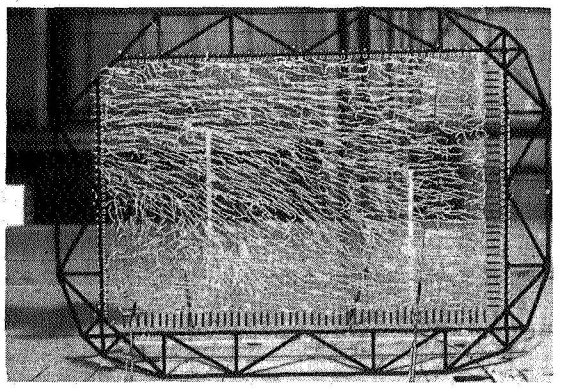

(d) V = 15 knots.

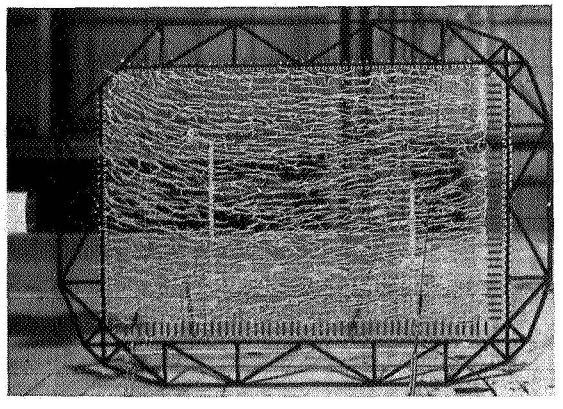

(e) V = 20 knots.

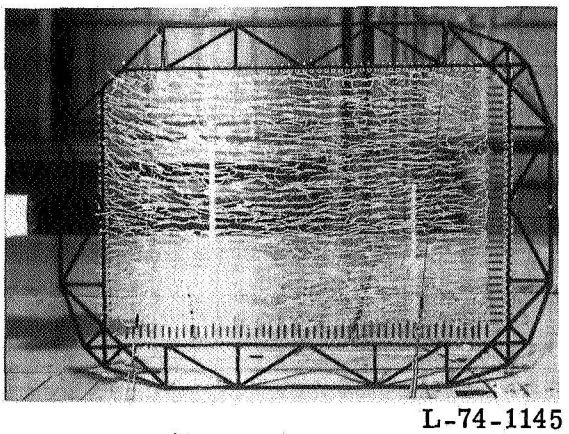

L-74-1145

(f) V = 25 knots.

Figure 5.- The ground vortex at $\beta = 180^{o}$ and a main-rotor disk loading of 220 N/m^2.

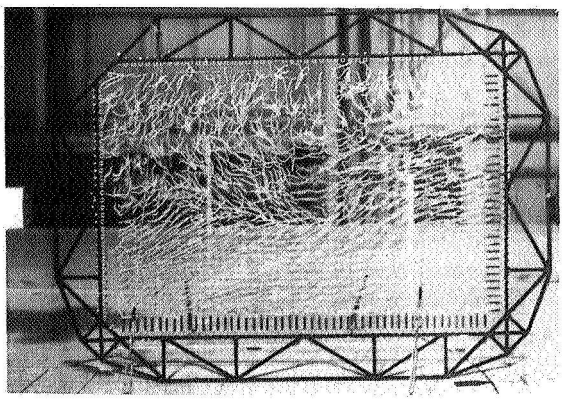

(a) V = 7.5 knots.

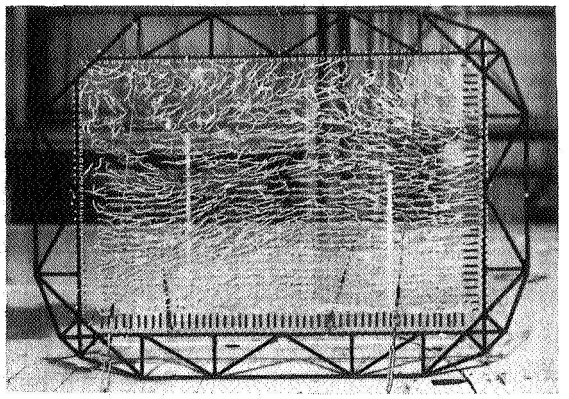

(b) V = 10 knots.

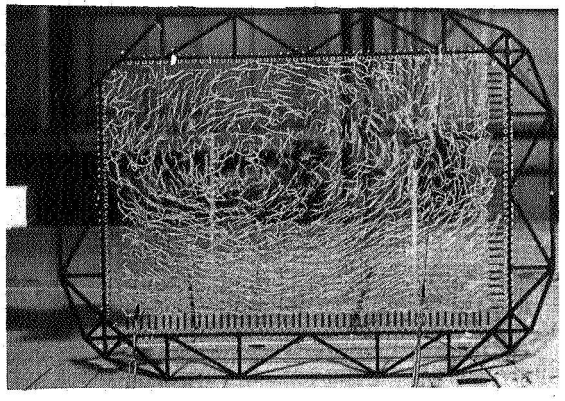

(c) V = 12.5 knots.

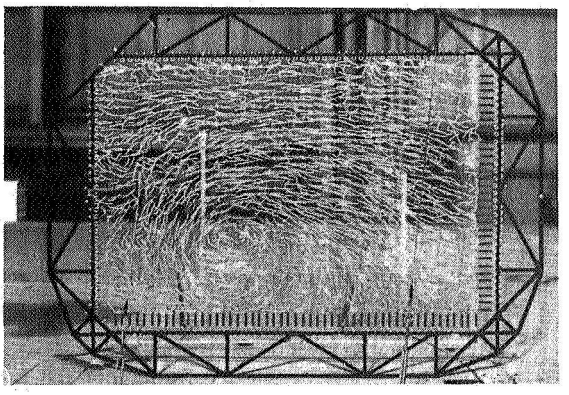

(d) V = 15 knots.

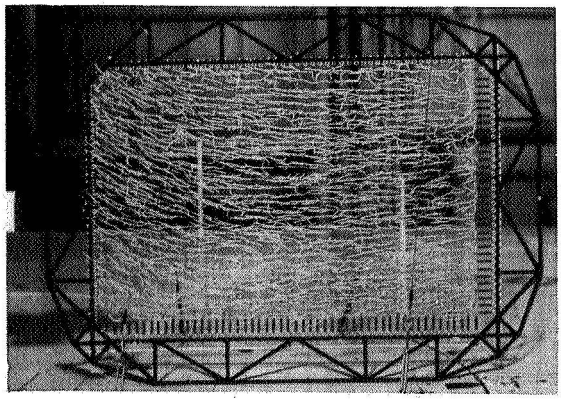

(e) V = 20 knots.

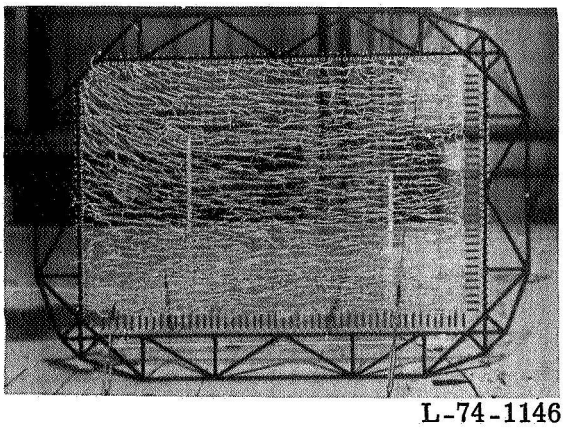

L-74-1146

(f) V = 25 knots.

Figure 6.- The ground vortex at $\beta = 180^{o}$ and a main-rotor disk loading of 250 N/m^2.

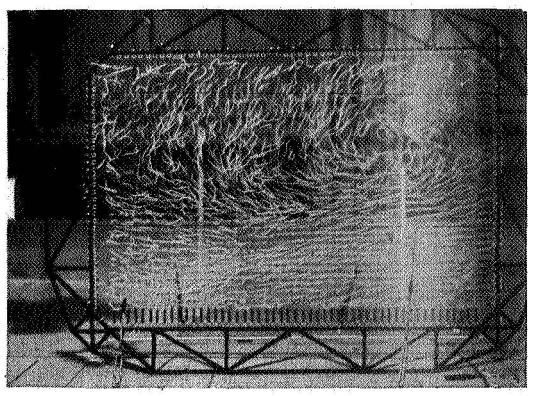

(a) V = 7.5 knots.

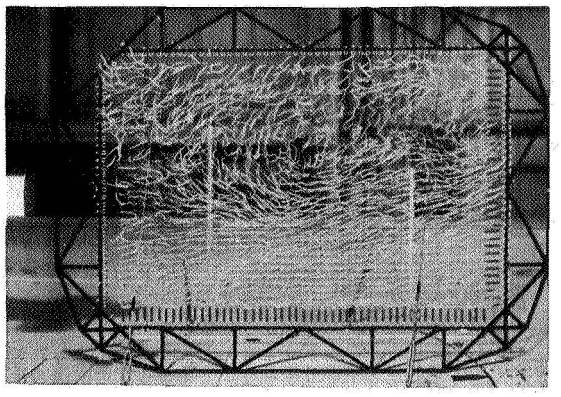

(b) V = 10 knots.

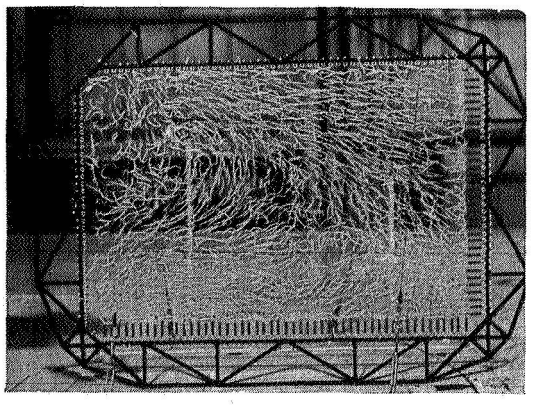

(c) V = 12.5 knots.

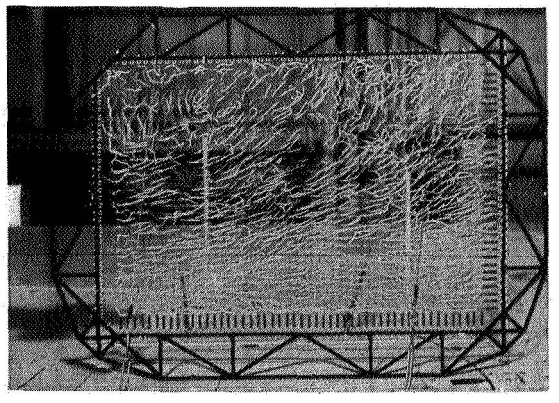

(d) V = 15 knots.

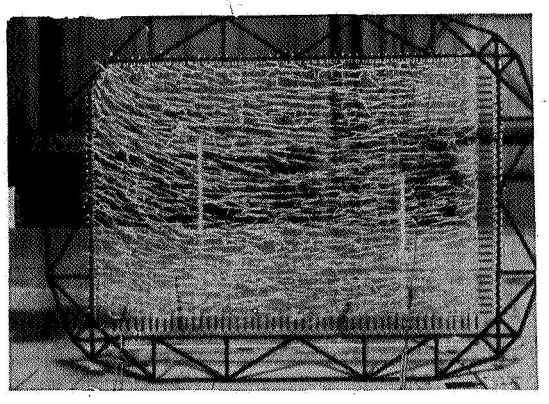

(e) V = 20 knots.

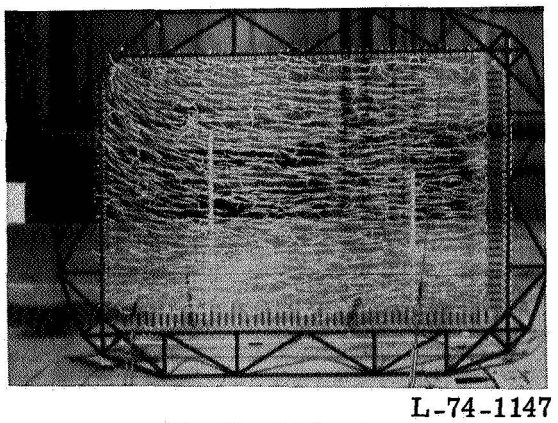

L-74-1147

(f) V = 25 knots.

Figure 7.- The ground vortex at $\beta = 180^{o}$ and a main-rotor disk loading of 284 N/m^2.

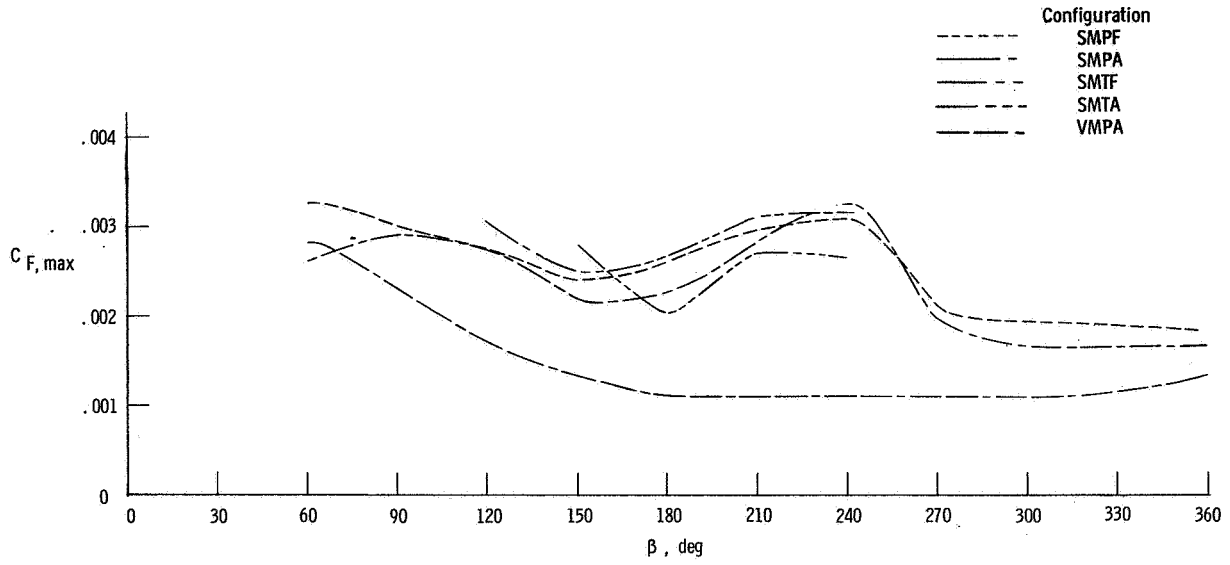

(a) Fin force.

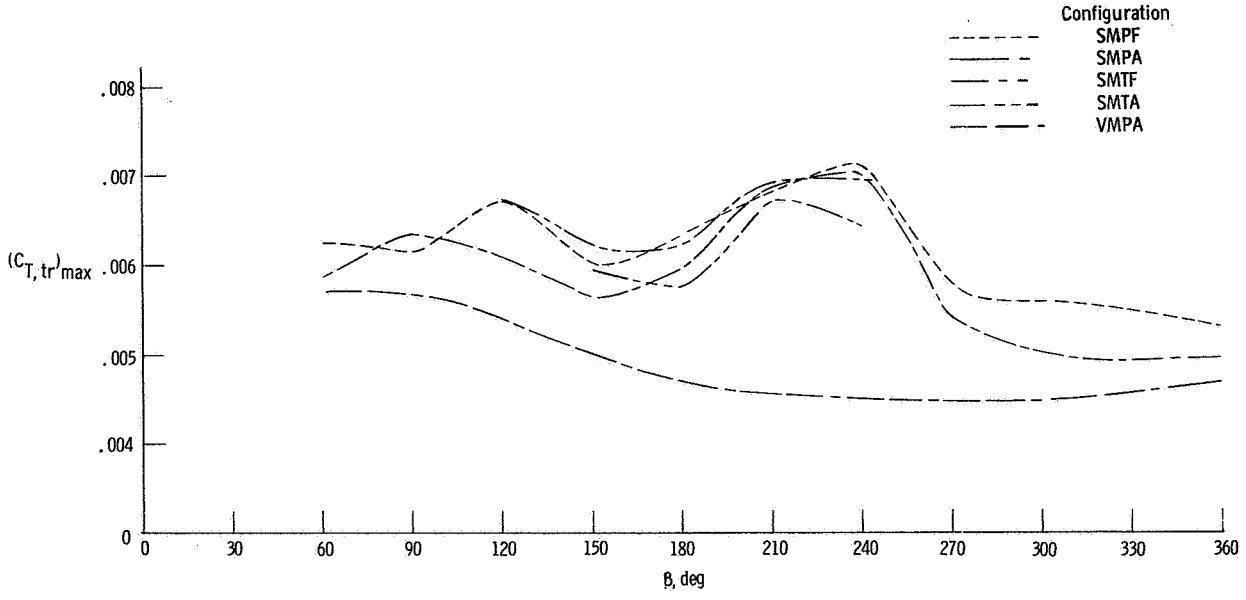

(b) Tail-rotor thrust.

Figure 8.- Variation of performance parameter maximums.

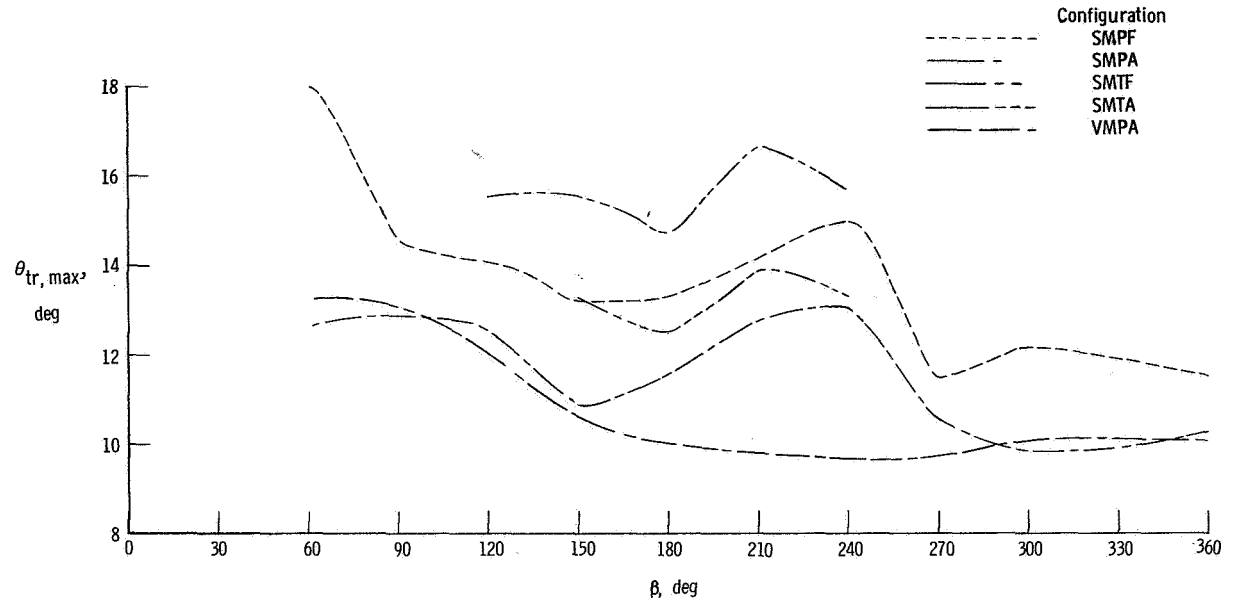

(c) Tail-rotor collective pitch.

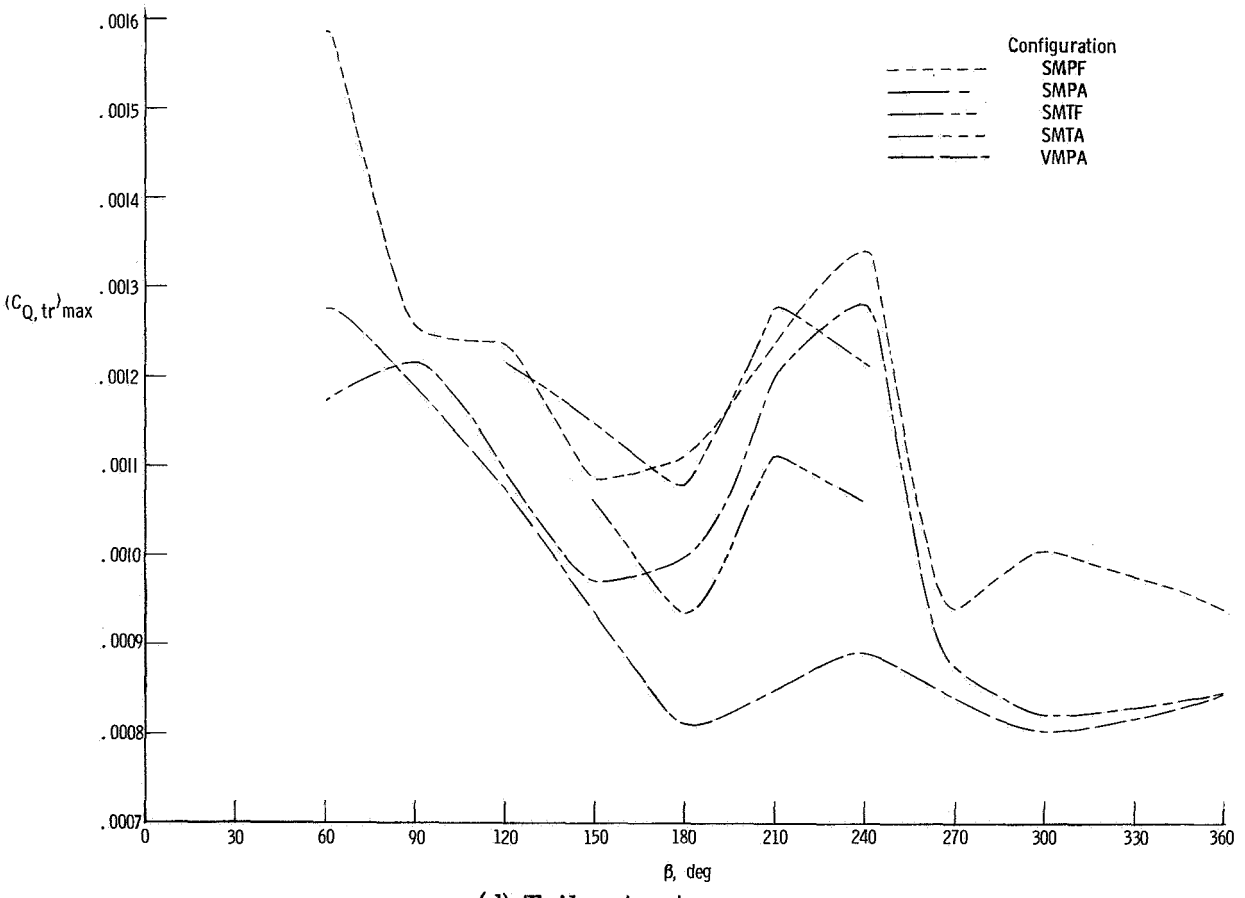

(d) Tail-rotor torque.

Figure 8.- Concluded.

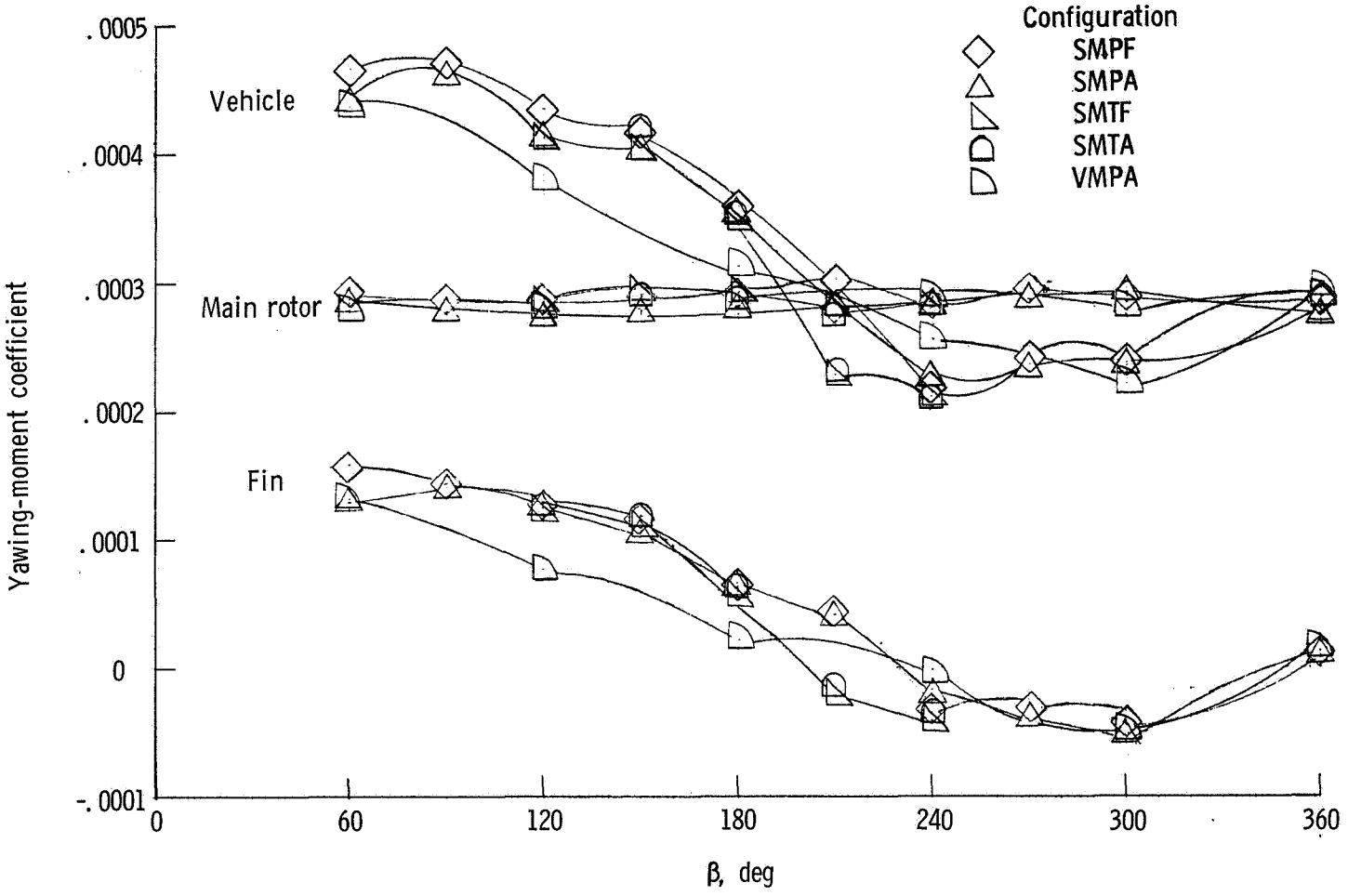

(a) Yawing-moment coefficients.

Figure 9.- Variation of performance parameters with wind azimuth at 25 knots. All points have been interpolated to a yaw trim condition for $C'_L = 0.00470$.

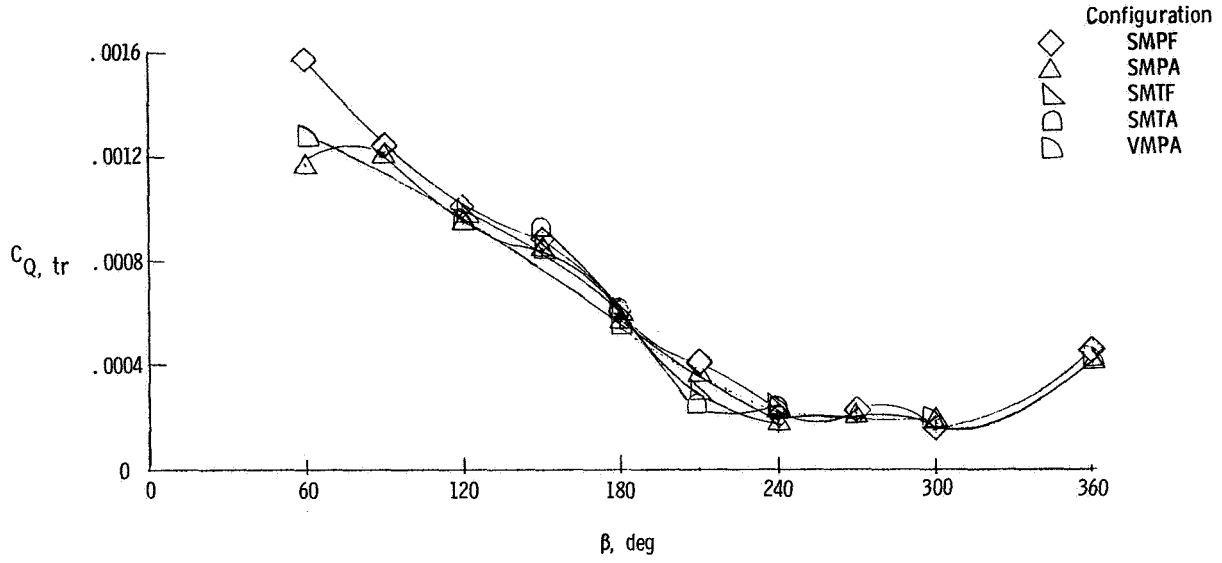

(b) Tail-rotor torque coefficient.

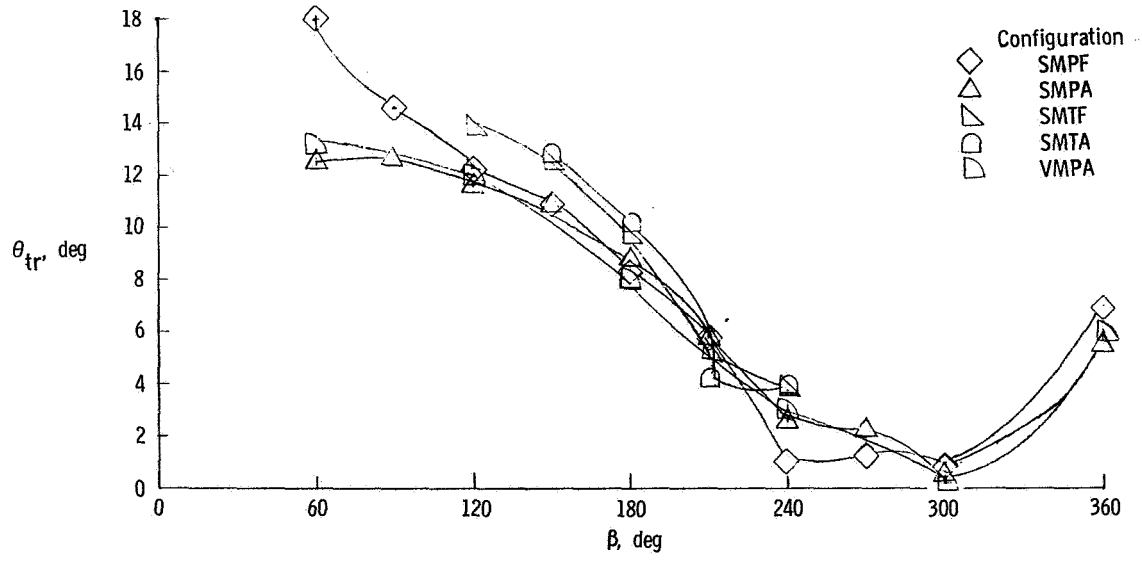

(c) Tail-rotor collective pitch.

Figure 9.- Concluded.

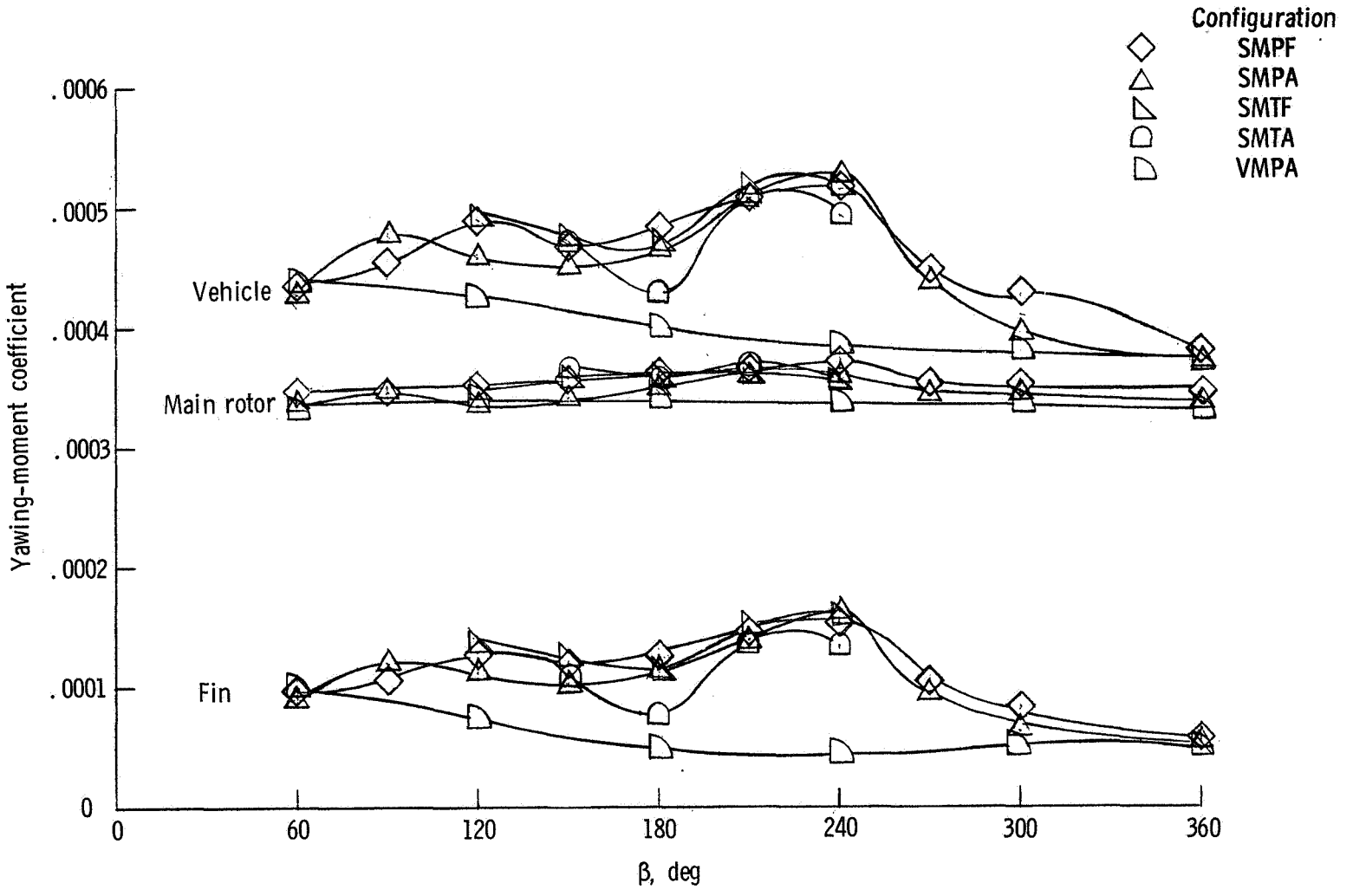

(a) Yawing-moment coefficients.

Figure 10.- Variation of performance parameters with wind azimuth at 12.5 knots. All points have been interpolated to a yaw trim condition for $C'_L = 0.00470$.

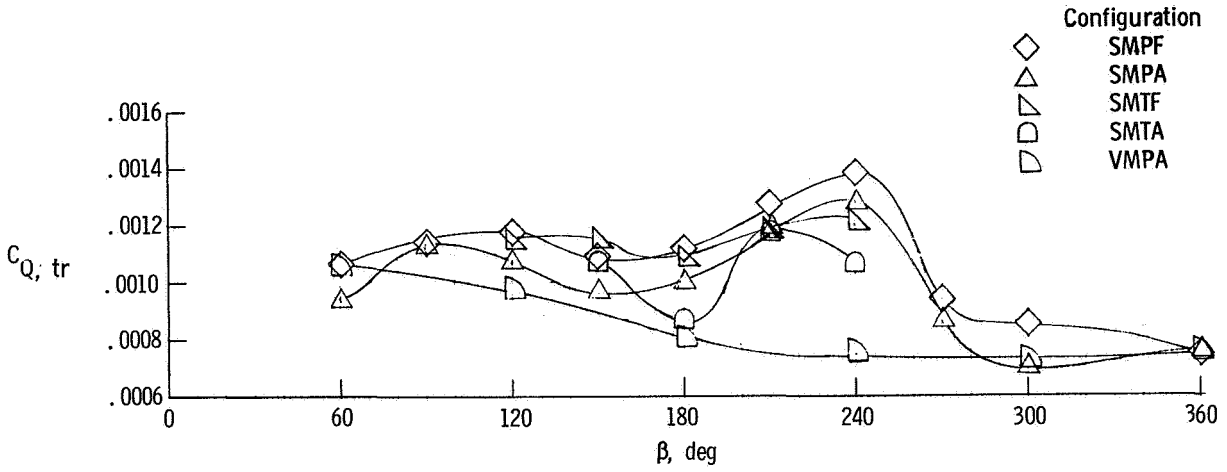

(b) Tail-rotor torque coefficient.

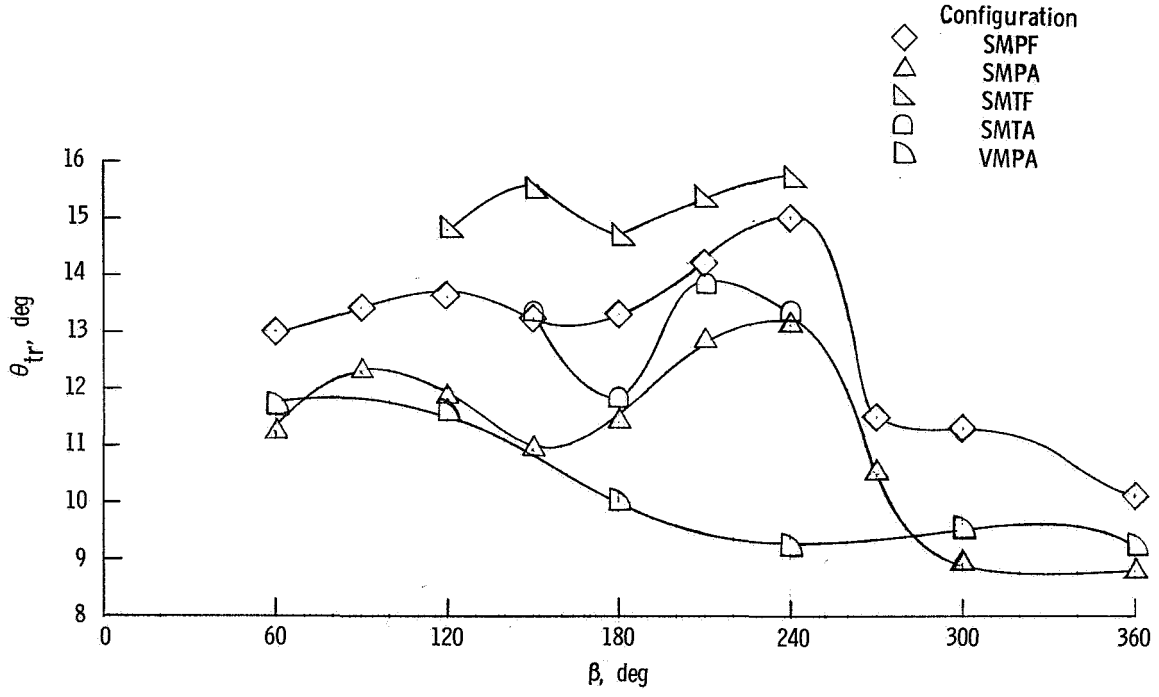

(c) Tail-rotor collective pitch.

Figure 10.- Concluded.

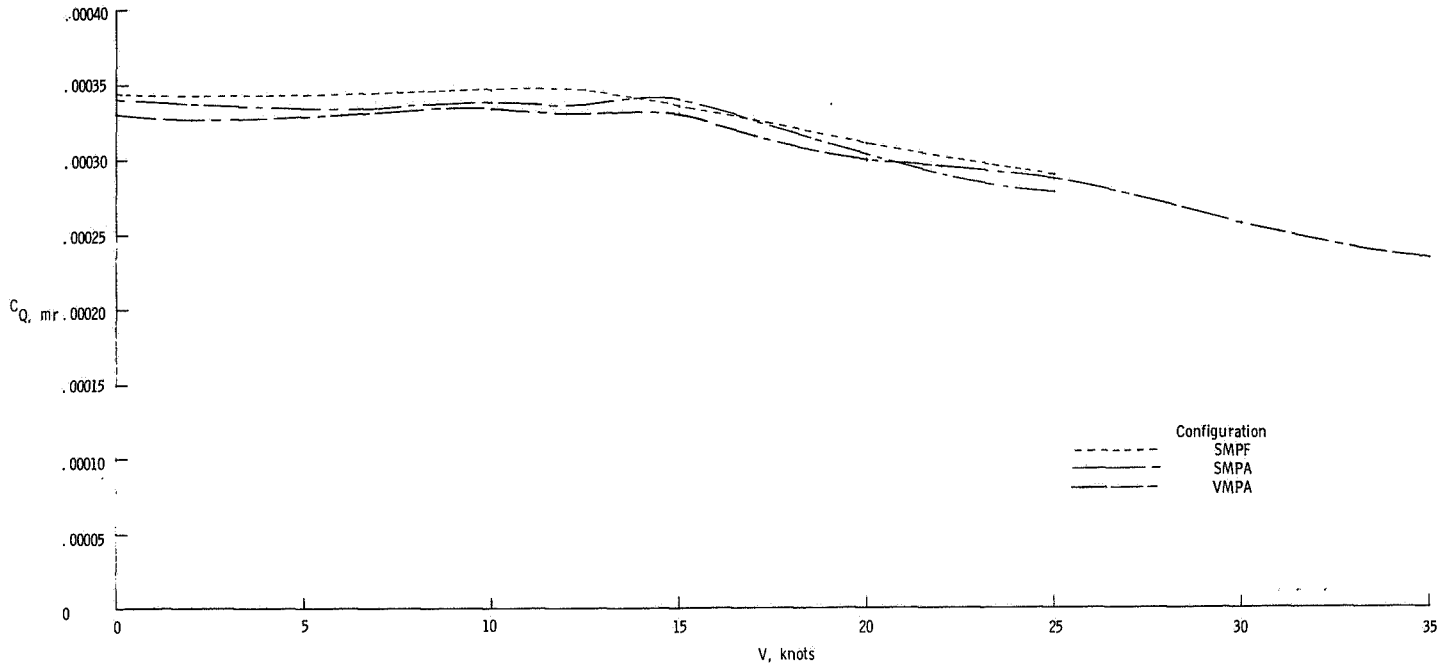

(a) Main-rotor torque.

Figure 11.- Variation of main-rotor, fin, and tail-rotor parameters with windspeed at $\beta = 0^{o}$.

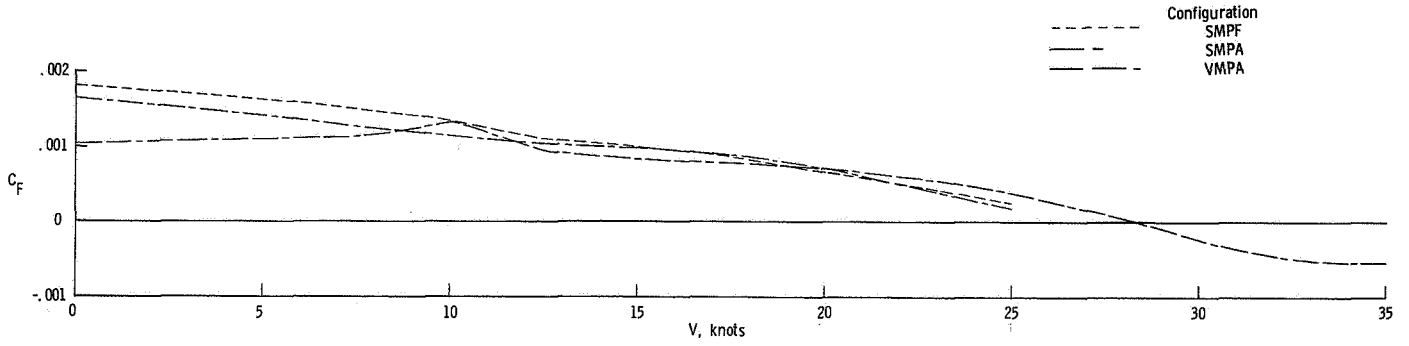

(b) Fin force.

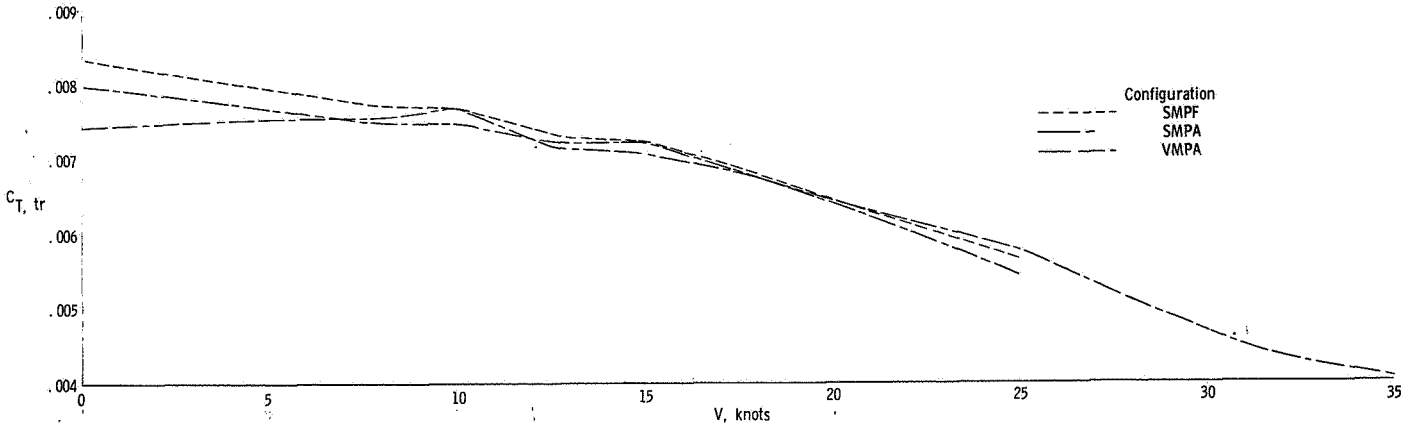

(c) Tail-rotor thrust.

Figure 11.- Continued.

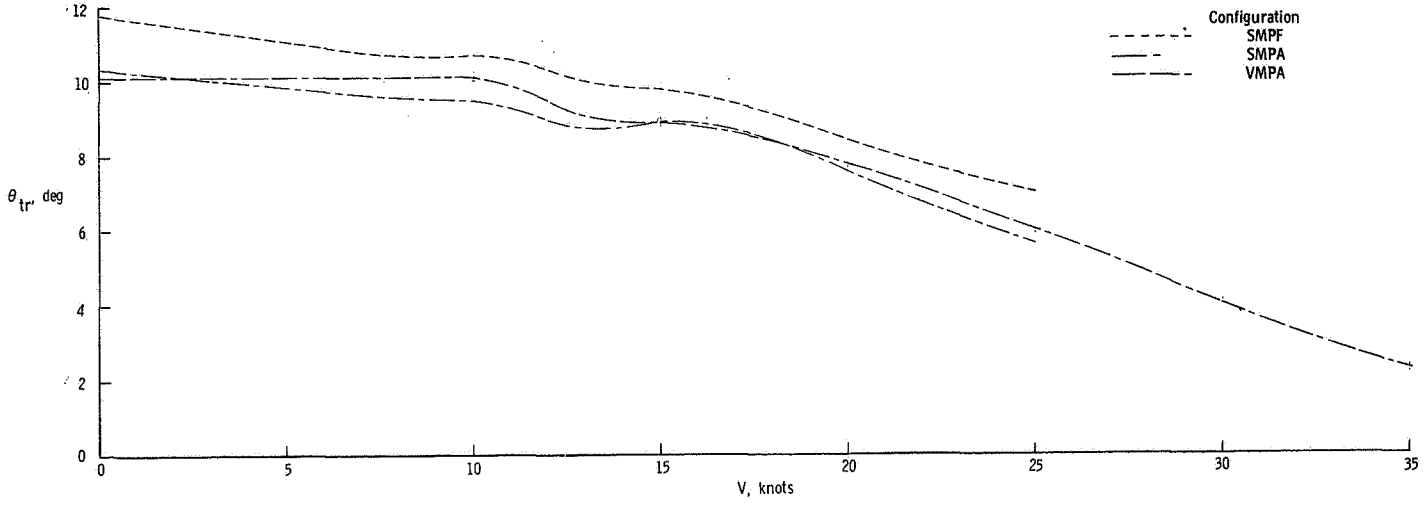

(d) Tail-rotor collective pitch.

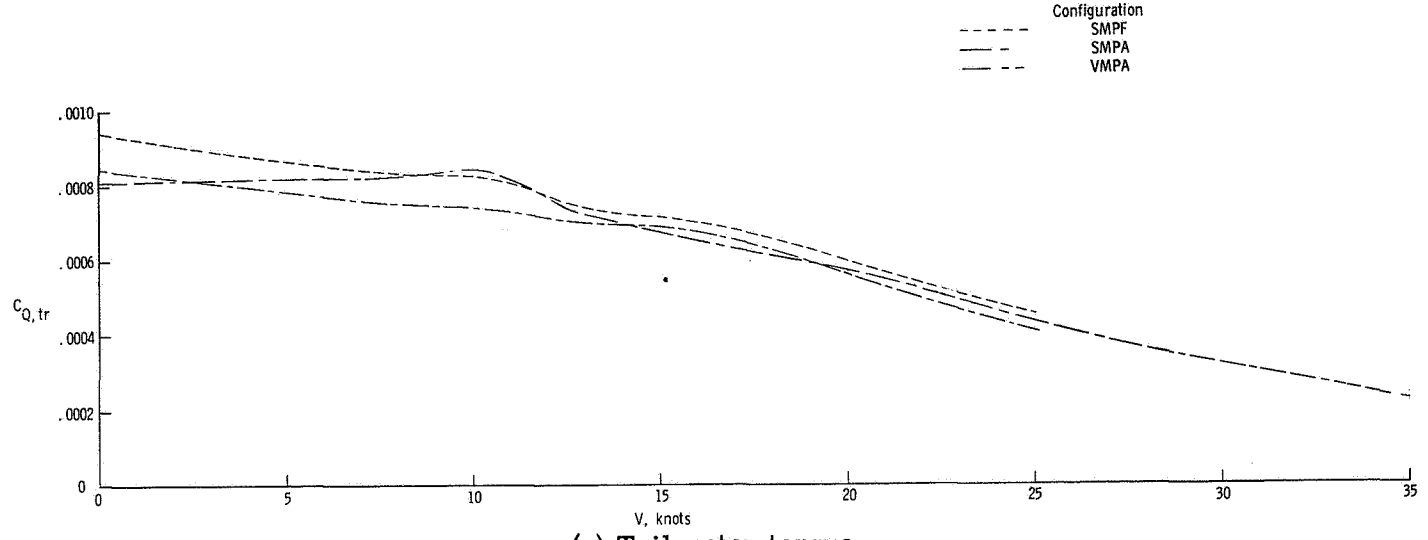

(e) Tail-rotor torque.

Figure 11.- Concluded.

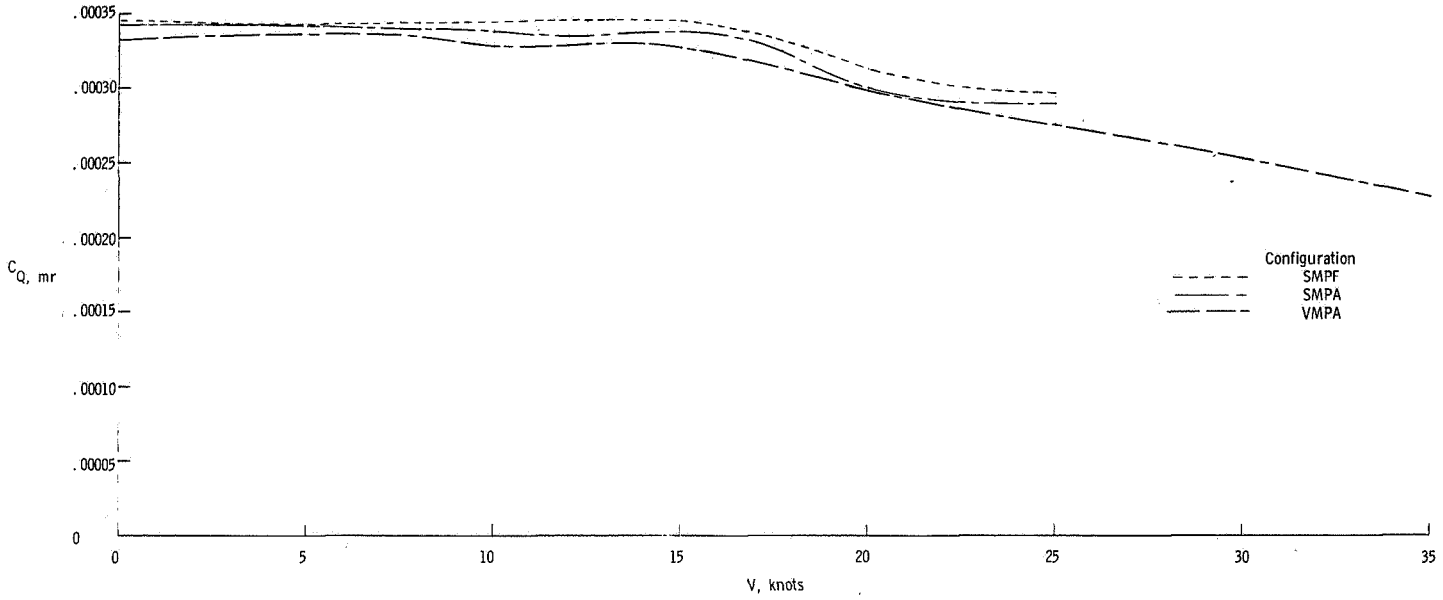

(a) Main-rotor torque.

Figure 12.- Variation of main-rotor, fin, and tail-rotor parameters with windspeed at $\beta = 60^{o}$.

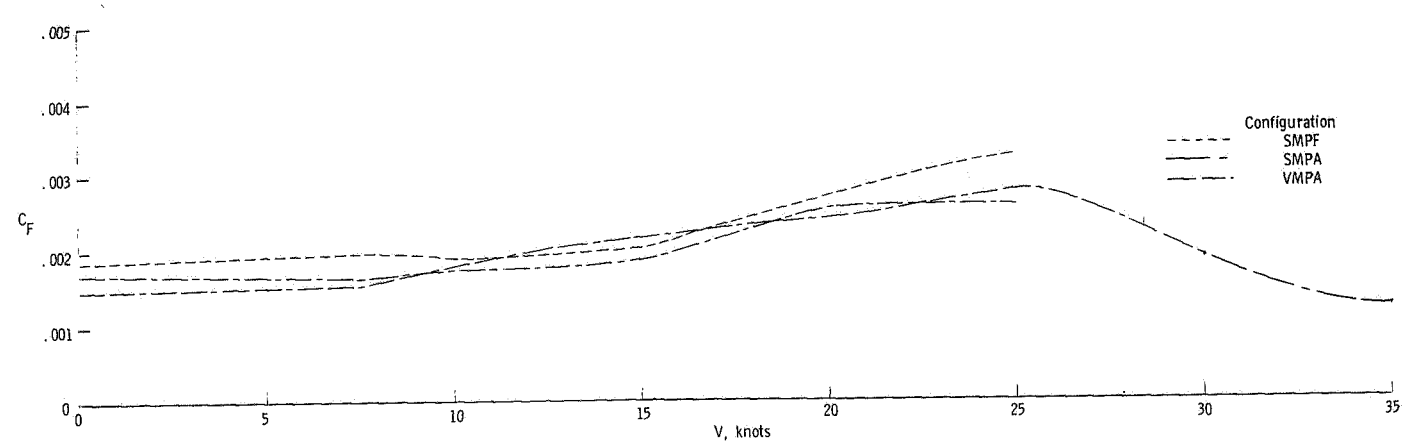

(b) Fin force.

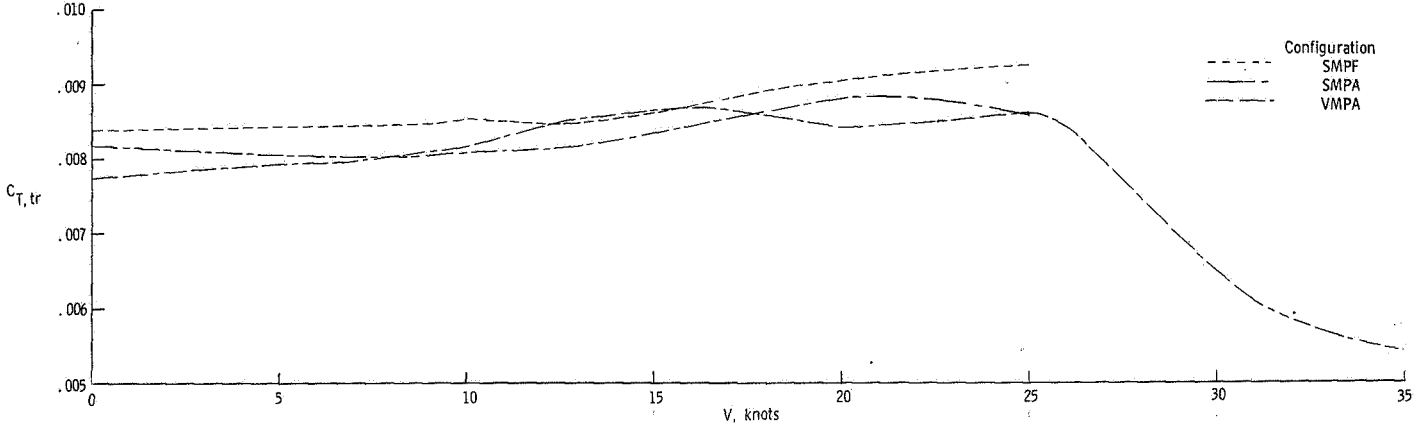

(c) Tail-rotor thrust.

Figure 12.- Continued.

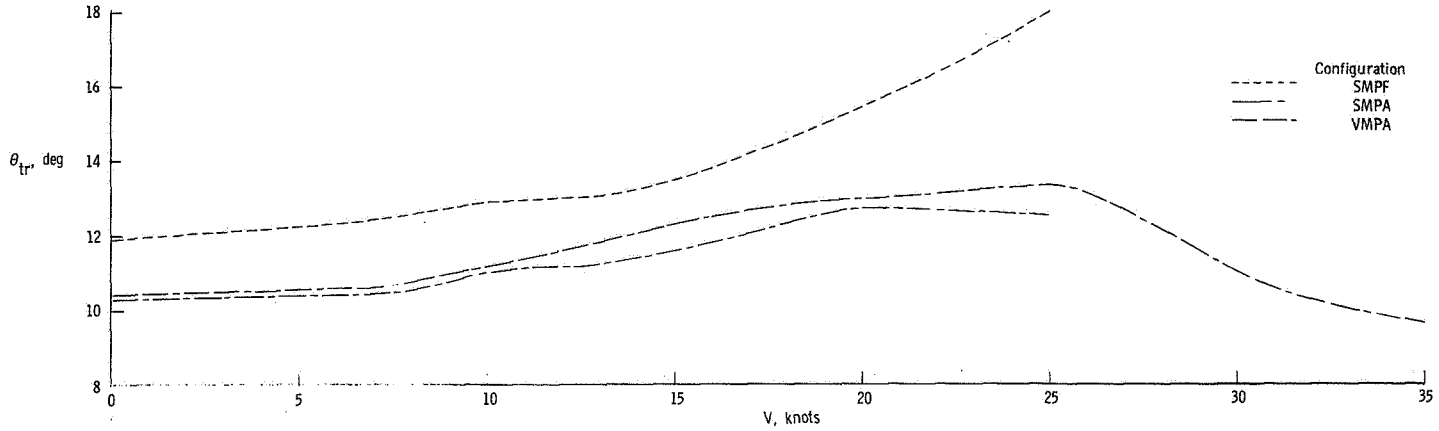

(d) Tail-rotor collective pitch.

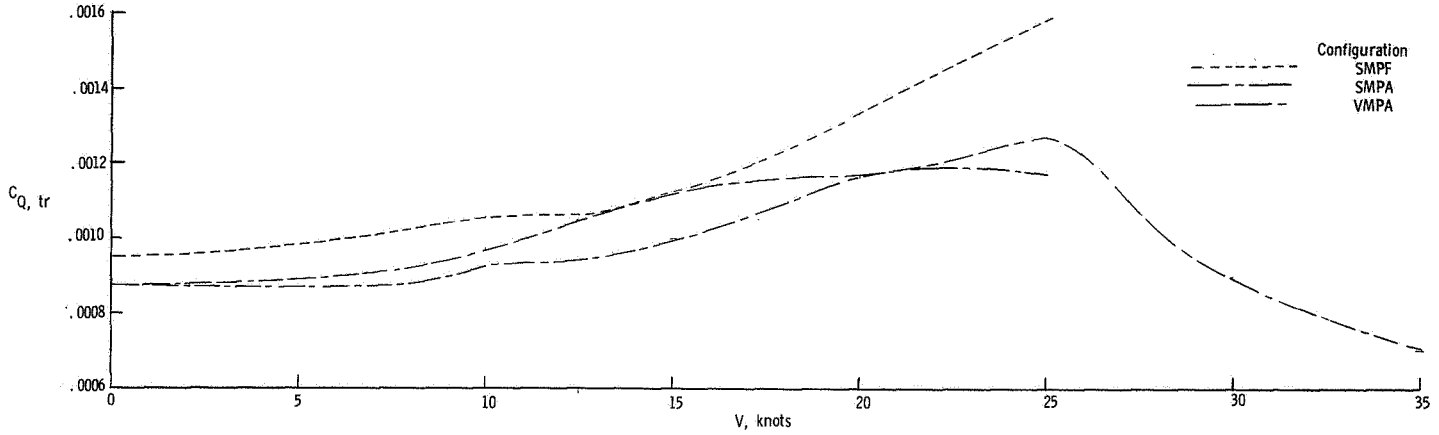

(e) Tail-rotor torque.

Figure 12.- Concluded.

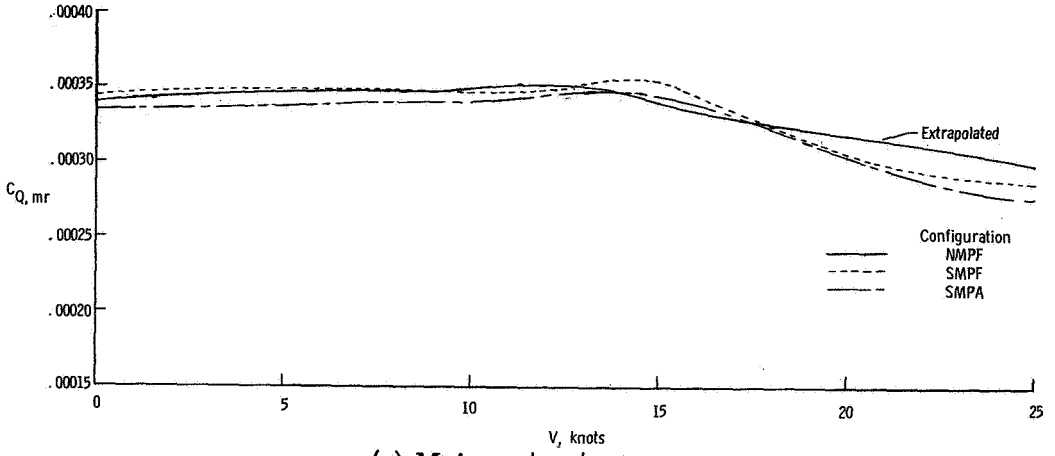

(a) Main-rotor torque.

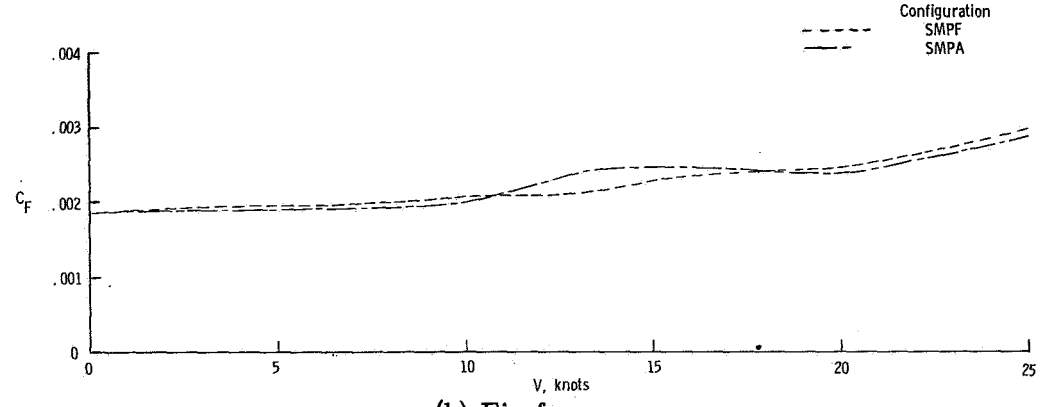

(b) Fin force.

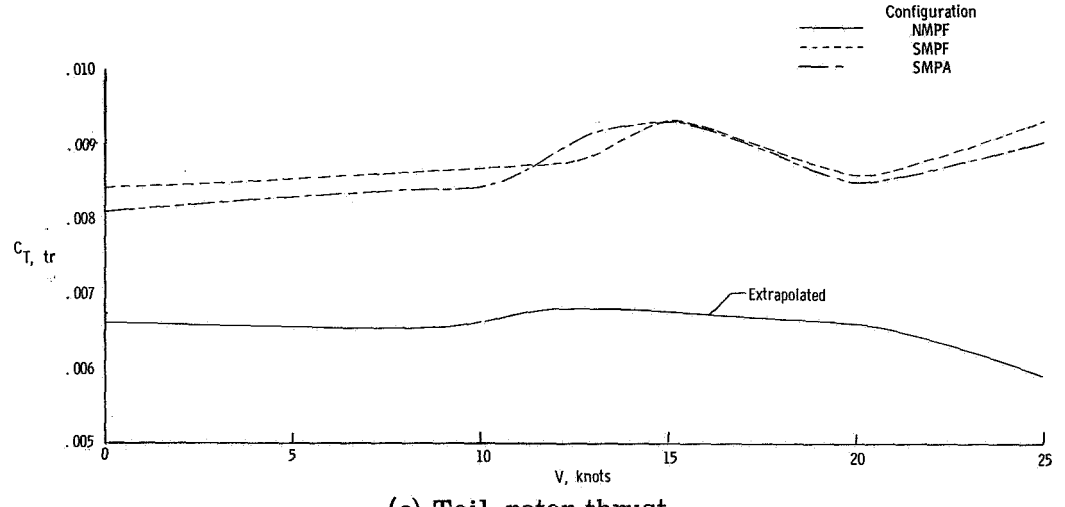

(c) Tail-rotor thrust.

Figure 13.- Variation of main-rotor, fin, and tail-rotor parameters with windspeed at $\beta = 90^{o}$.

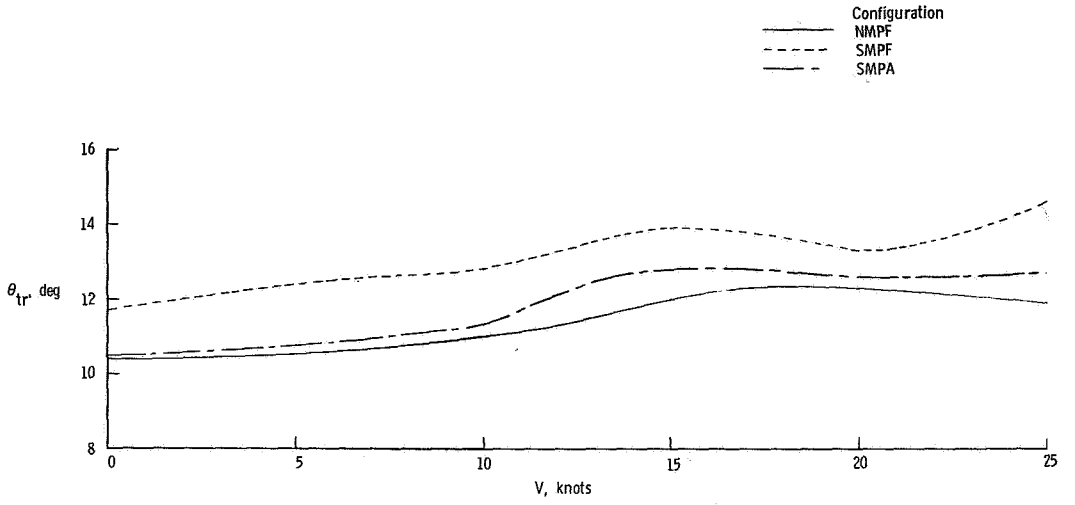

(d) Tail-rotor collective pitch.

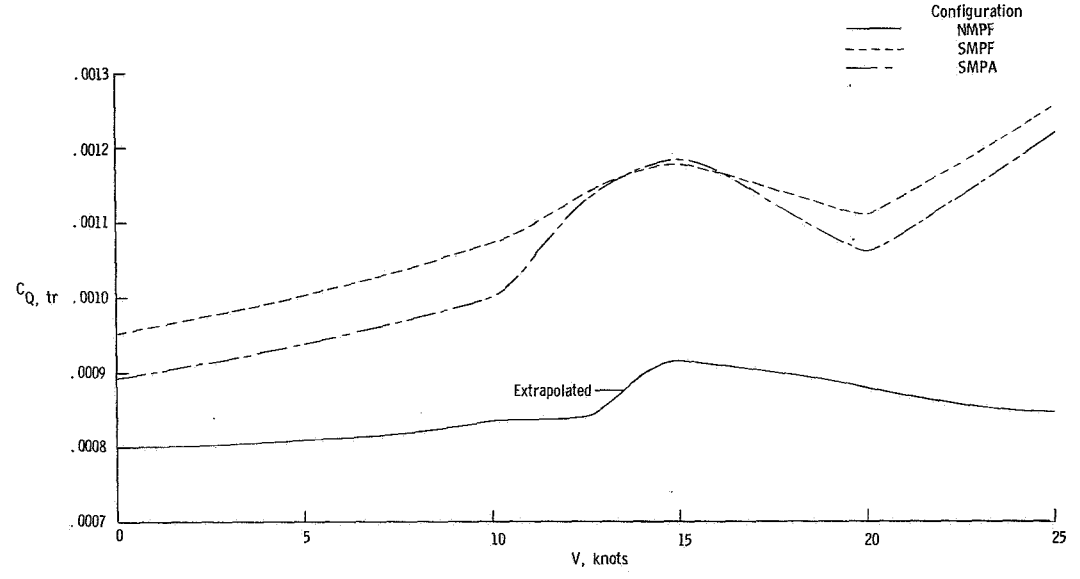

(e) Tail-rotor torque.

Figure 13.- Concluded.

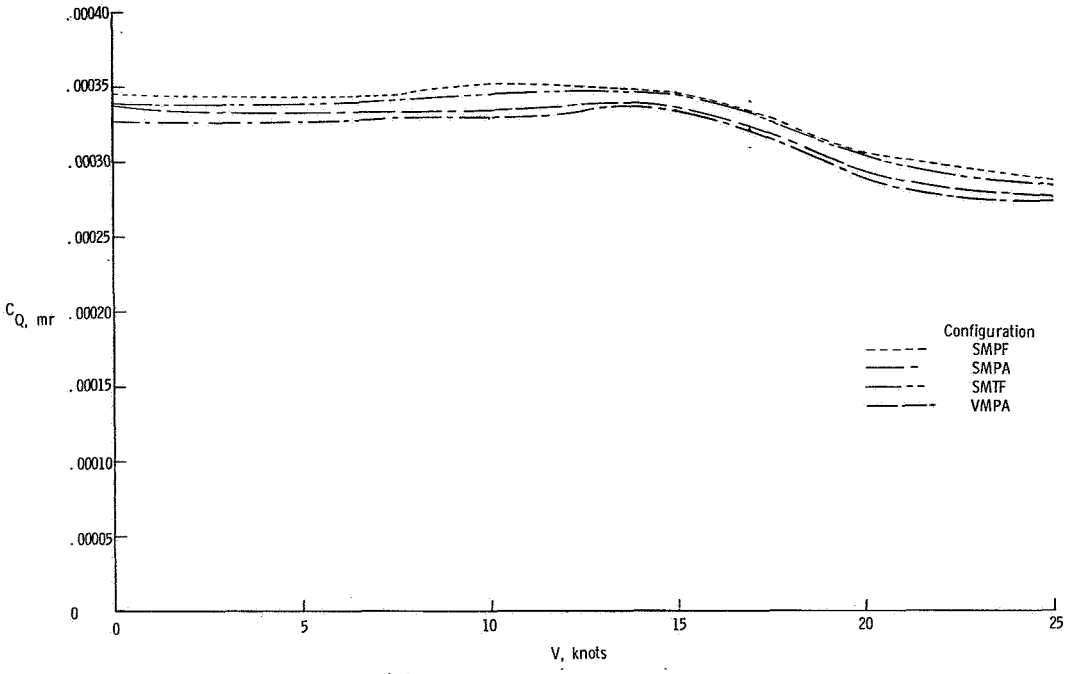

(a) Main-rotor torque.

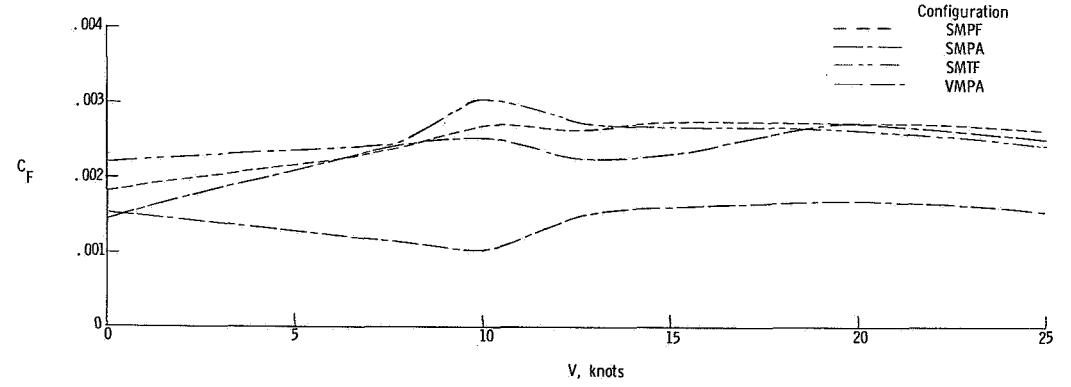

(b) Fin force.

Figure 14.- Variation of main-rotor, fin, and tail-rotor parameters with windspeed at $\beta = 120^{o}$.

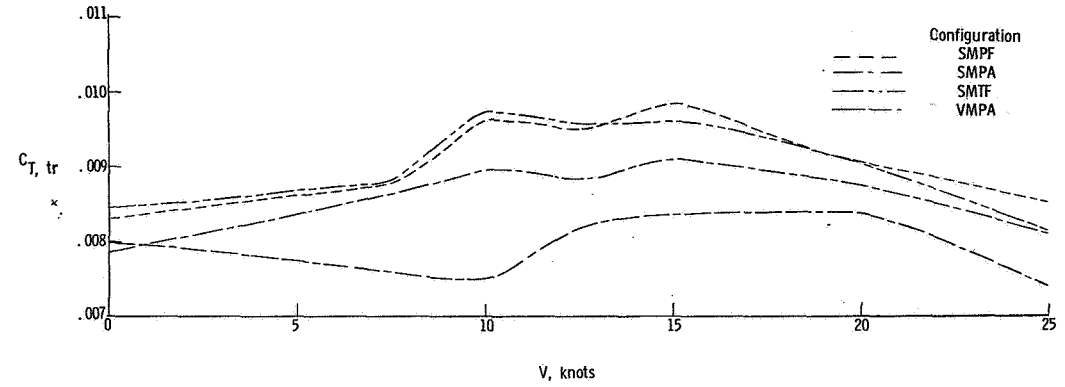

(c) Tail-rotor thrust.

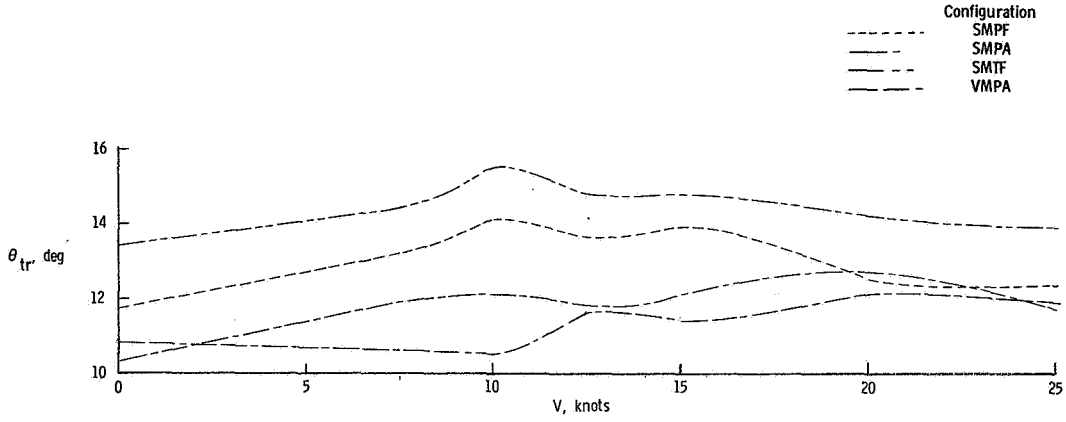

(d) Tail-rotor collective pitch.

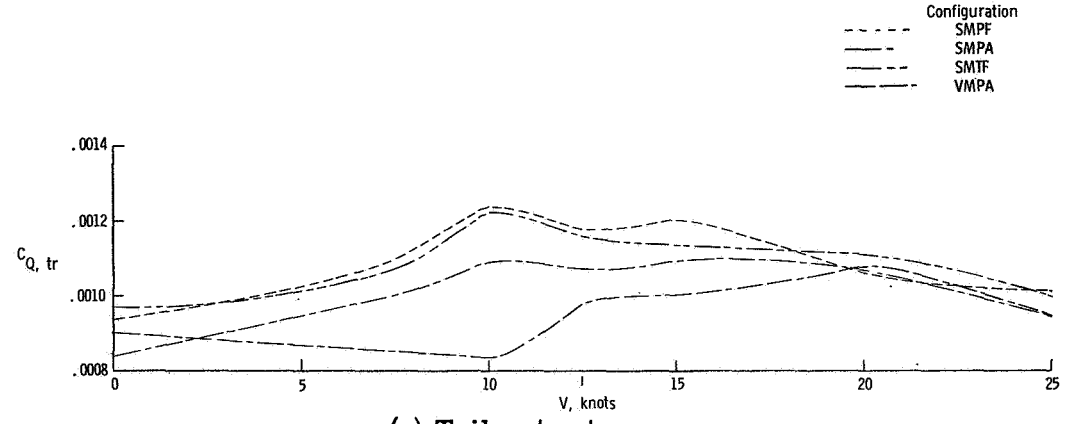

(e) Tail-rotor torque.

Figure 14.- Concluded.

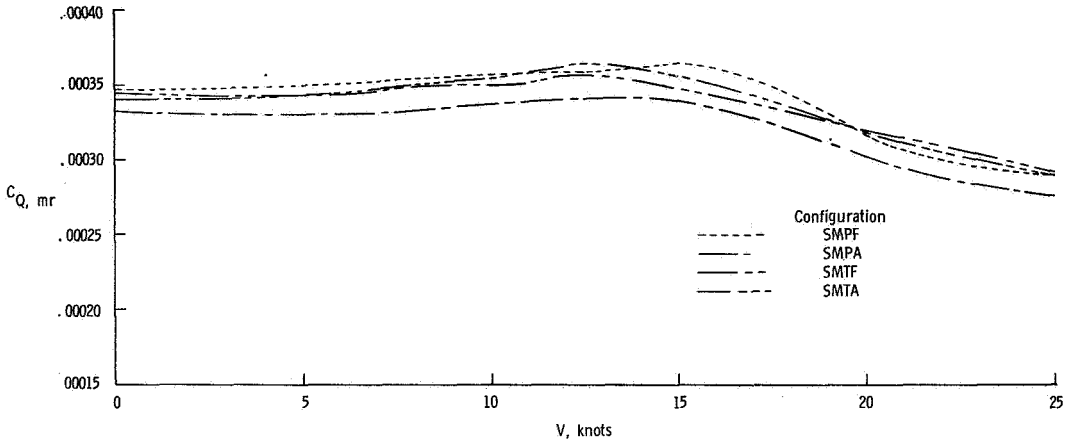

(a) Main-rotor torque.

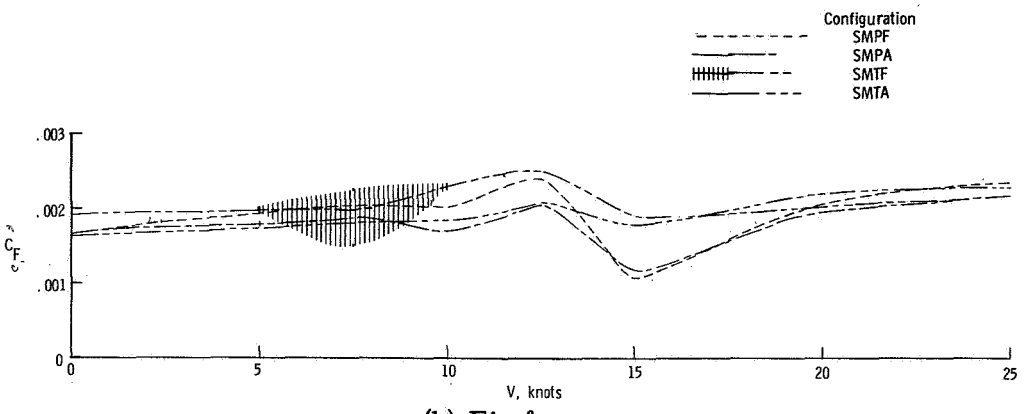

(b) Fin force.

Figure 15.- Variation of main-rotor, fin, and tail-rotor parameters with windspeed at $\beta = 150^{o}$.

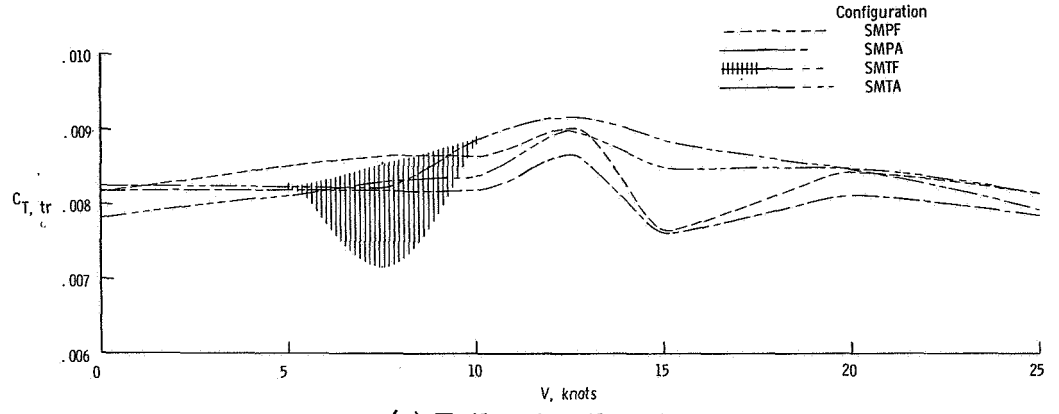

(c) Tail-rotor thrust.

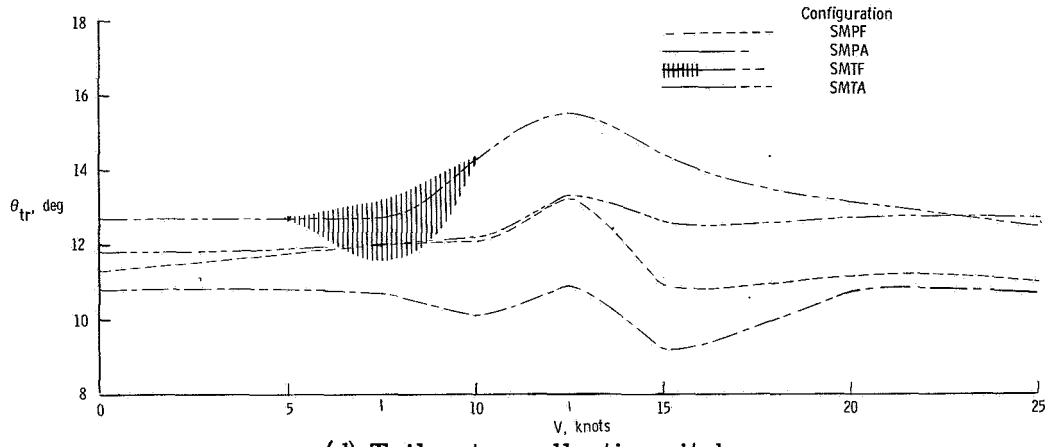

(d) Tail-rotor collective pitch.

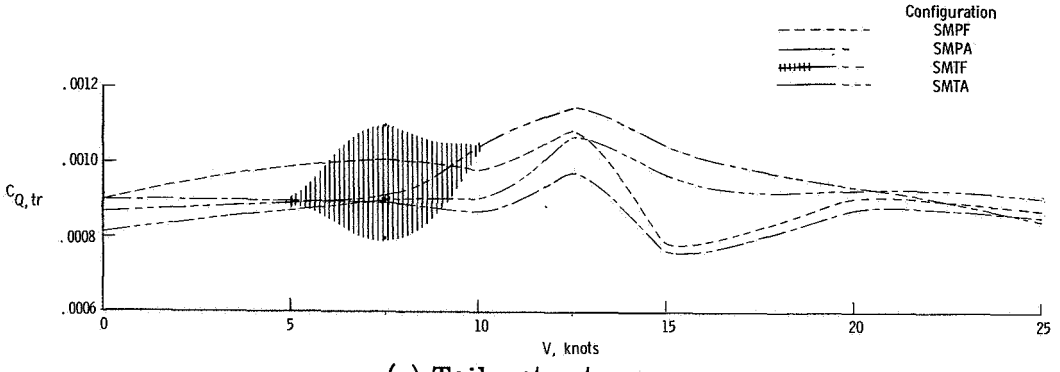

(e) Tail-rotor torque.

Figure 15.- Concluded.

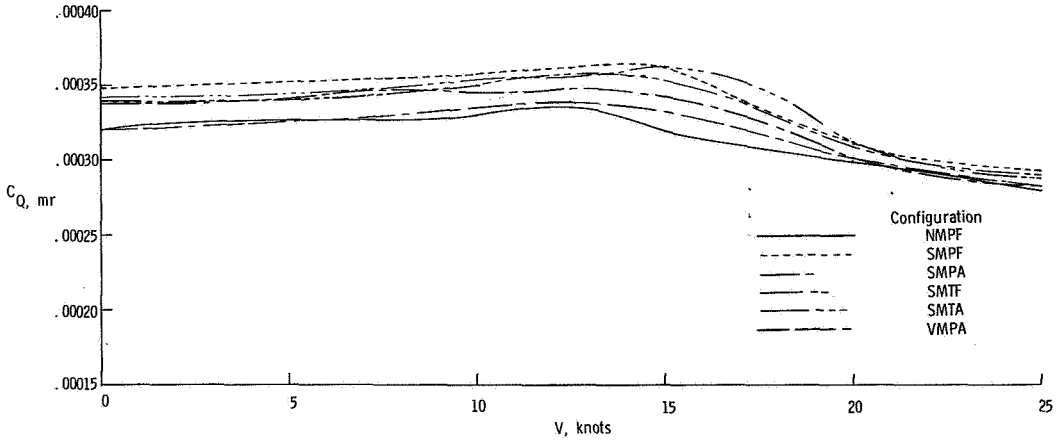

(a) Main-rotor torque.

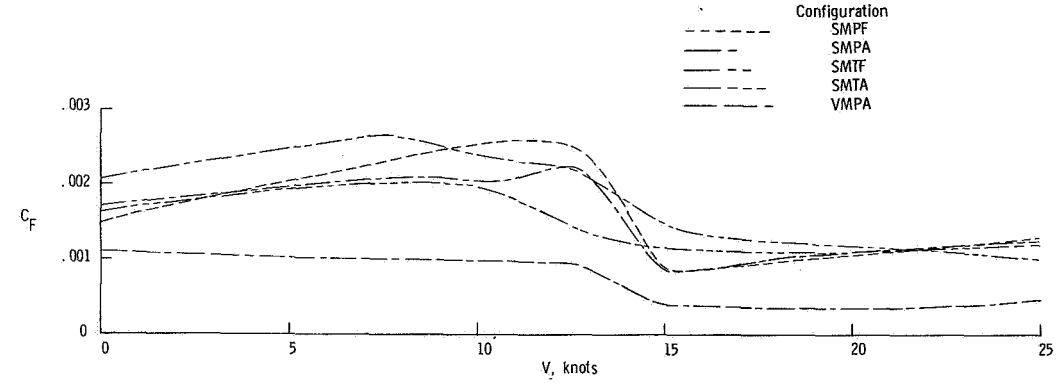

(b) Fin force.

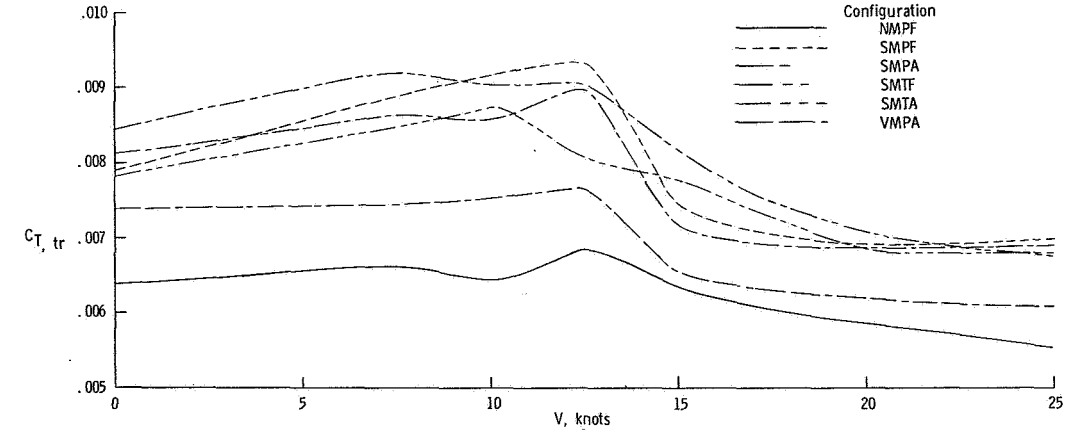

(c) Tail-rotor thrust.

Figure 16.- Variation of main-rotor, fin, and tail-rotor parameters with windspeed at $\beta = 180^{o}$.

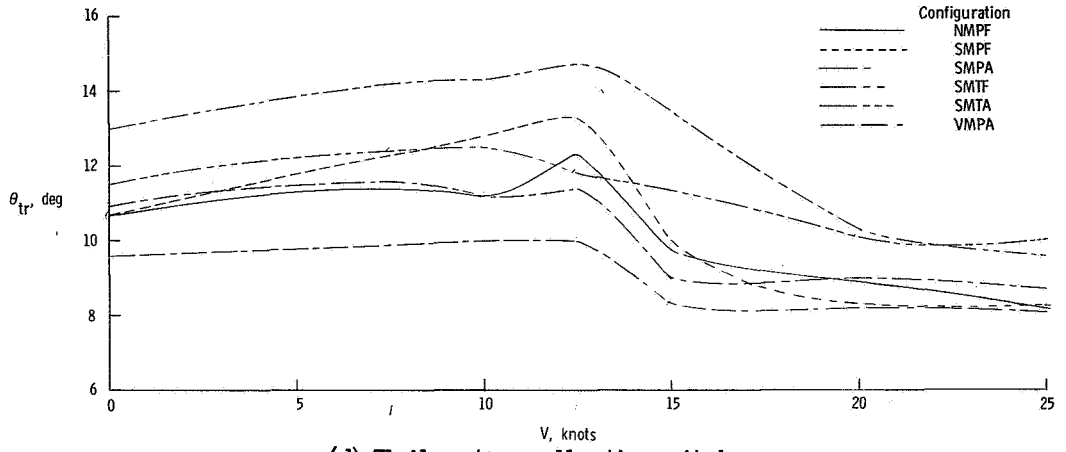

(d) Tail-rotor collective pitch.

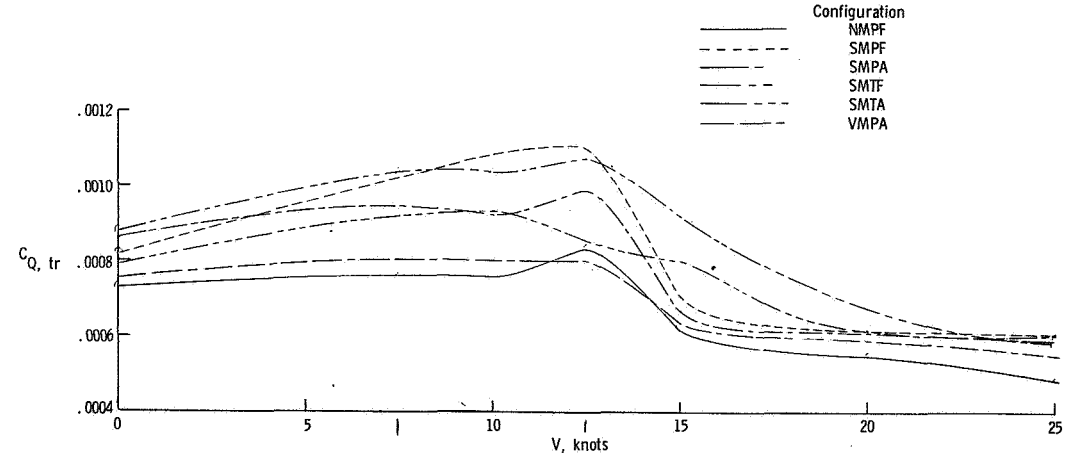

(e) Tail-rotor torque.

Figure 16.- Concluded.

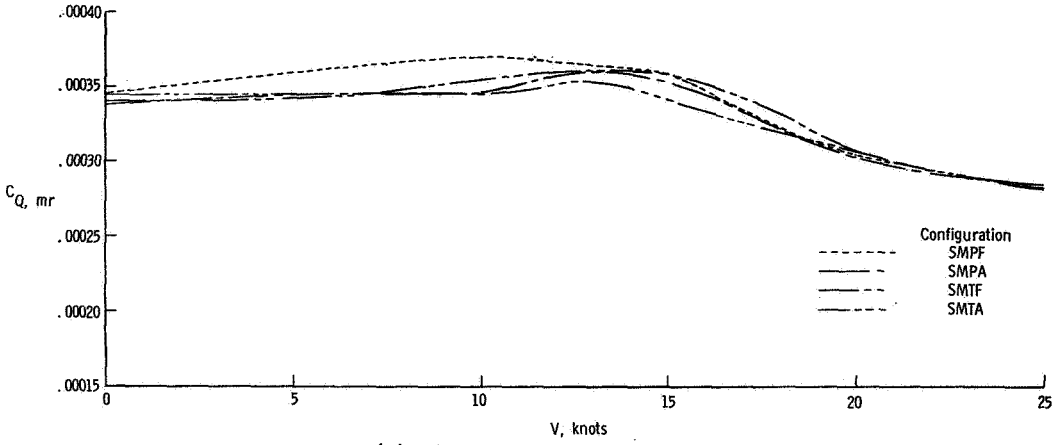

(a) Main-rotor torque.

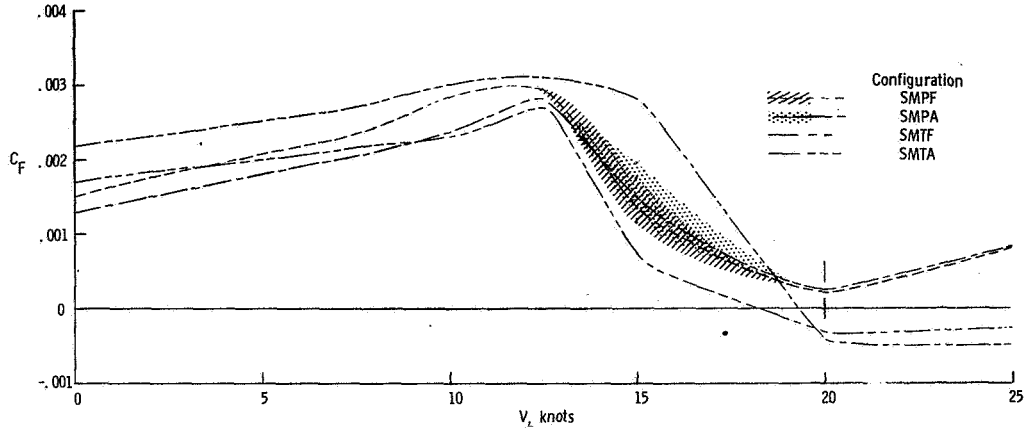

(b) Fin force.

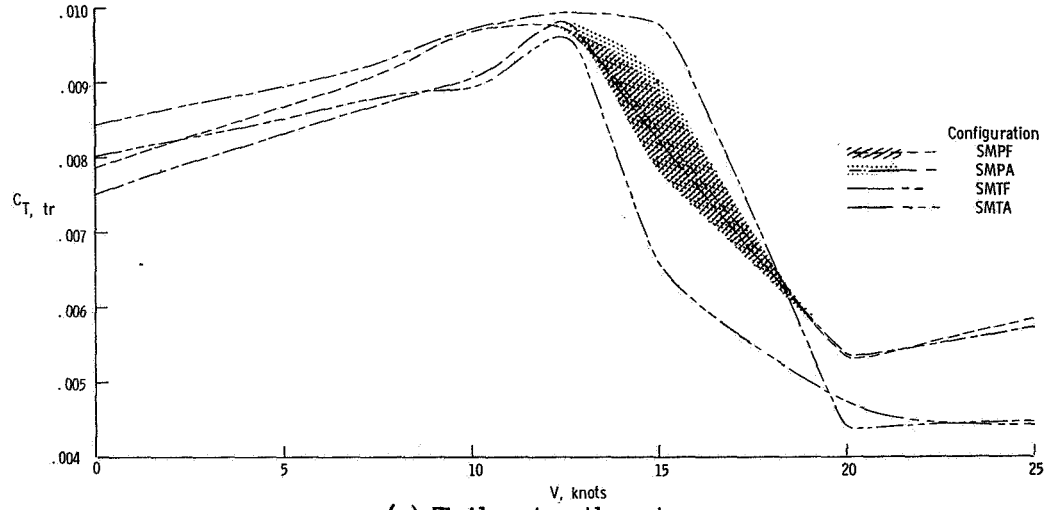

(c) Tail-rotor thrust.

Figure 17.- Variation of main-rotor, fin, and tail-rotor parameters with windspeed at $\beta = 210^{o}$.

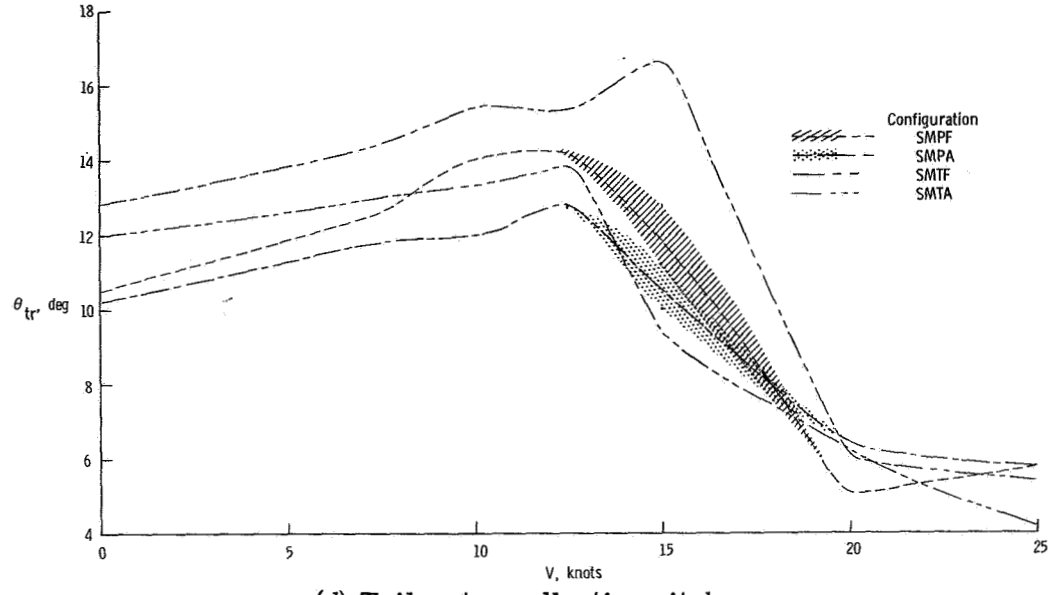

(d) Tail-rotor collective pitch.

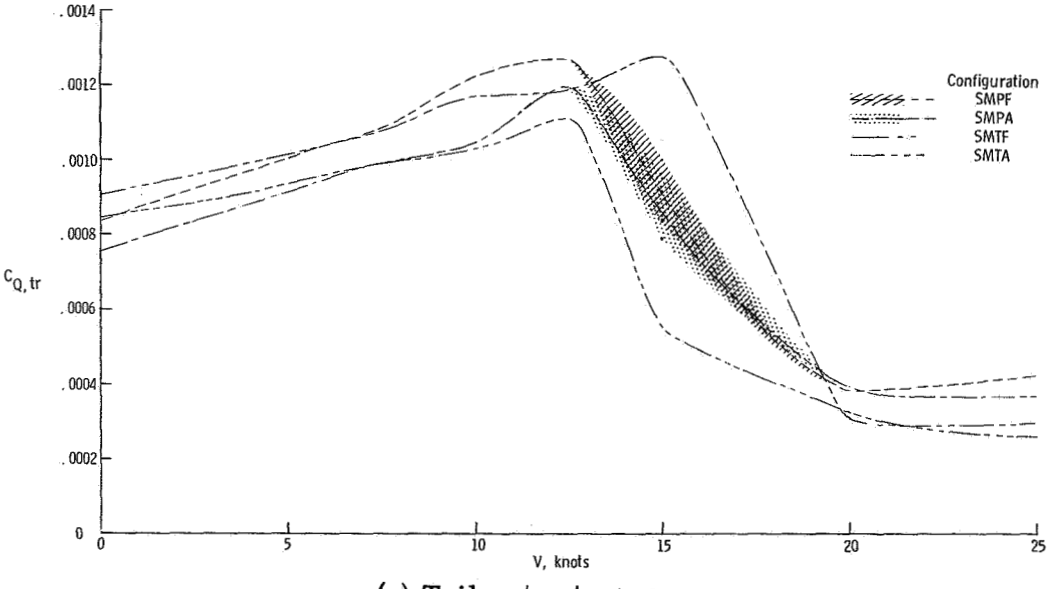

(e) Tail-rotor torque.

Figure 17.- Concluded.

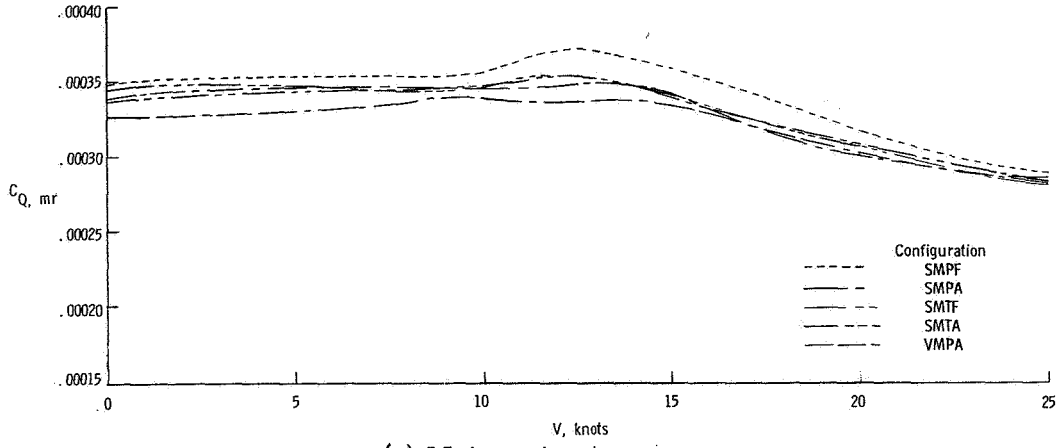

(a) Main-rotor torque.

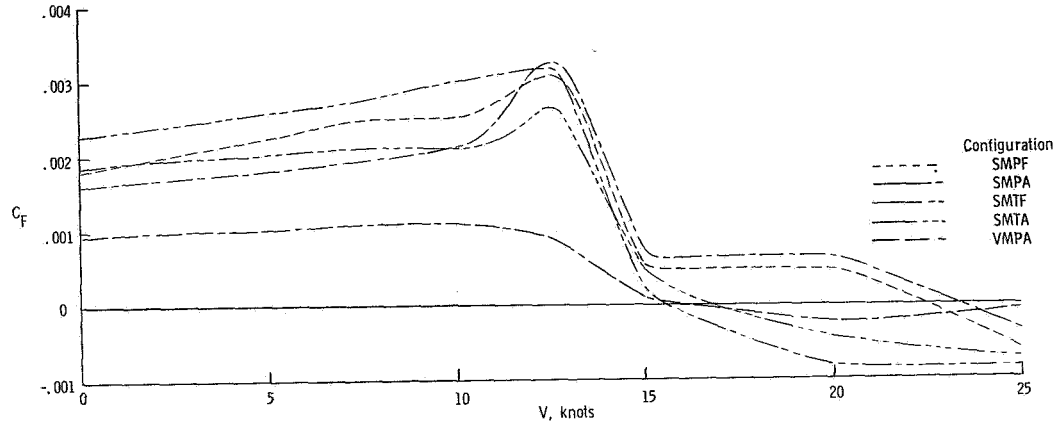

(b) Fin force.

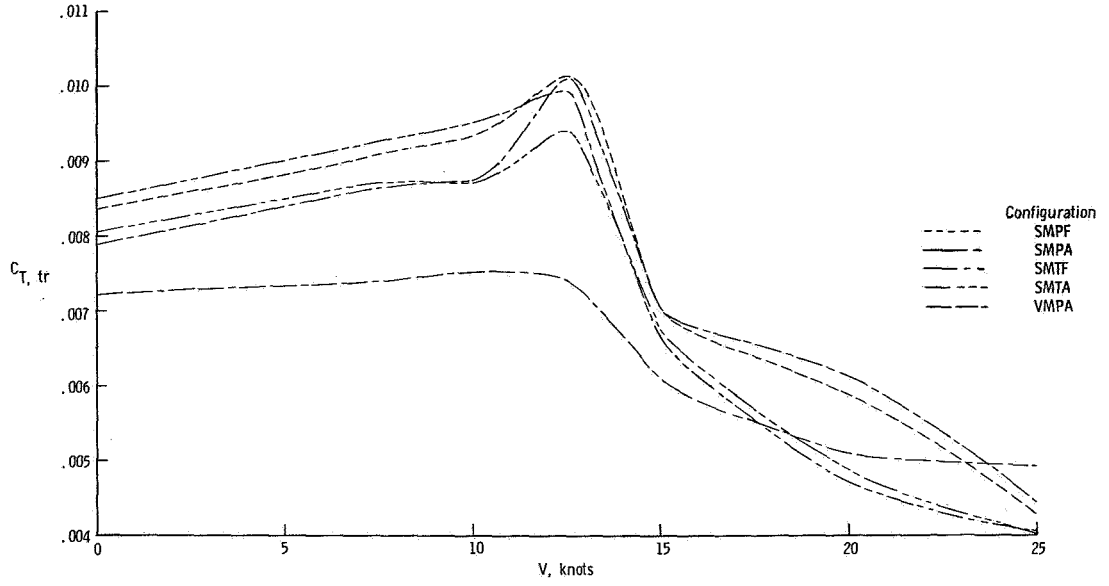

(c) Tail-rotor thrust.

Figure 18.- Variation of main-rotor, fin, and tail-rotor parameters with windspeed at $\beta = 240^{o}$.

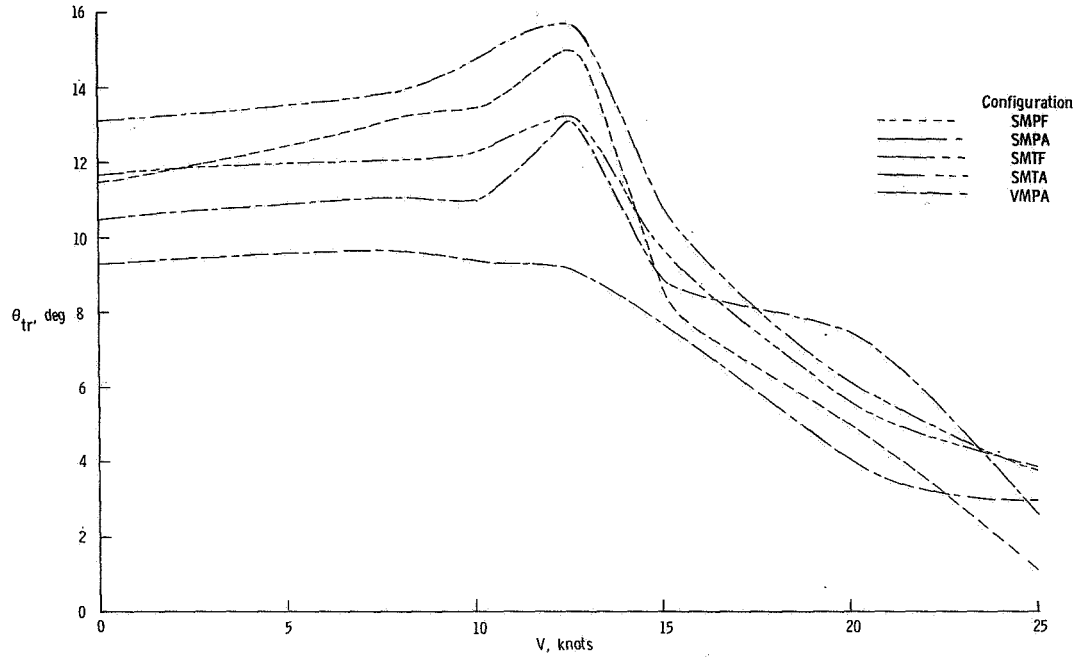

(d) Tail-rotor collective pitch.

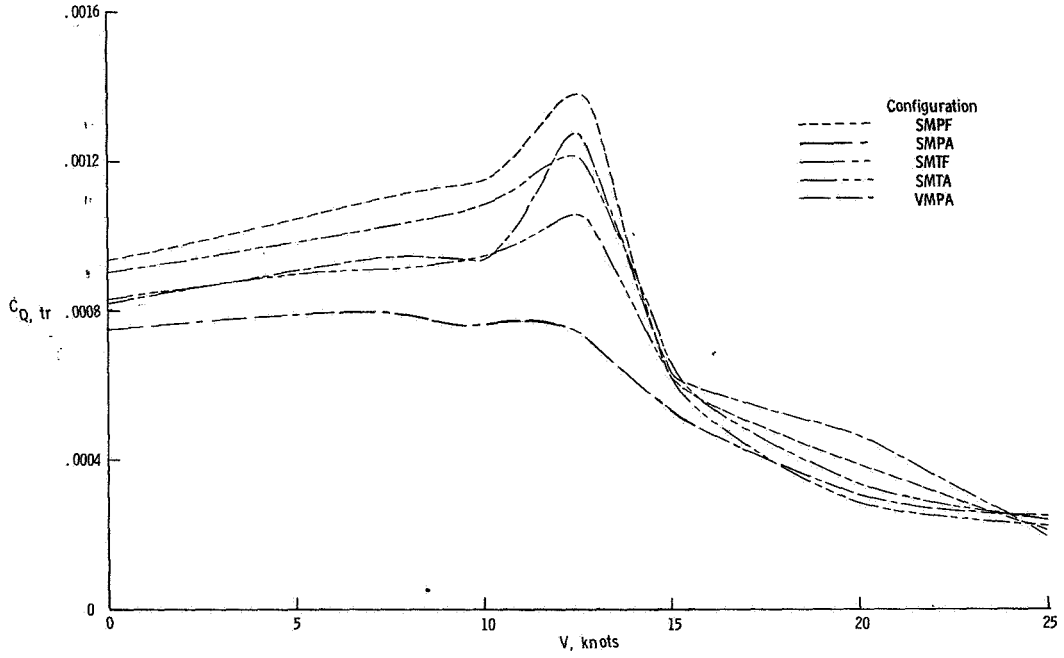

(e) Tail-rotor torque.

Figure 18.- Concluded.

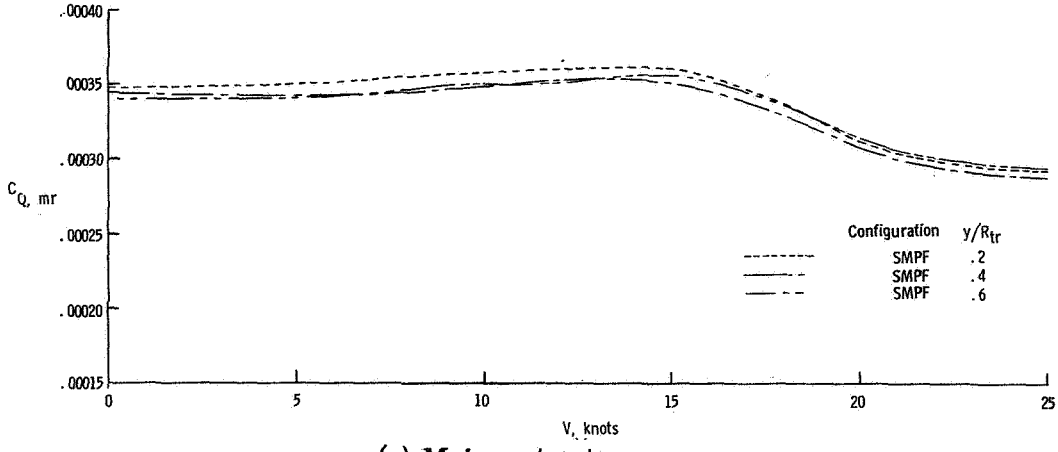

(a) Main-rotor torque.

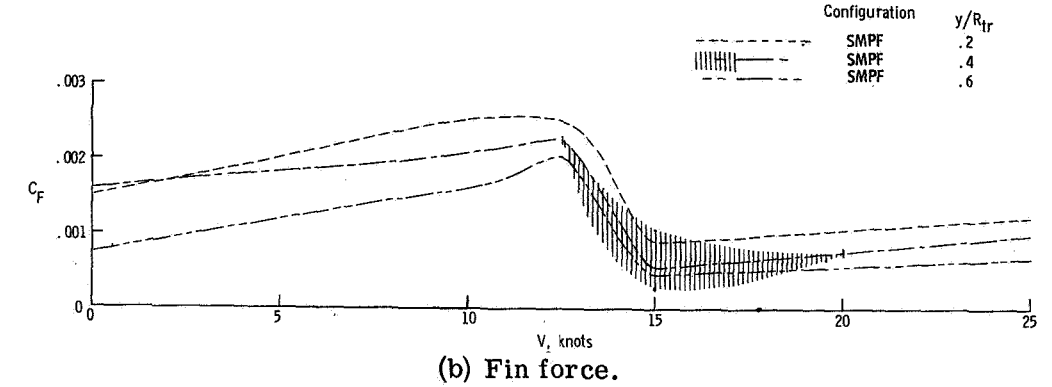

(b) Fin force.

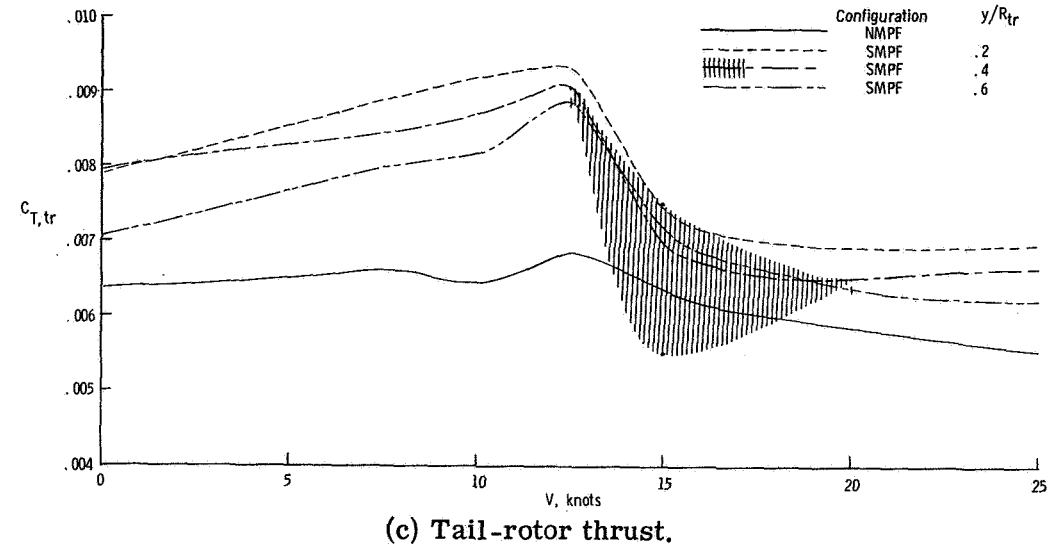

(c) Tail-rotor thrust.

Figure 19.- Effect of fin/tail-rotor gap on main-rotor, fin, and tail-rotor parameters at $\beta = 180^{o}$.

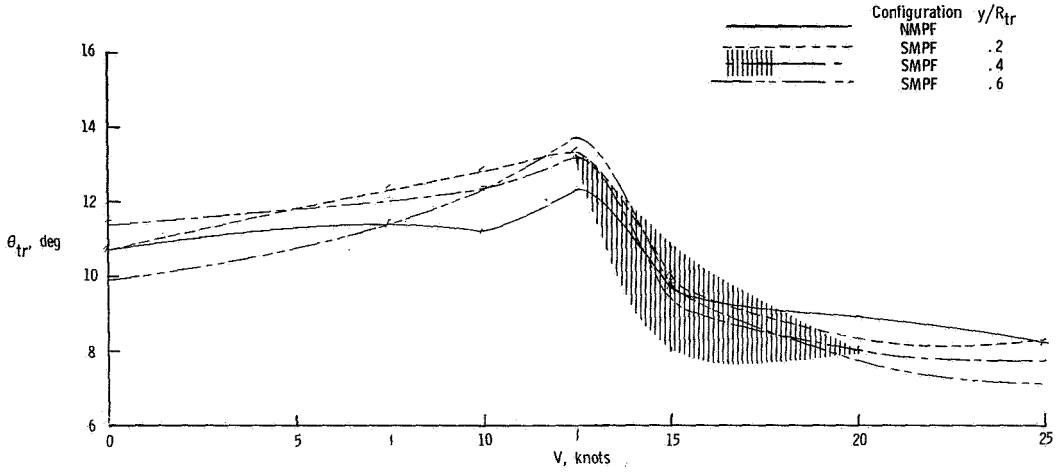

(d) Tail-rotor collective pitch.

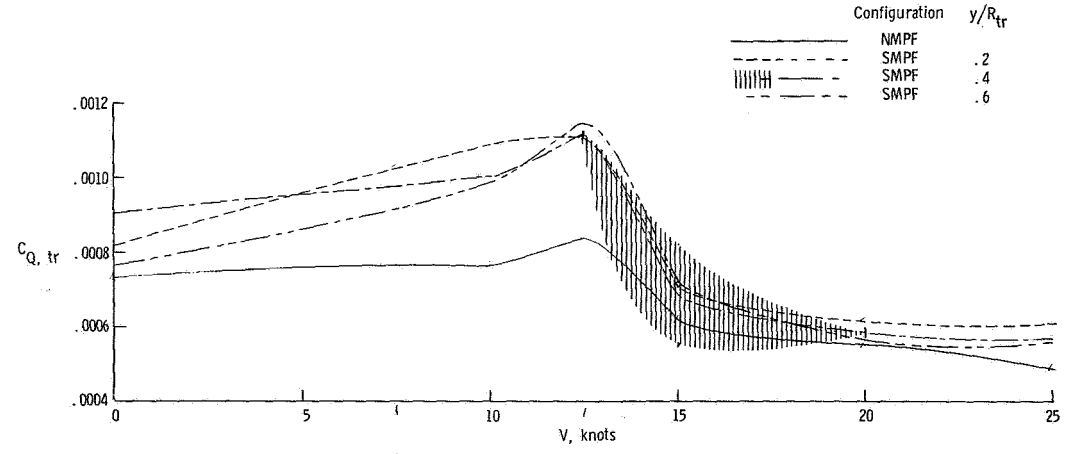

(e) Tail-rotor torque.

Figure 19.- Concluded.

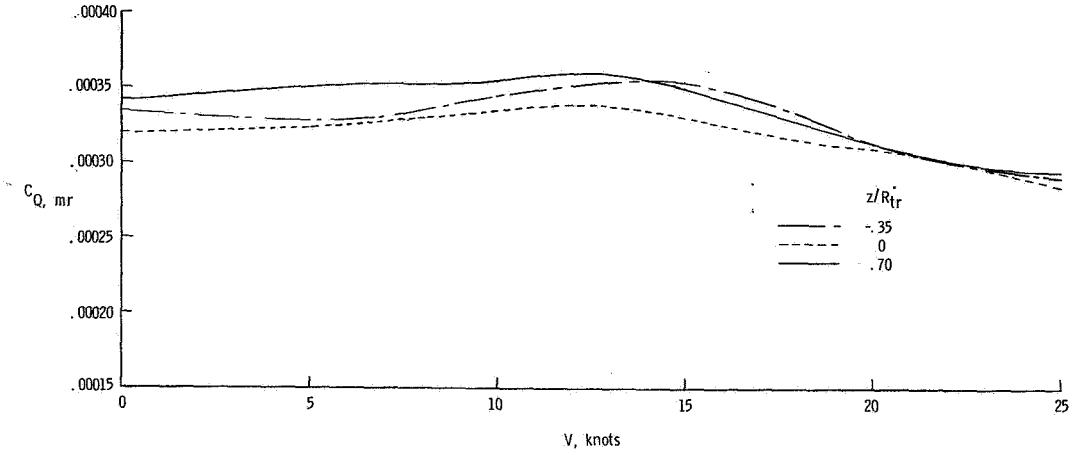

(a) Main-rotor torque.

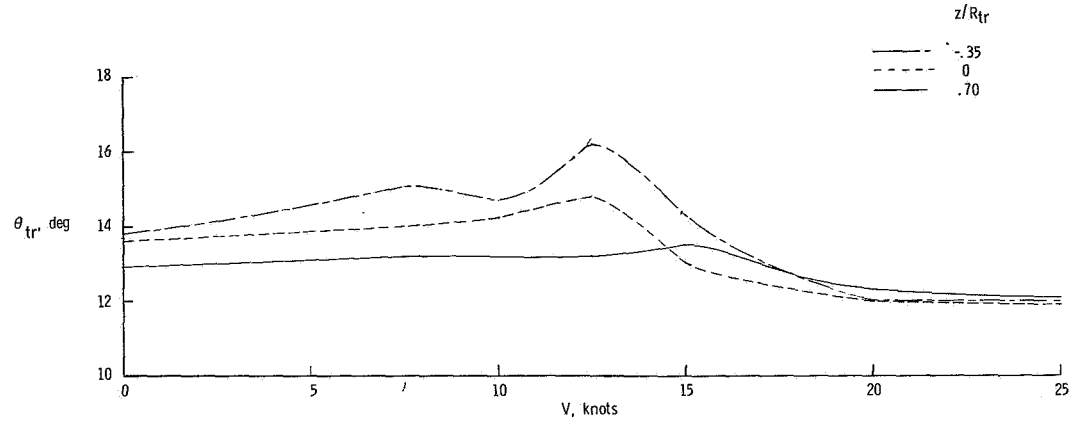

(b) Tail-rotor collective pitch.

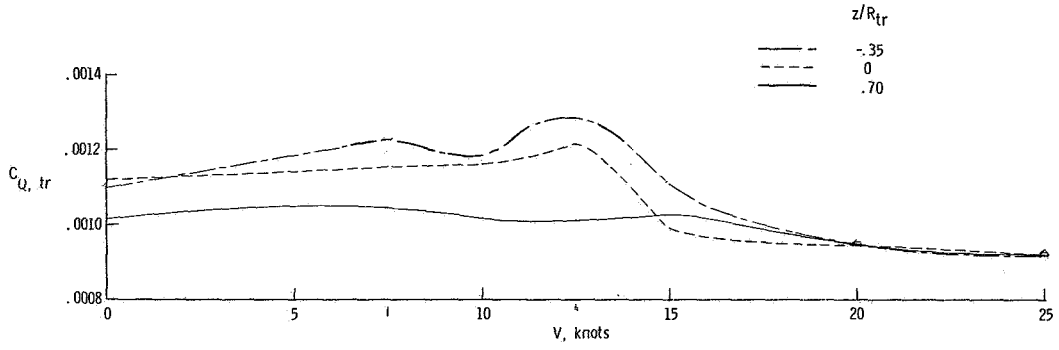

(c) Tail-rotor torque.

Figure 20.- Effect of tail-rotor height on main-rotor and tail-rotor parameters of configuration NMPF at $\beta = 180^{o}$. $C_{T,tr} = 0.009$.

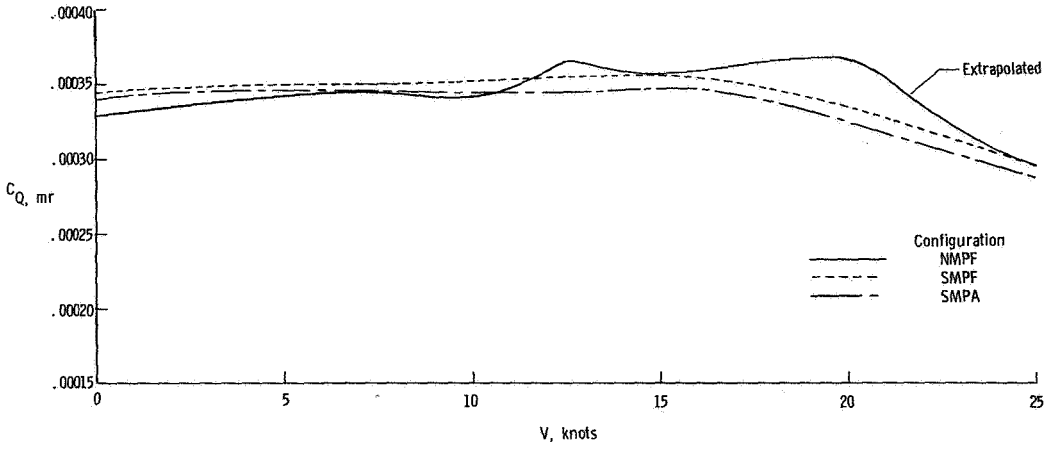

(a) Main-rotor torque.

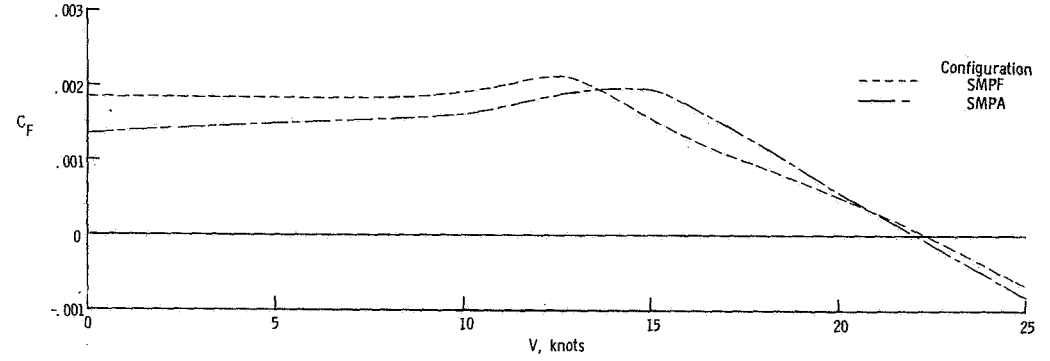

(b) Fin force.

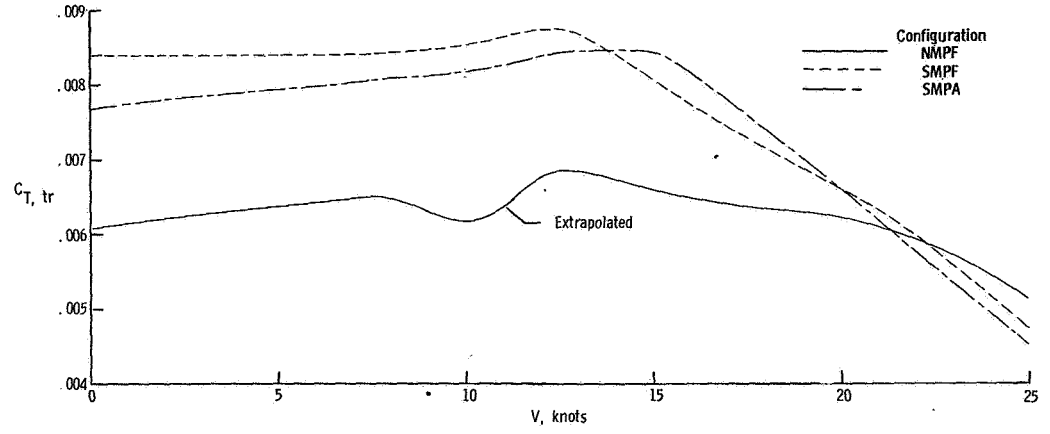

(c) Tail-rotor thrust.

Figure 21.- Variation of main-rotor, fin, and tail-rotor parameters with windspeed at $\beta = 270^{o}$.

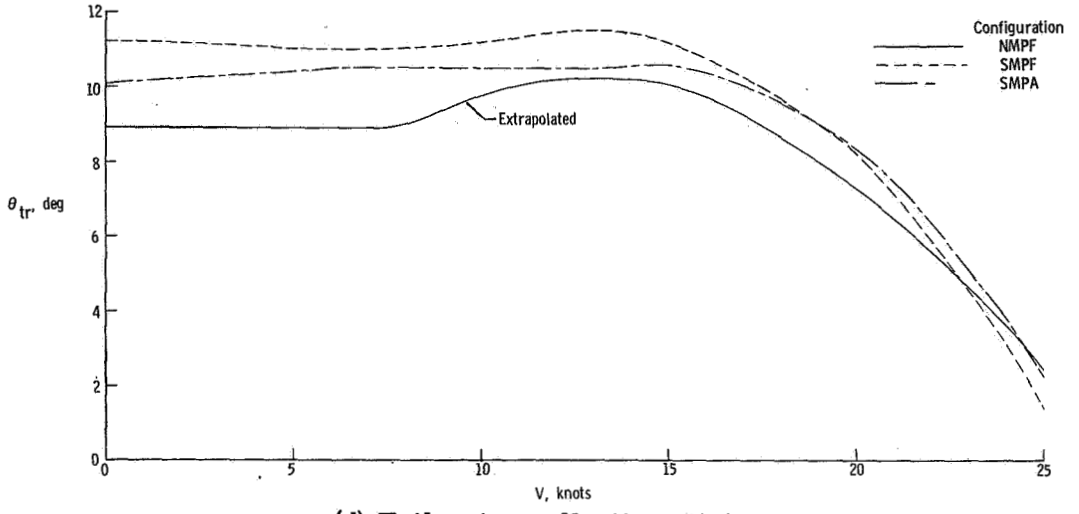

(d) Tail-rotor collective pitch.

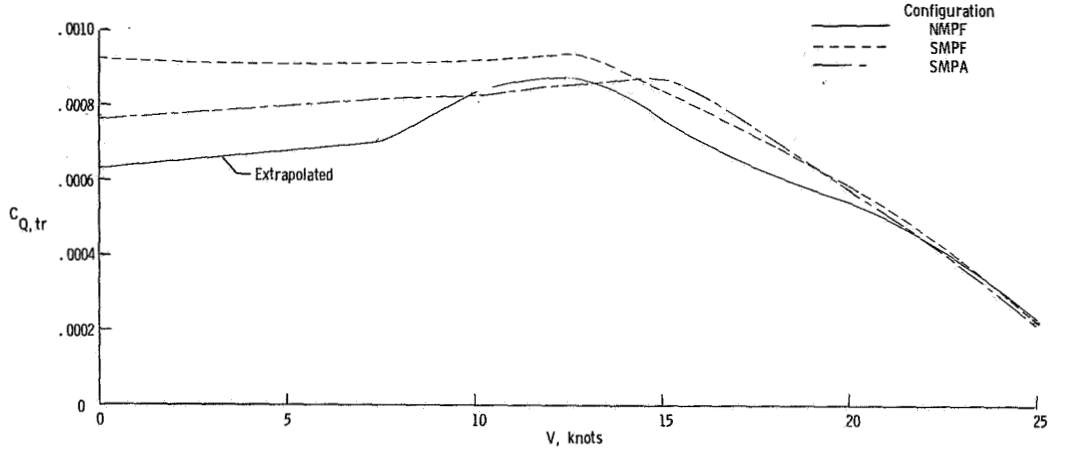

(e) Tail-rotor torque.

Figure 21.- Concluded.

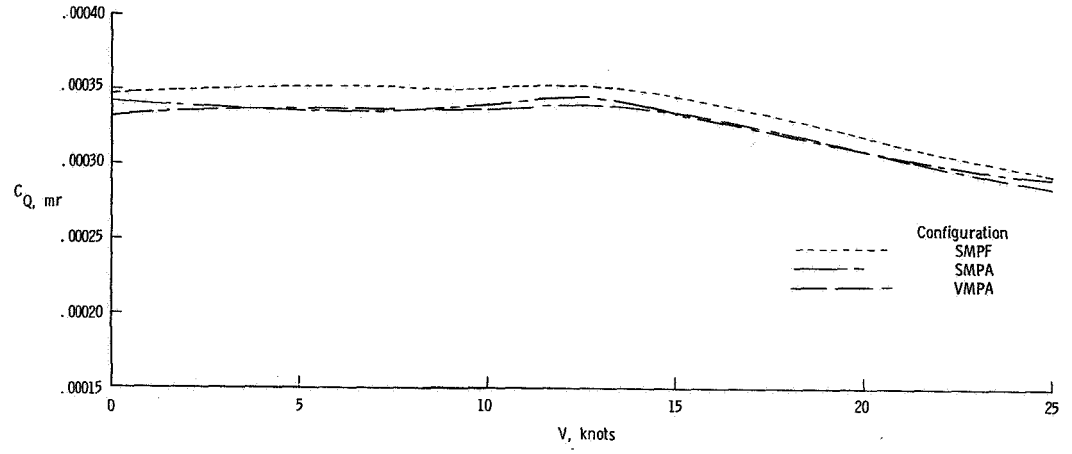

(a) Main-rotor torque.

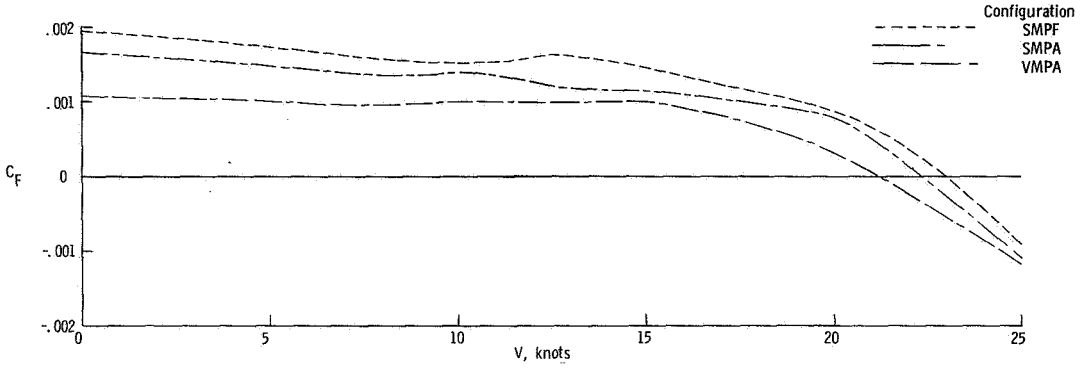

(b) Fin force.

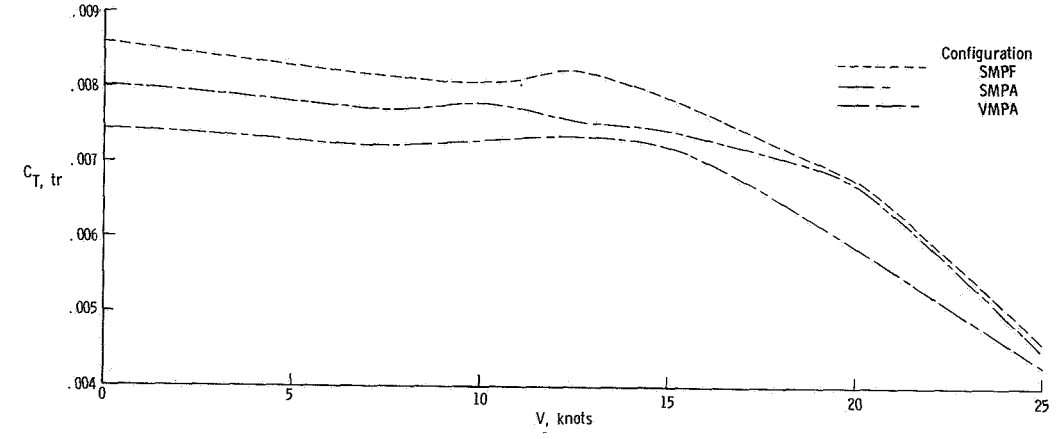

(c) Tail-rotor thrust.

Figure 22.- Variation of main-rotor, fin, and tail-rotor parameters with windspeed at $\beta = 300^{o}$.

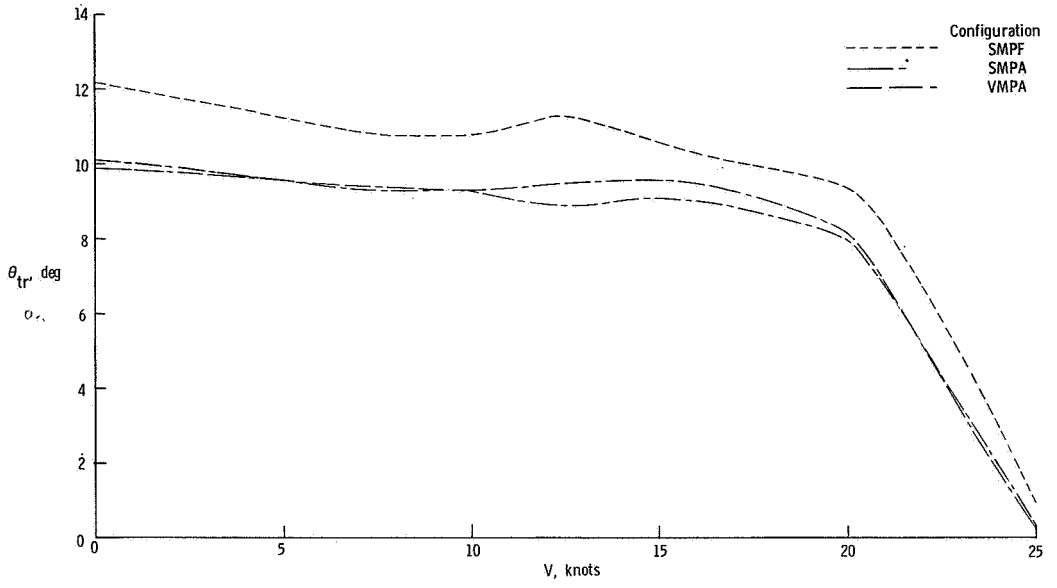

(d) Tail-rotor collective pitch.

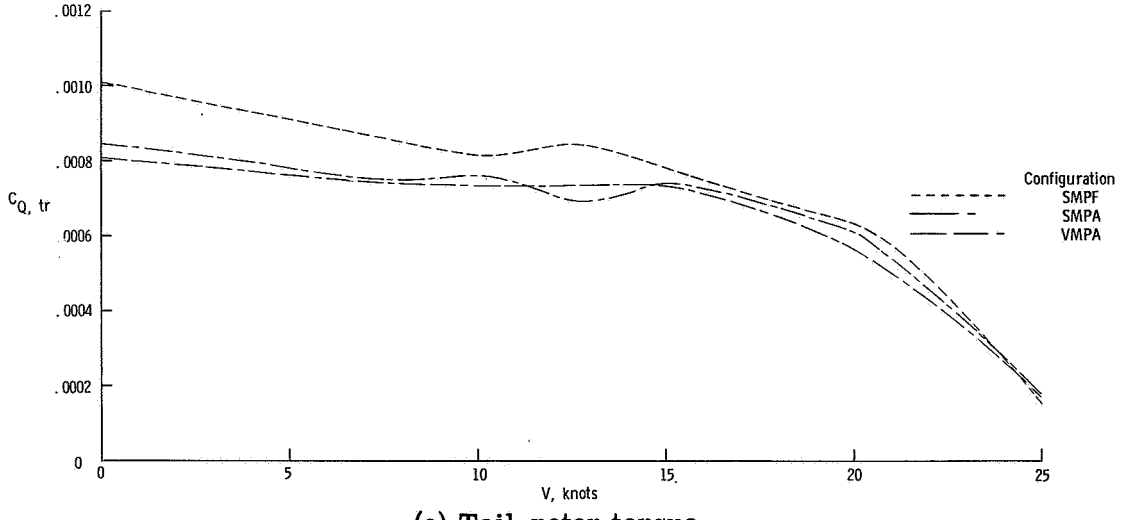

(e) Tail-rotor torque.

Figure 22.- Concluded.

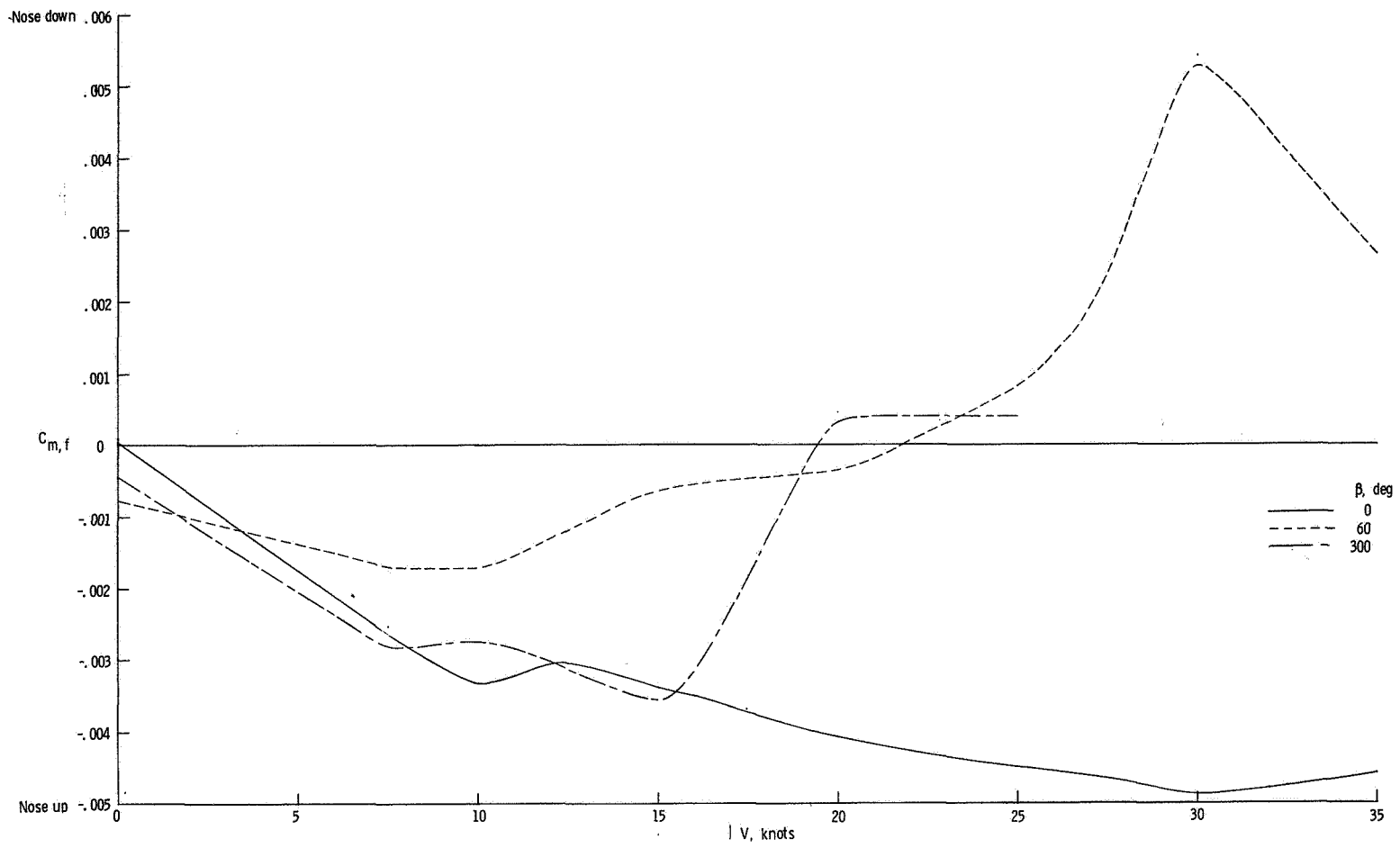

Figure 23.- Vehicle pitching-moment coefficient due to V-tail.

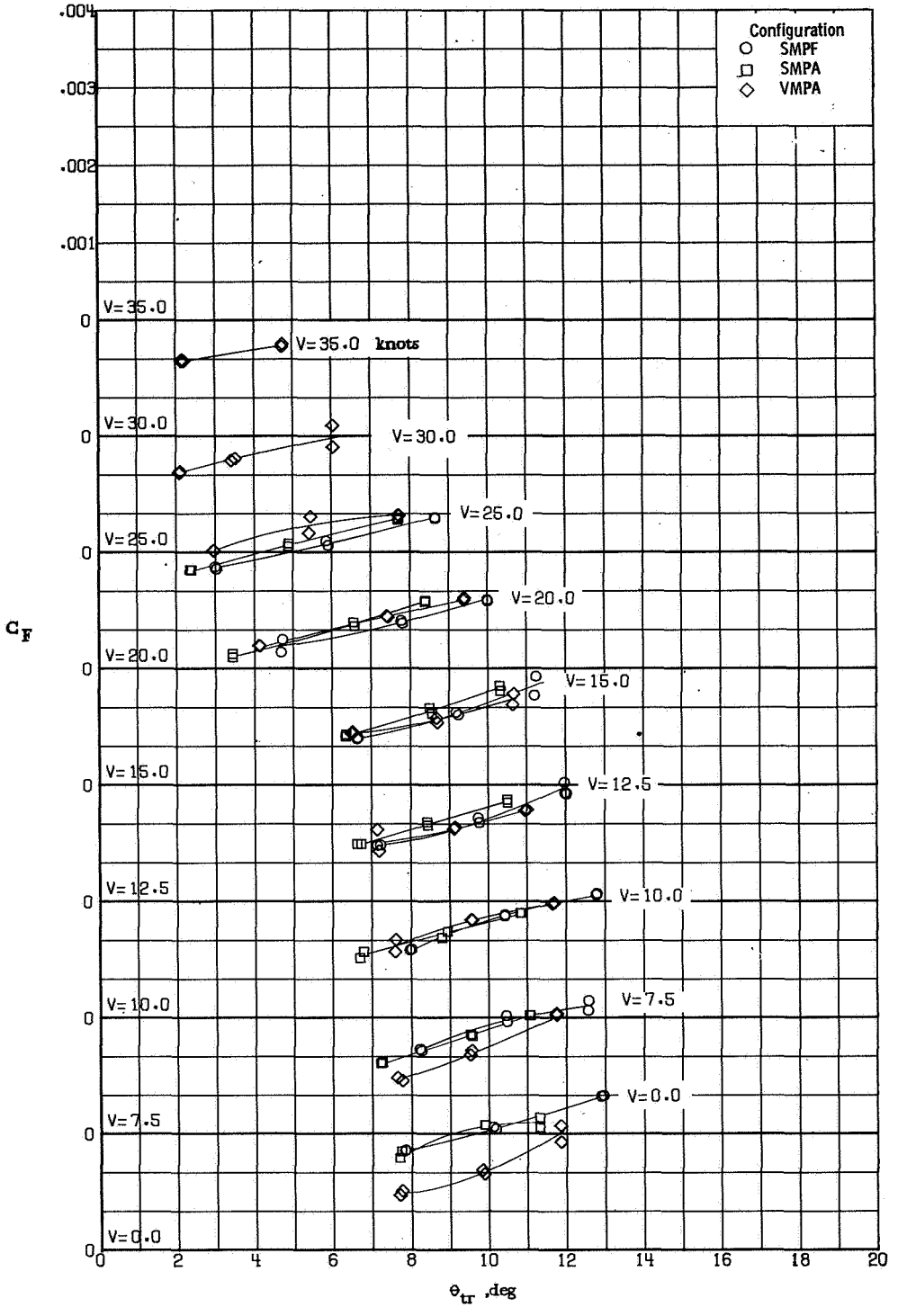

(a) Fin force.

Figure 24.- Aerodynamic characteristics of various configurations at $\beta = 0^o$.

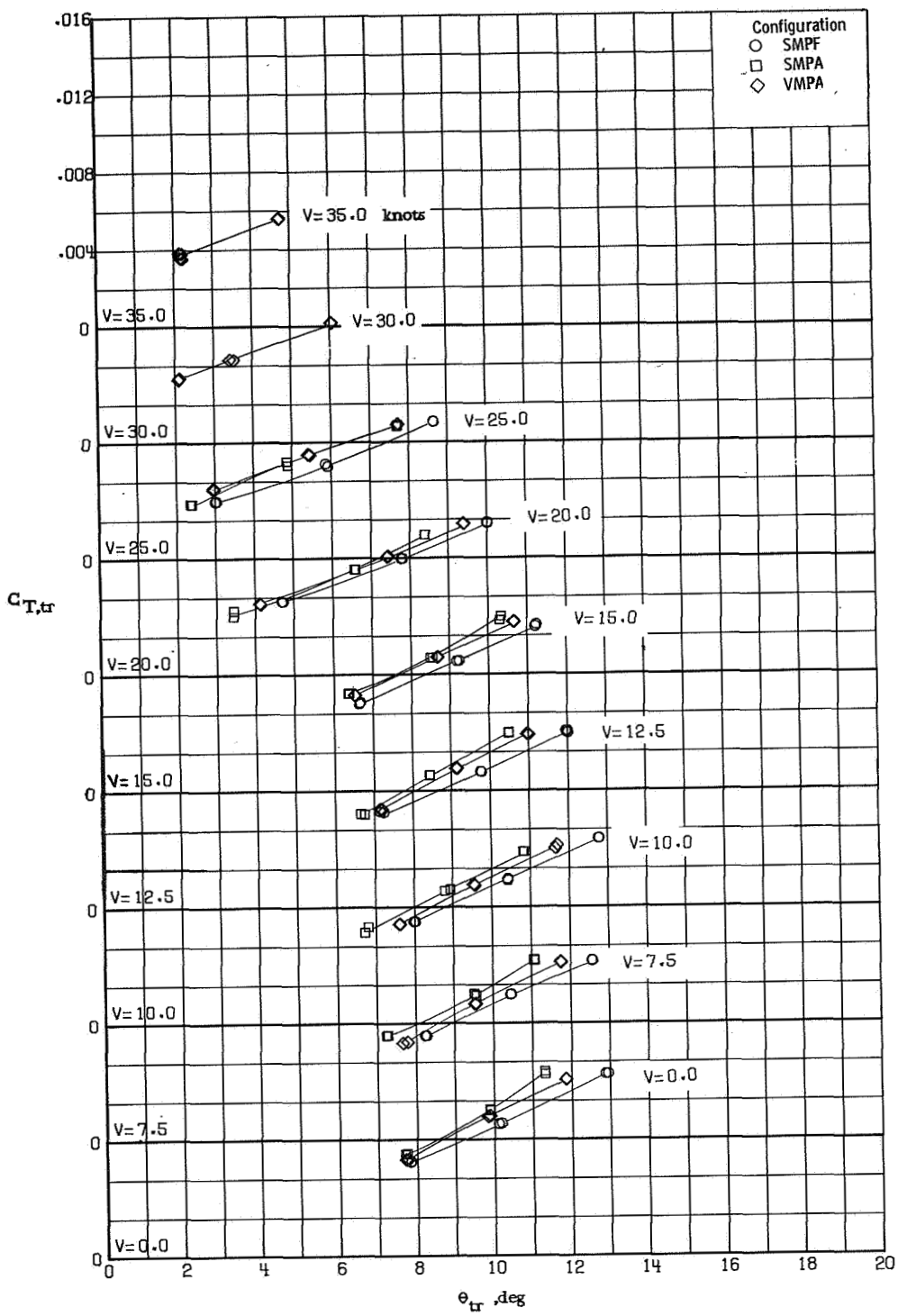

(b) Tail-rotor thrust.

Figure 24.- Continued.

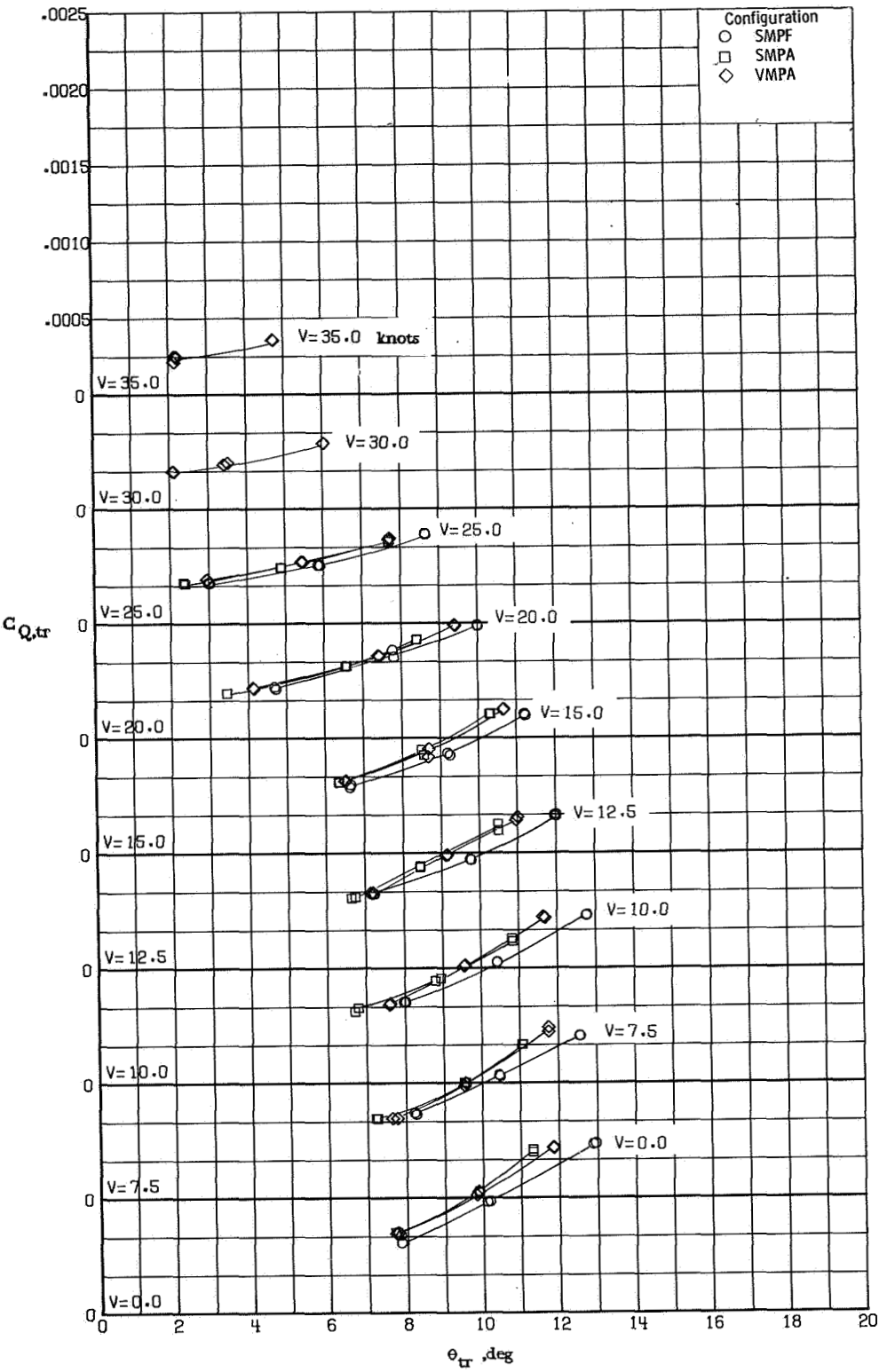

(c) Tail-rotor torque.

Figure 24.- Continued.

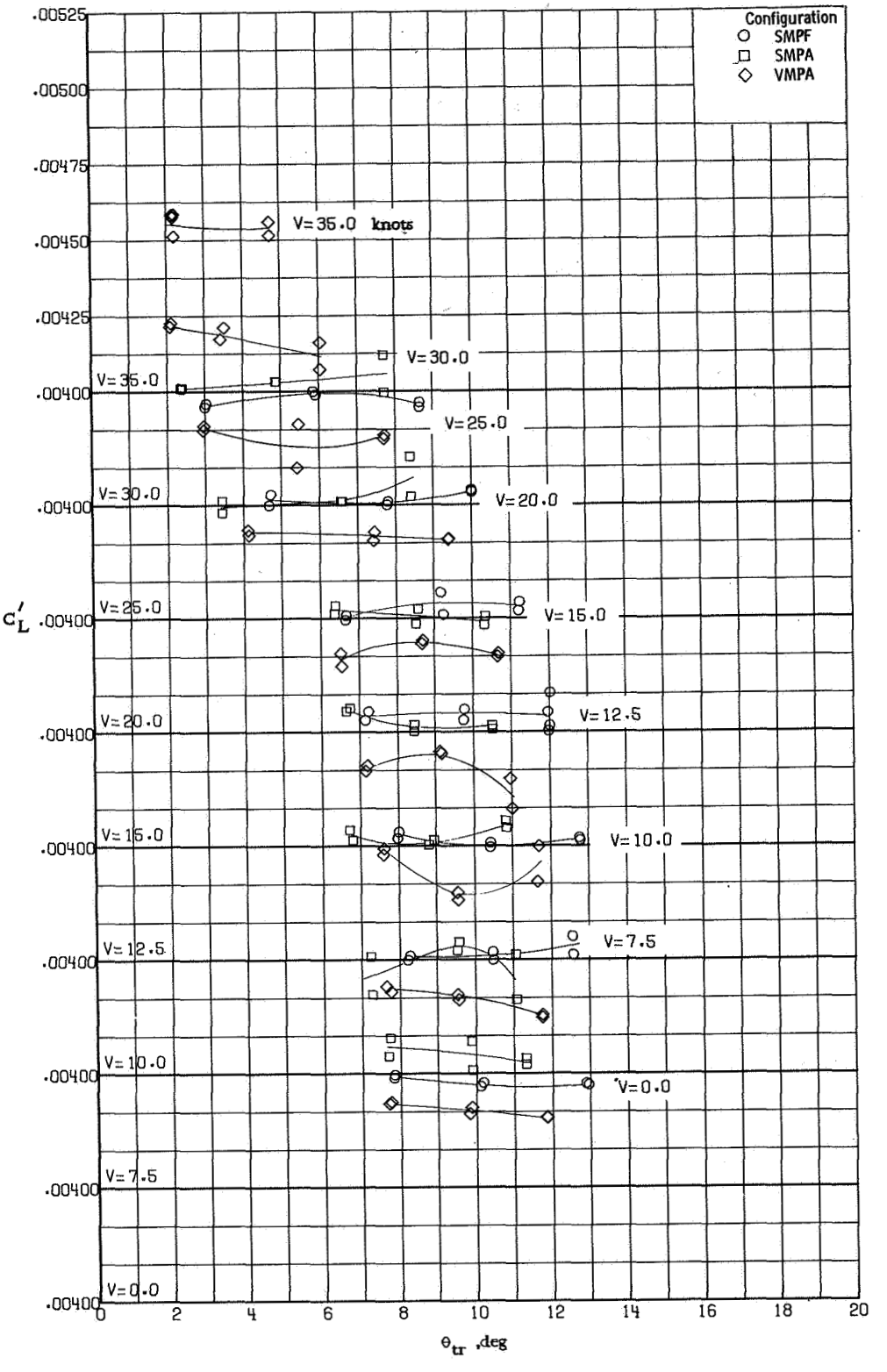

(d) Main-rotor lift.

Figure 24.- Continued.

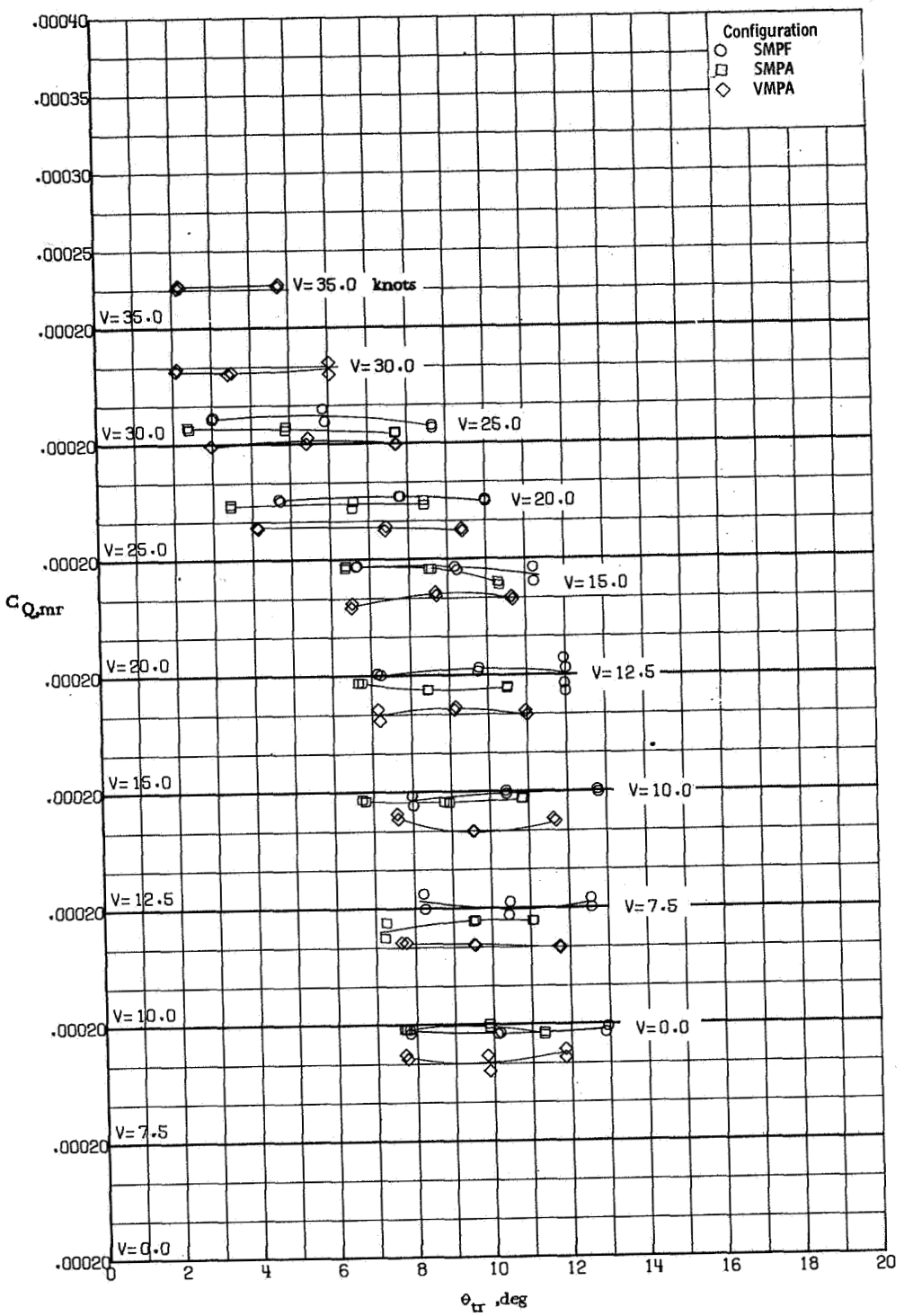

(e) Main-rotor torque.

Figure 24.- Continued.

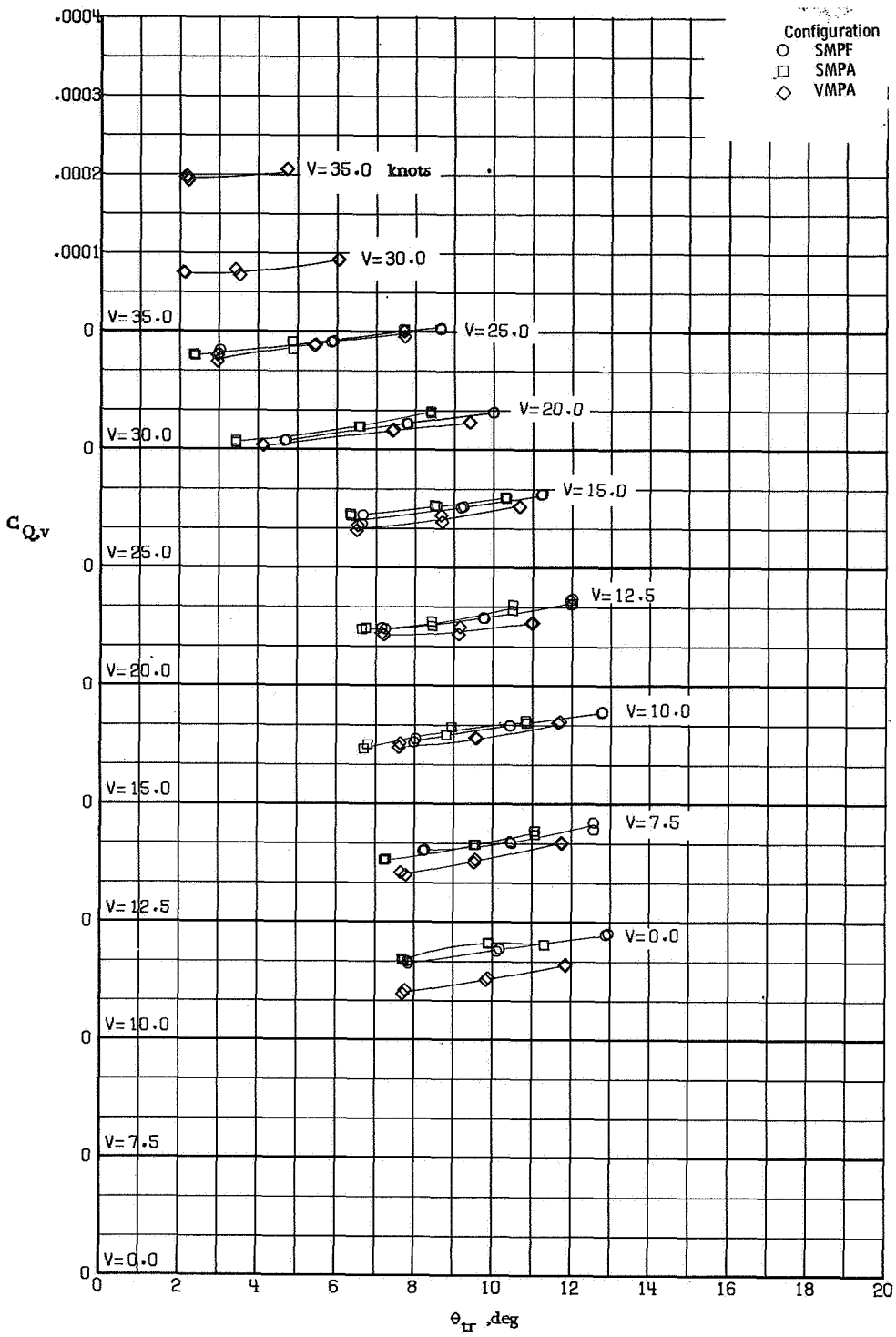

(f) Vehicle torque.

Figure 24.- Continued.

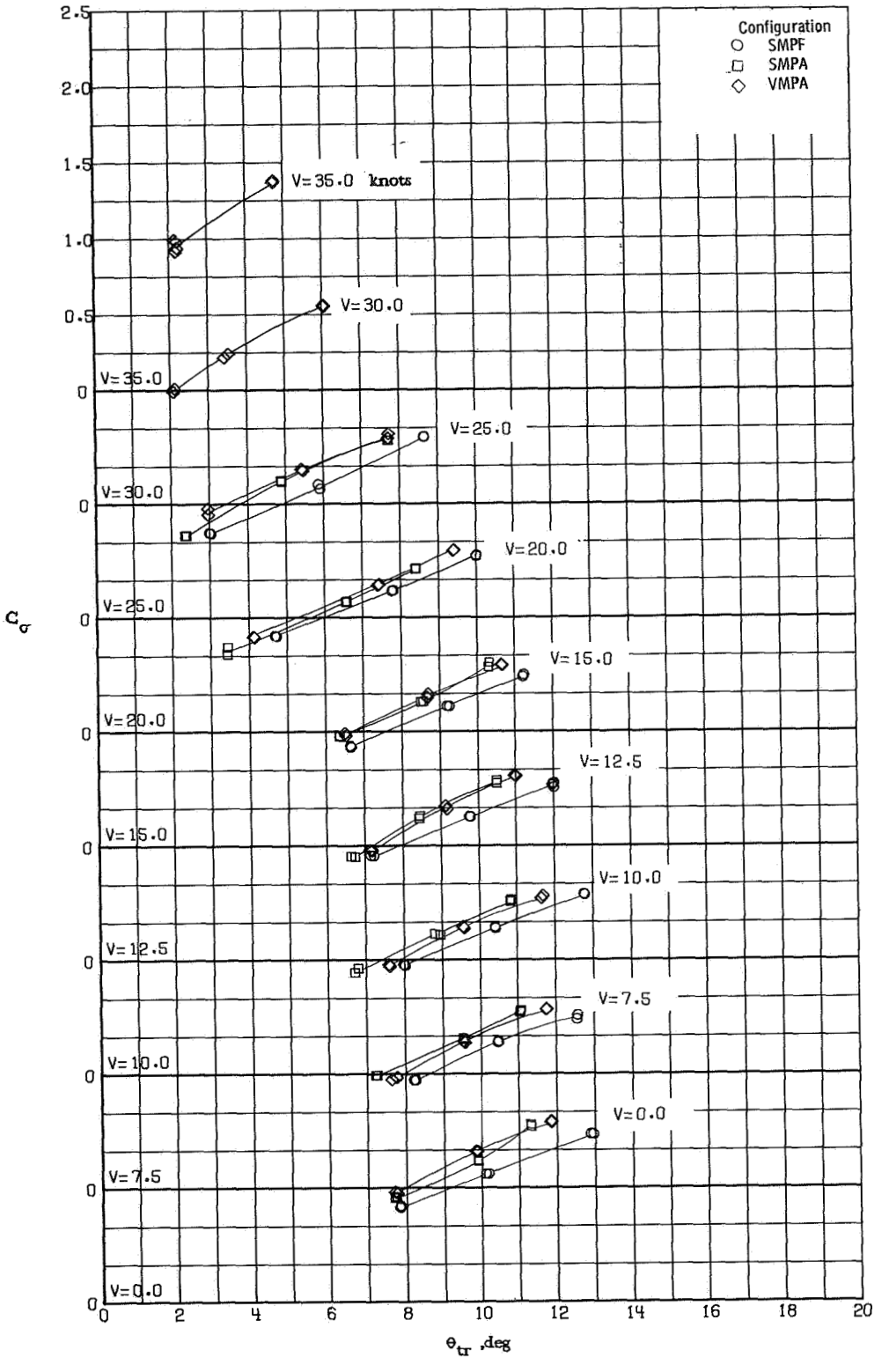

(g) Torque balance factor.

Figure 24.- Concluded.

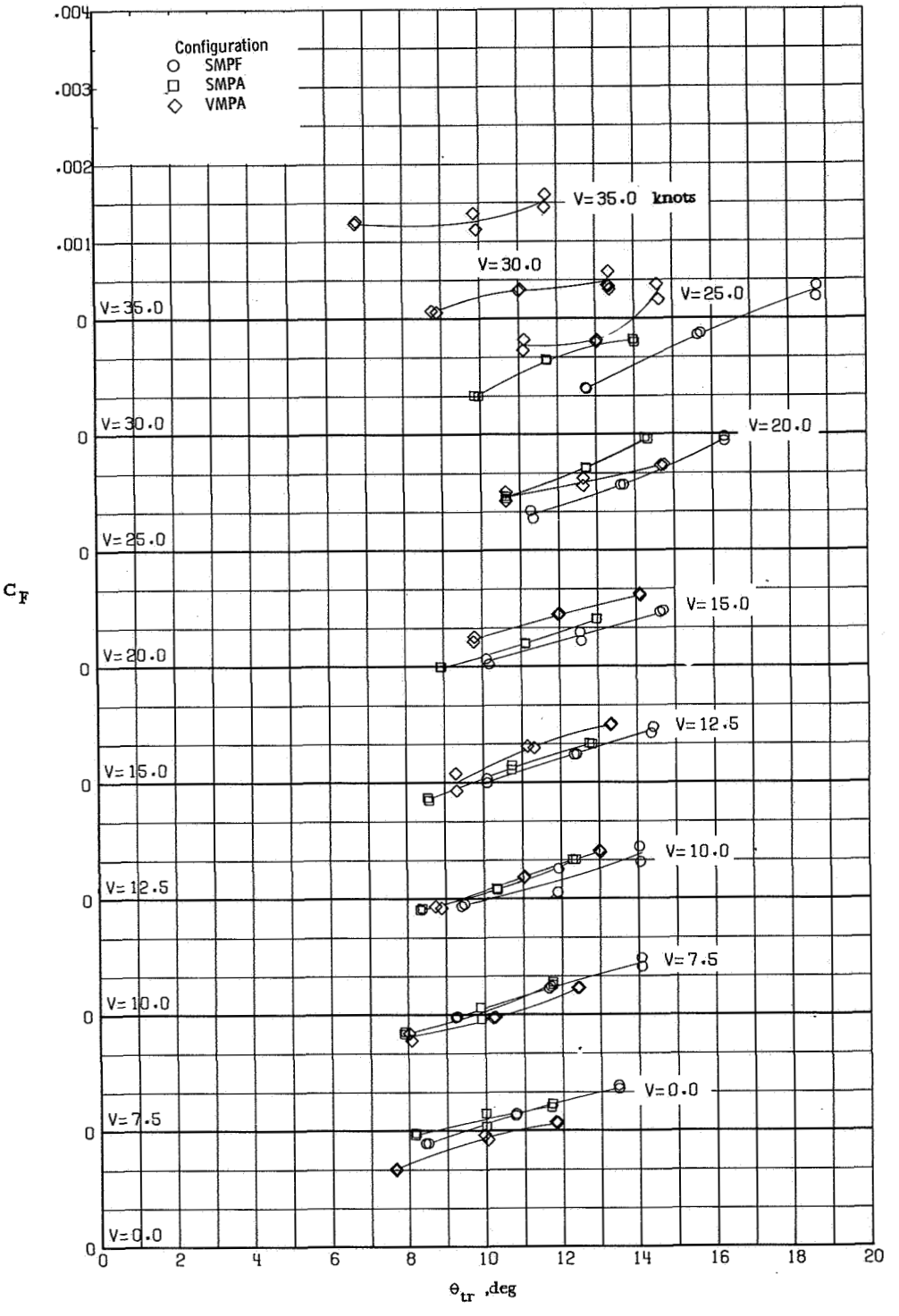

(a) Fin force.

Figure 25.- Aerodynamic characteristics of various configurations at $\beta = 60^{o}$.

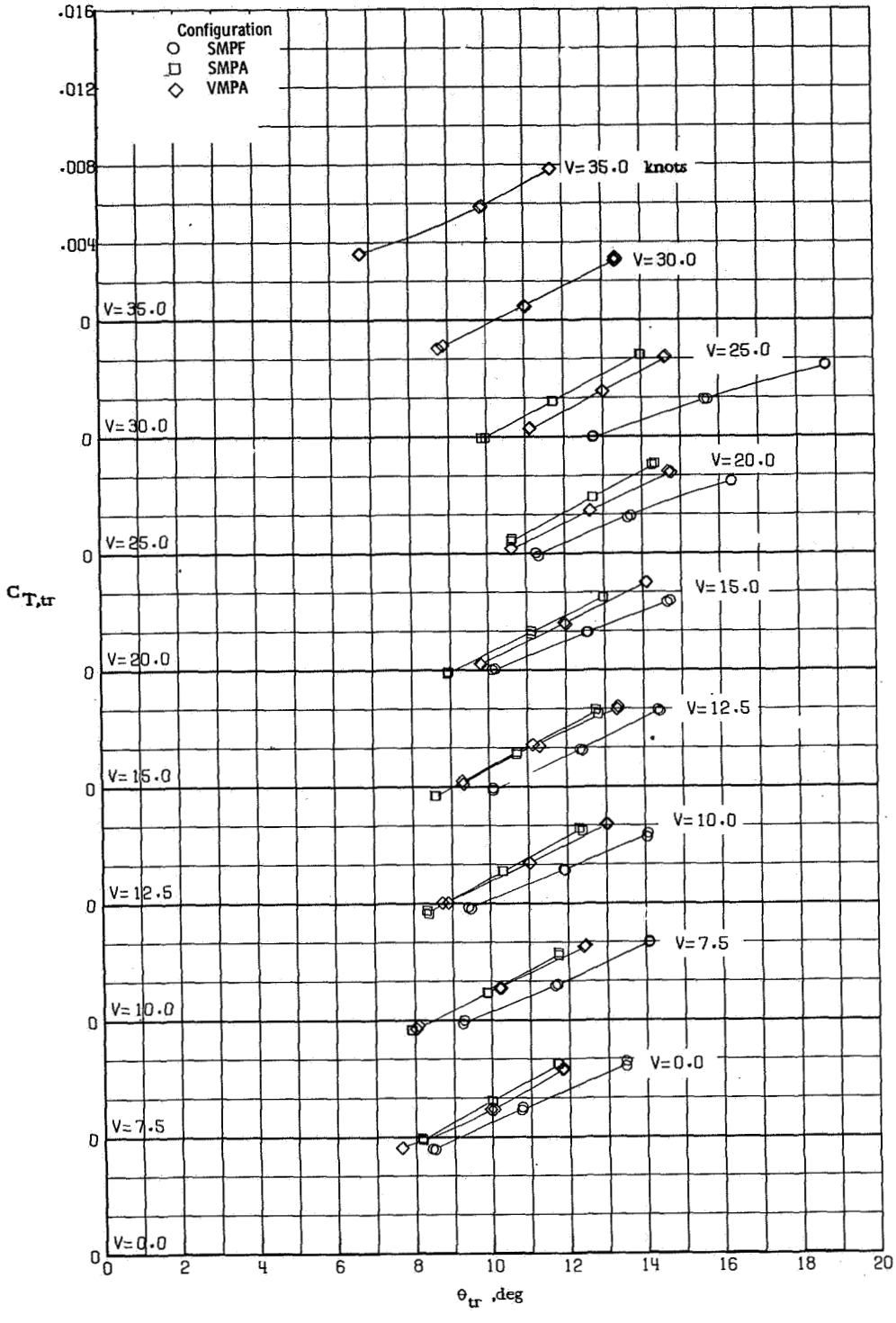

(b) Tail-rotor thrust.

Figure 25.- Continued.

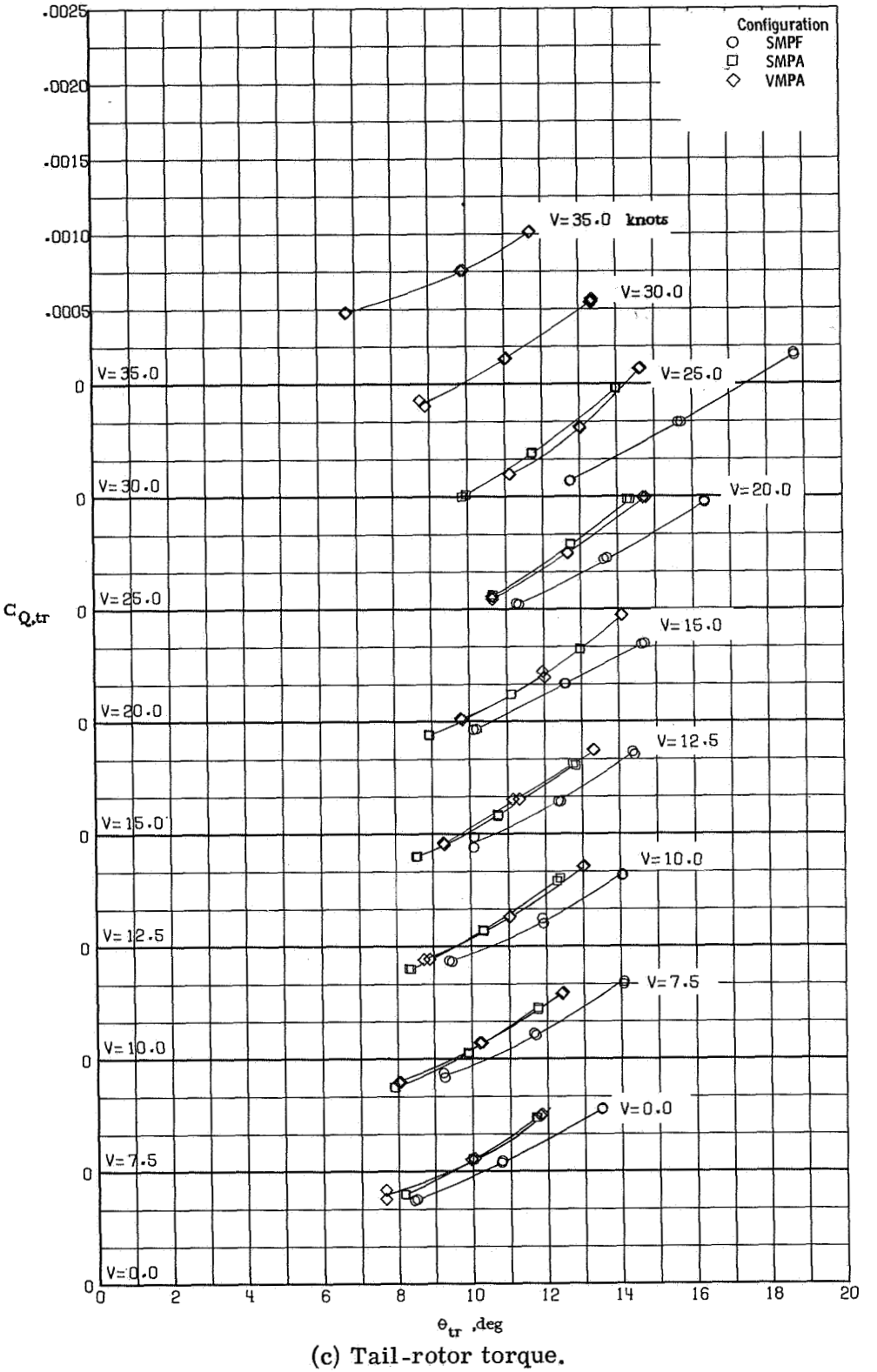

(c) Tail-rotor torque.

Figure 25.- Continued.

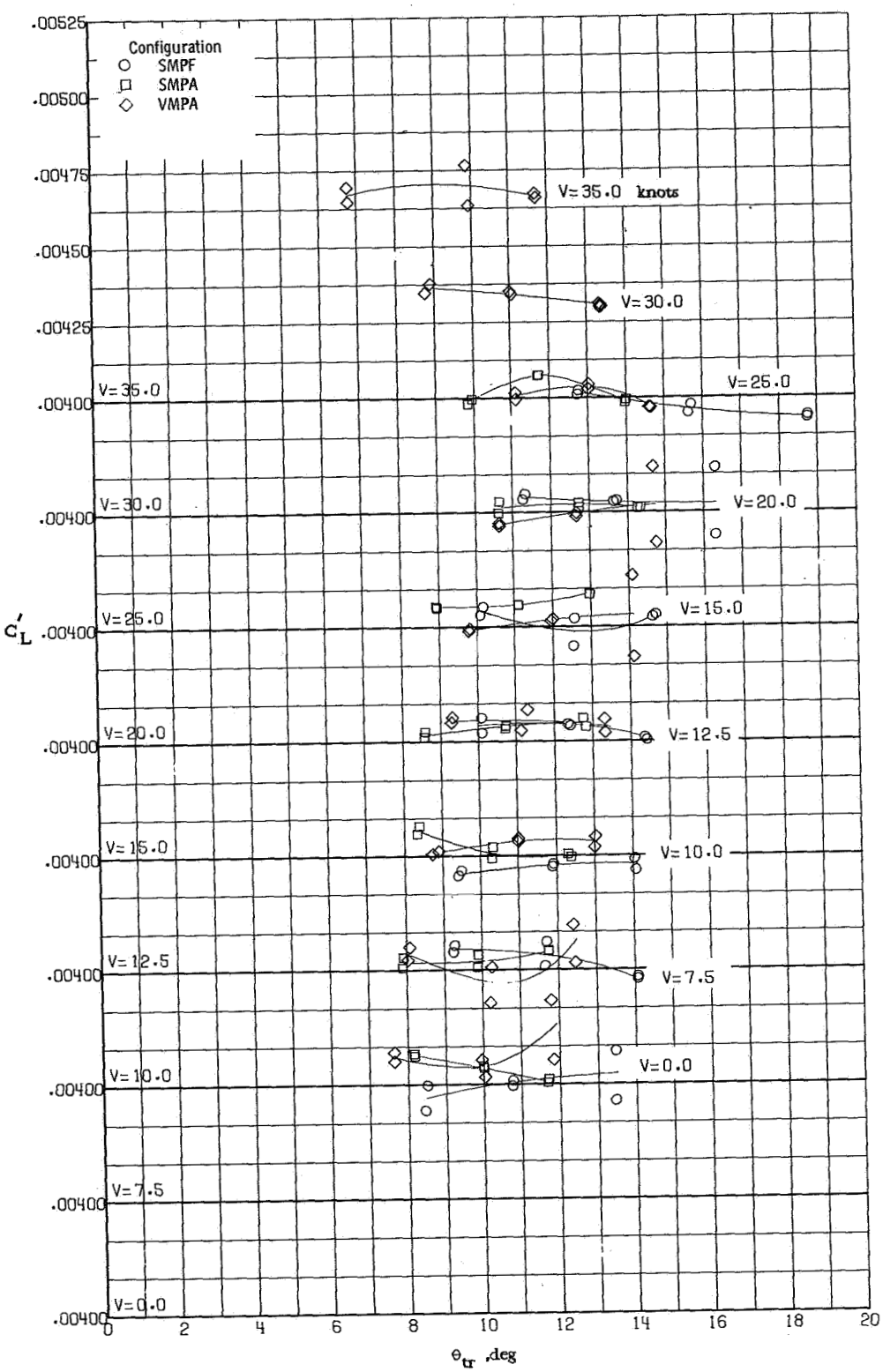

(d) Main-rotor lift.

Figure 25.- Continued.

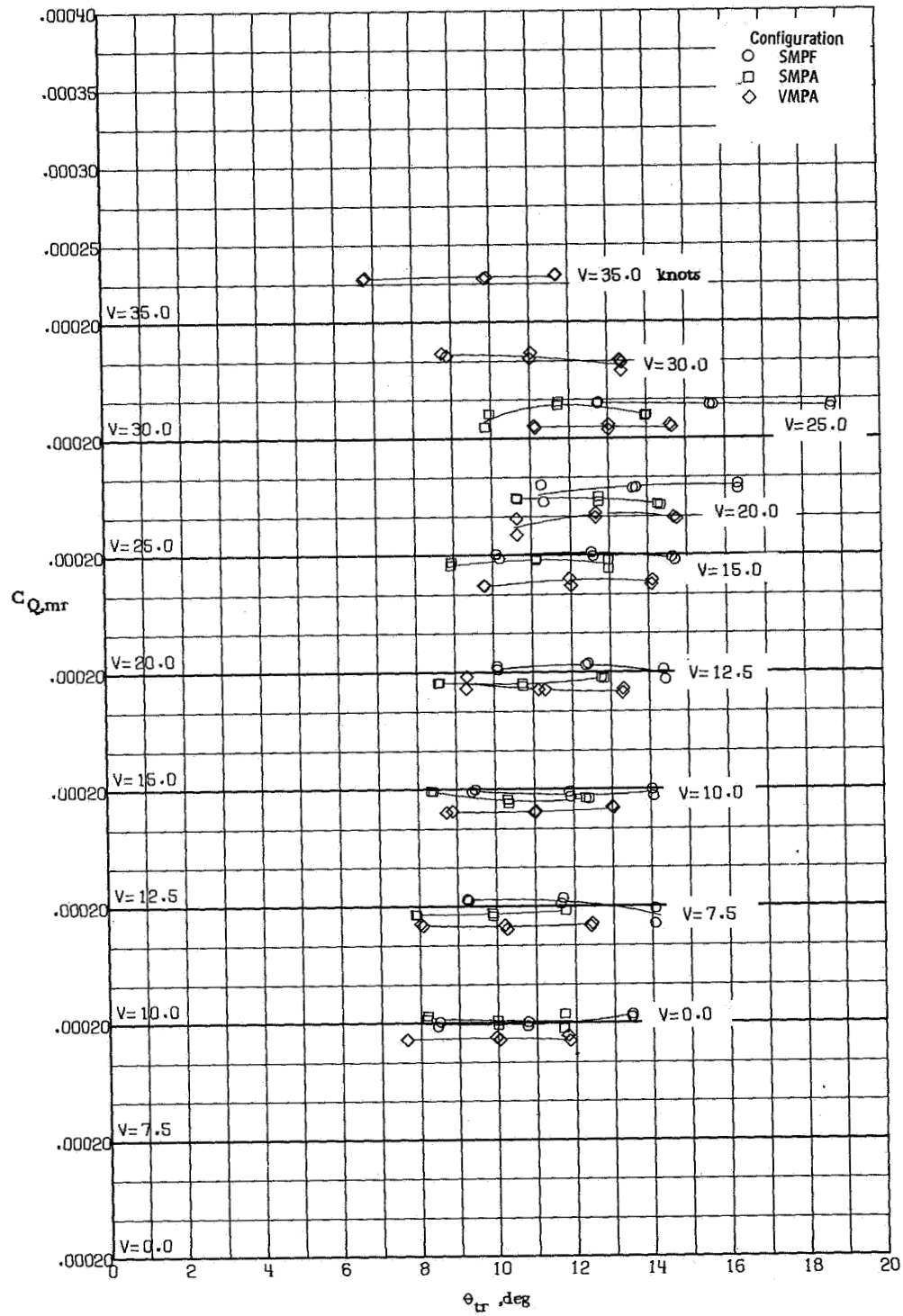

(e) Main-rotor torque.

Figure 25.- Continued.

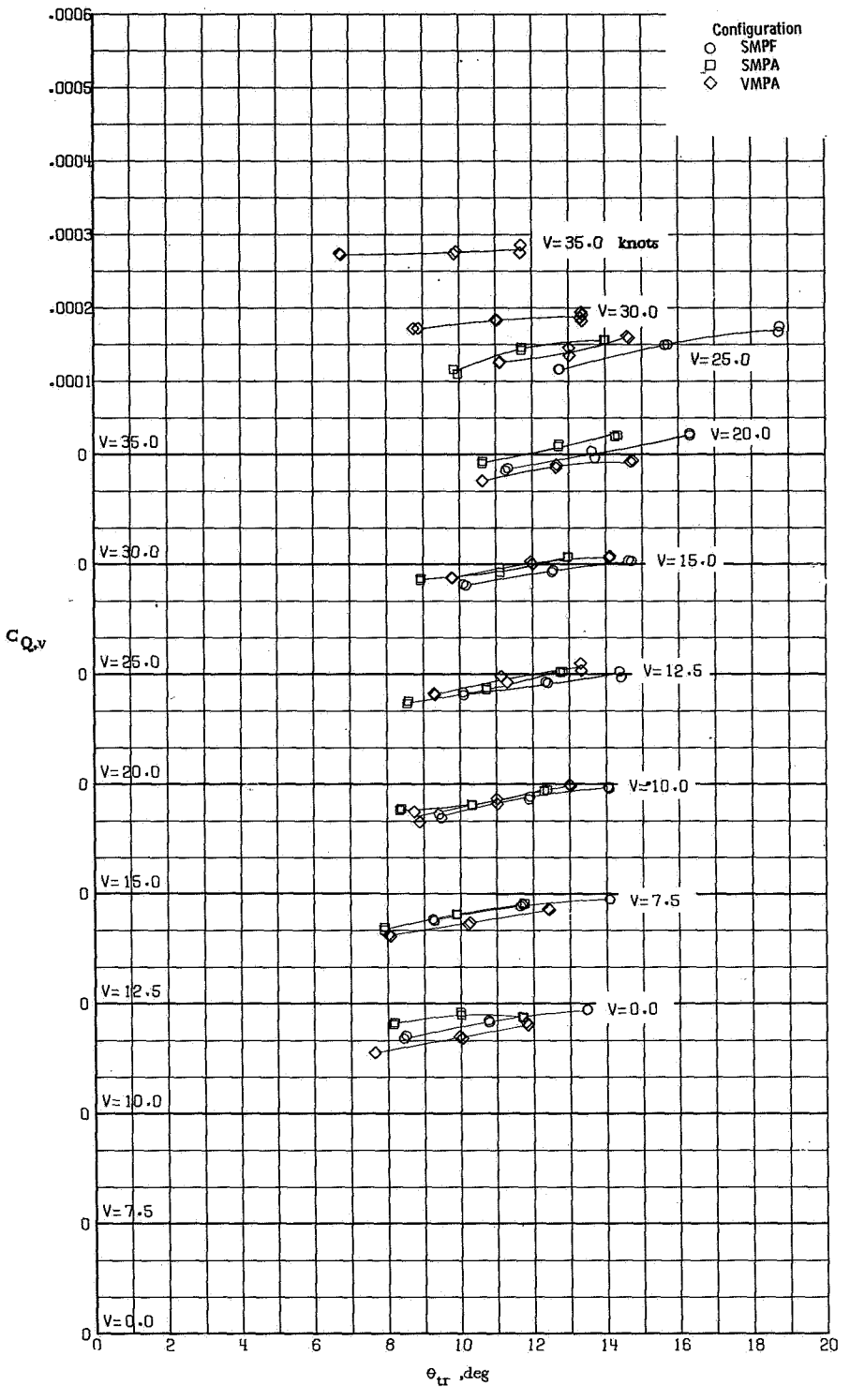

(f) Vehicle torque.

Figure 25.- Continued.

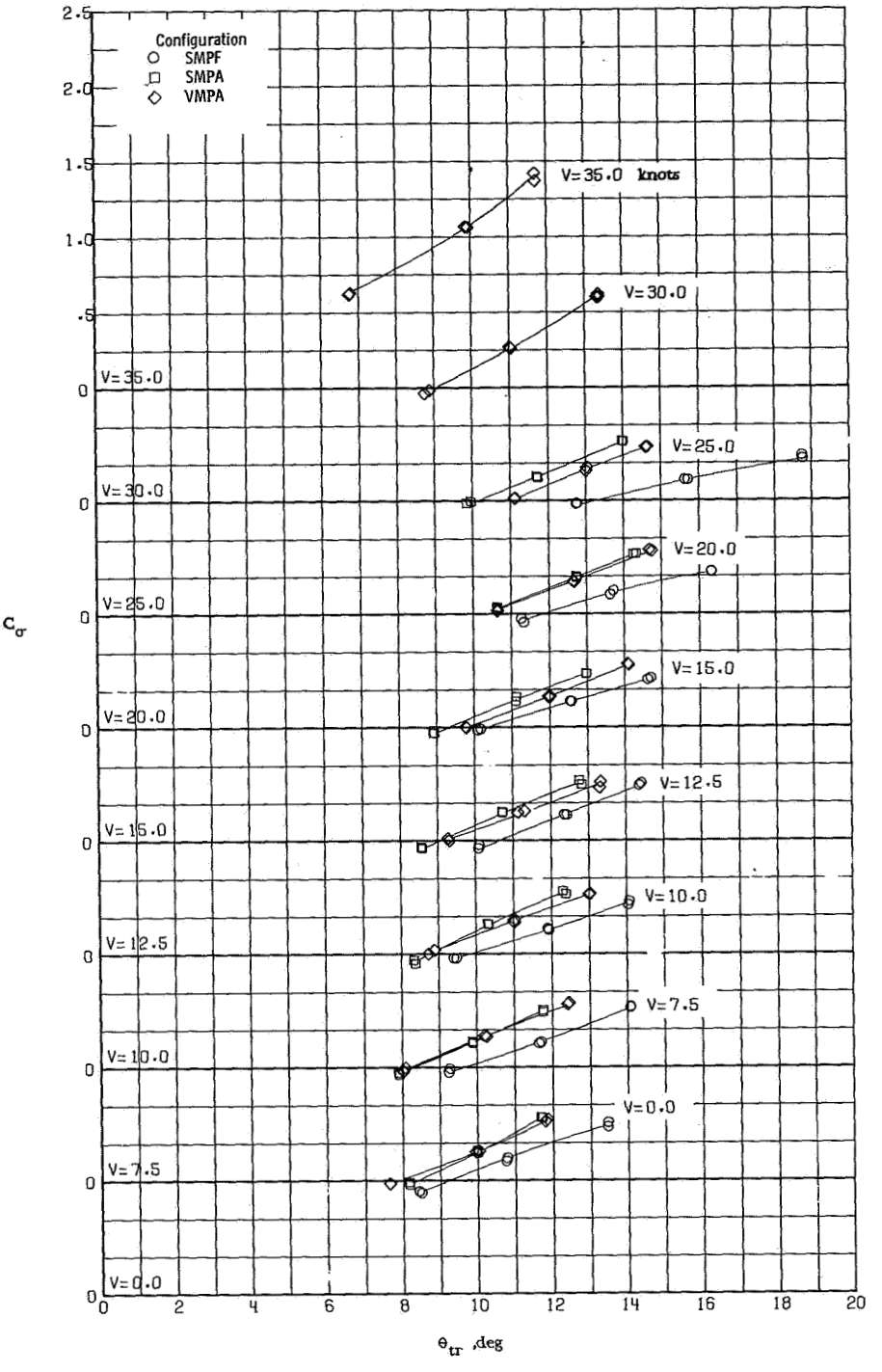

(g) Torque balance factor.

Figure 25.- Concluded.

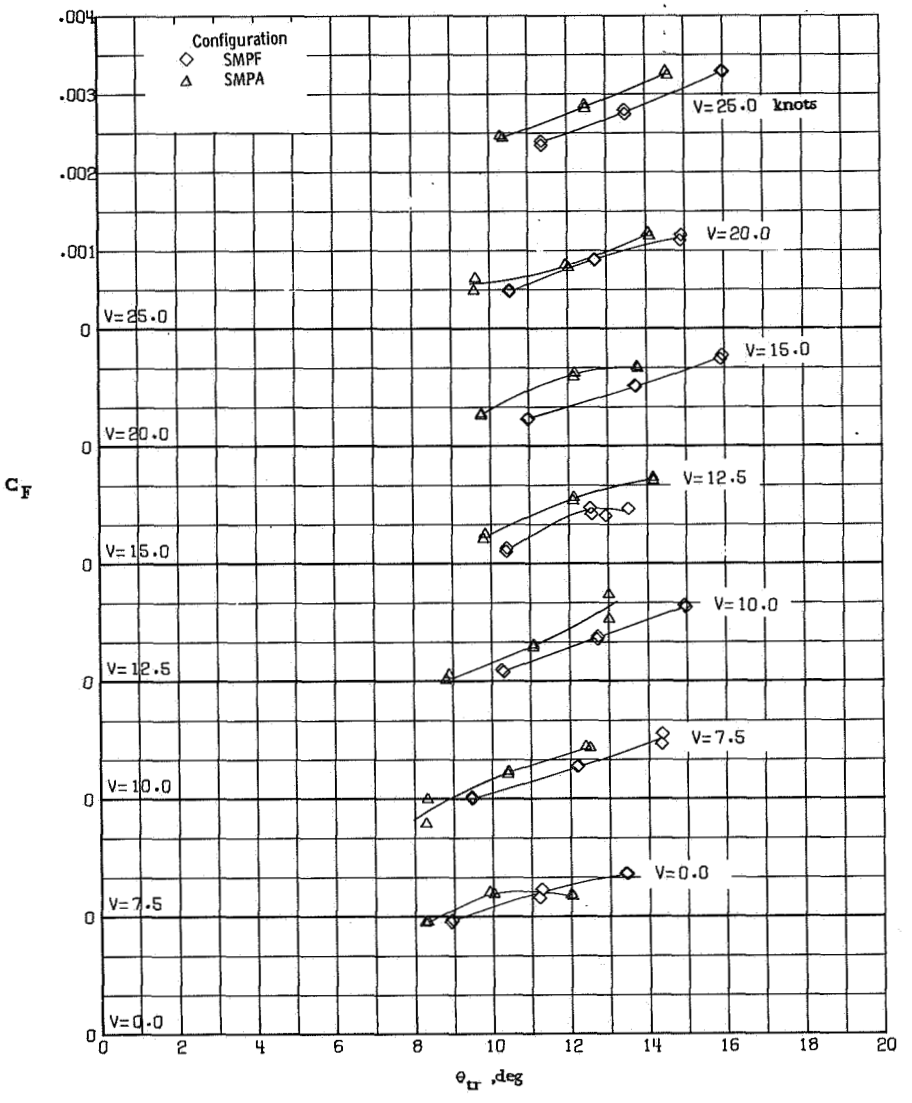

(a) Fin force.

Figure 26.- Aerodynamic characteristics of various configurations at $\beta = 90^{o}$.

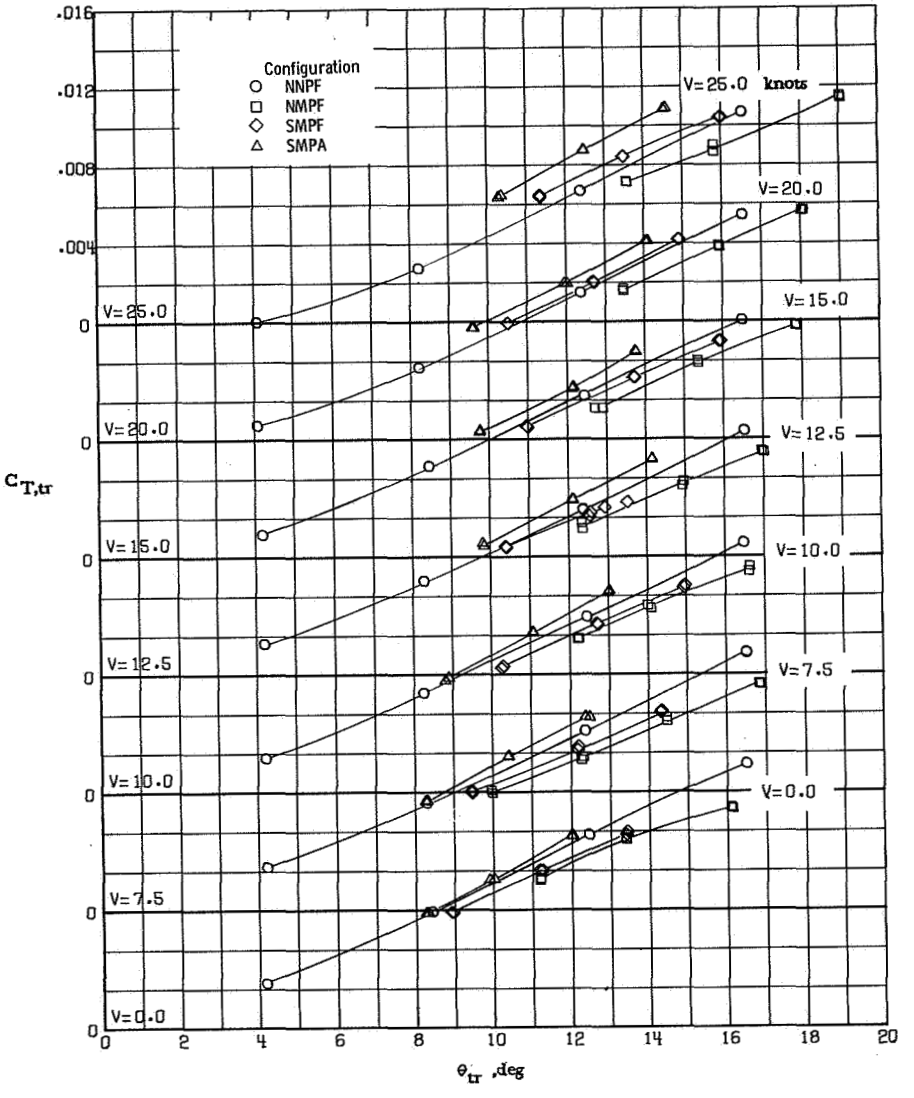

(b) Tail-rotor thrust.

Figure 26.- Continued.

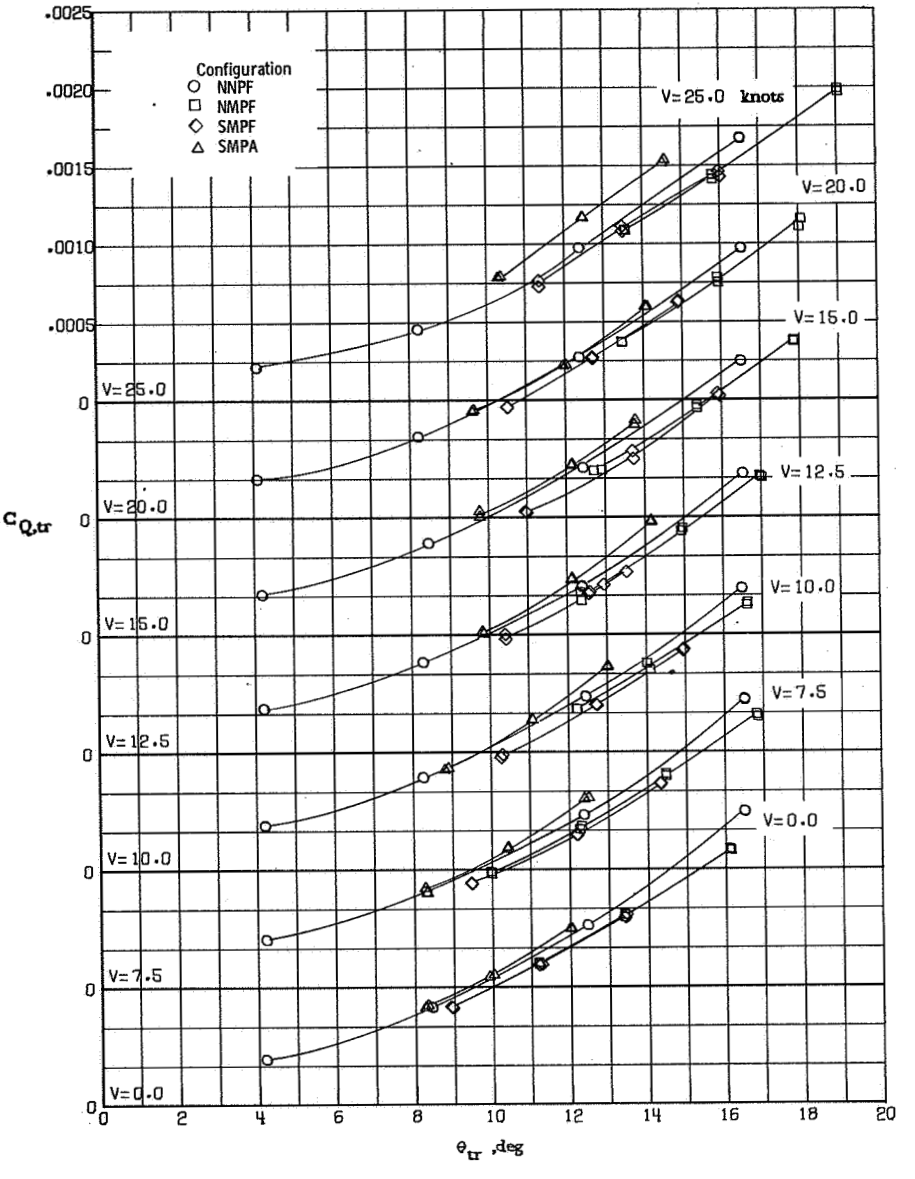

(c) Tail-rotor torque.

Figure 26.- Continued.

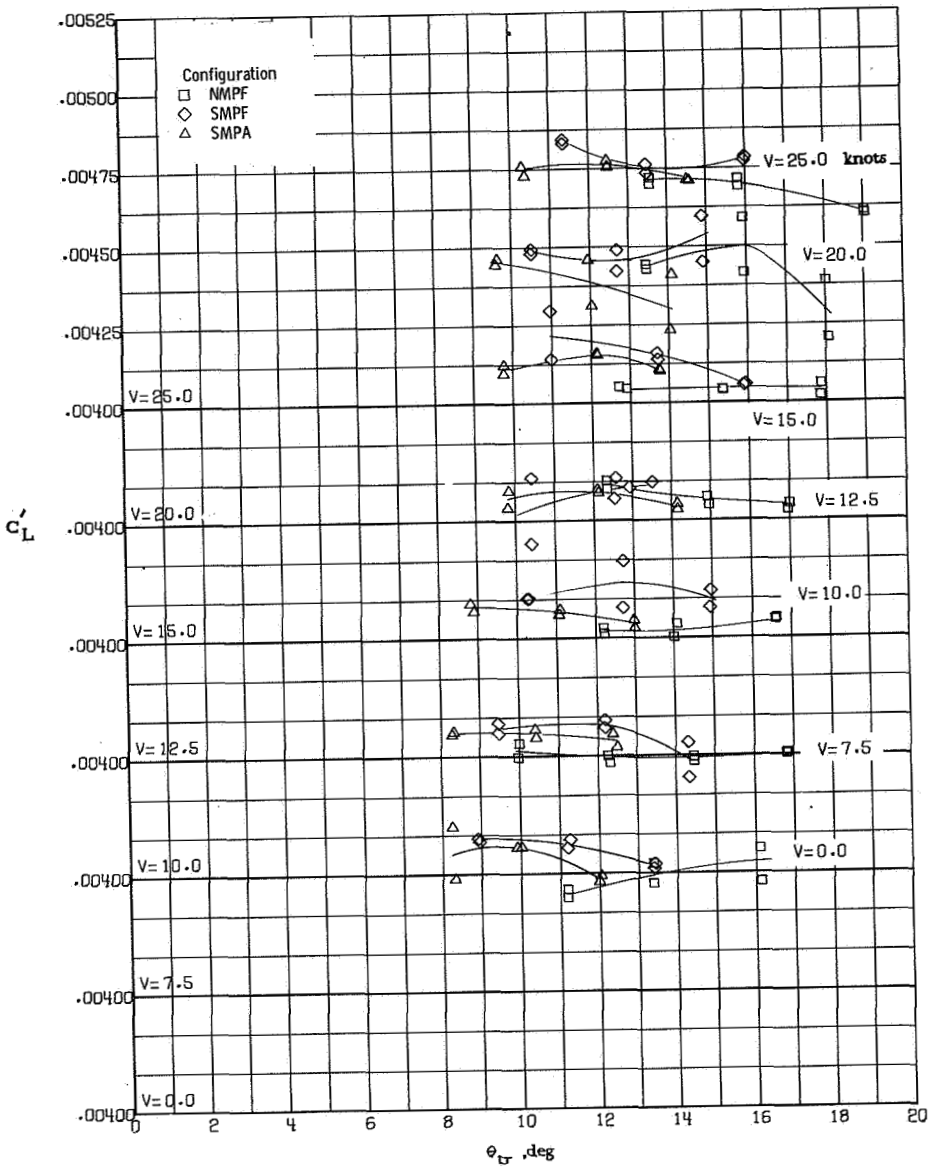

(d) Main-rotor lift.

Figure 26.- Continued.

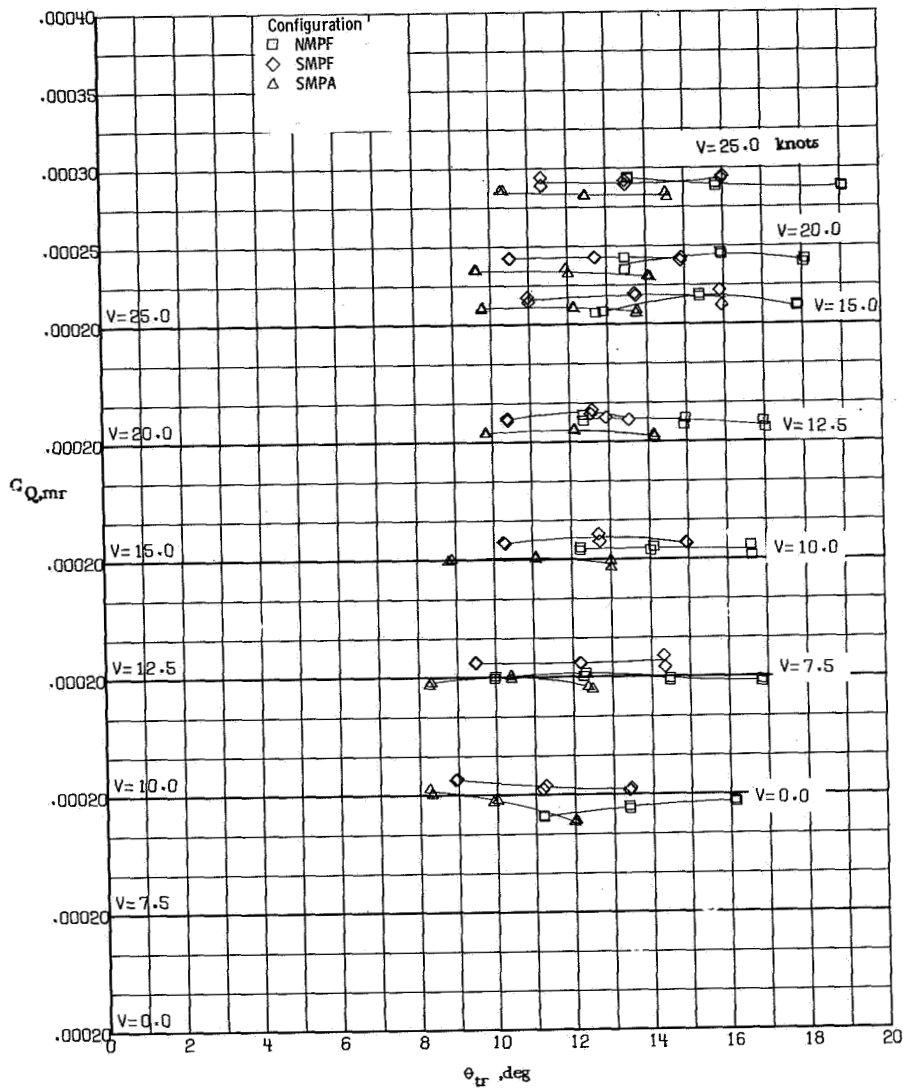

(e) Main-rotor torque.

Figure 26.- Continued.

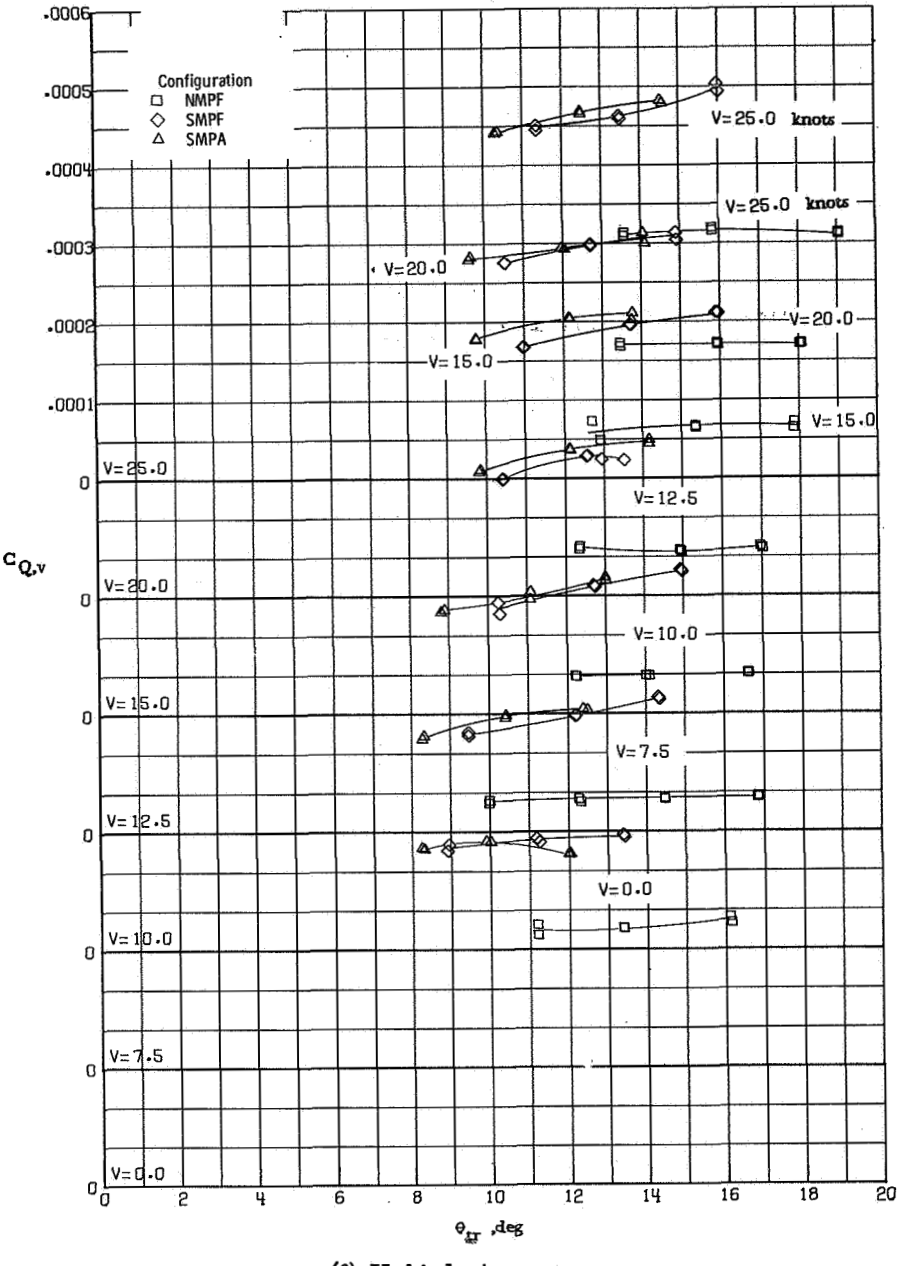

(f) Vehicle torque.

Figure 26.- Continued.

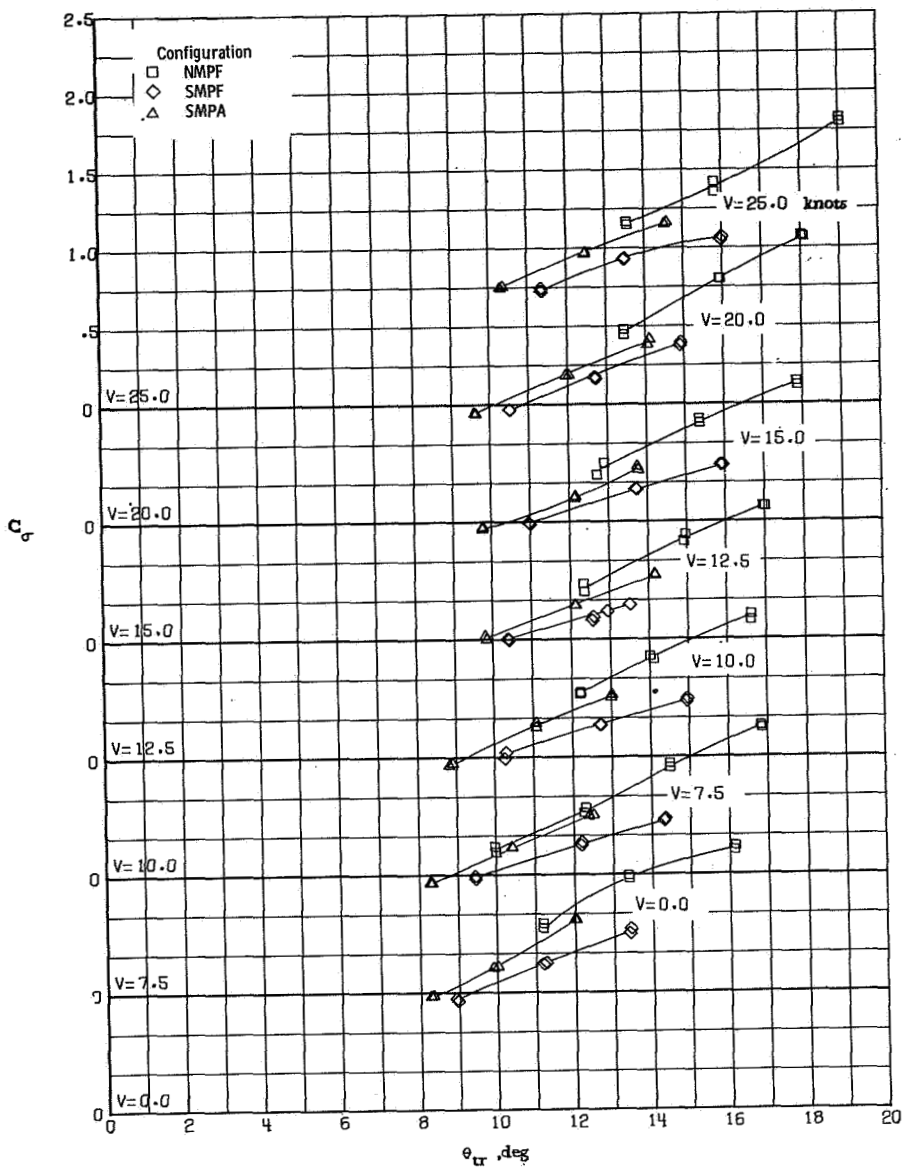

(g) Torque balance factor.

Figure 26.- Concluded.

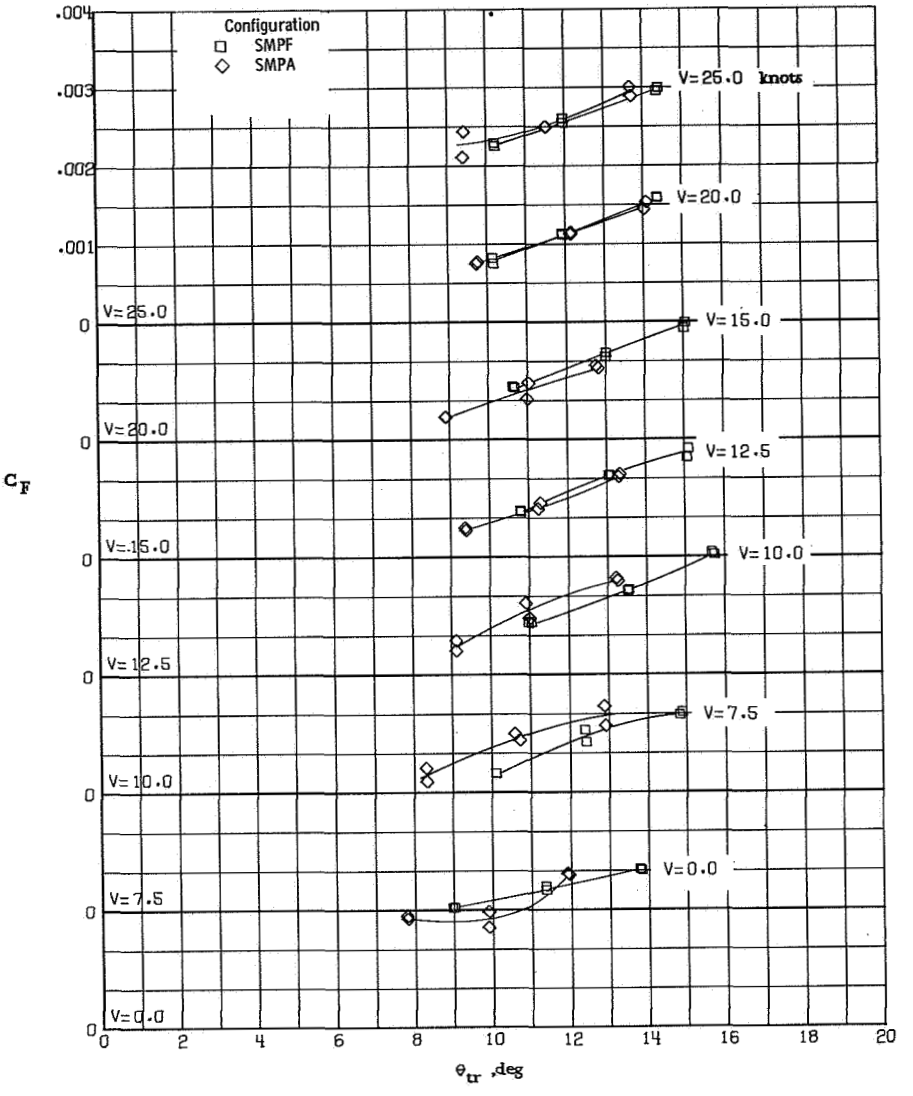

(a) Fin force.

Figure 27.- Aerodynamic characteristics of configurations with a pusher tail rotor at $\beta = 120^{o}$.

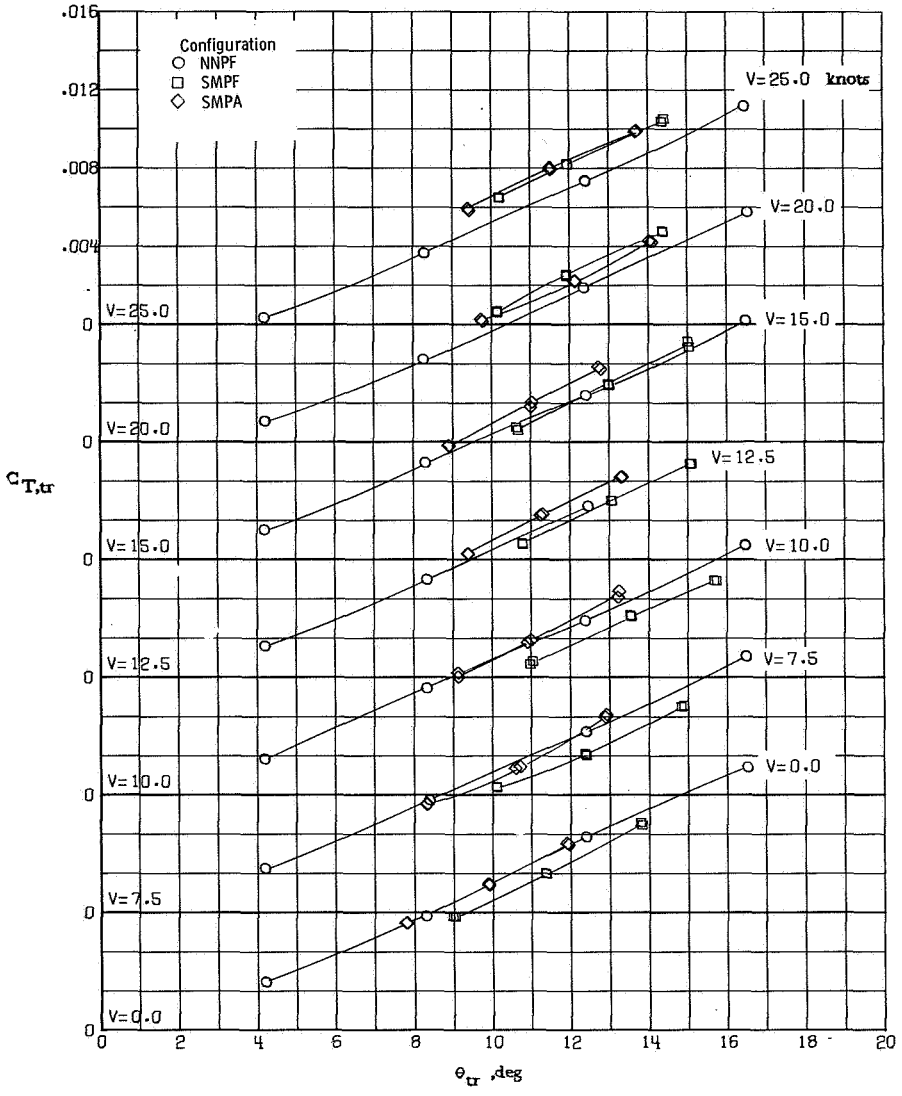

(b) Tail-rotor thrust.

Figure 27.- Continued.

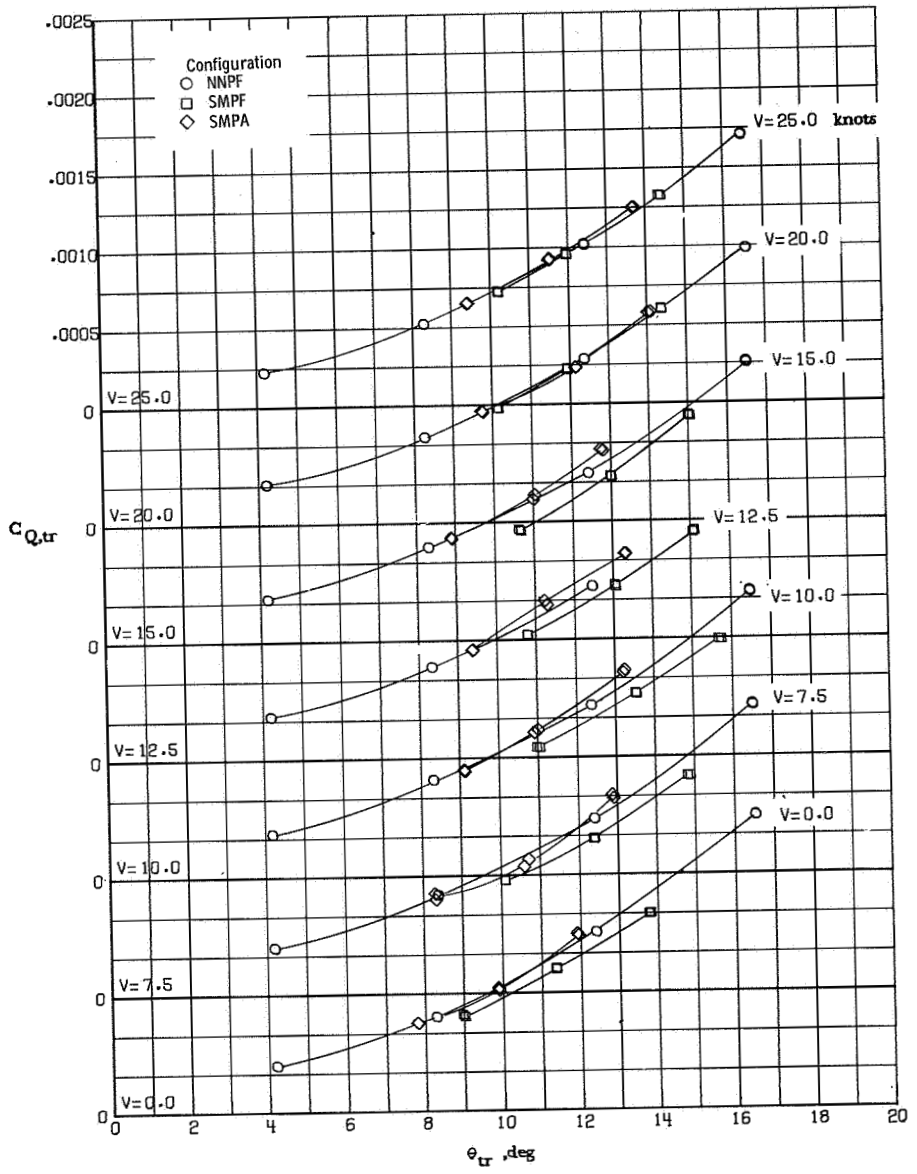

(c) Tail-rotor torque.

Figure 27.- Continued.

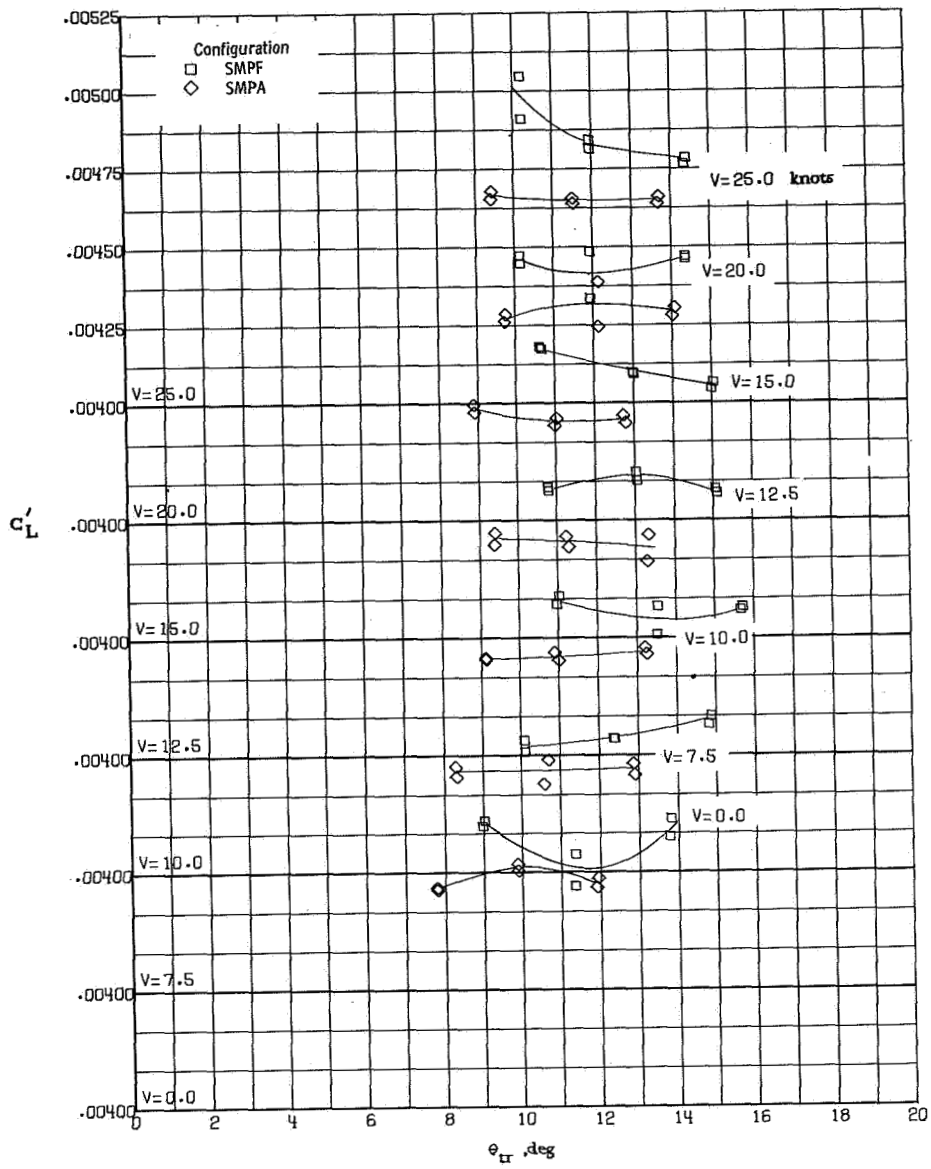

(d) Main-rotor lift.

Figure 27.- Continued.

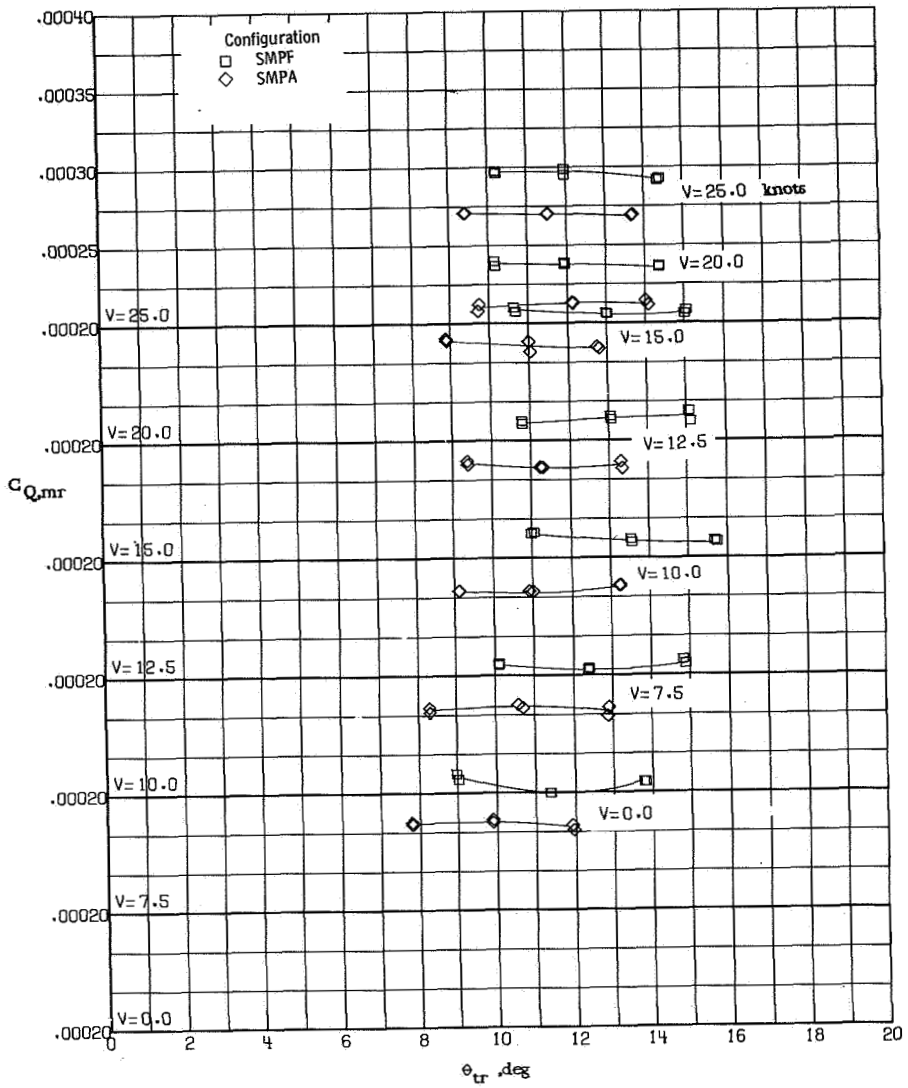

(e) Main-rotor torque.

Figure 27.- Continued.

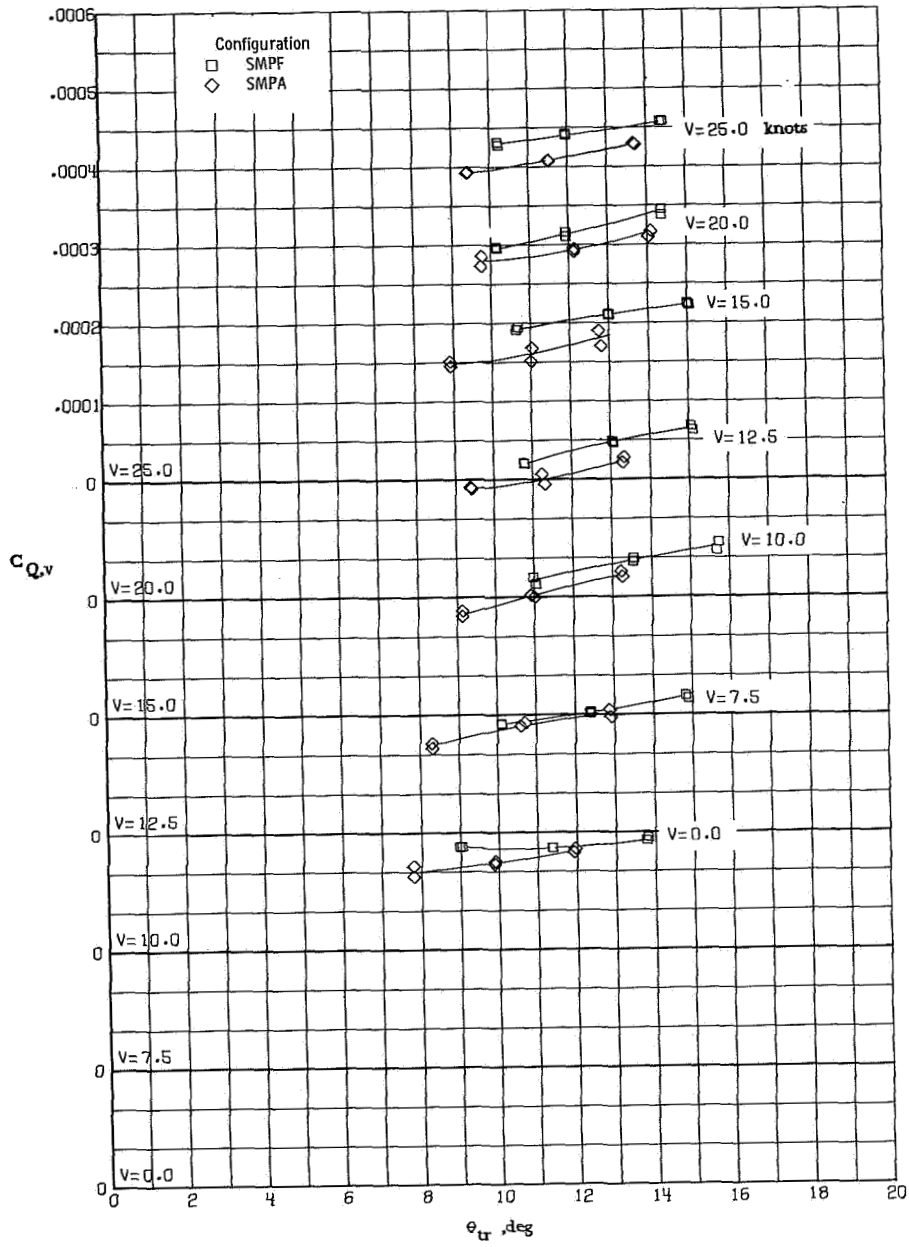

(f) Vehicle torque.

Figure 27.- Continued.

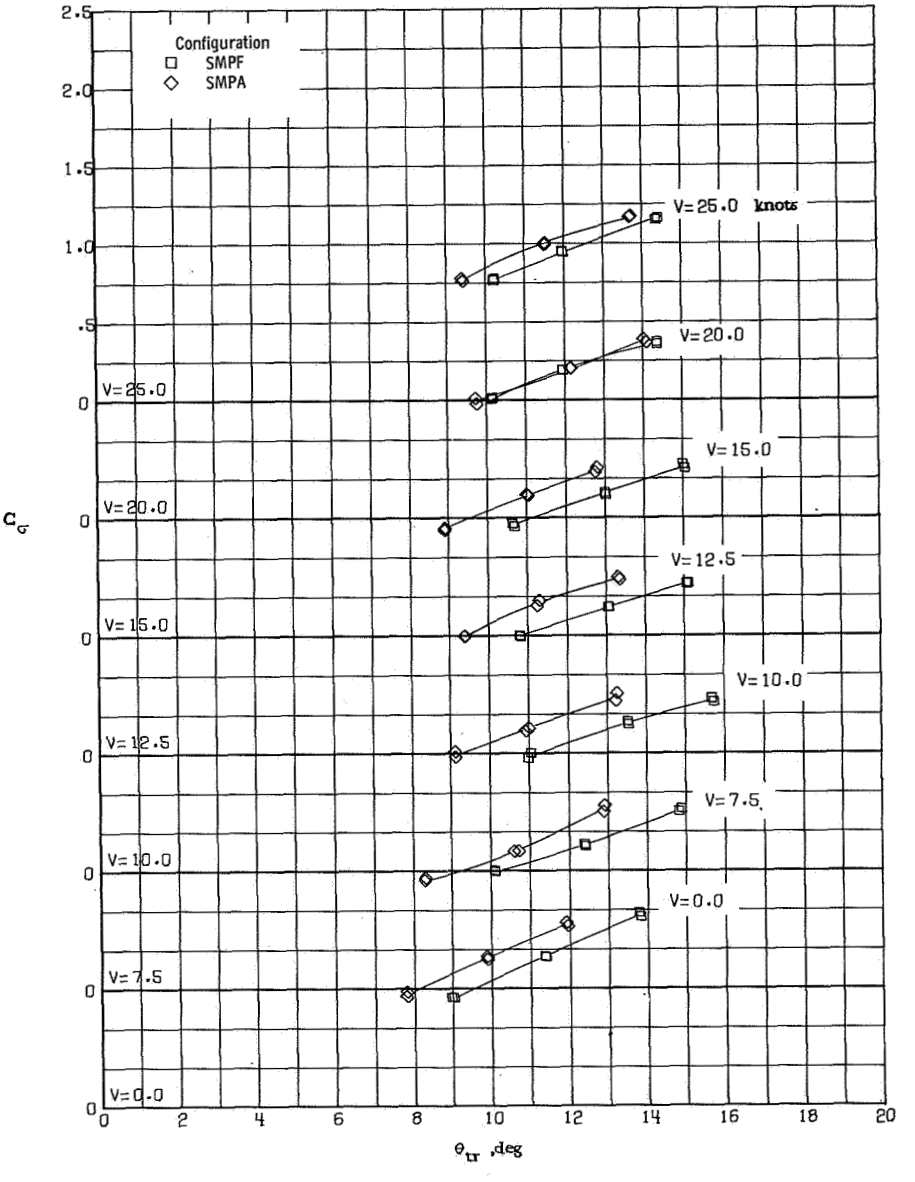

(g) Torque balance factor.

Figure 27.- Concluded.

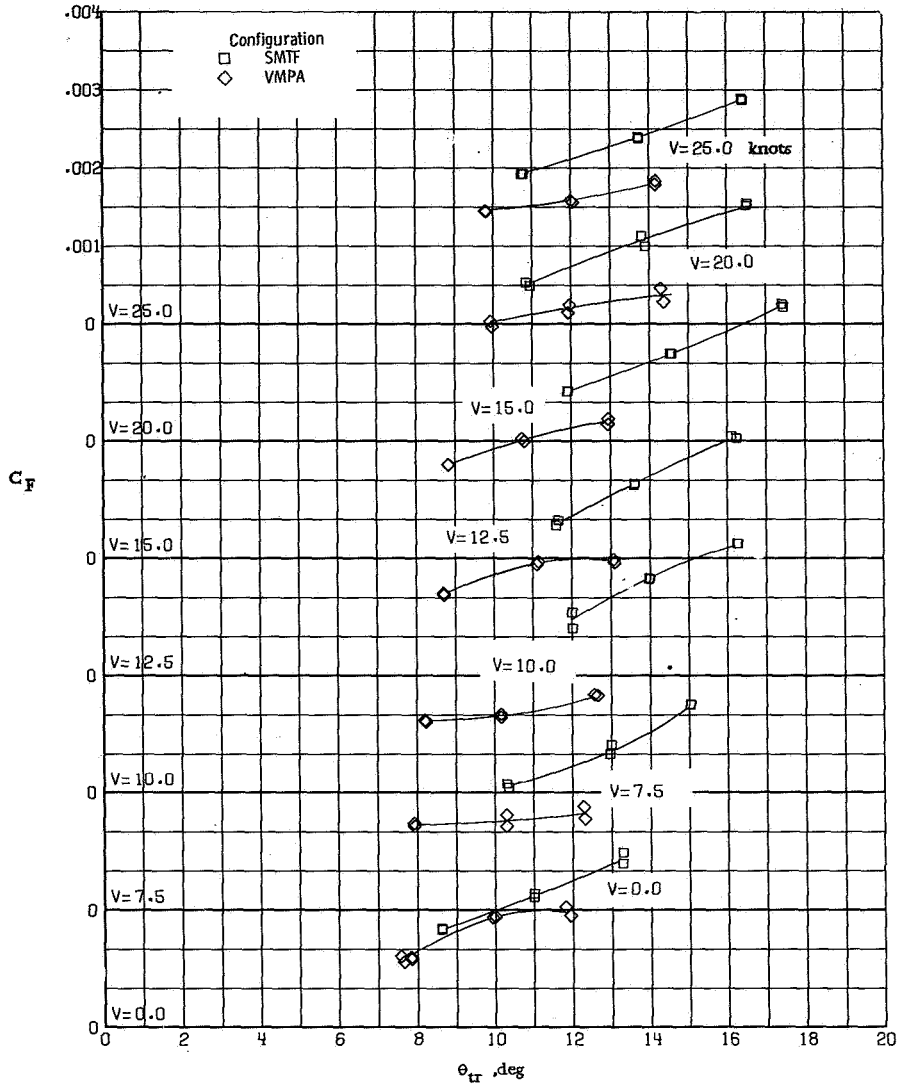

(a) Fin force.

Figure 28.- Aerodynamic characteristics of various configurations with and without the main rotor at $\beta = 120^{o}$.

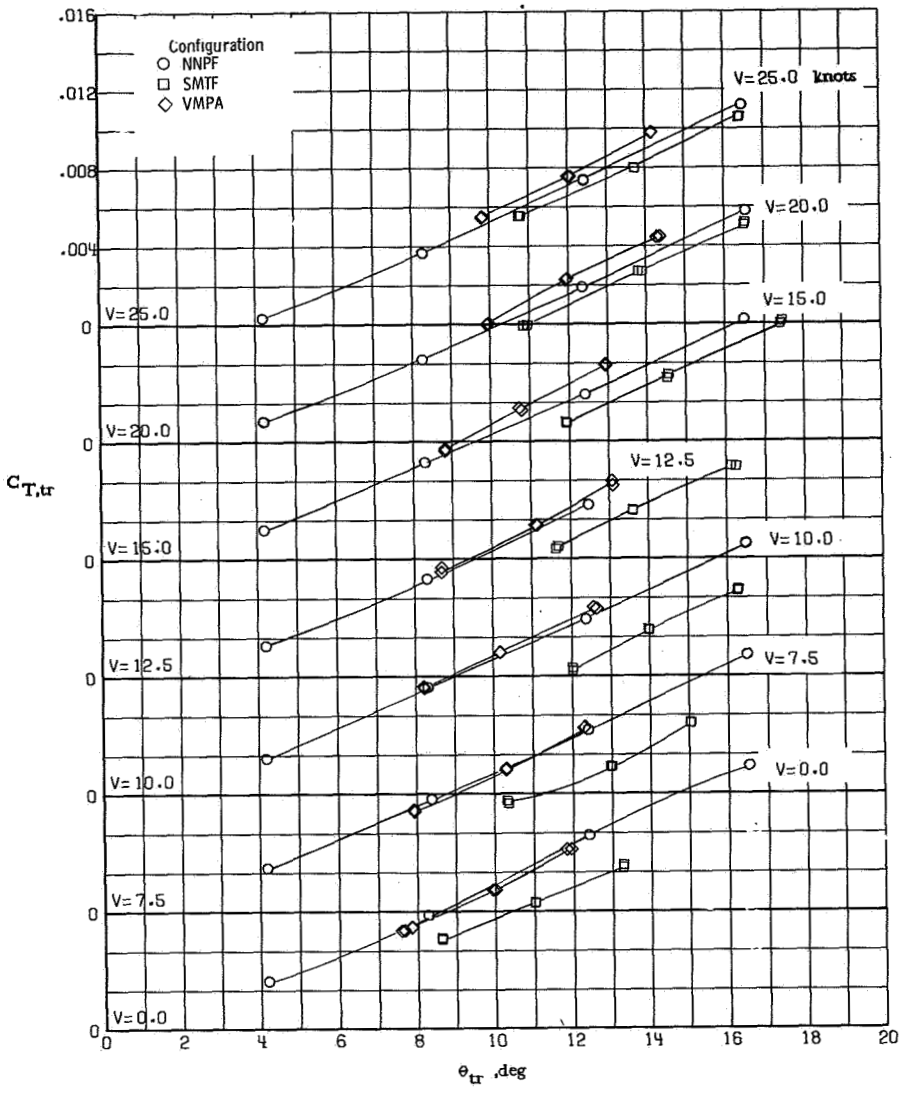

(b) Tail-rotor thrust.

Figure 28.- Continued.

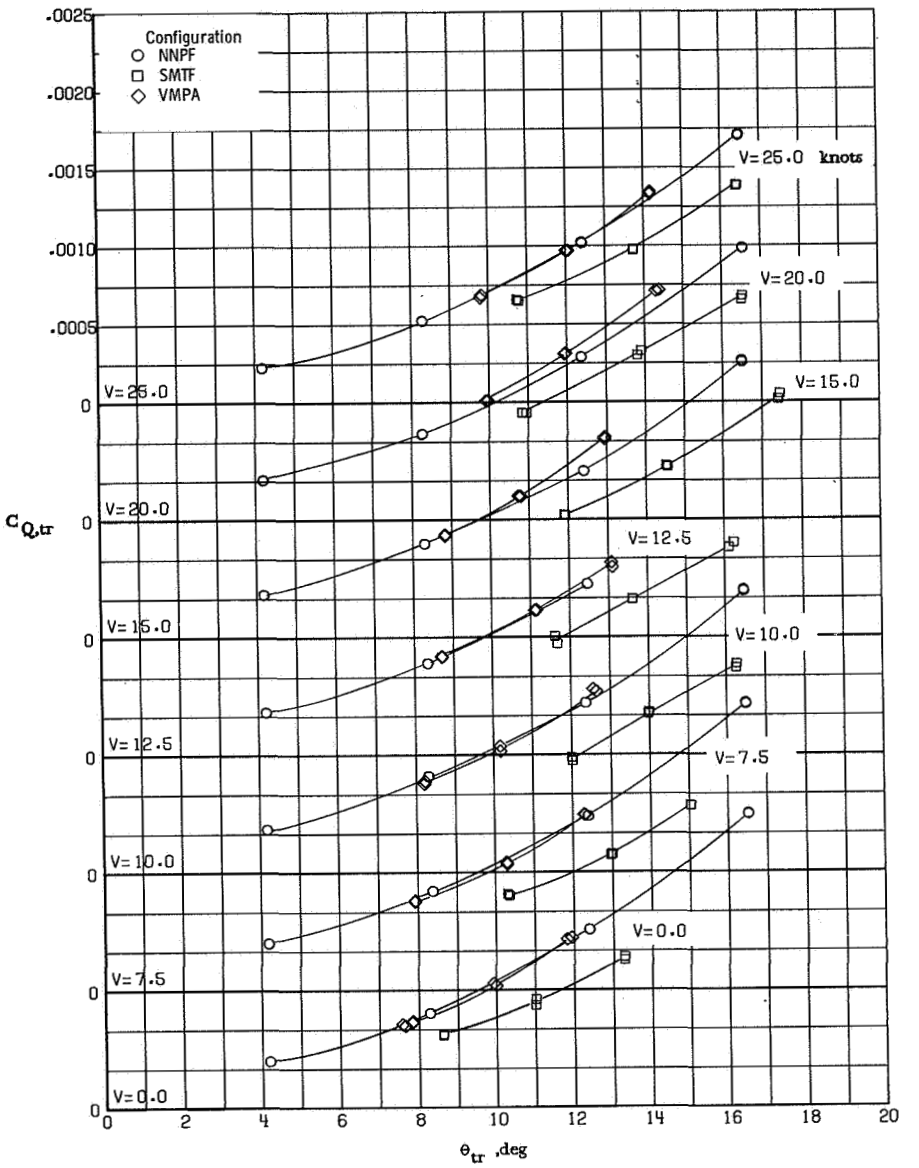

(c) Tail-rotor torque.

Figure 28.- Continued.

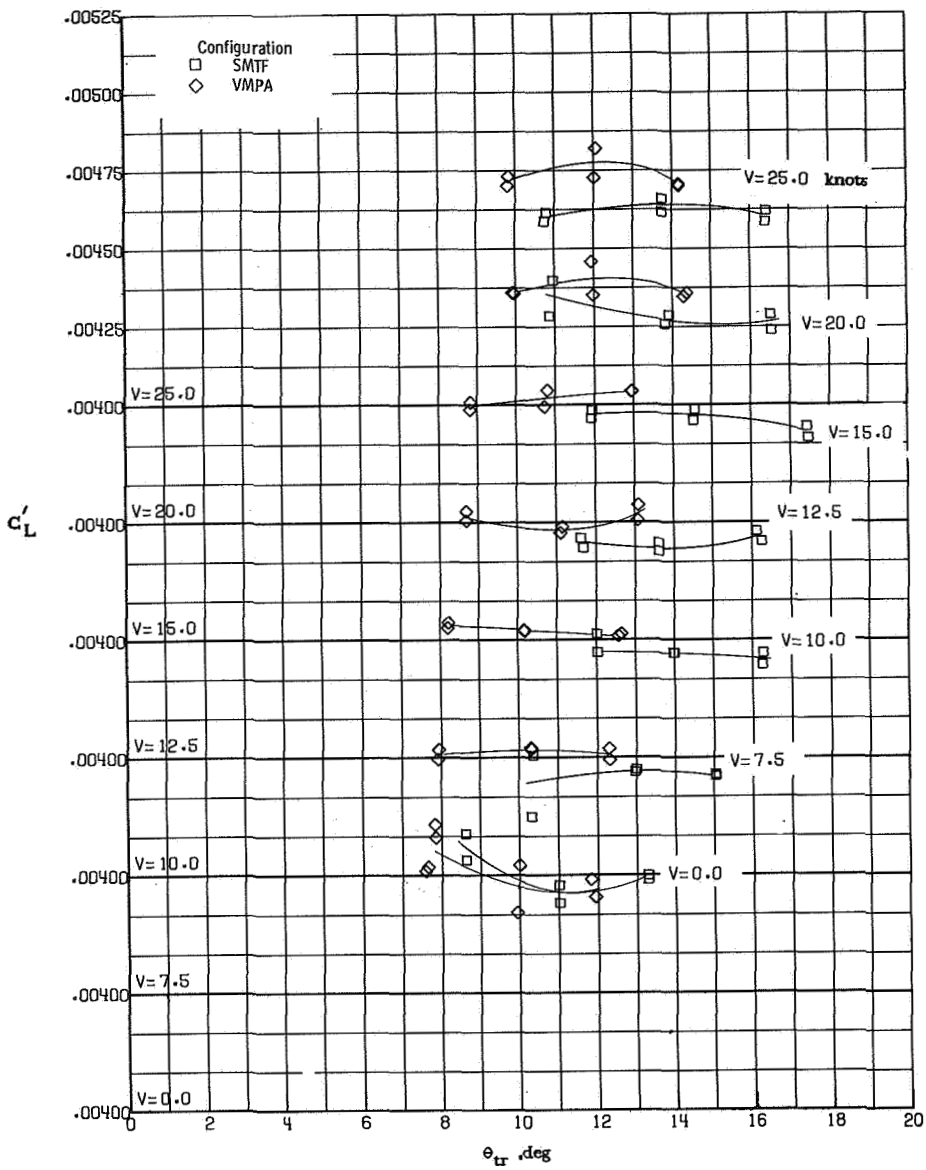

(d) Main-rotor lift.

Figure 28.- Continued.

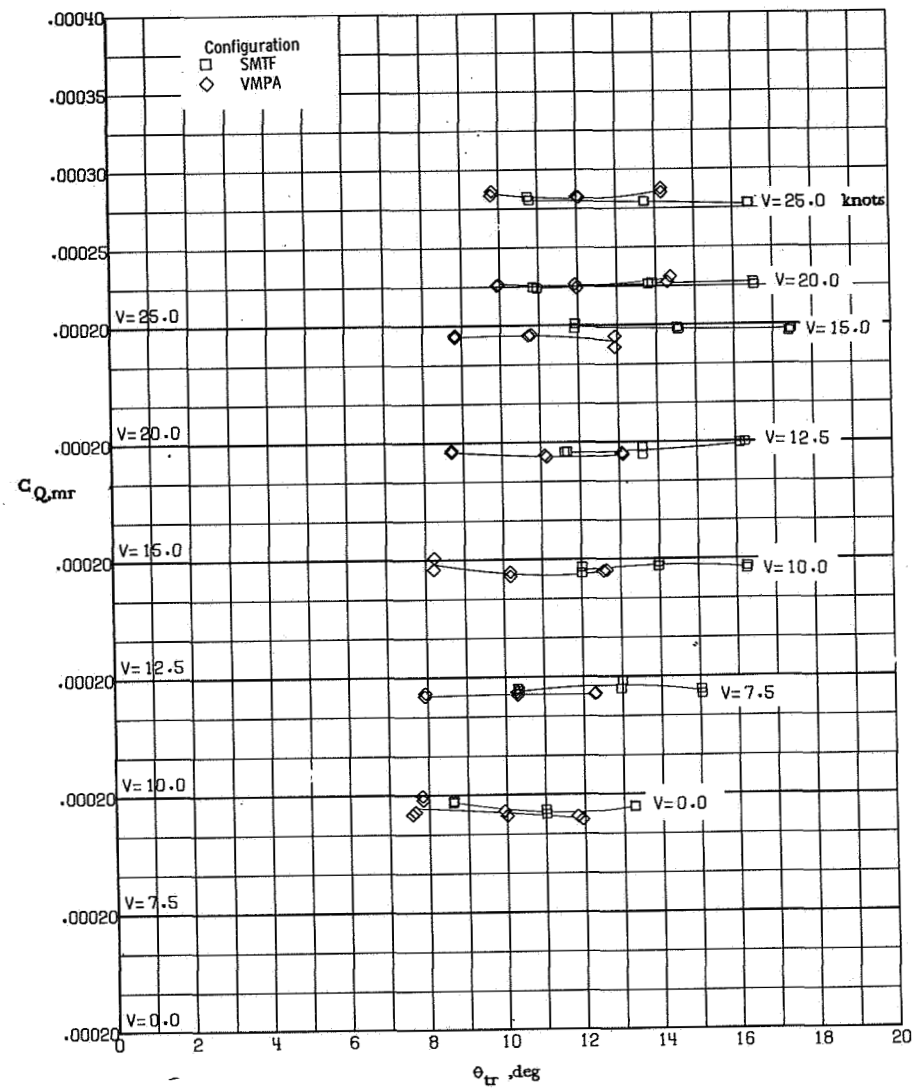

(e) Main-rotor torque.

Figure 28.- Continued.

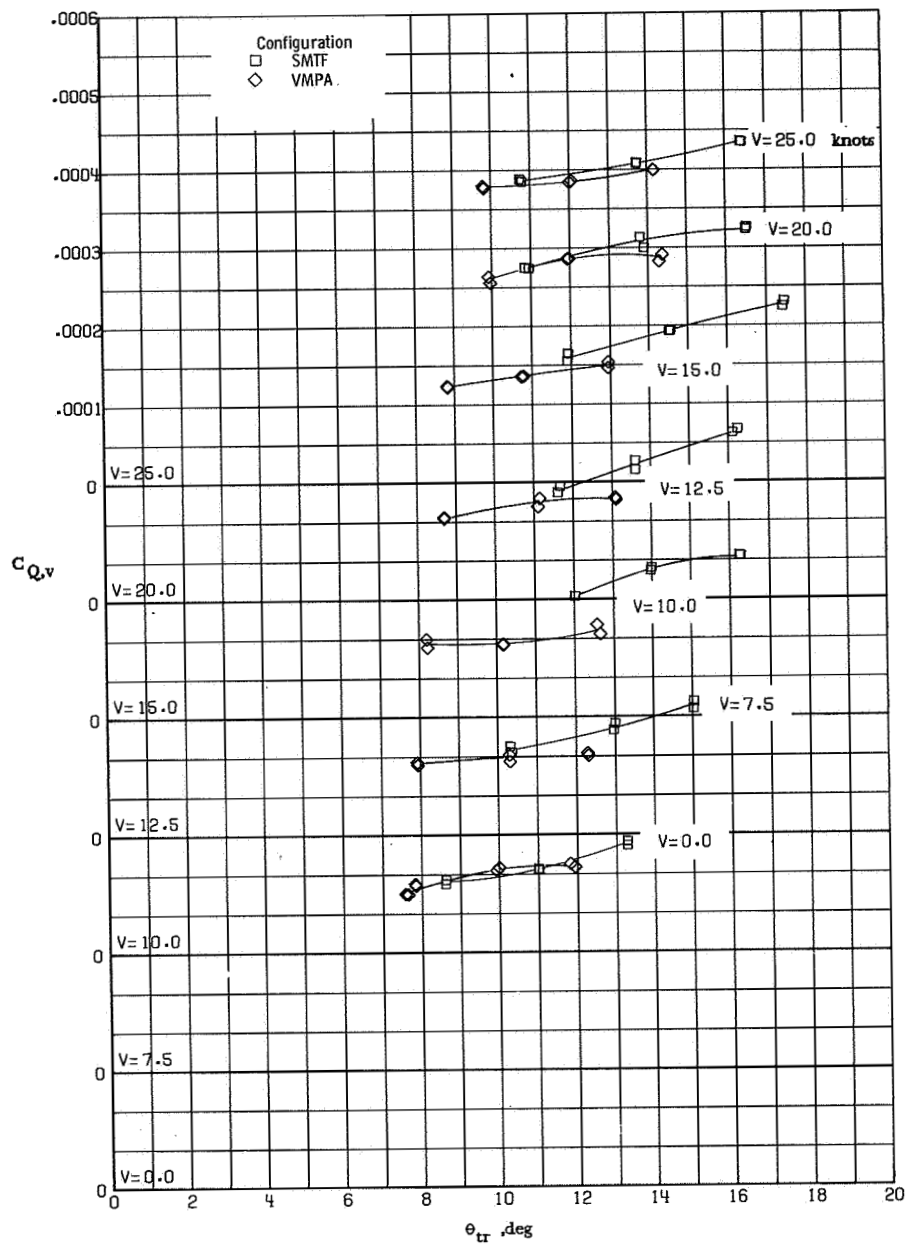

(f) Vehicle torque.

Figure 28.- Continued.

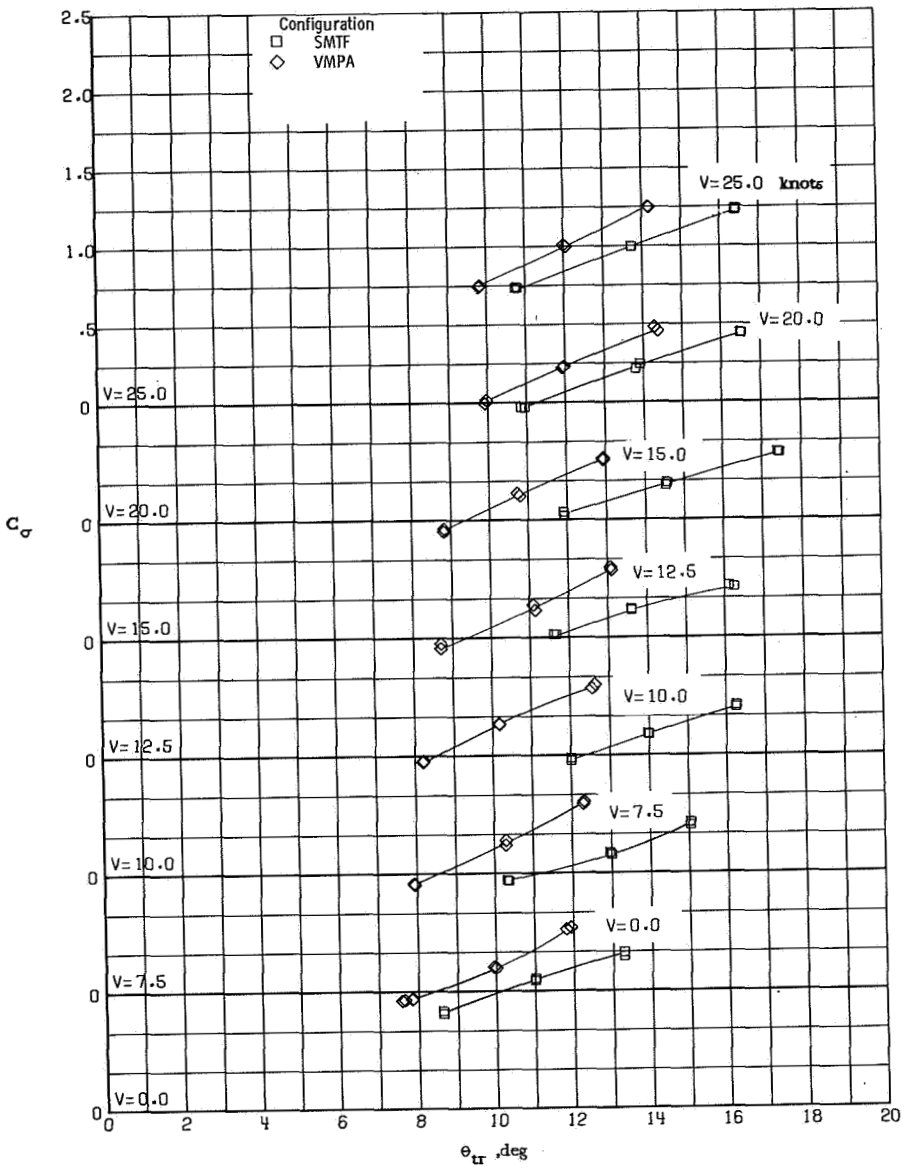

(g) Torque balance factor.

Figure 28.- Concluded.

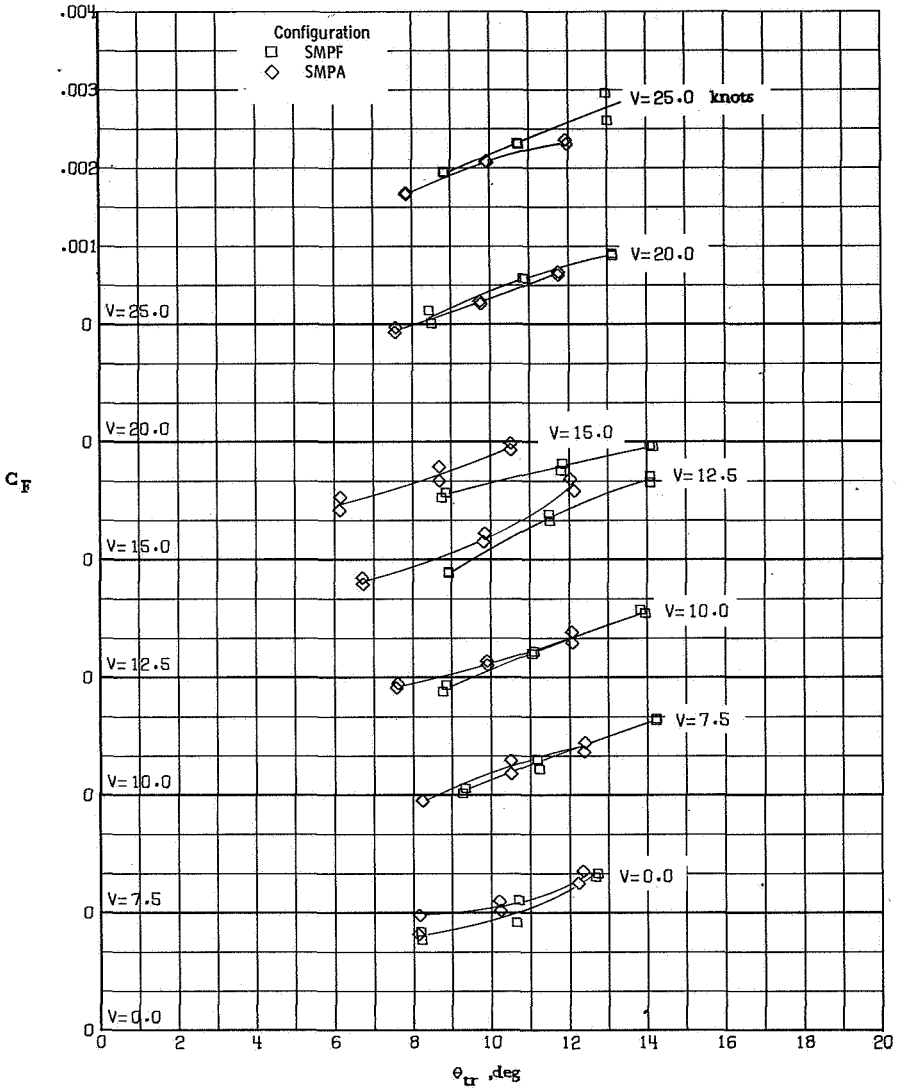

(a) Fin force.

Figure 29.- Aerodynamic characteristics of configurations with a pusher tail rotor at $\beta = 150^{o}$.

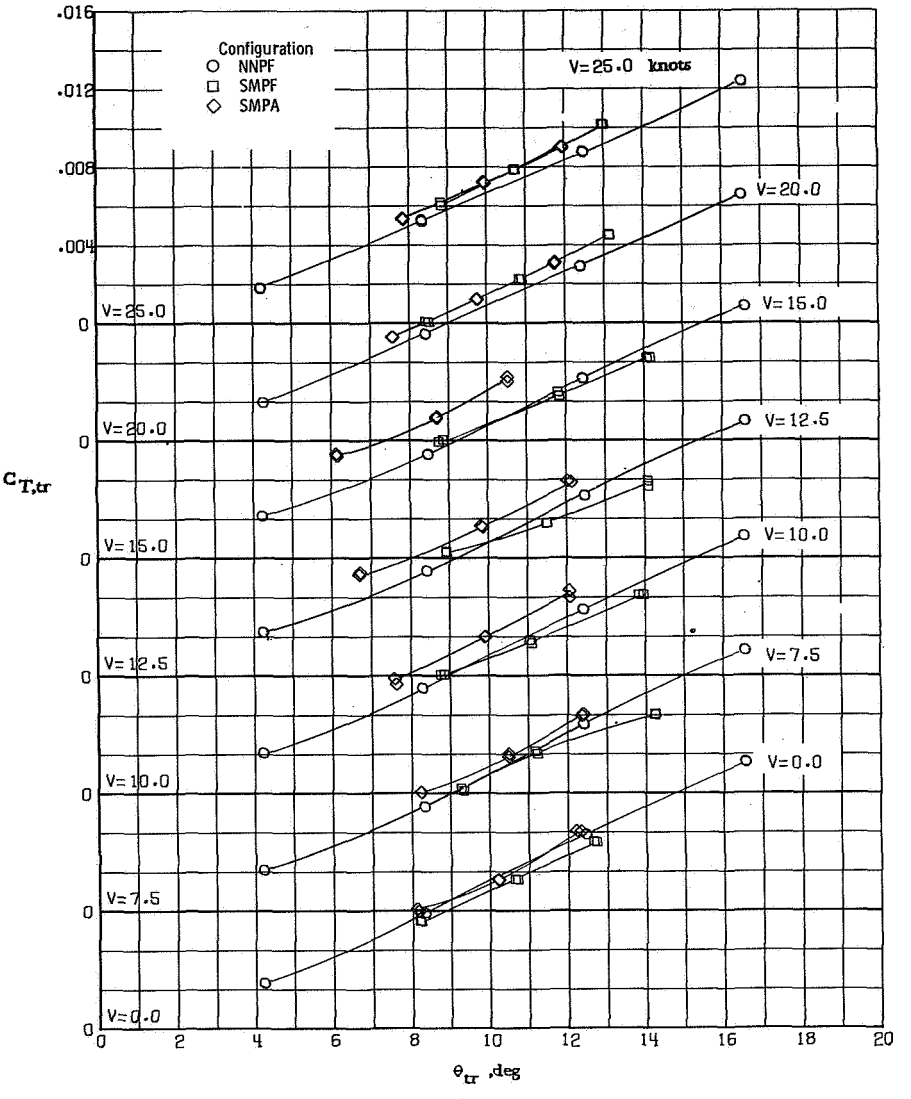

(b) Tail-rotor thrust.

Figure 29.- Continued.

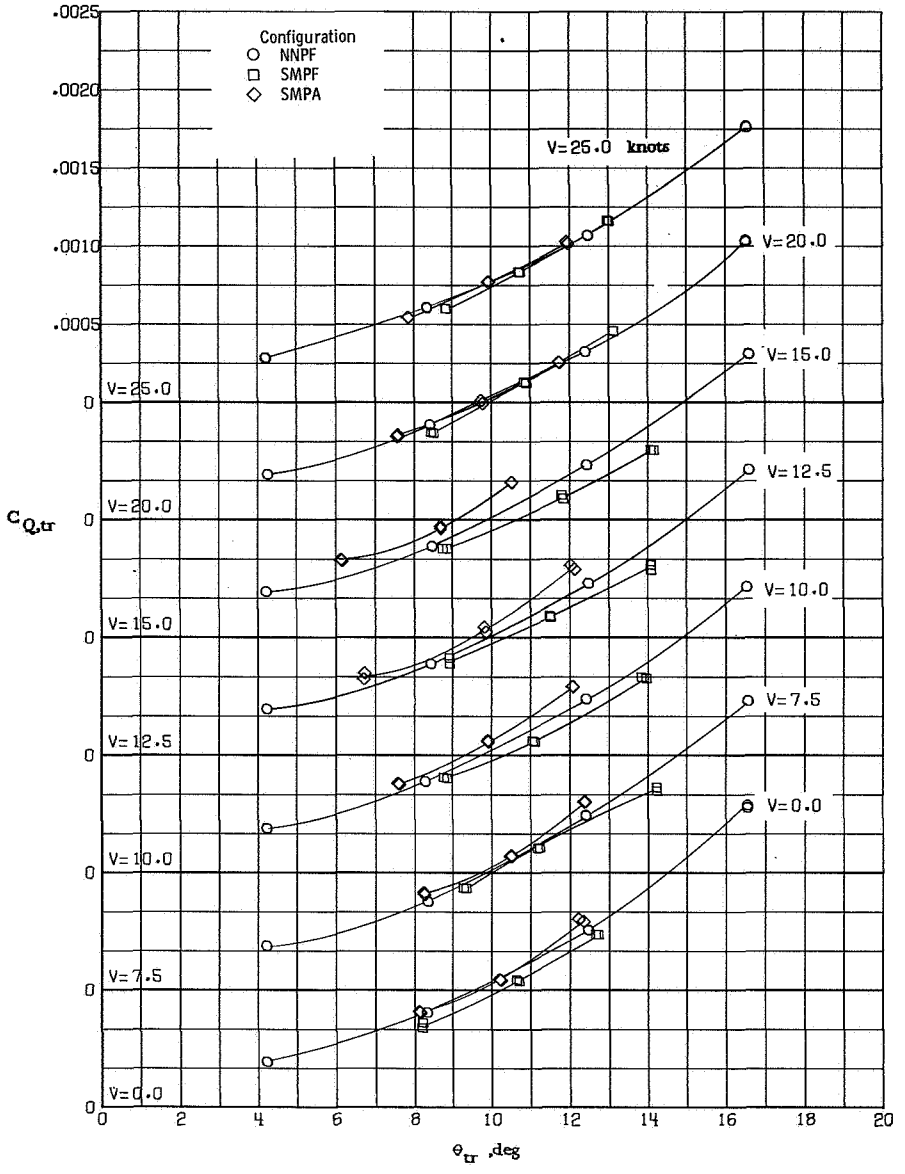

(c) Tail-rotor torque.

Figure 29.- Continued.

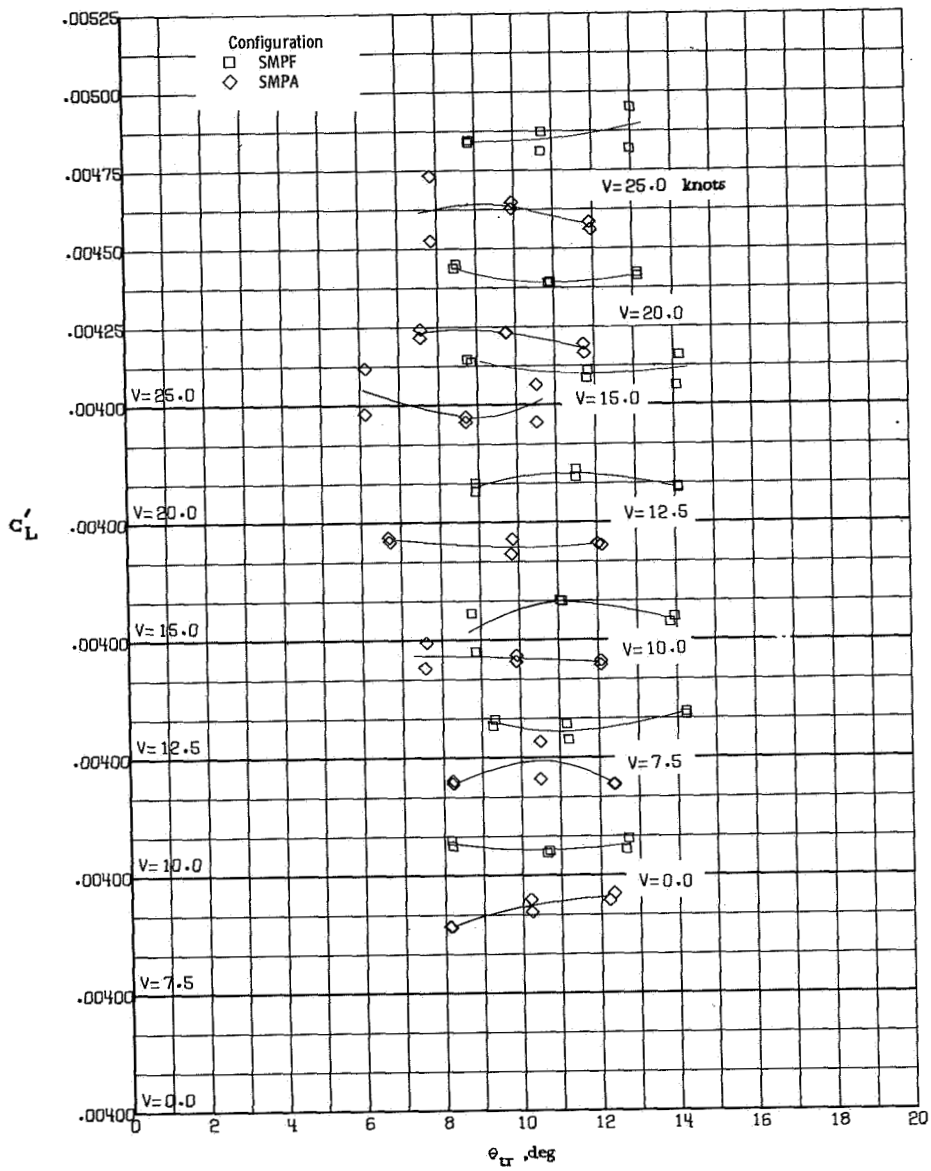

(d) Main-rotor lift.

Figure 29.- Continued.

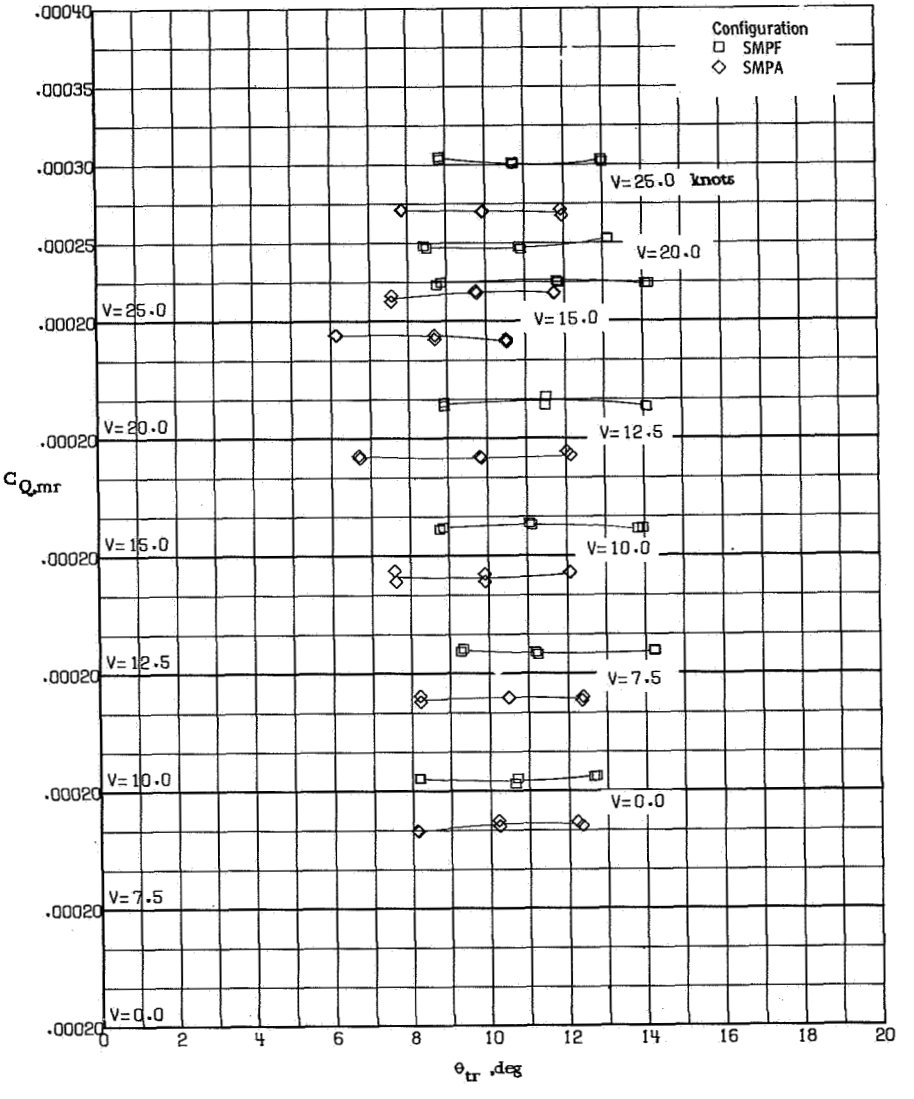

(e) Main-rotor torque.

Figure 29.- Continued.

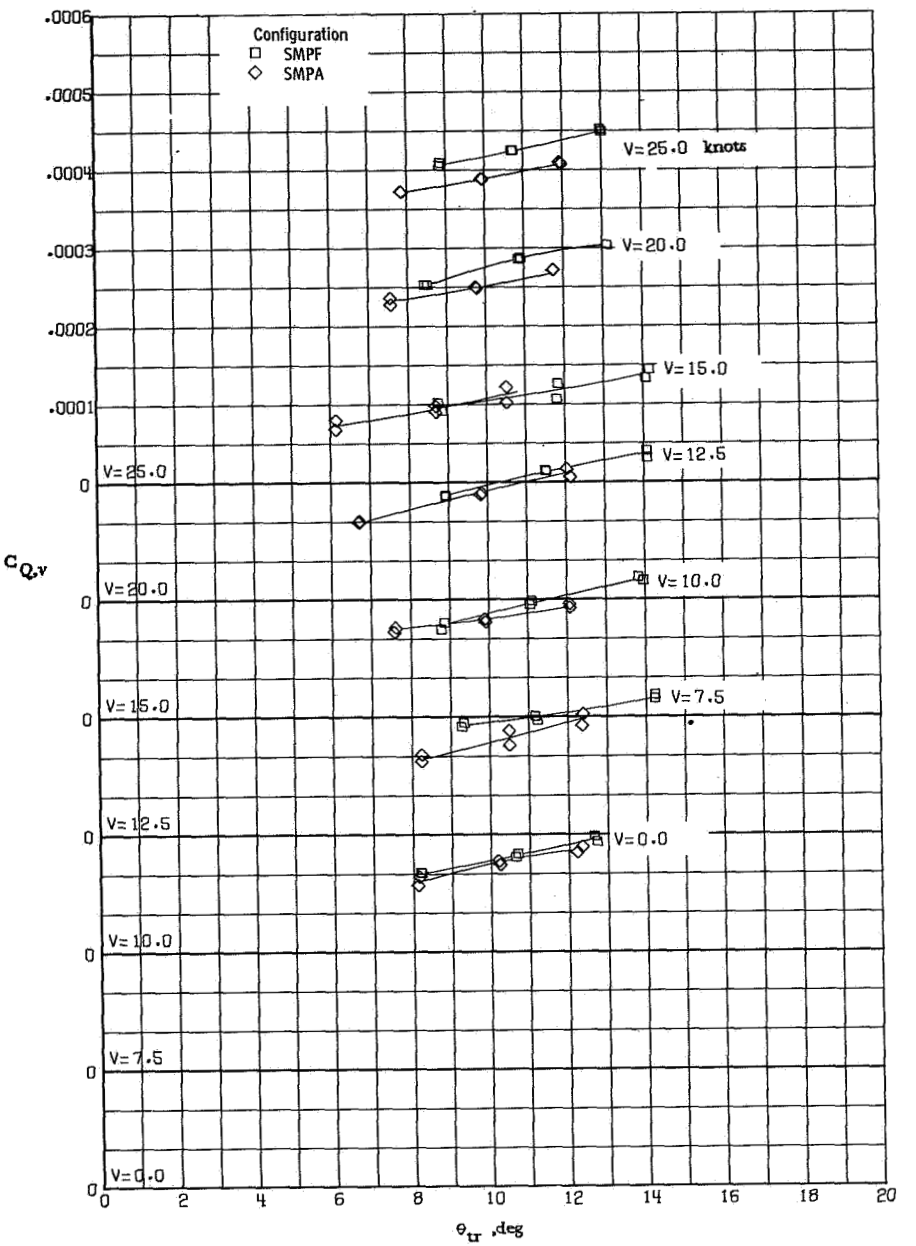

(f) Vehicle torque.

Figure 29.- Continued.

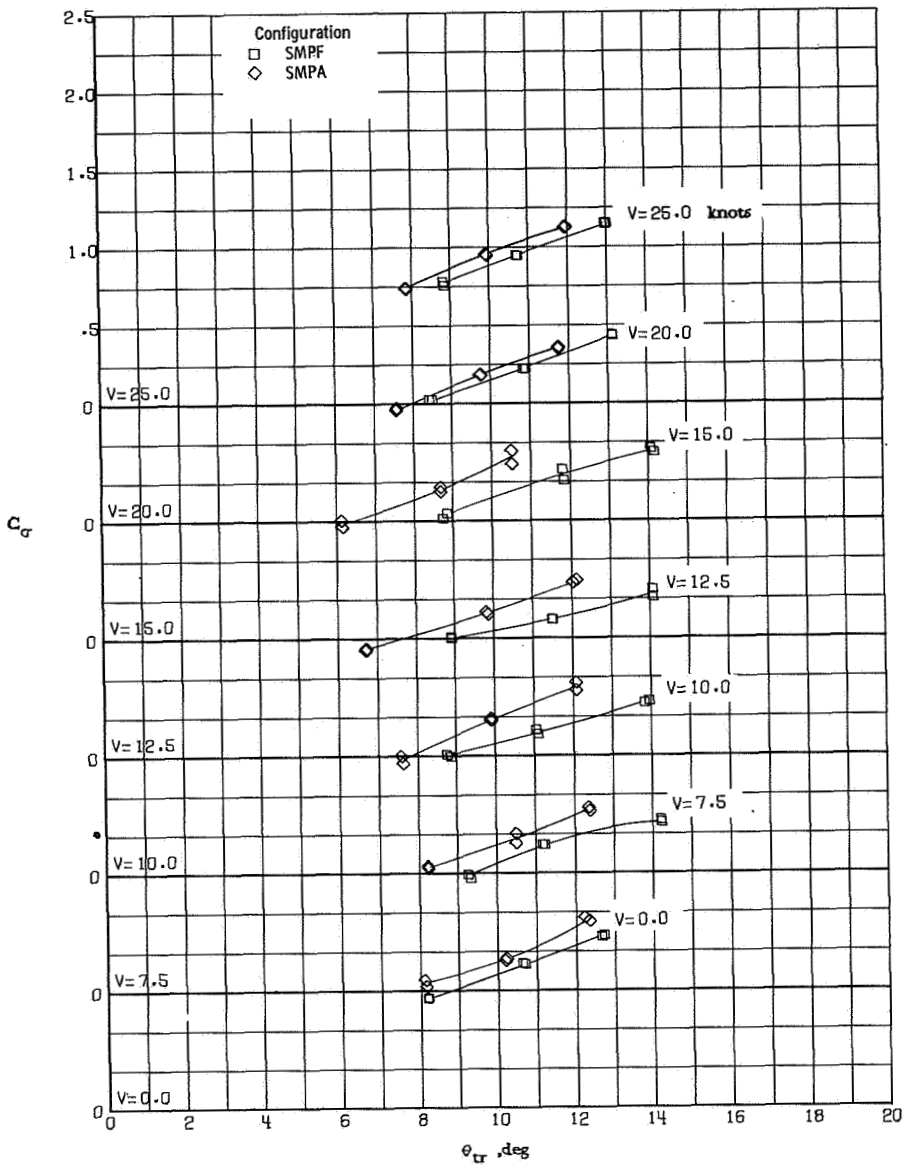

(g) Torque balance factor.

Figure 29.- Concluded.

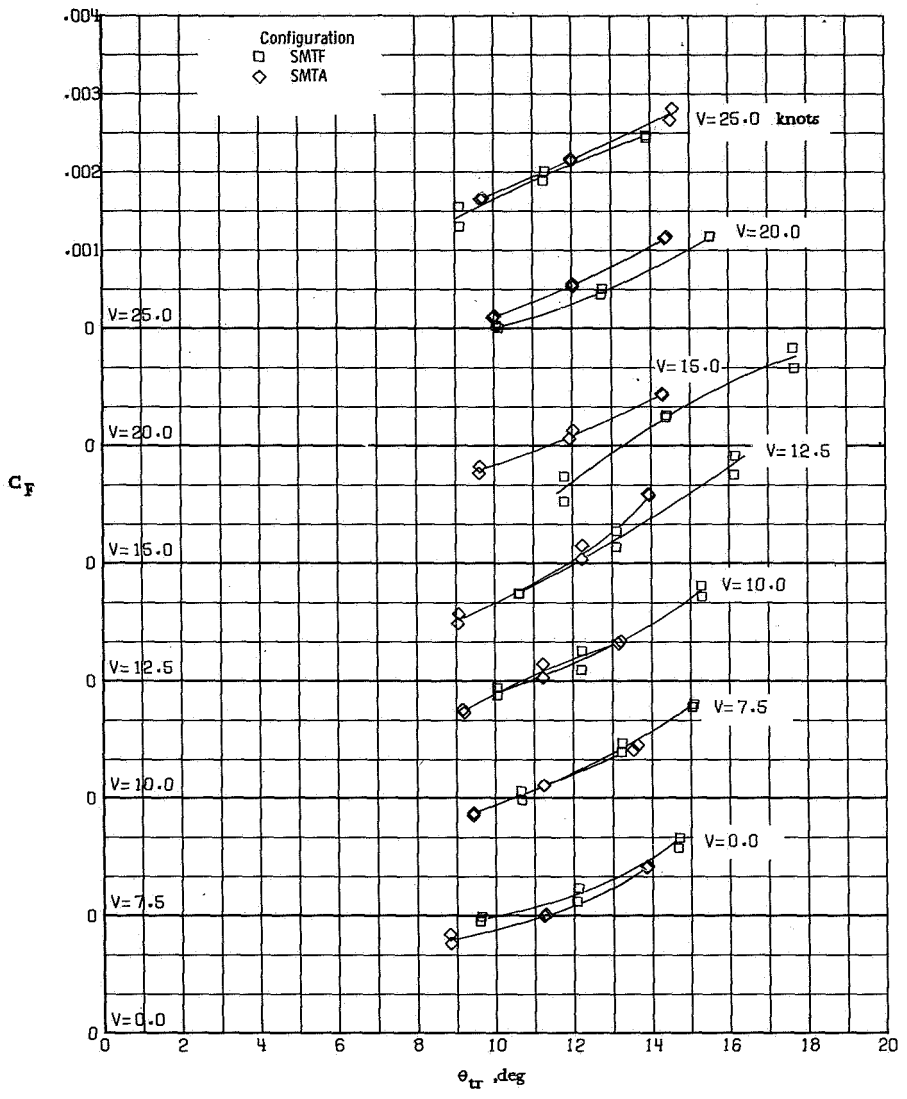

(a) Fin force.

Figure 30.- Aerodynamic characteristics of various configurations with and without the main rotor at $\beta = 150^{o}$.

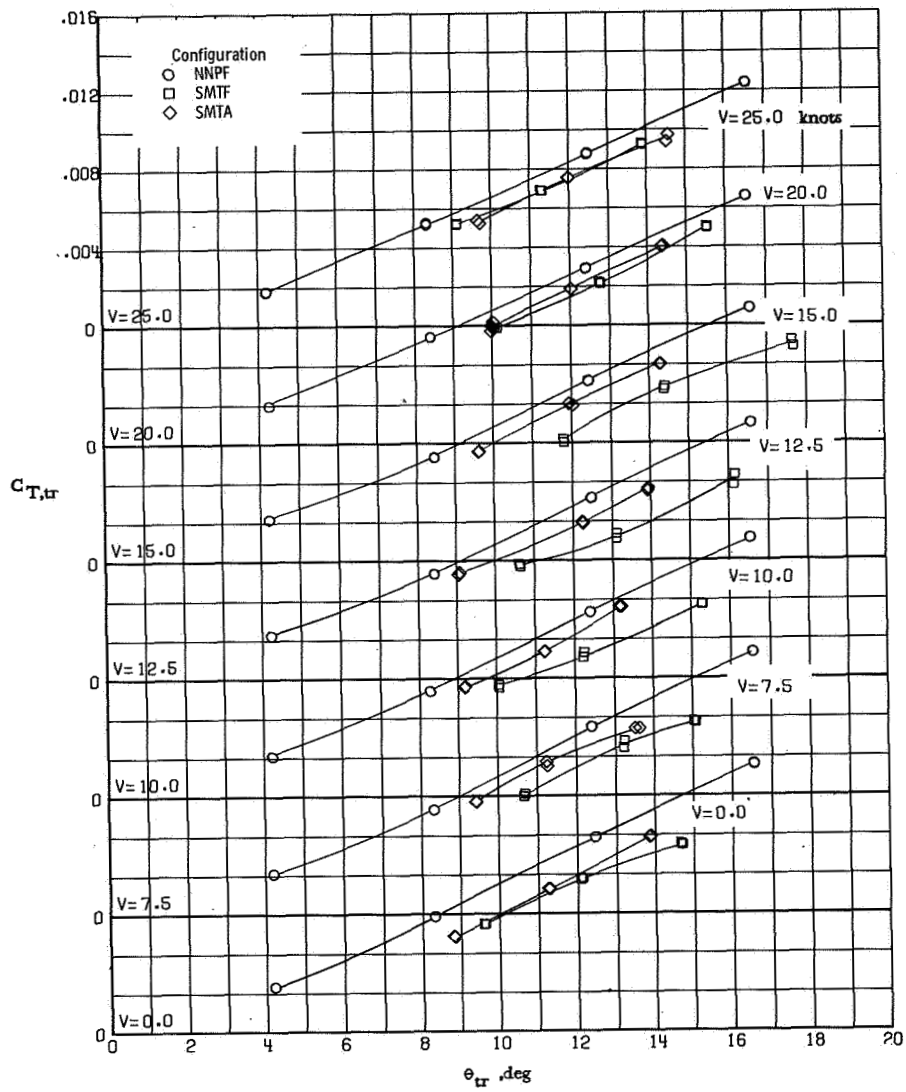

(b) Tail-rotor thrust.

Figure 30.- Continued.

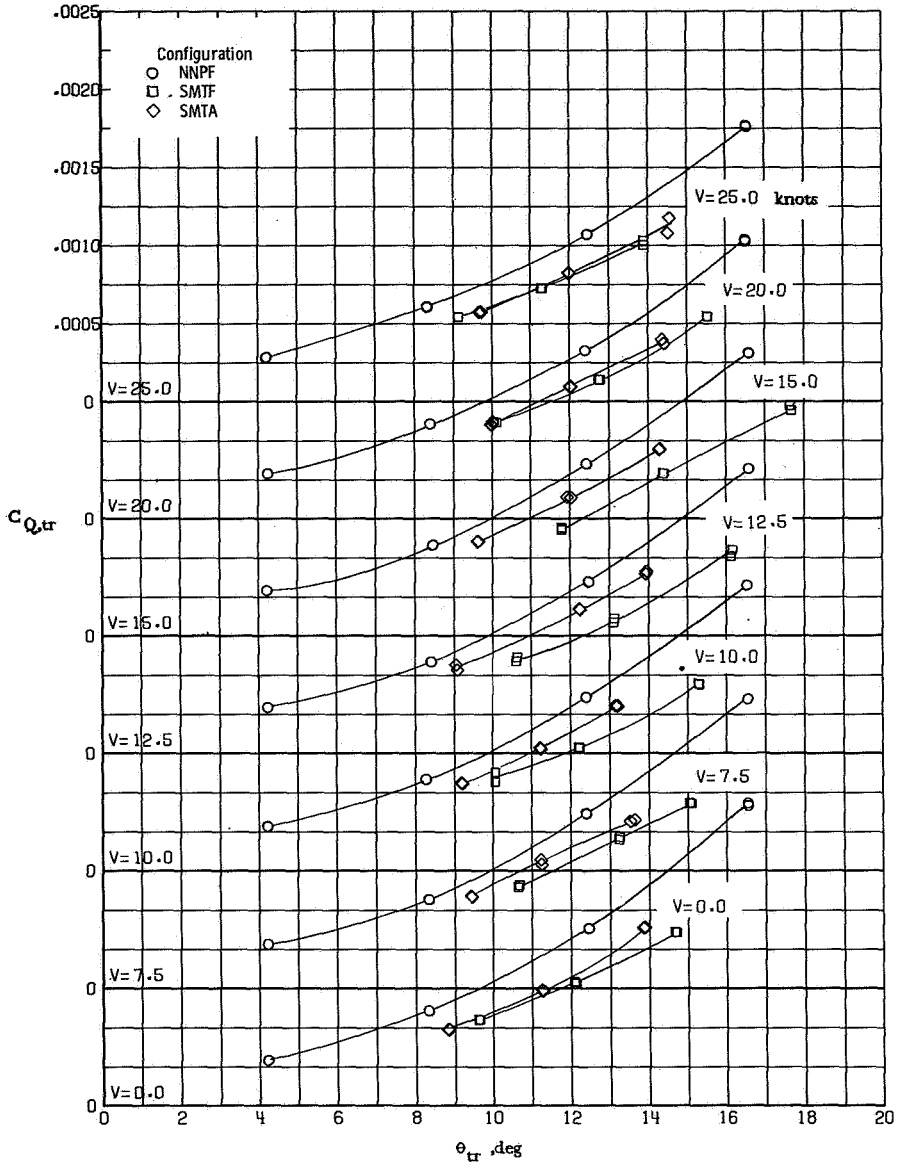

(c) Tail-rotor torque.

Figure 30.- Continued.

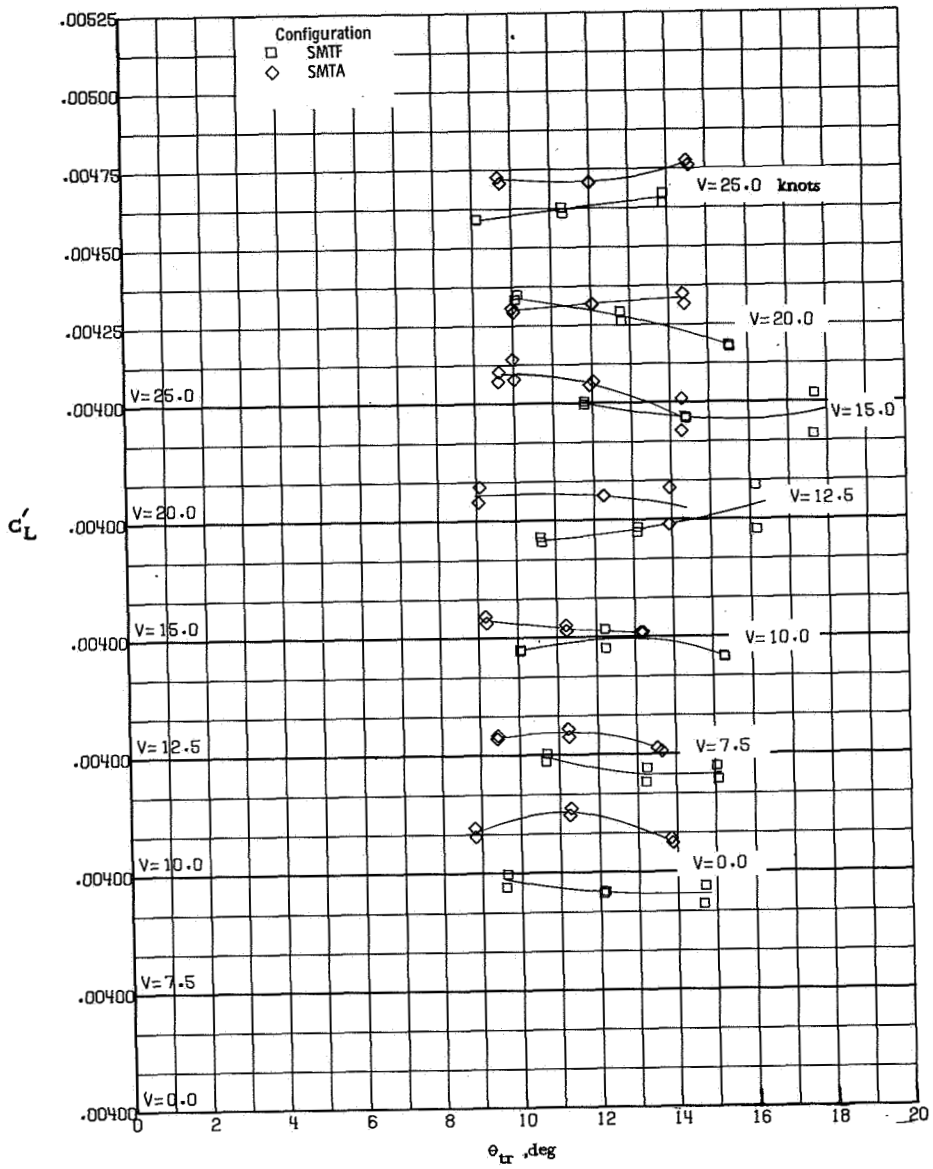

(d) Main-rotor lift.

Figure 30.- Continued.

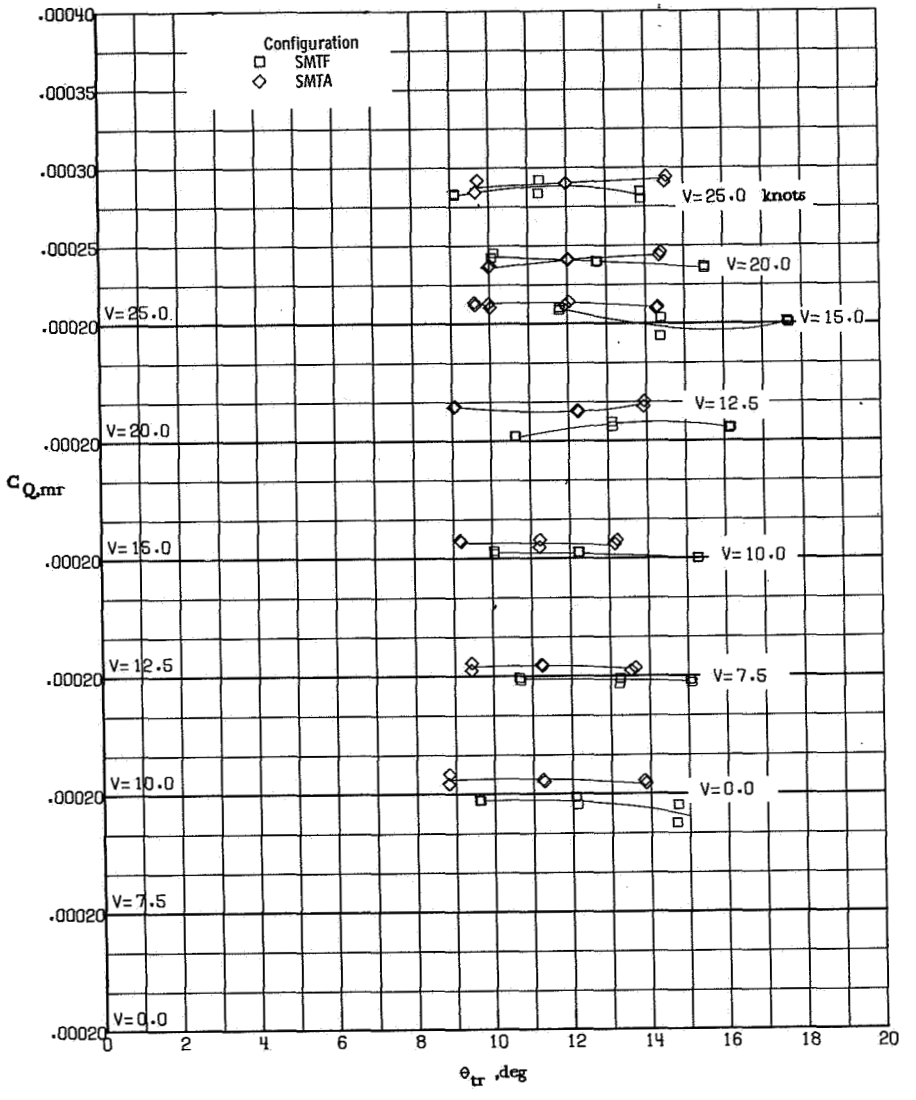

(e) Main-rotor torque.

Figure 30.- Continued.

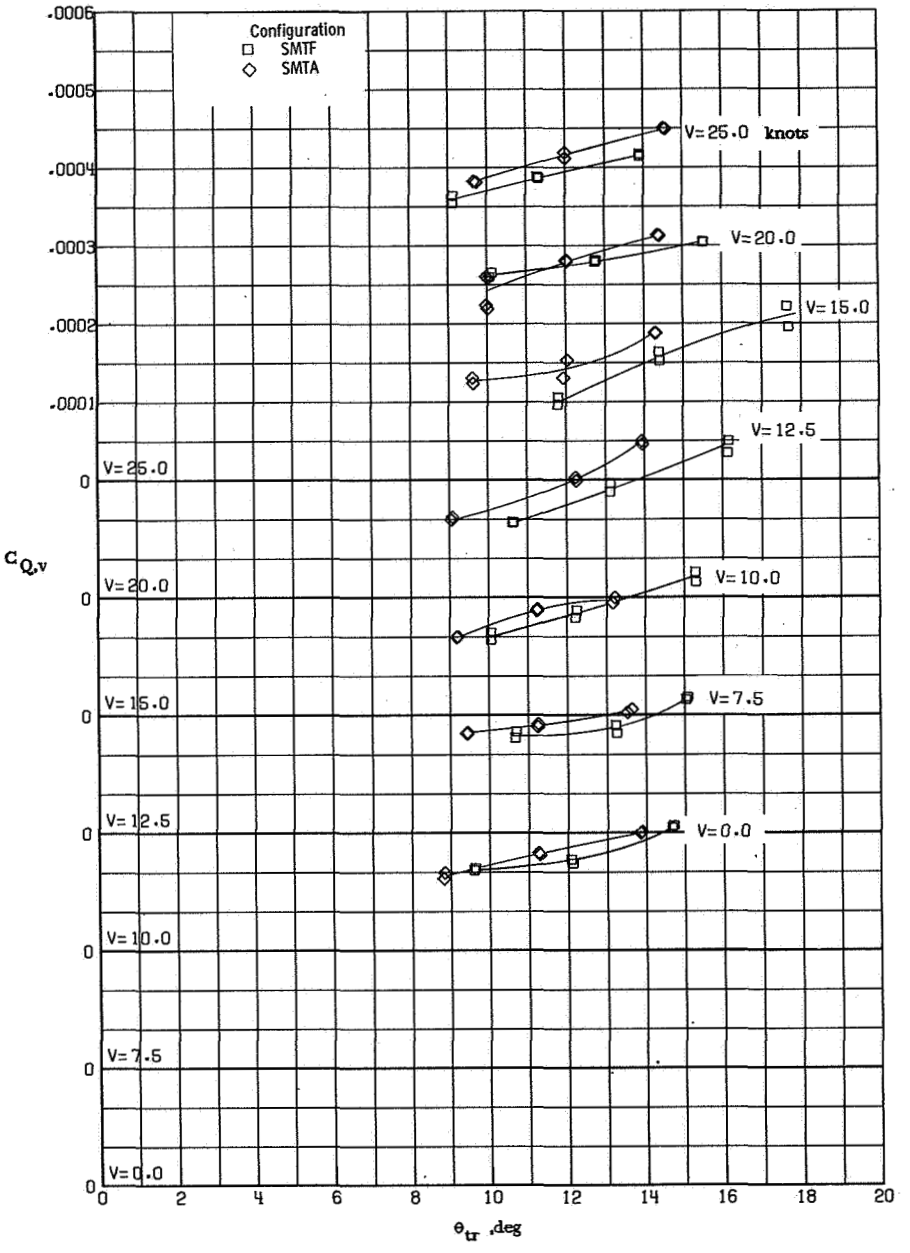

(f) Vehicle torque.

Figure 30.- Continued.

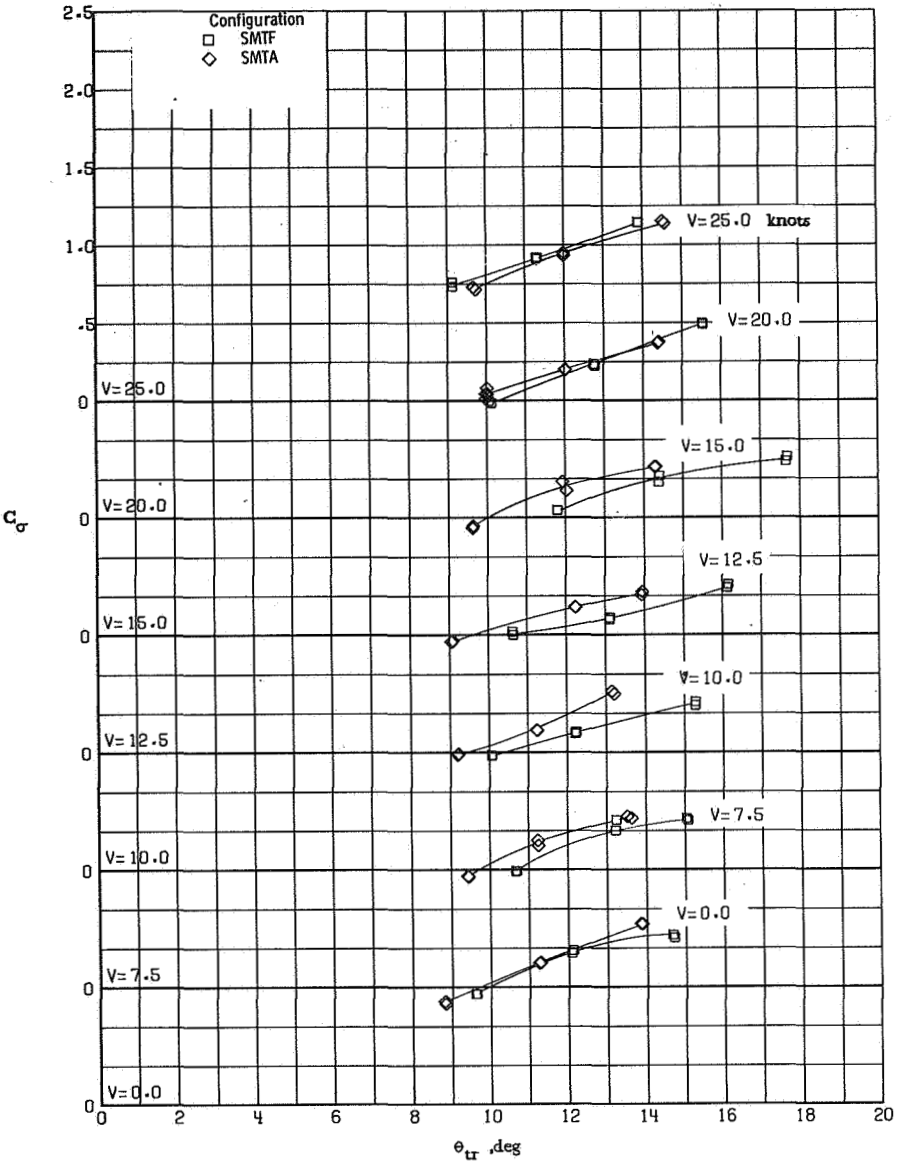

(g) Torque balance factor.

Figure 30.- Concluded.

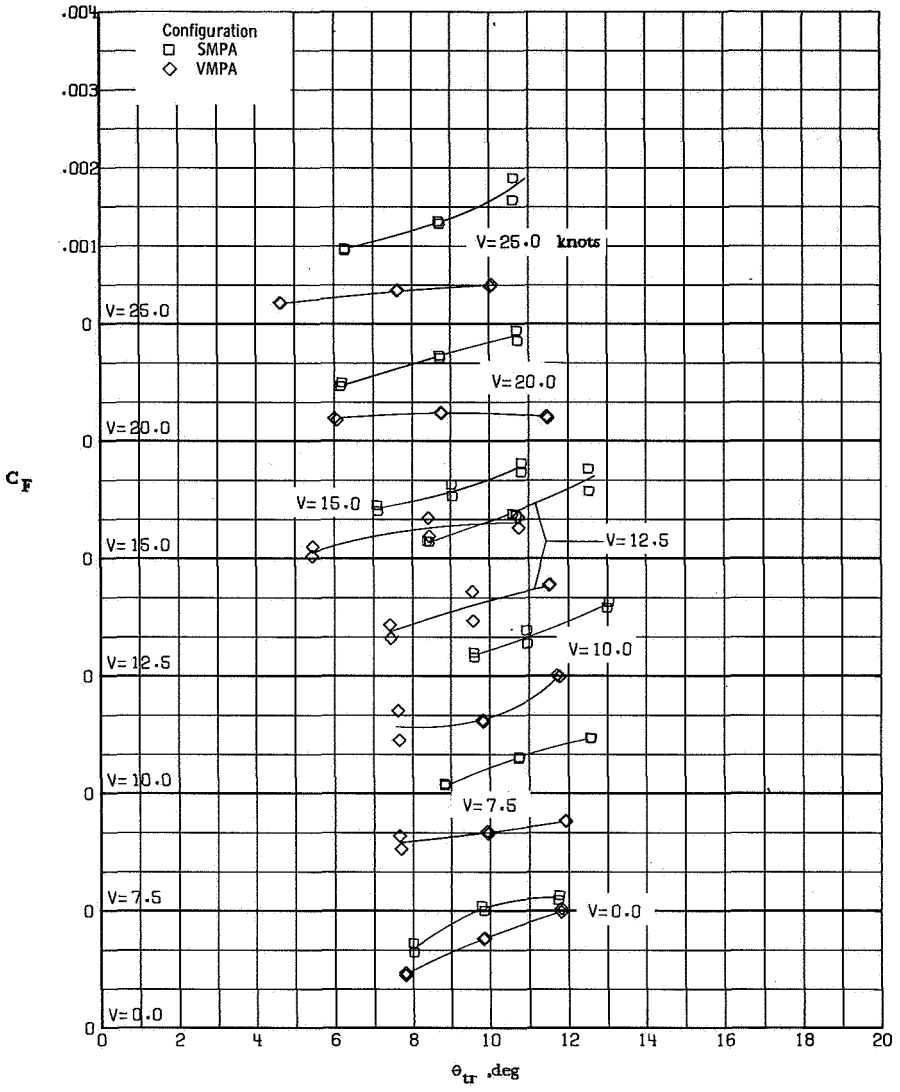

(a) Fin force.

Figure 31.- Aerodynamic characteristics of configurations with a pusher tail rotor at $\beta = 180^{o}$.

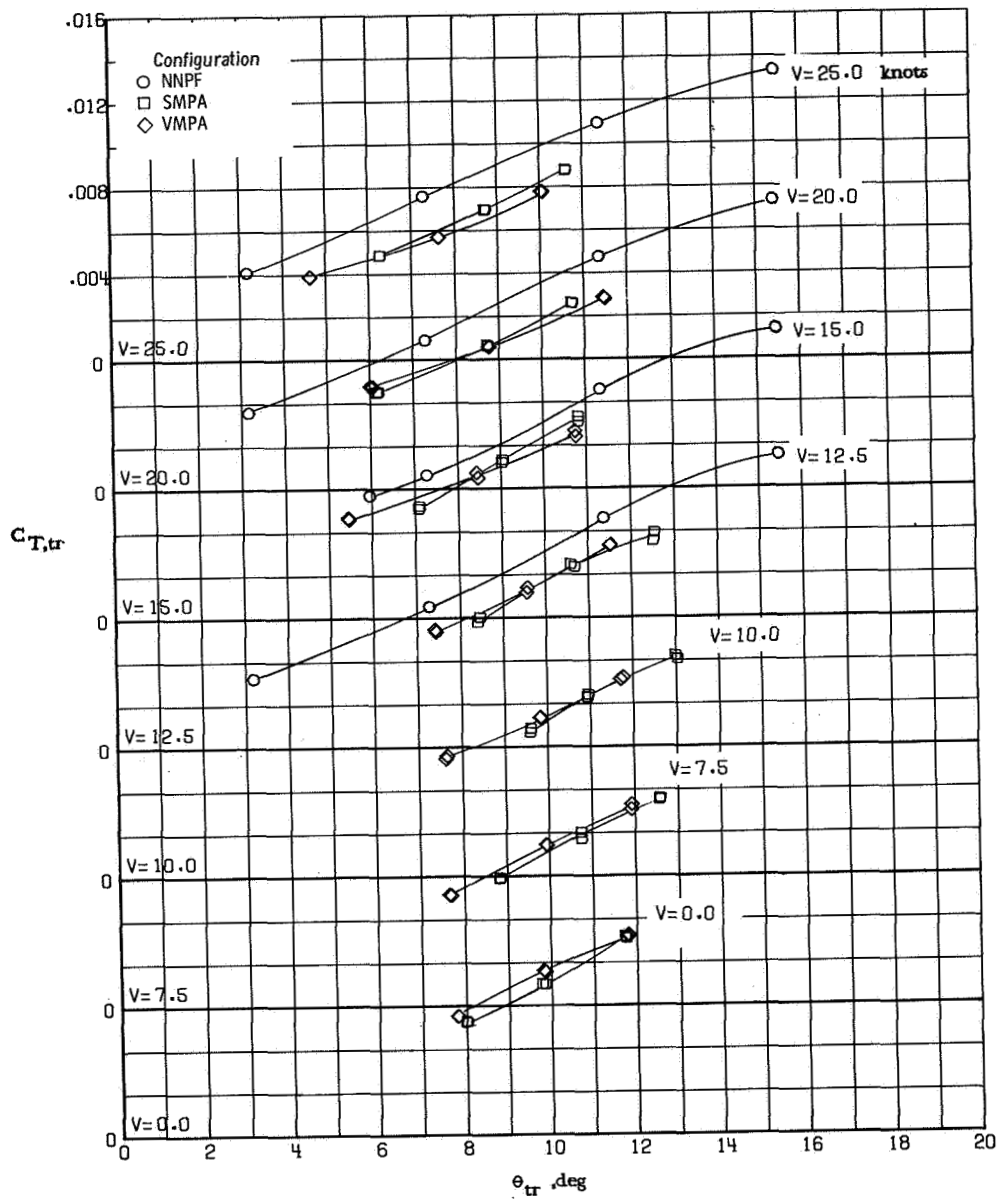

(b) Tail-rotor thrust.

Figure 31.- Continued.

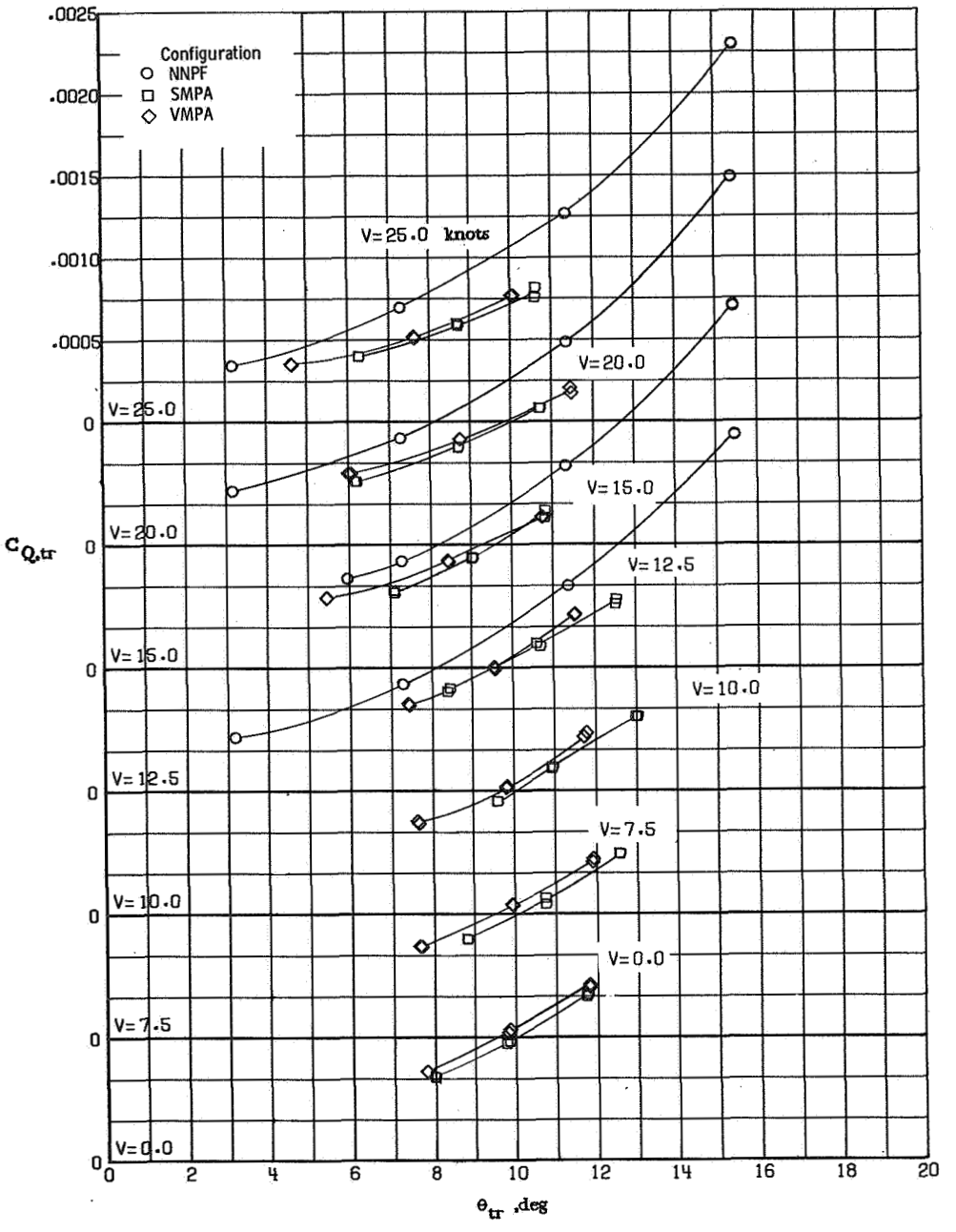

(c) Tail-rotor torque.

Figure 31.- Continued.

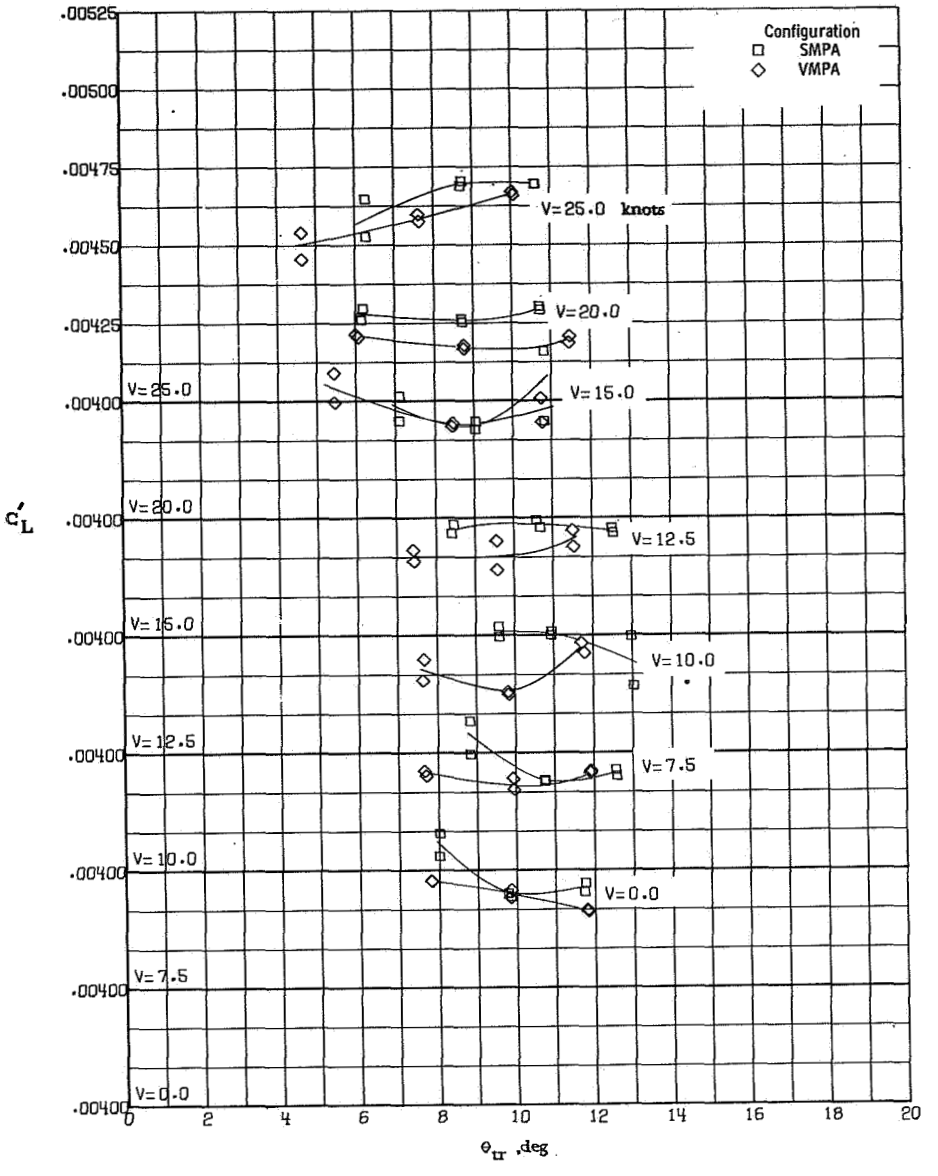

(d) Main-rotor lift.

Figure 31.- Continued.

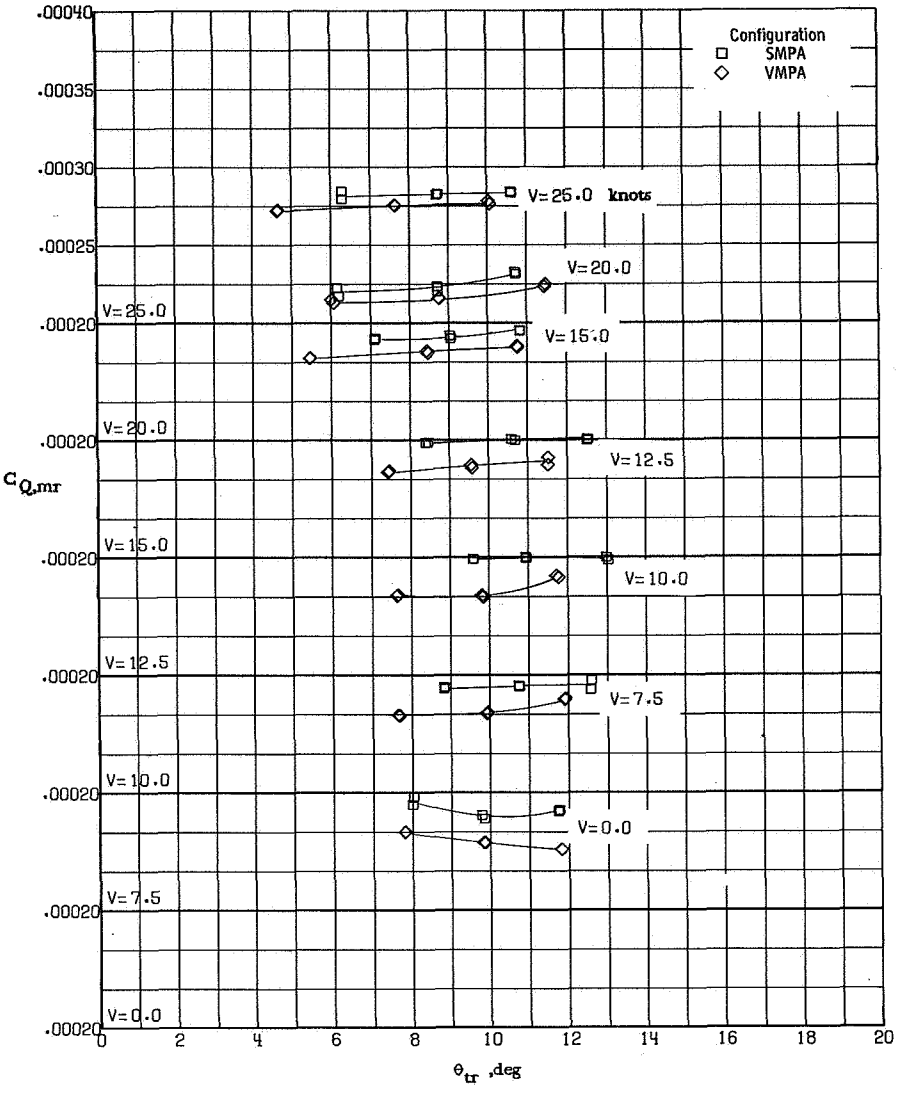

(e) Main-rotor torque.

Figure 31.- Continued.

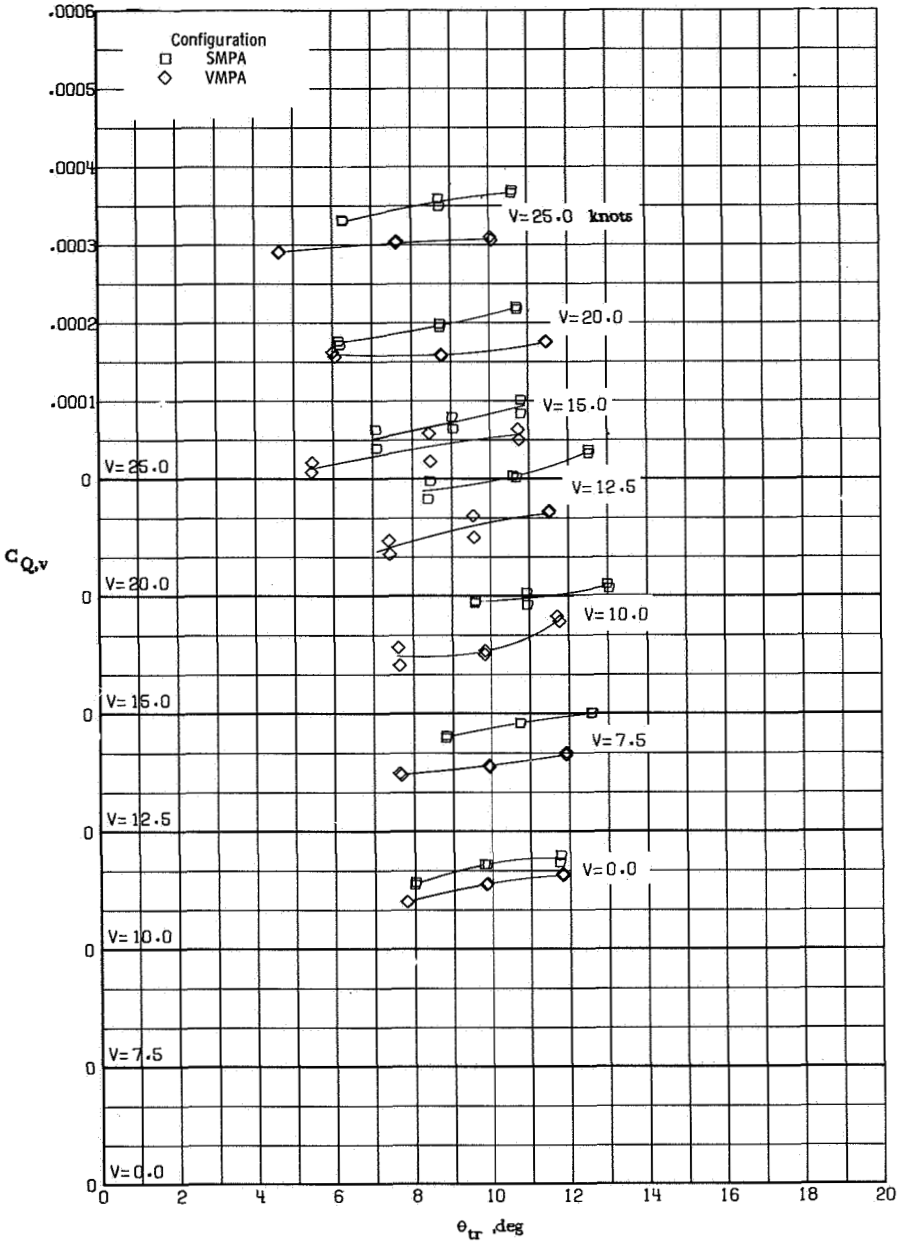

(f) Vehicle torque.

Figure 31.- Continued.

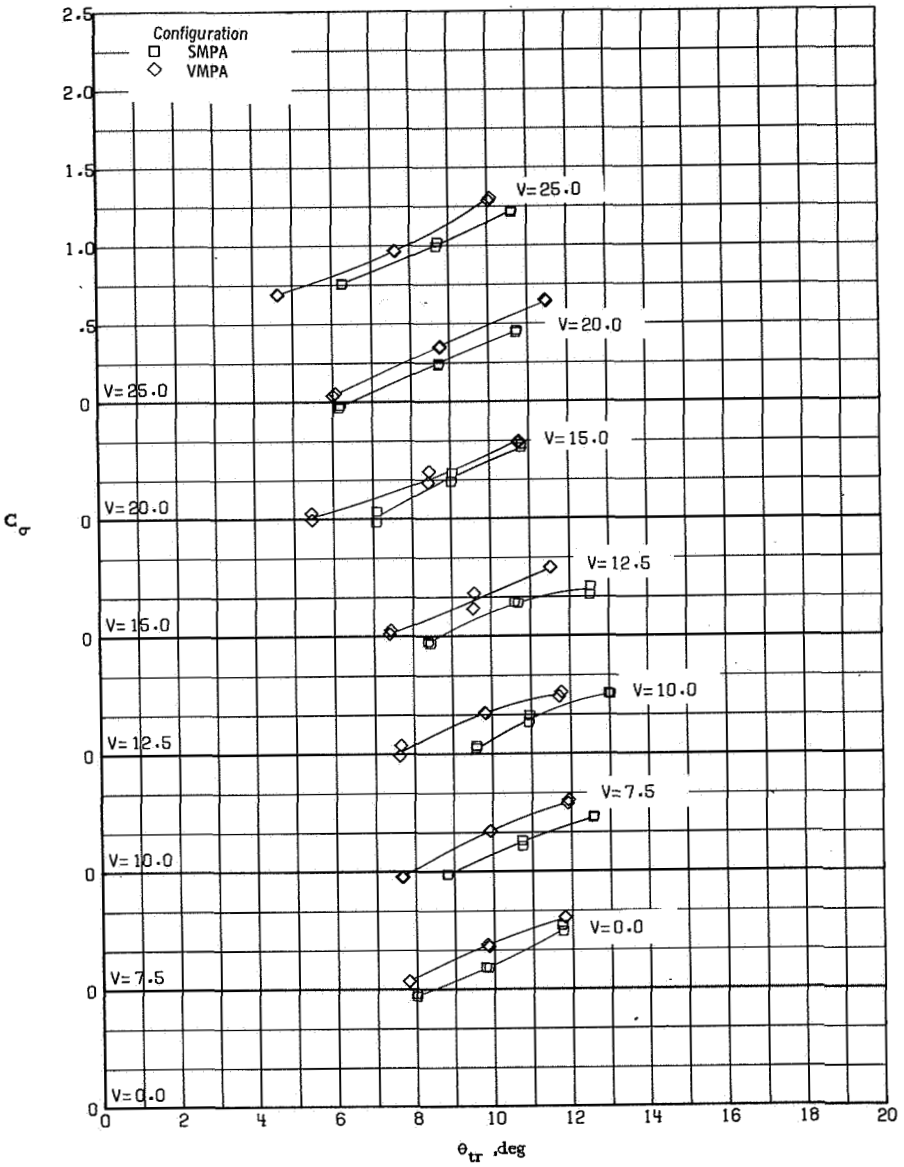

(g) Torque balance factor.

Figure 31.- Concluded.

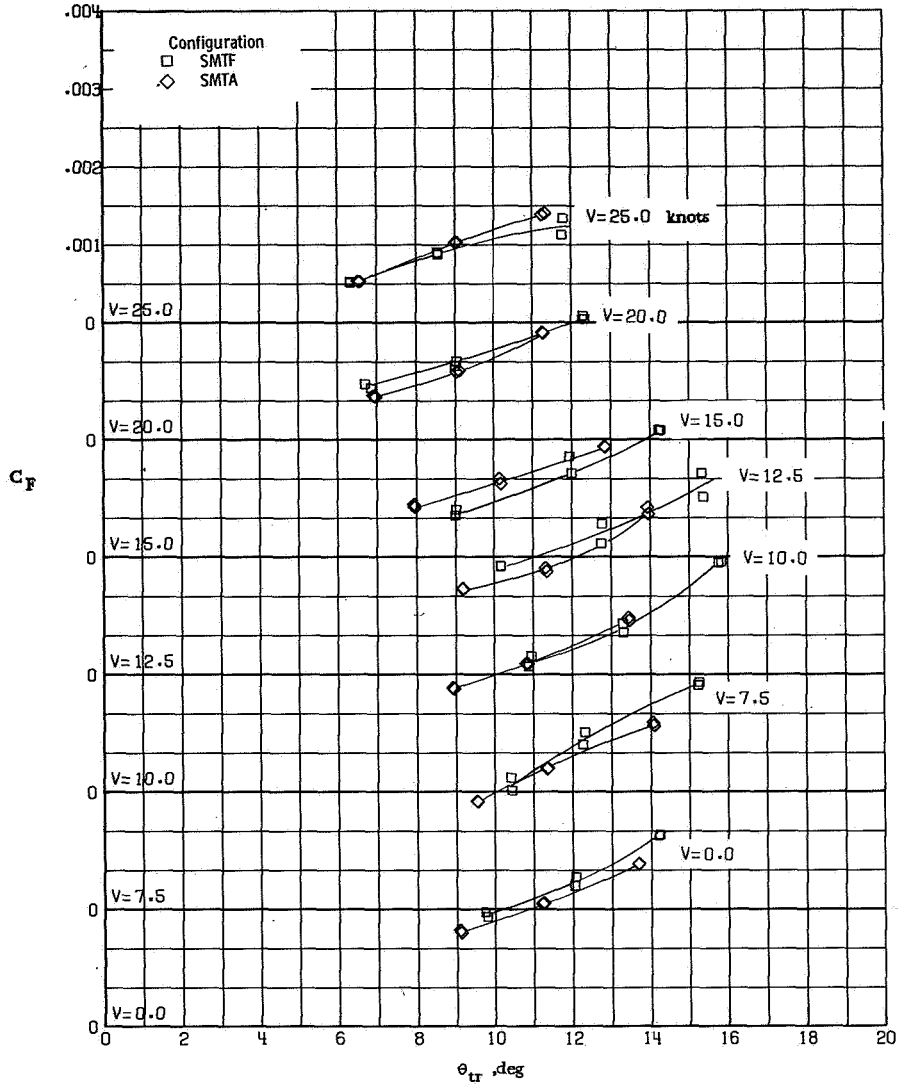

(a) Fin force.

Figure 32.- Aerodynamic characteristics of various configurations with and without the main rotor at $\beta = 180^{o}$.

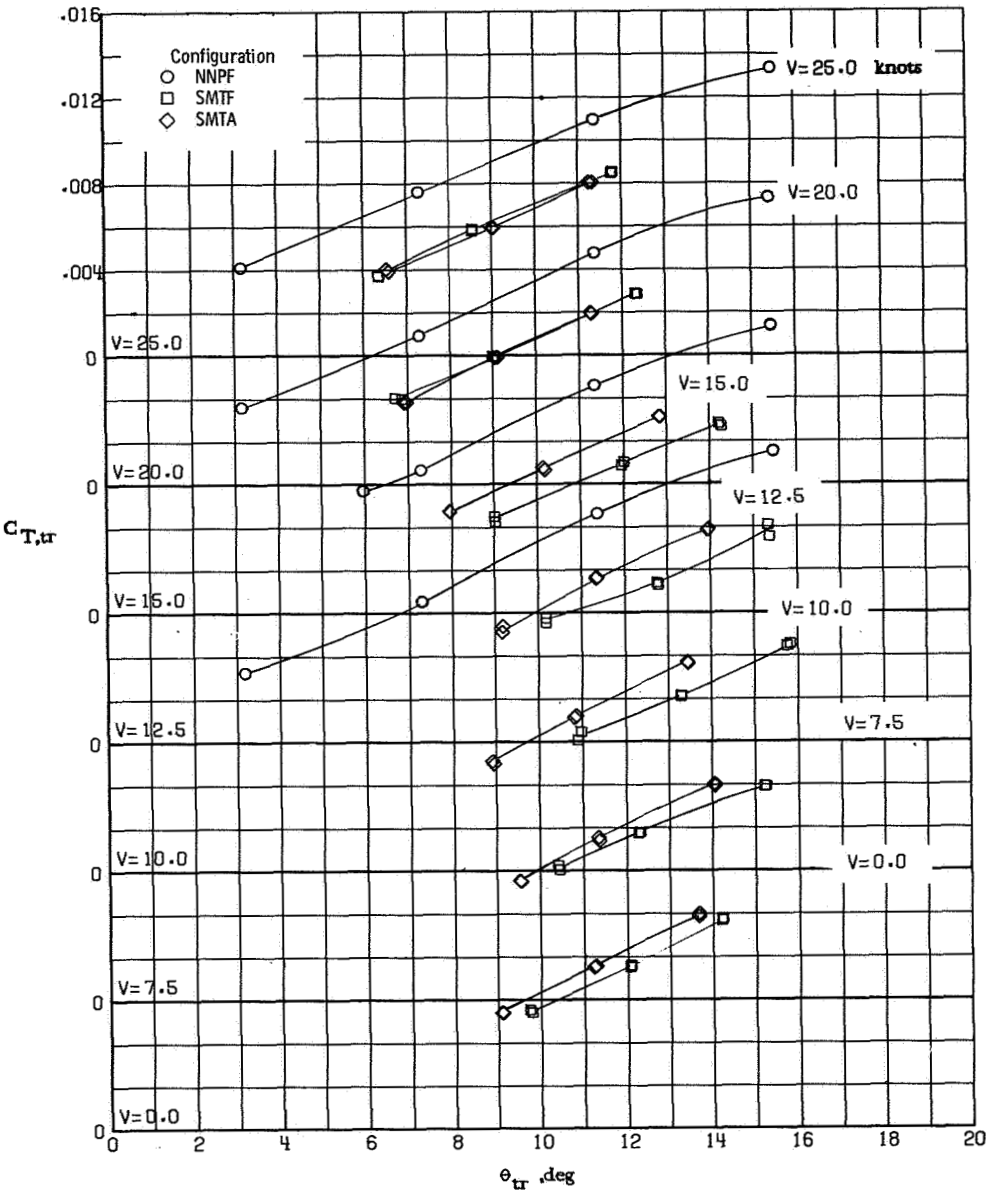

(b) Tail-rotor thrust.

Figure 32.- Continued.

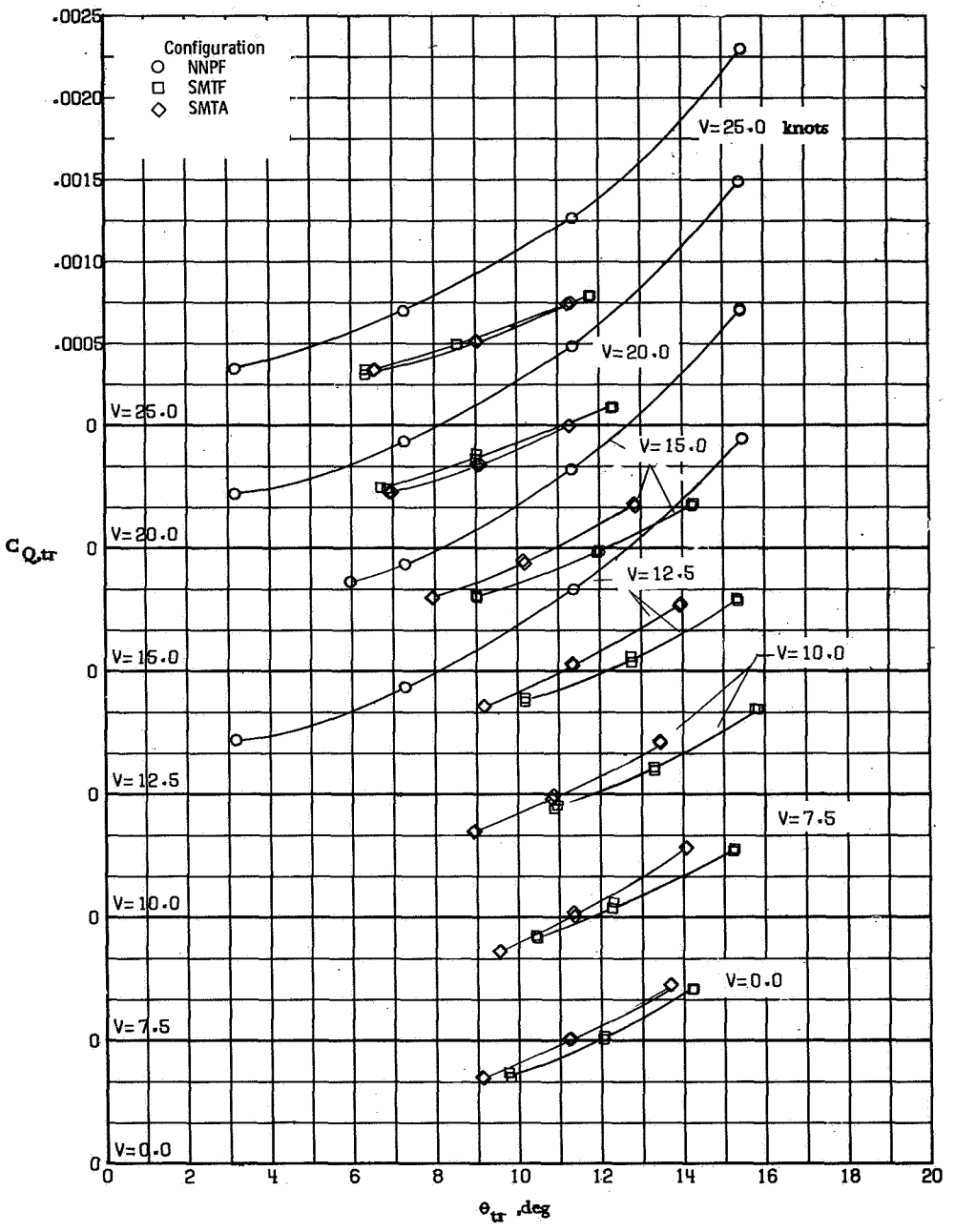

(c) Tail-rotor torque.

Figure 32.- Continued.

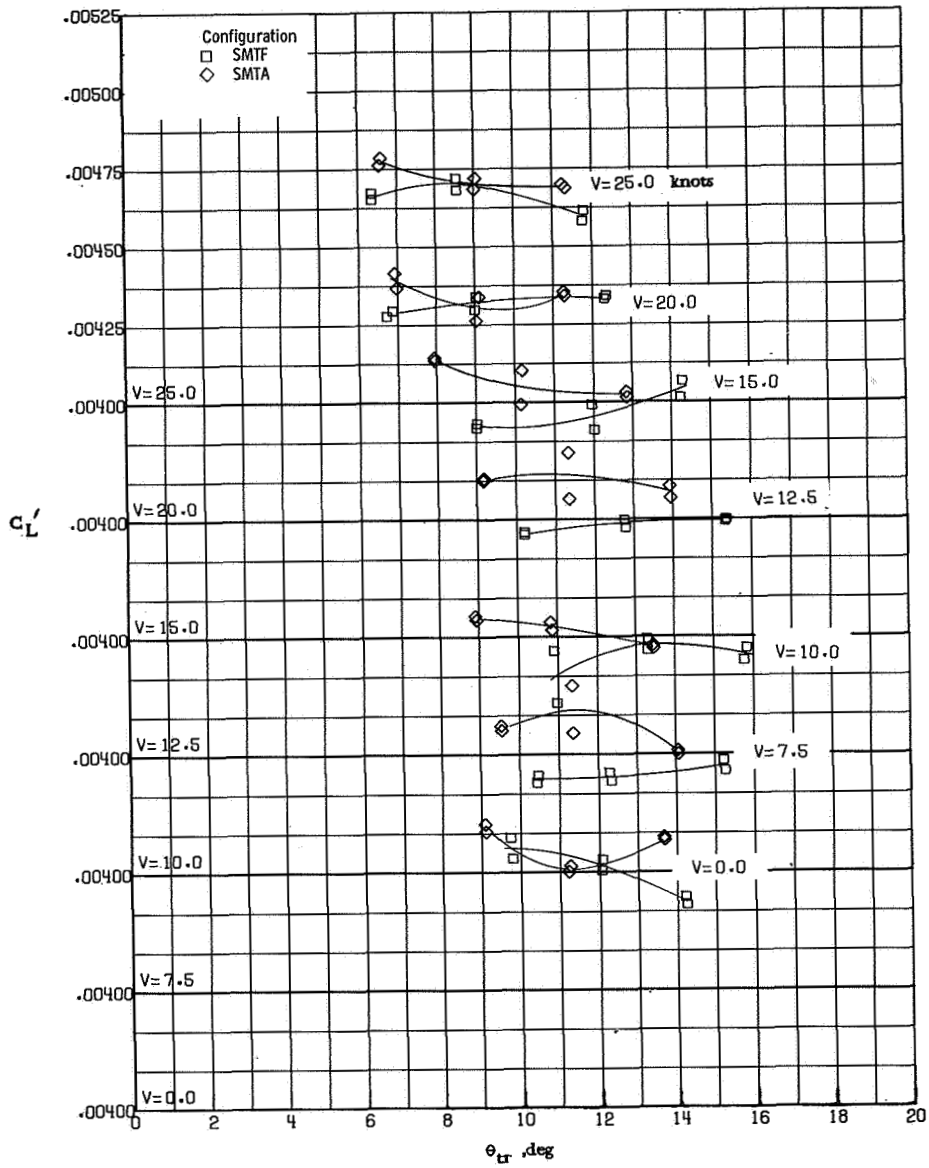

(d) Main-rotor lift.

Figure 32.- Continued.

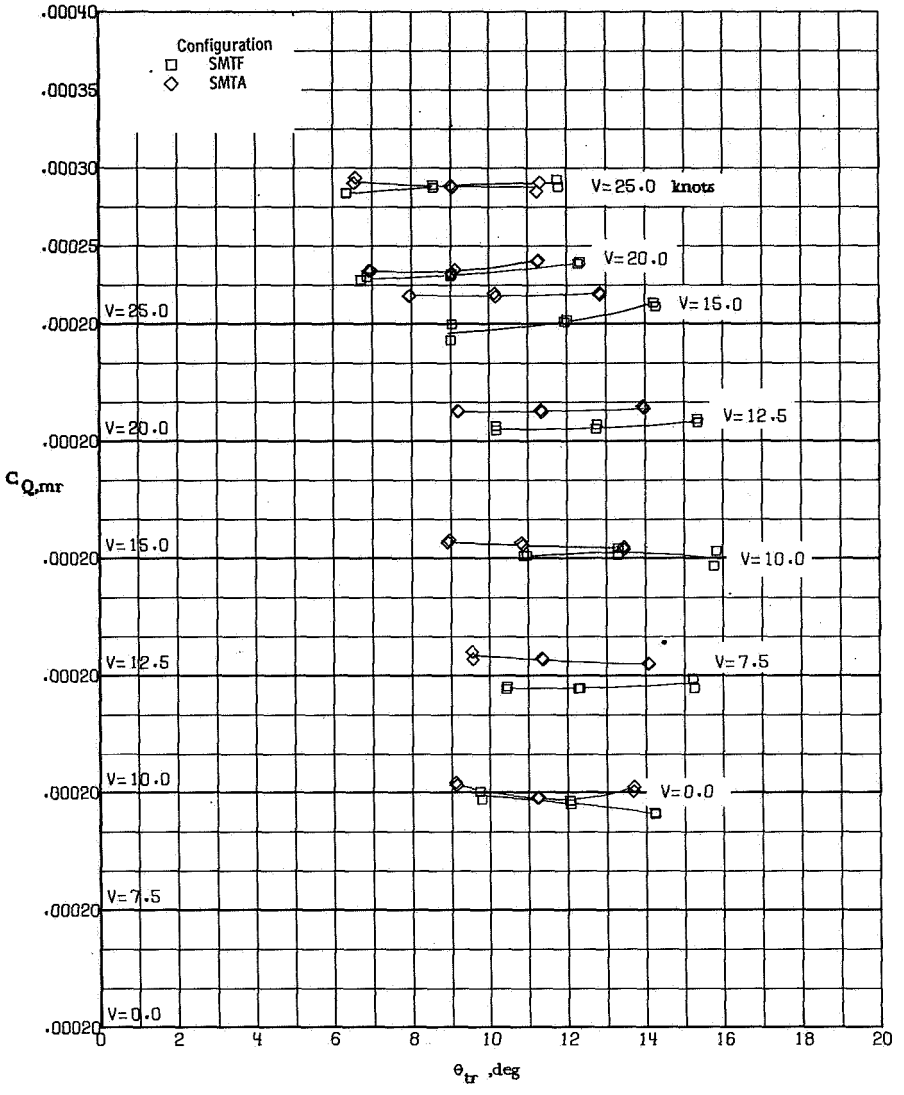

(e) Main-rotor torque.

Figure 32.- Continued.

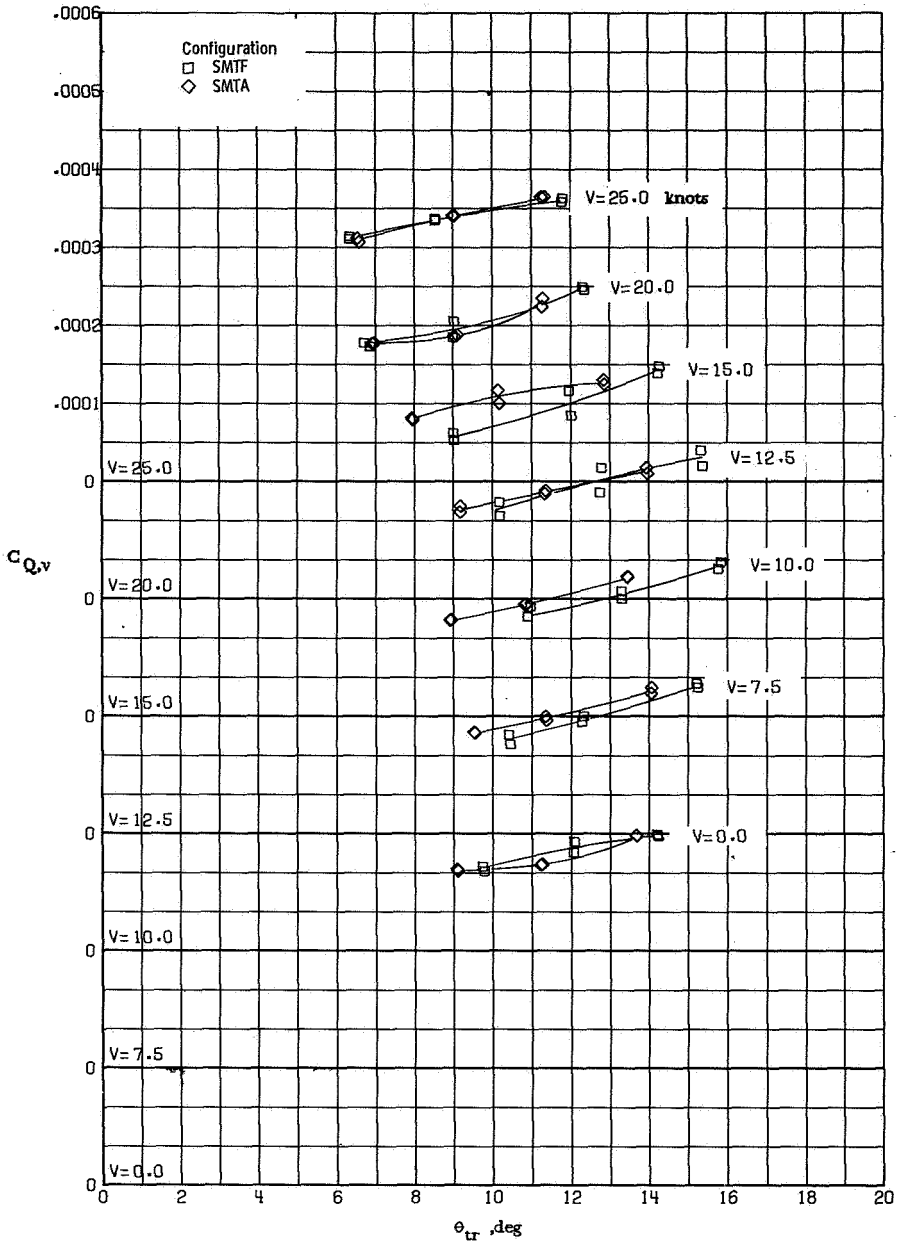

(f) Vehicle torque.

Figure 32.- Continued.

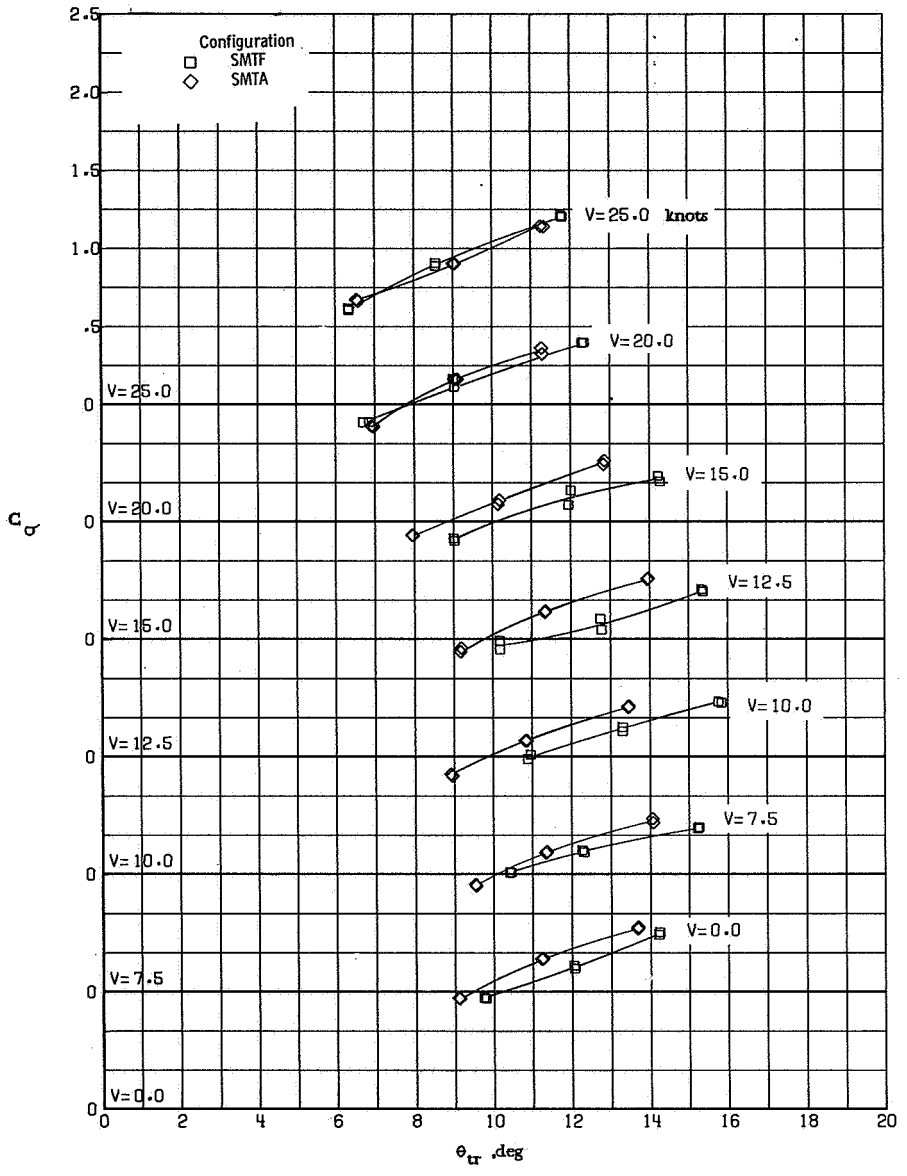

(g) Torque balance factor.

Figure 32.- Concluded.

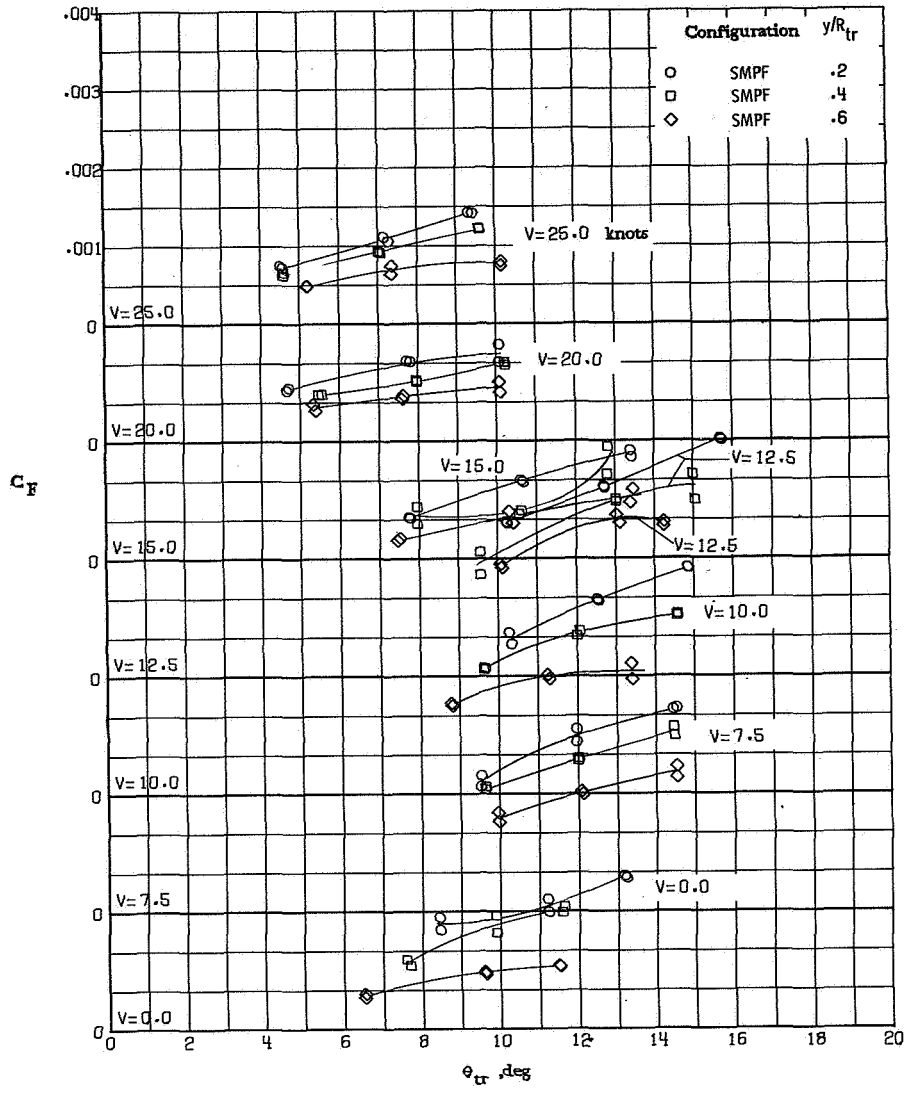

(a) Fin force.

Figure 33.- Aerodynamic characteristics of the pusher configuration with top blade forward rotation for different fin/tail-rotor gaps at $\beta = 180^{o}$.

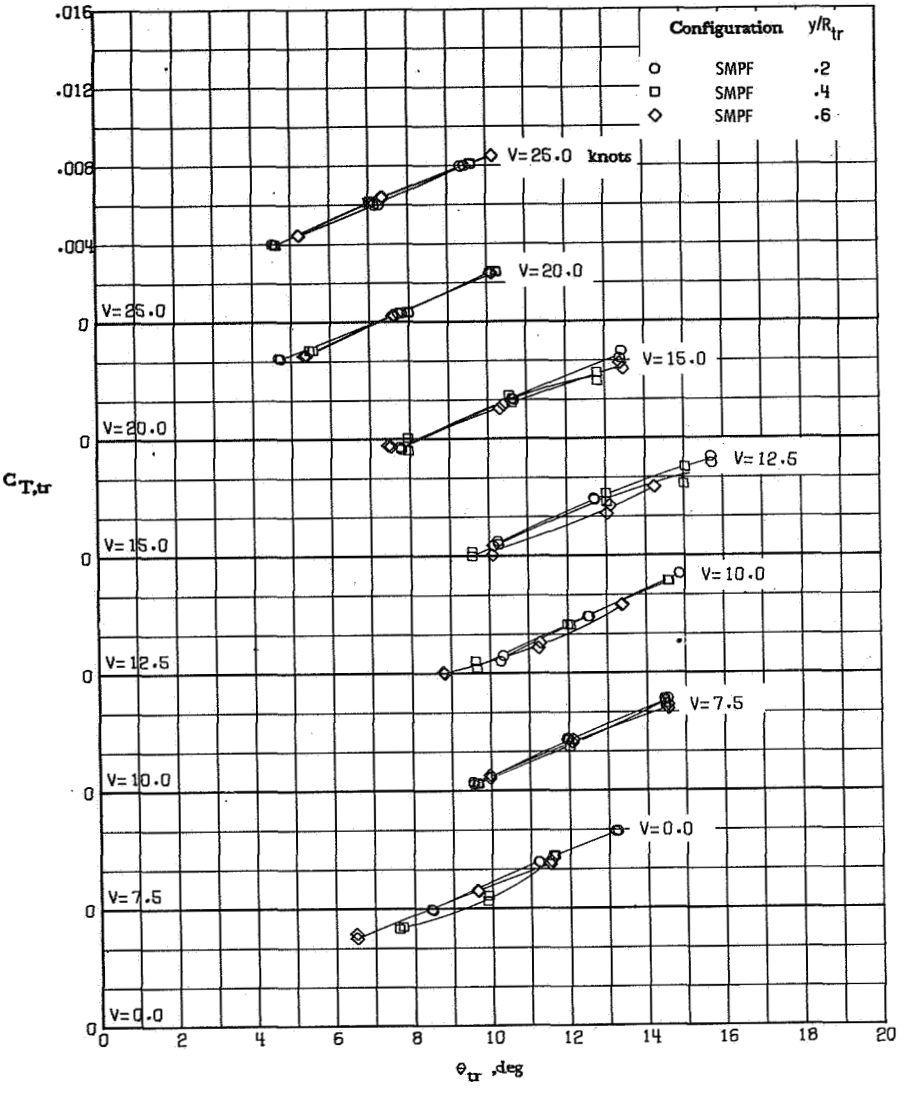

(b) Tail-rotor thrust.

Figure 33.- Continued.

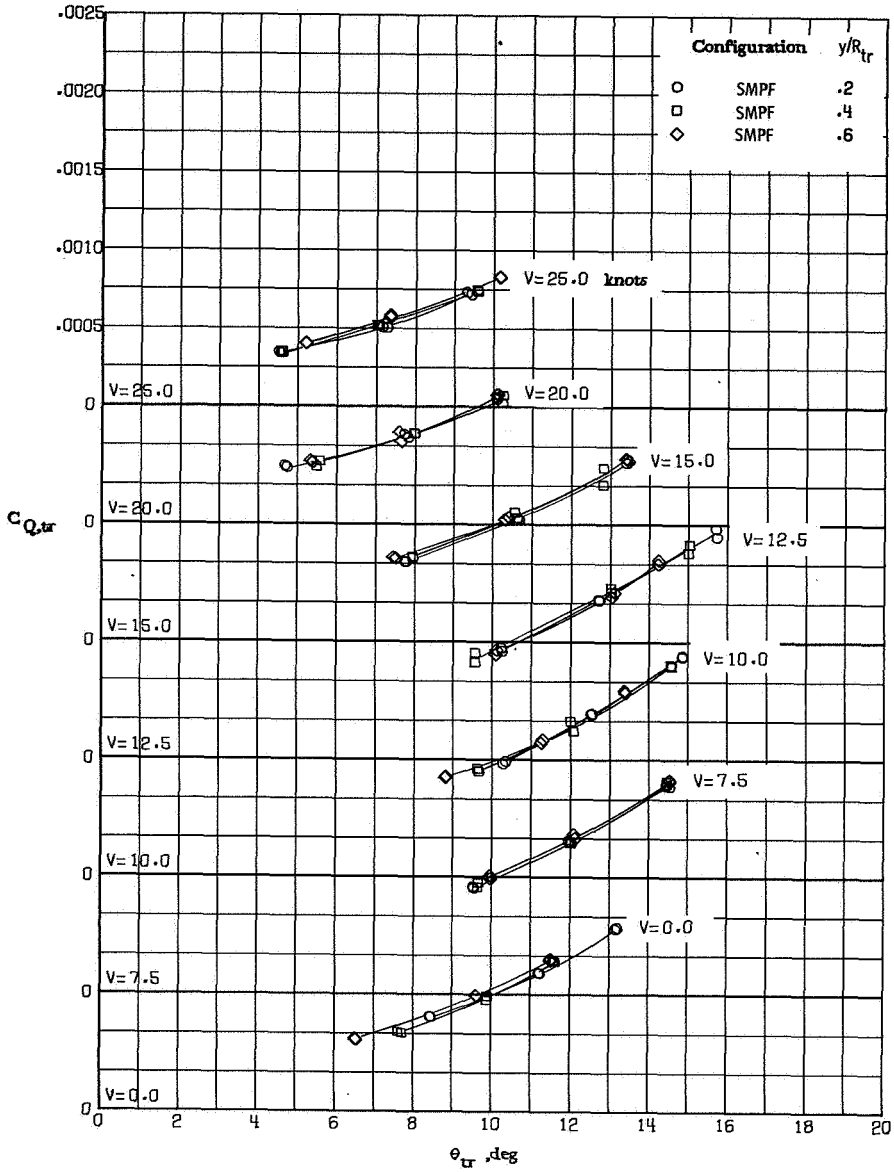

(c) Tail-rotor torque.

Figure 33.- Continued.

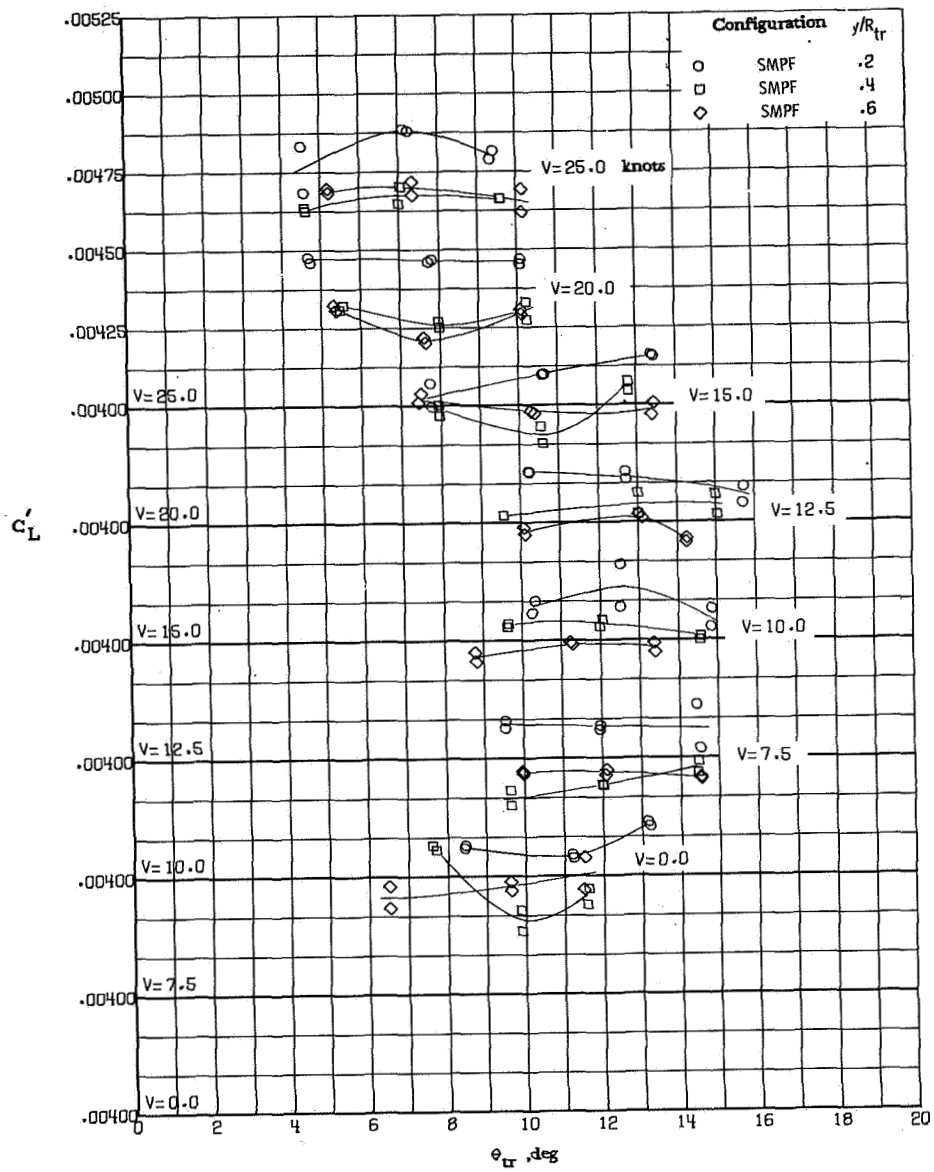

(d) Main-rotor lift.

Figure 33.- Continued.

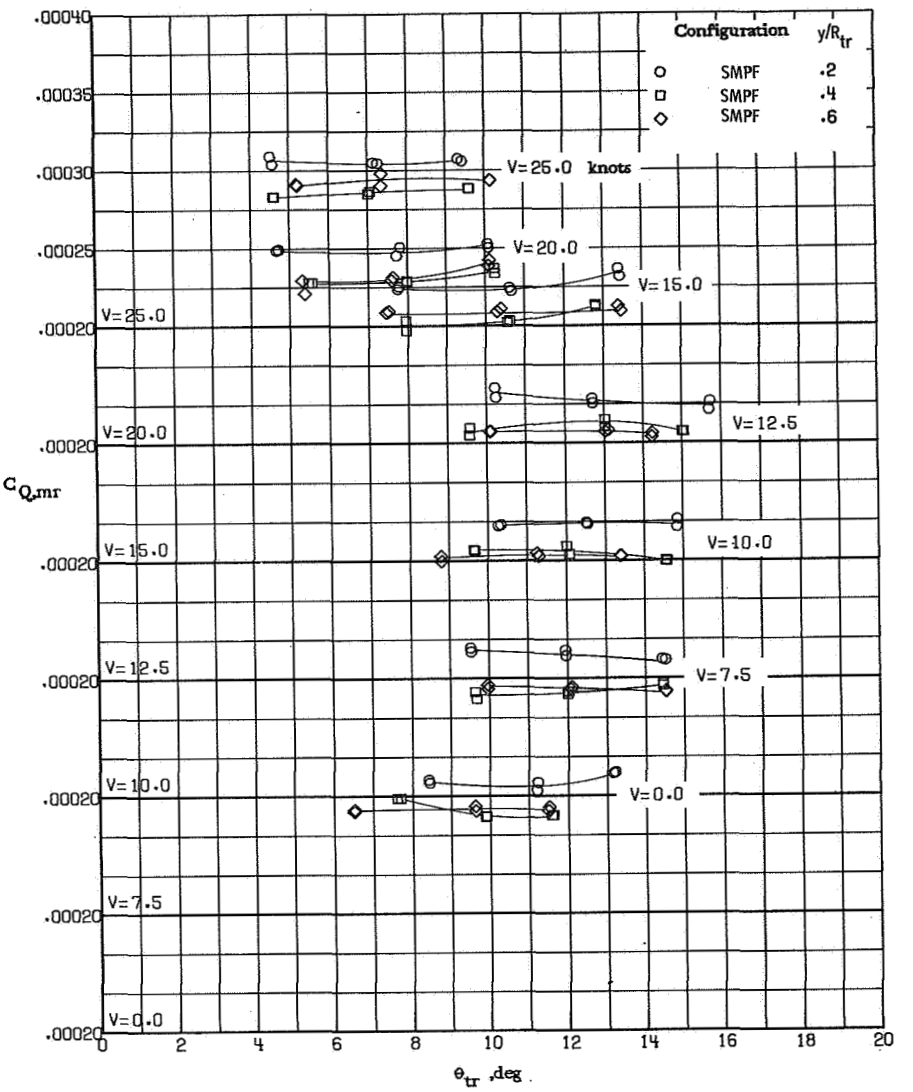

(e) Main-rotor torque.

Figure 33.- Continued.

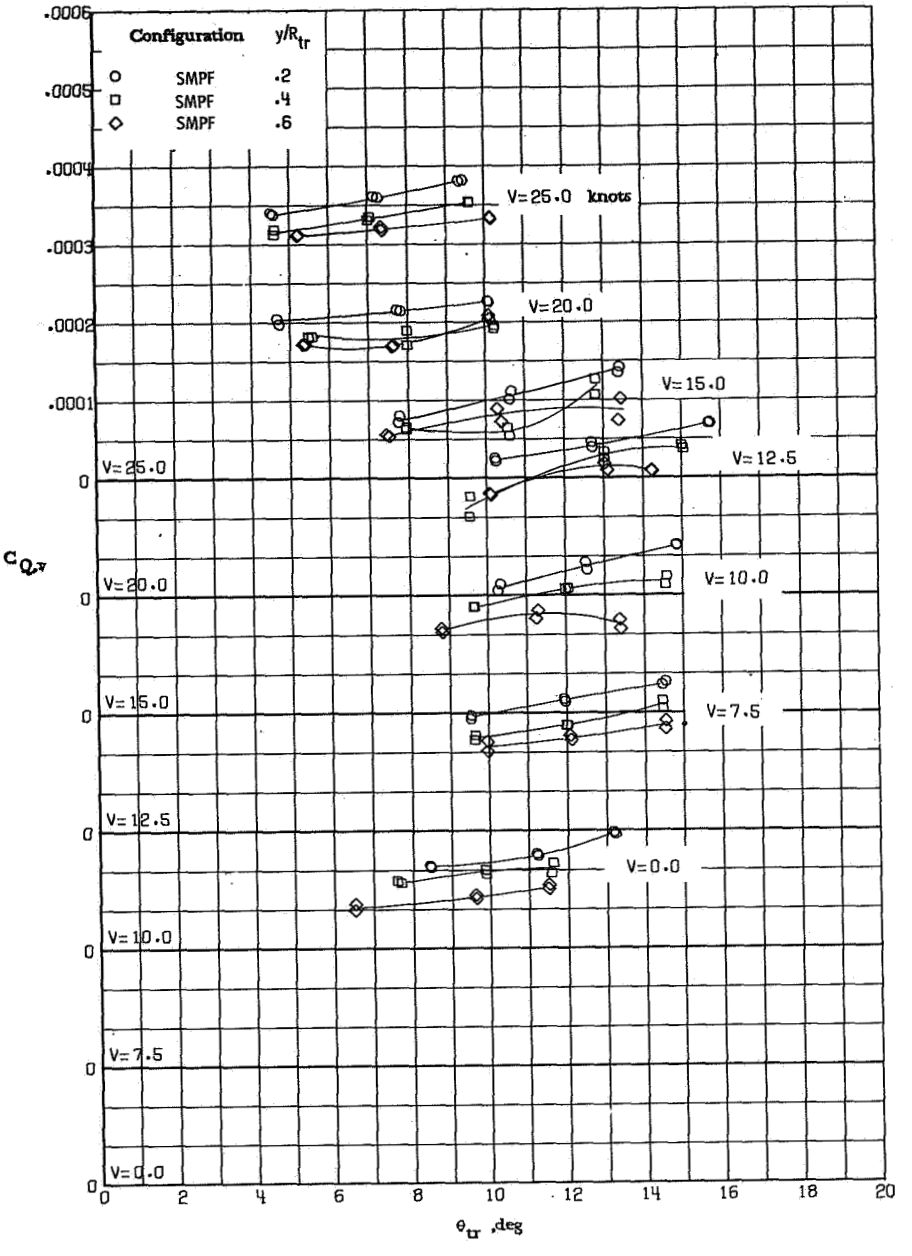

(f) Vehicle torque.

Figure 33.- Continued.

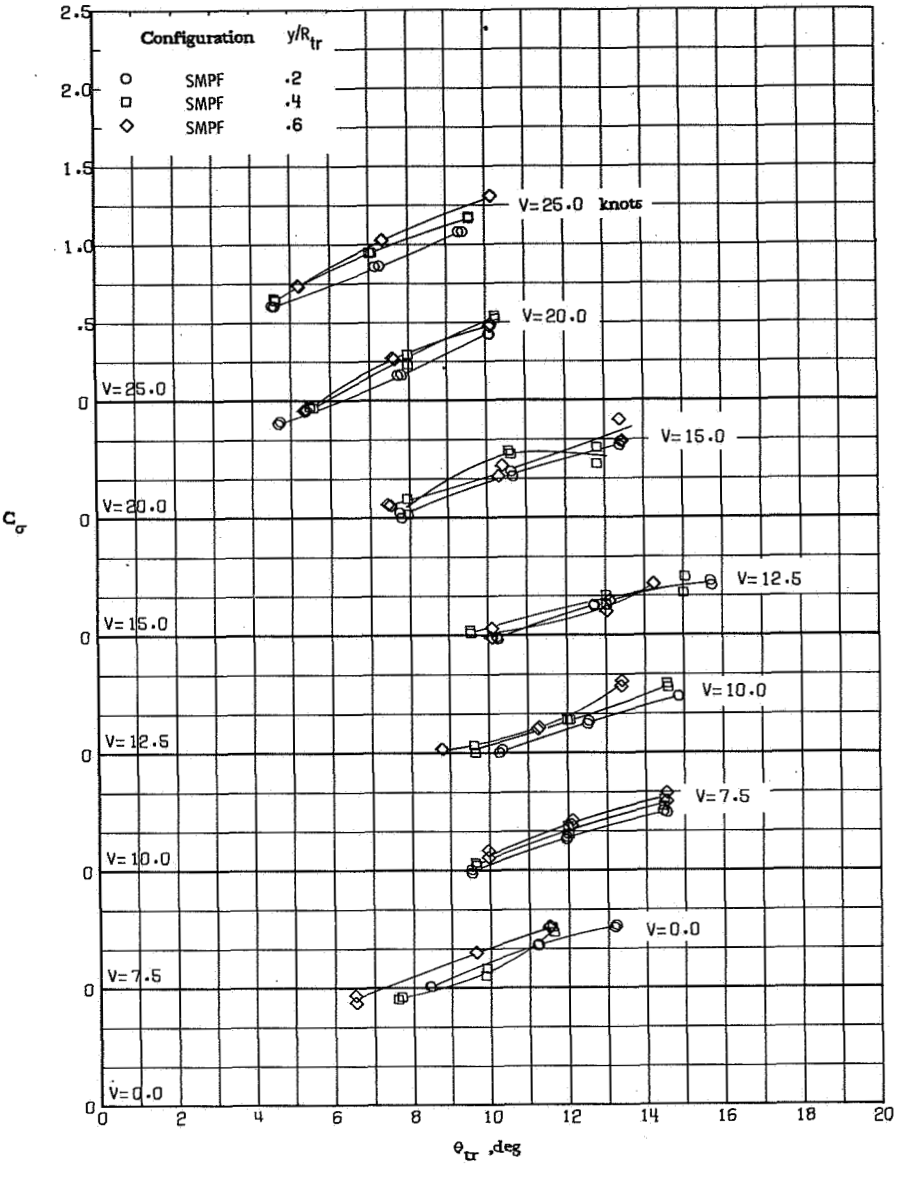

(g) Torque balance factor.

Figure 33.- Concluded.

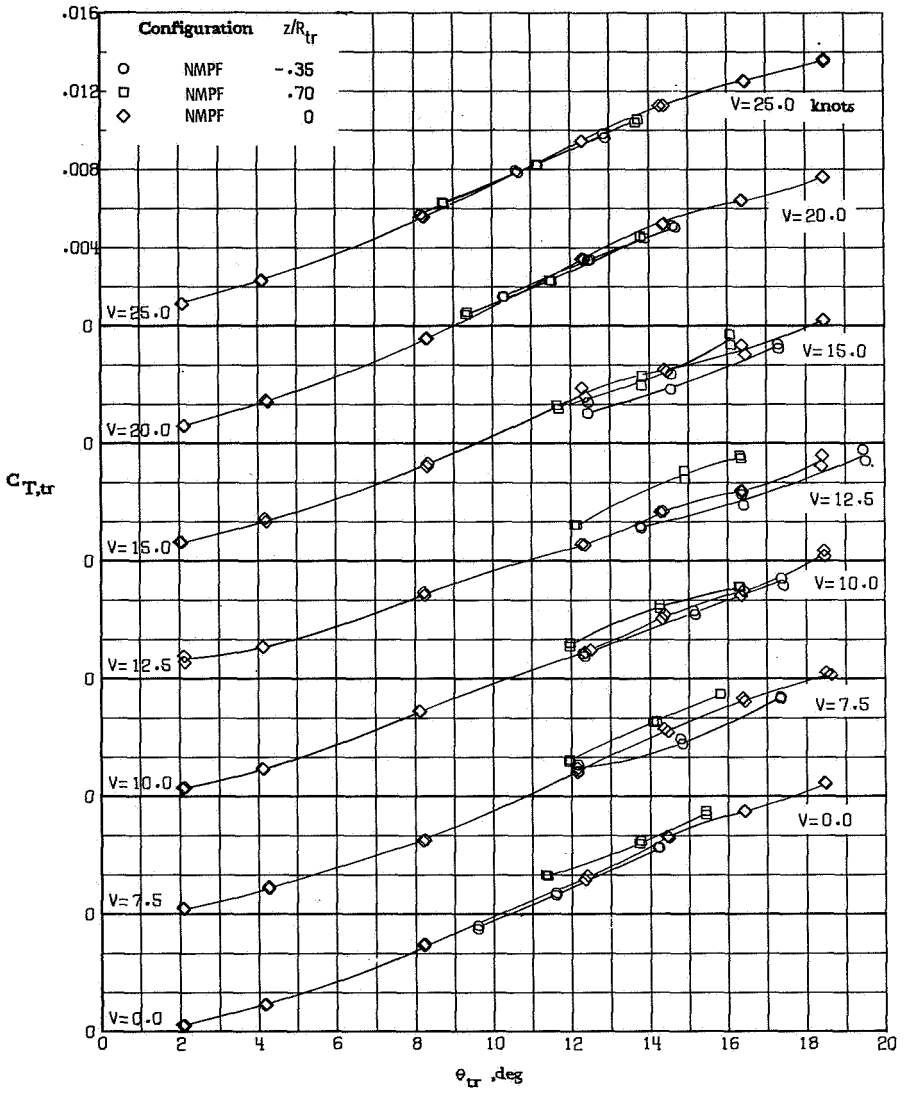

(a) Tail-rotor thrust.

Figure 34.- Aerodynamic characteristics of the fin-off configuration for different tail-rotor heights at $\beta = 180^{o}$.

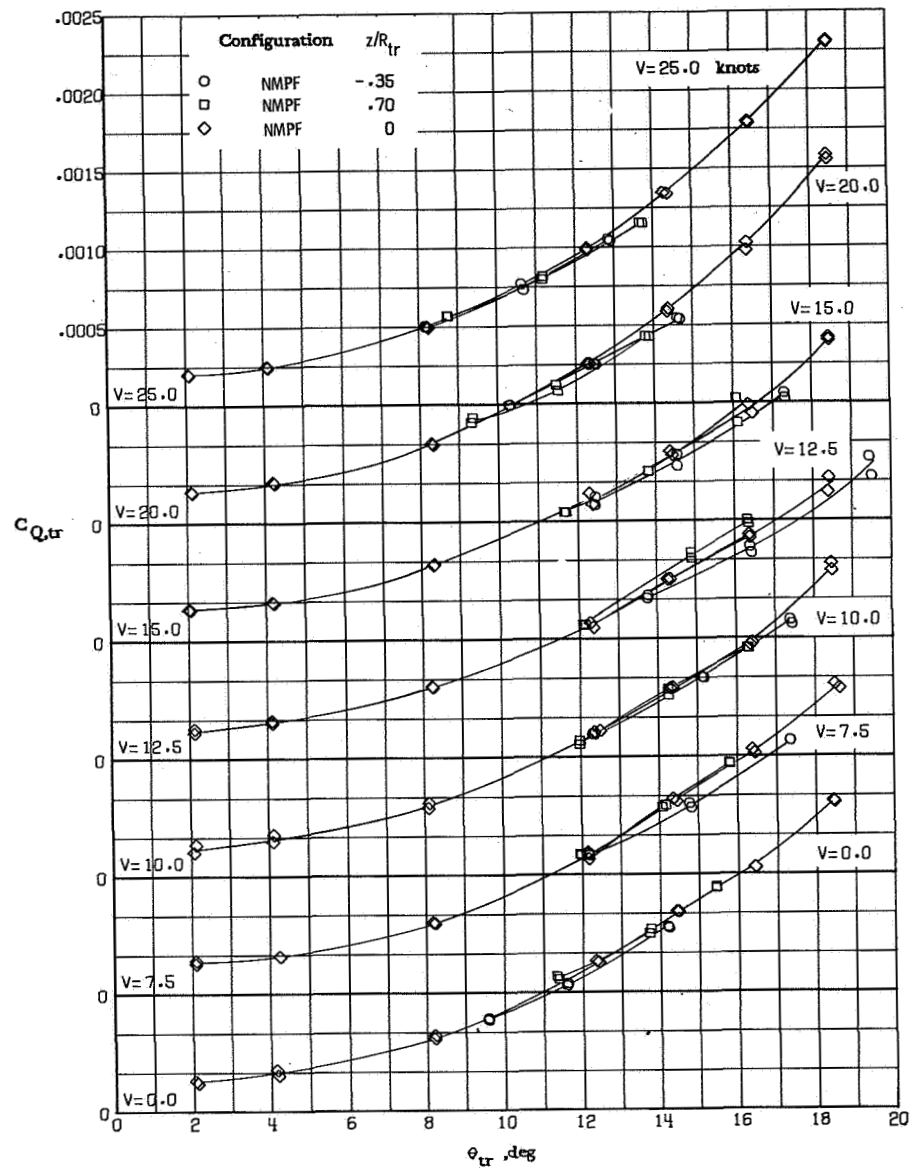

(b) Tail-rotor torque.

Figure 34.- Continued.

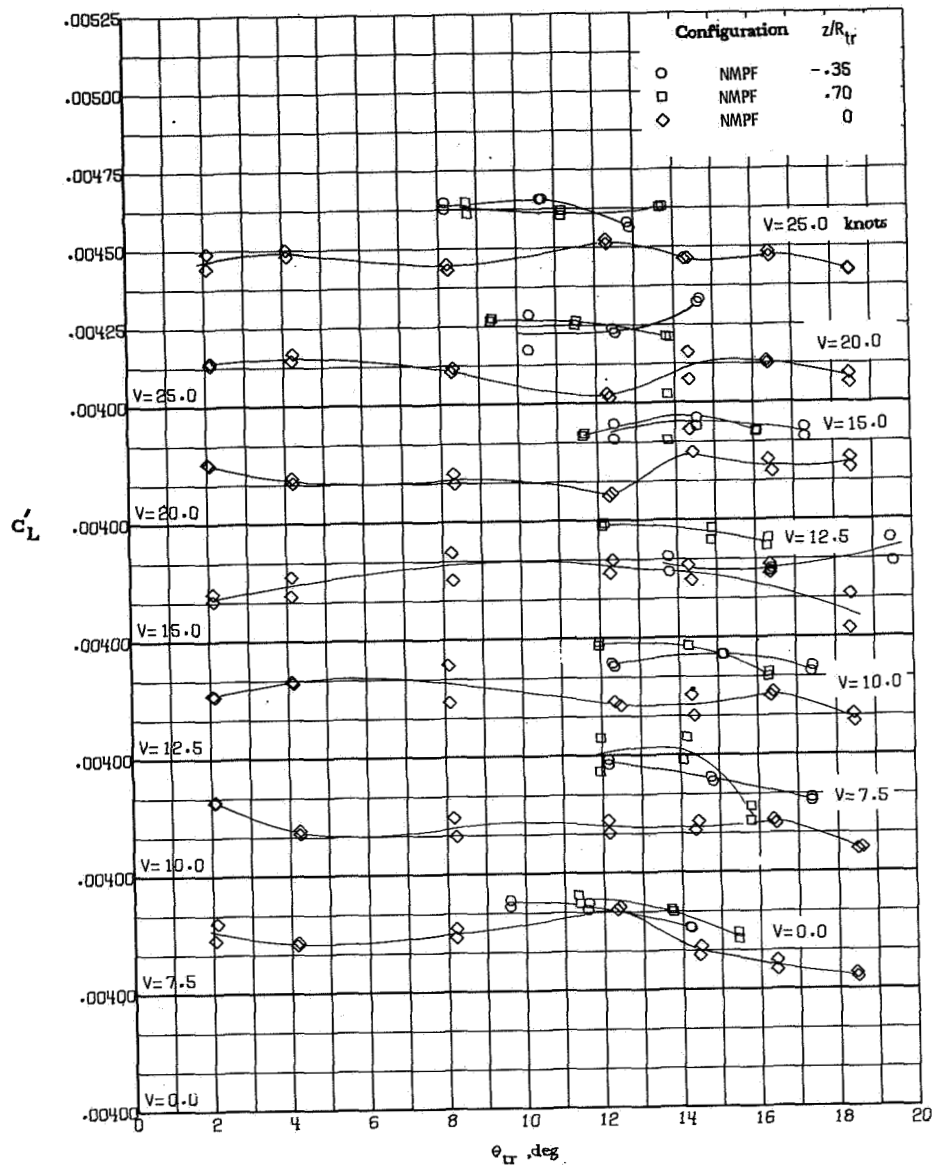

(c) Main-rotor lift.

Figure 34.- Continued.

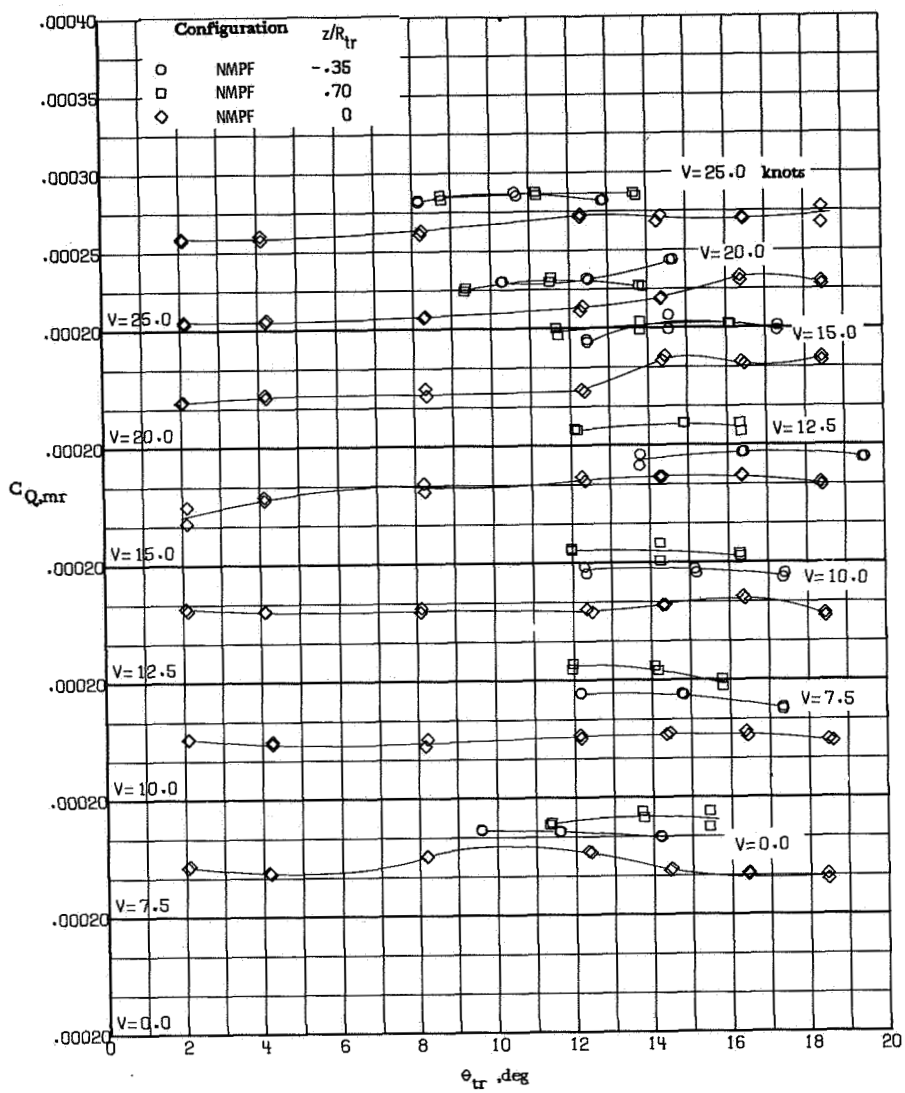

(d) Main-rotor torque.

Figure 34.- Continued.

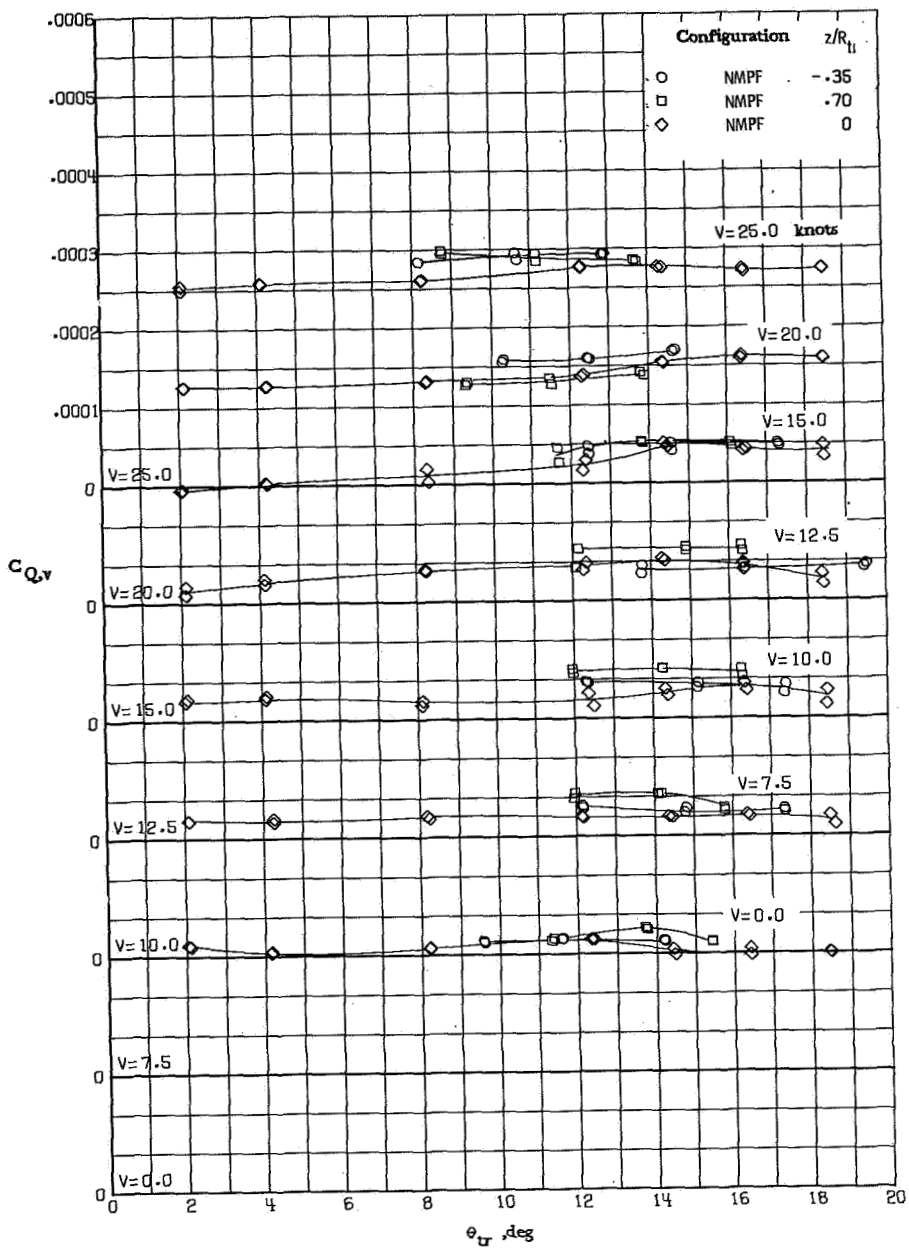

(e) Vehicle torque.

Figure 34.- Continued.

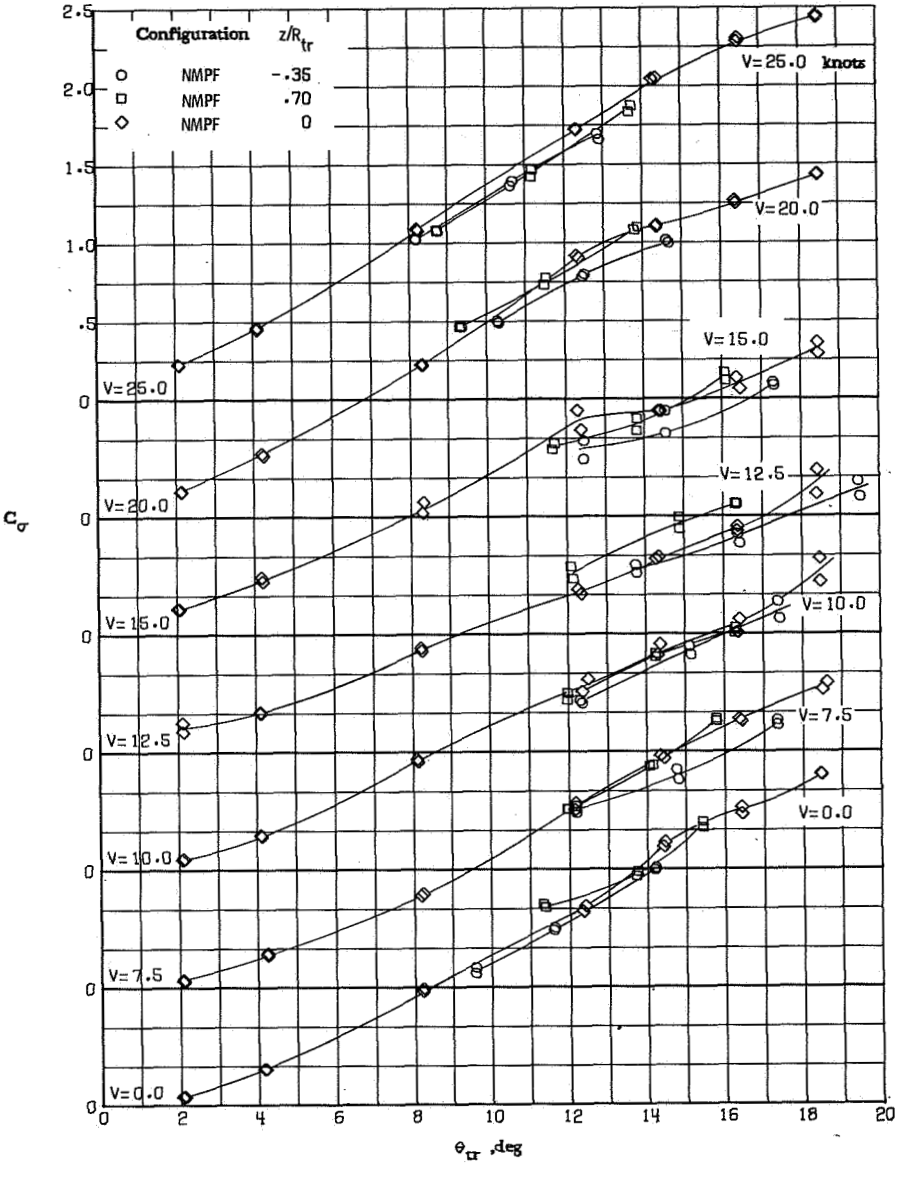

(f) Torque balance factor.

Figure 34.- Concluded.

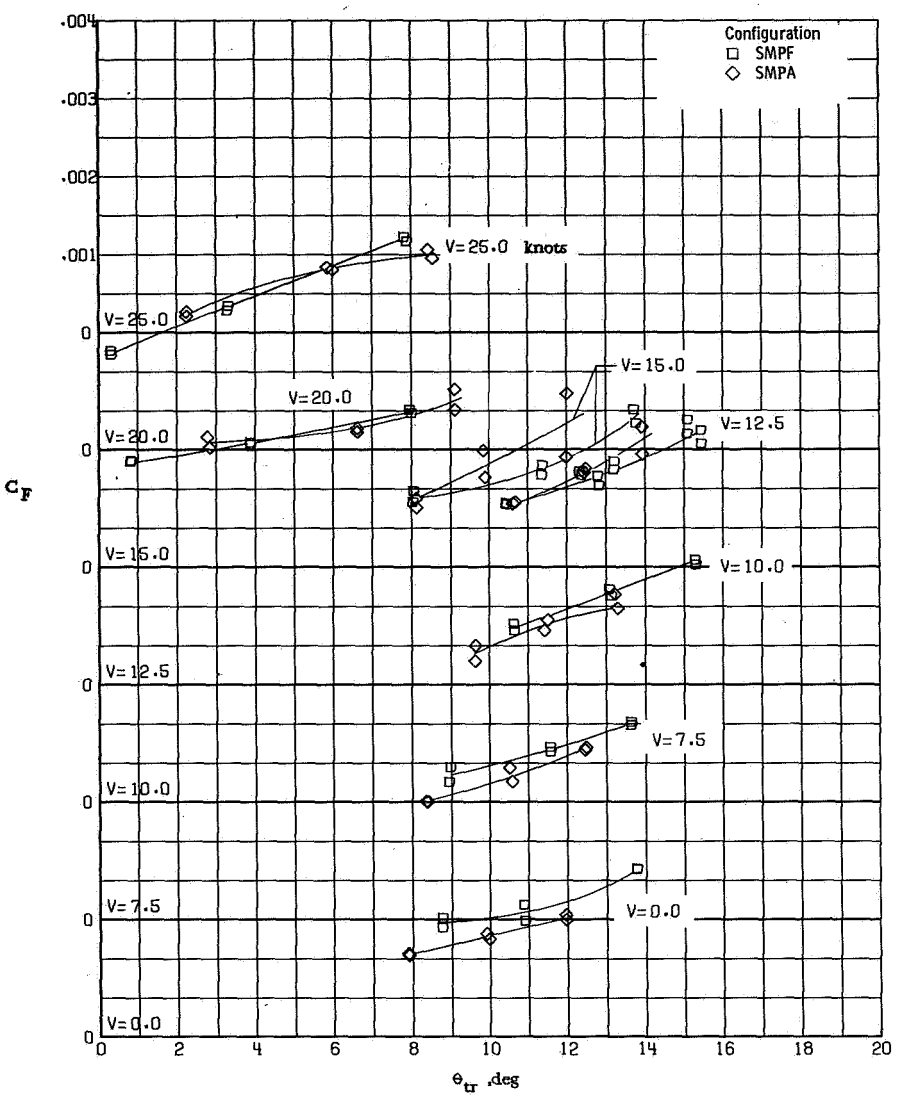

(a) Fin force.

Figure 35.- Aerodynamic characteristics of configurations with a pusher tail rotor at $\beta = 210^{o}$.

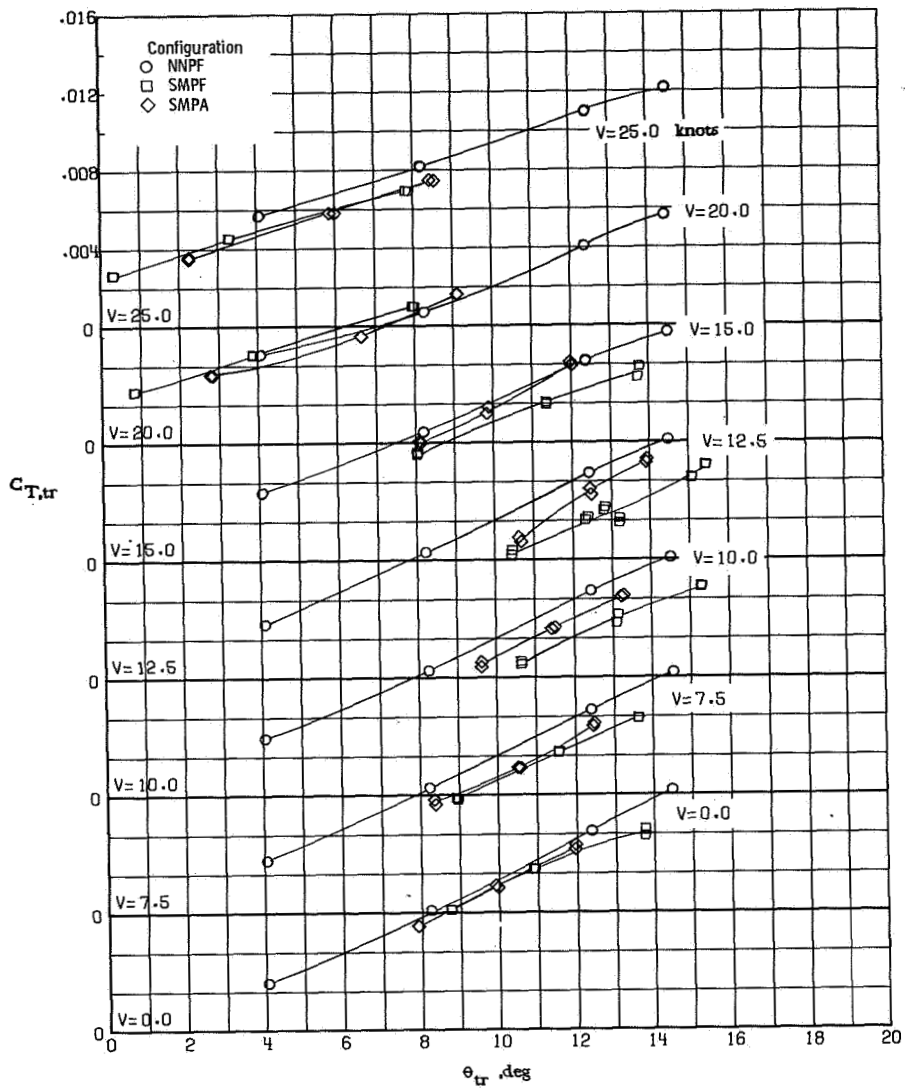

(b) Tail-rotor thrust.

Figure 35.- Continued.

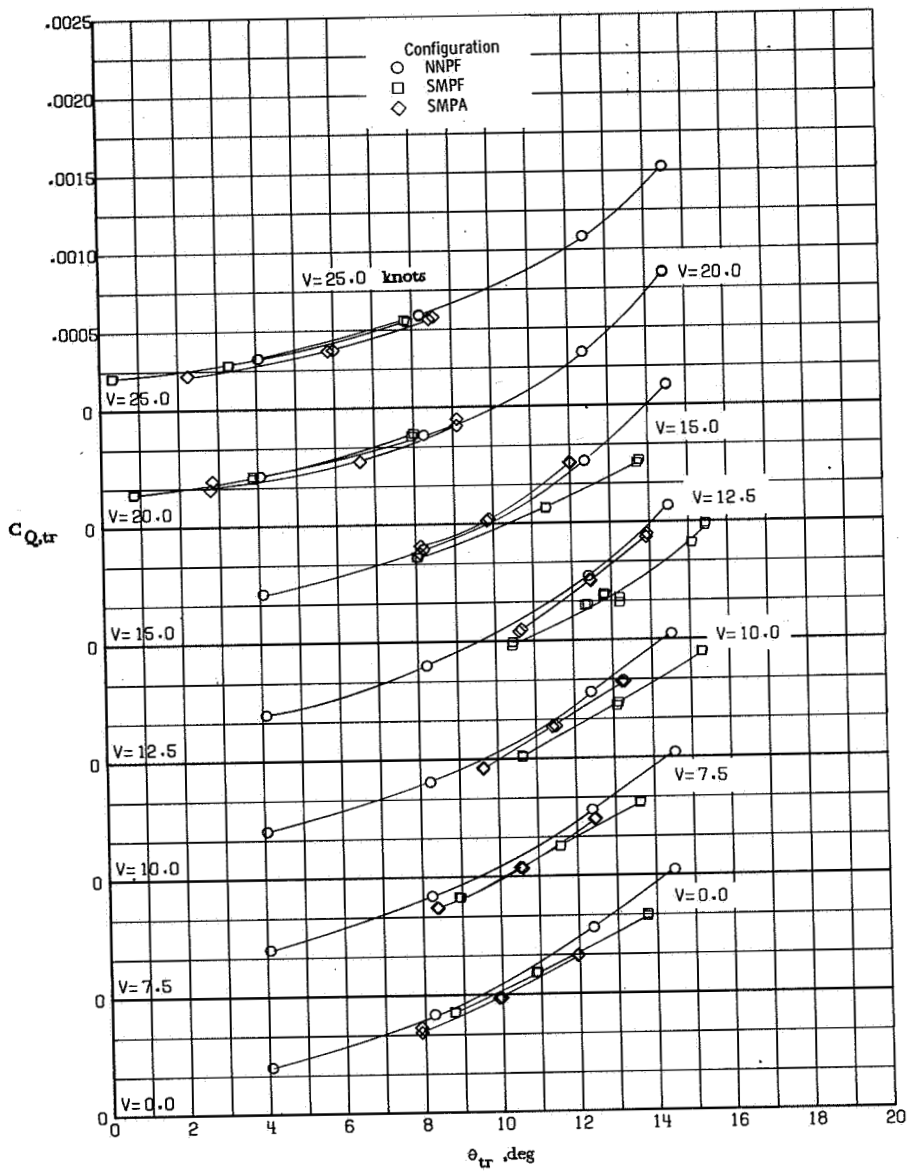

(c) Tail-rotor torque.

Figure 35.- Continued.

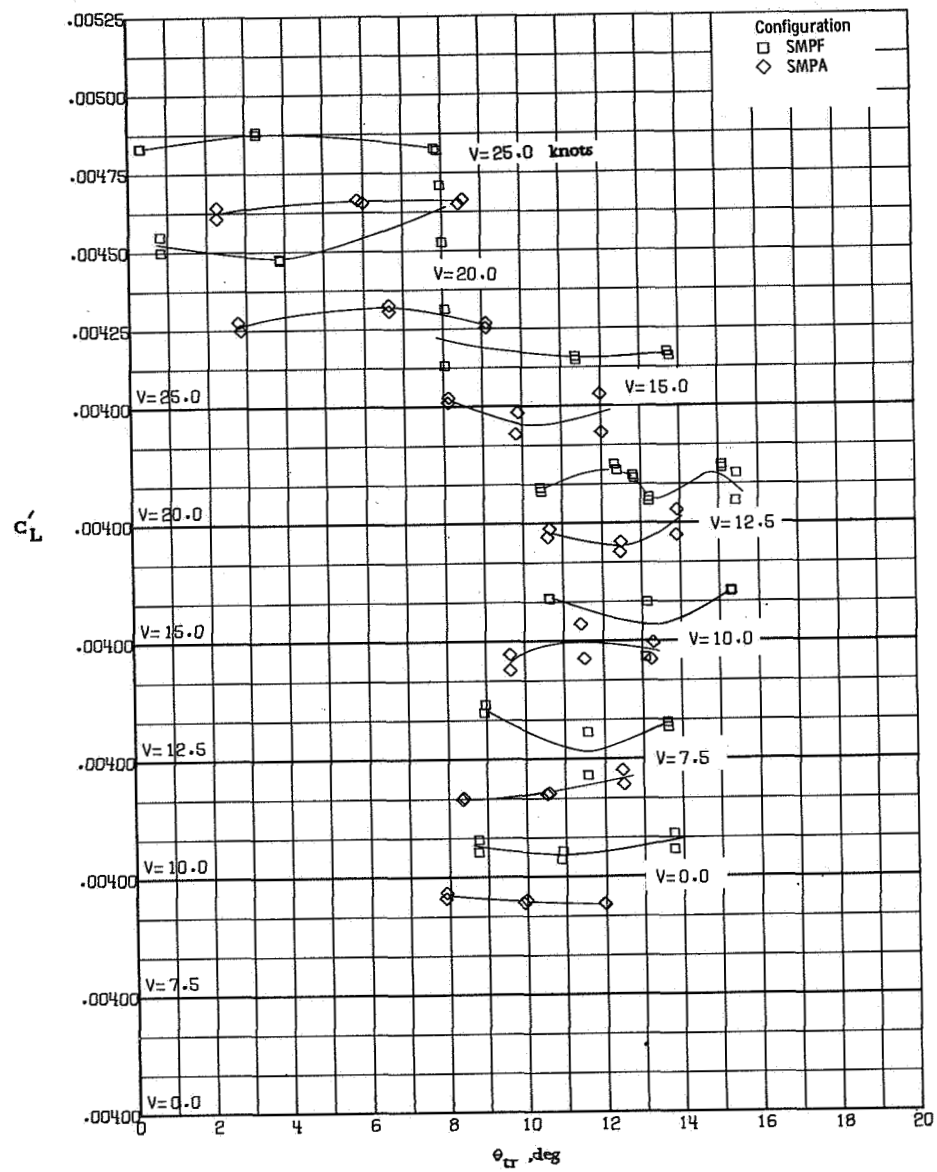

(d) Main-rotor lift.

Figure 35.- Continued.

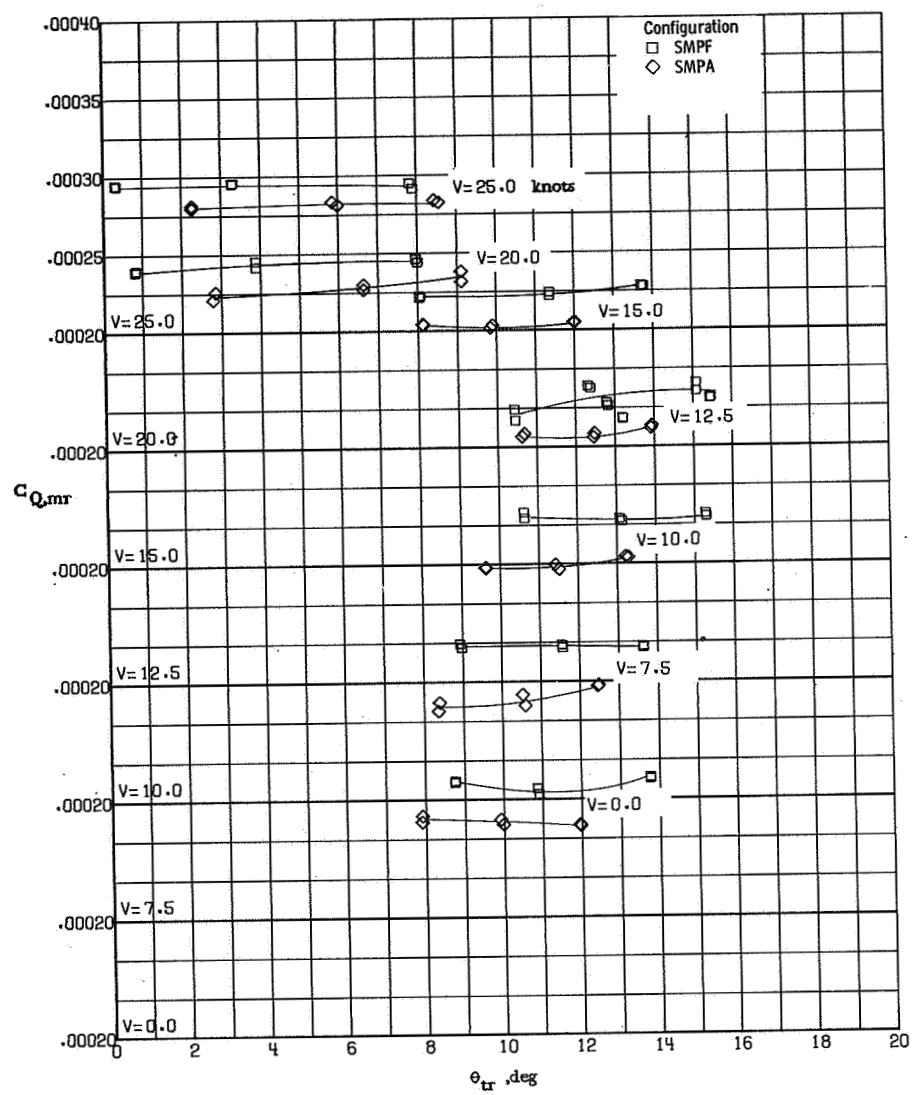

(e) Main-rotor torque.

Figure 35.- Continued.

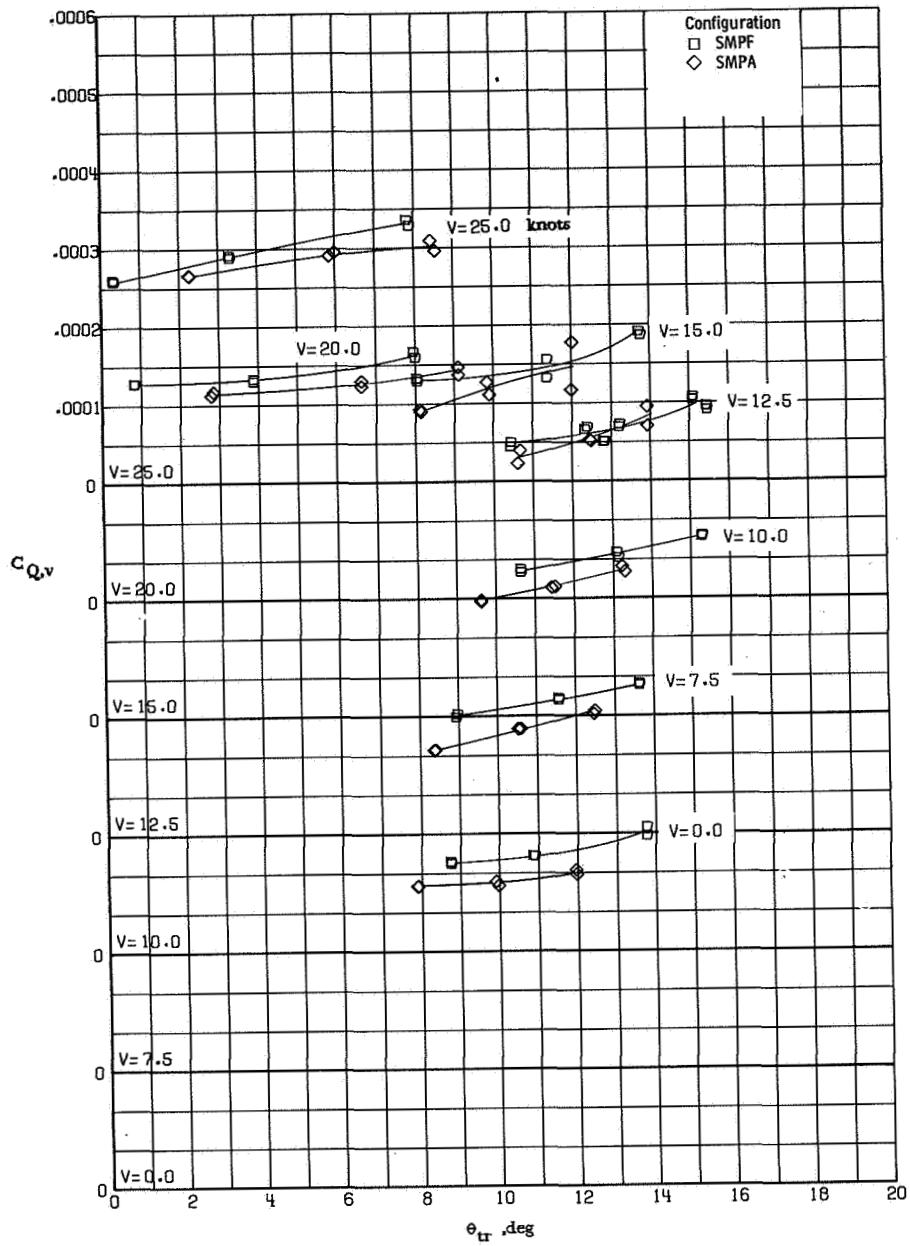

(f) Vehicle torque.

Figure 35.- Continued.

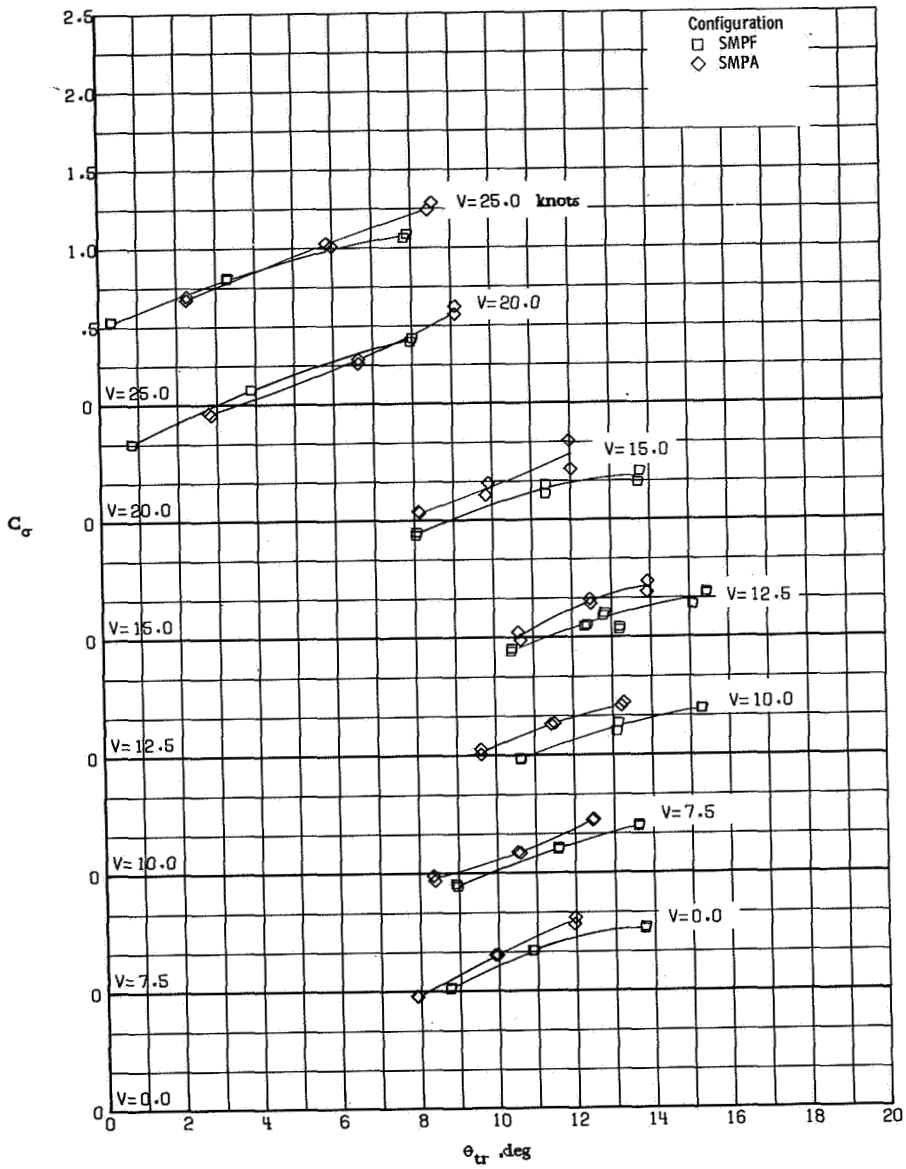

(g) Torque balance factor.

Figure 35.- Concluded.

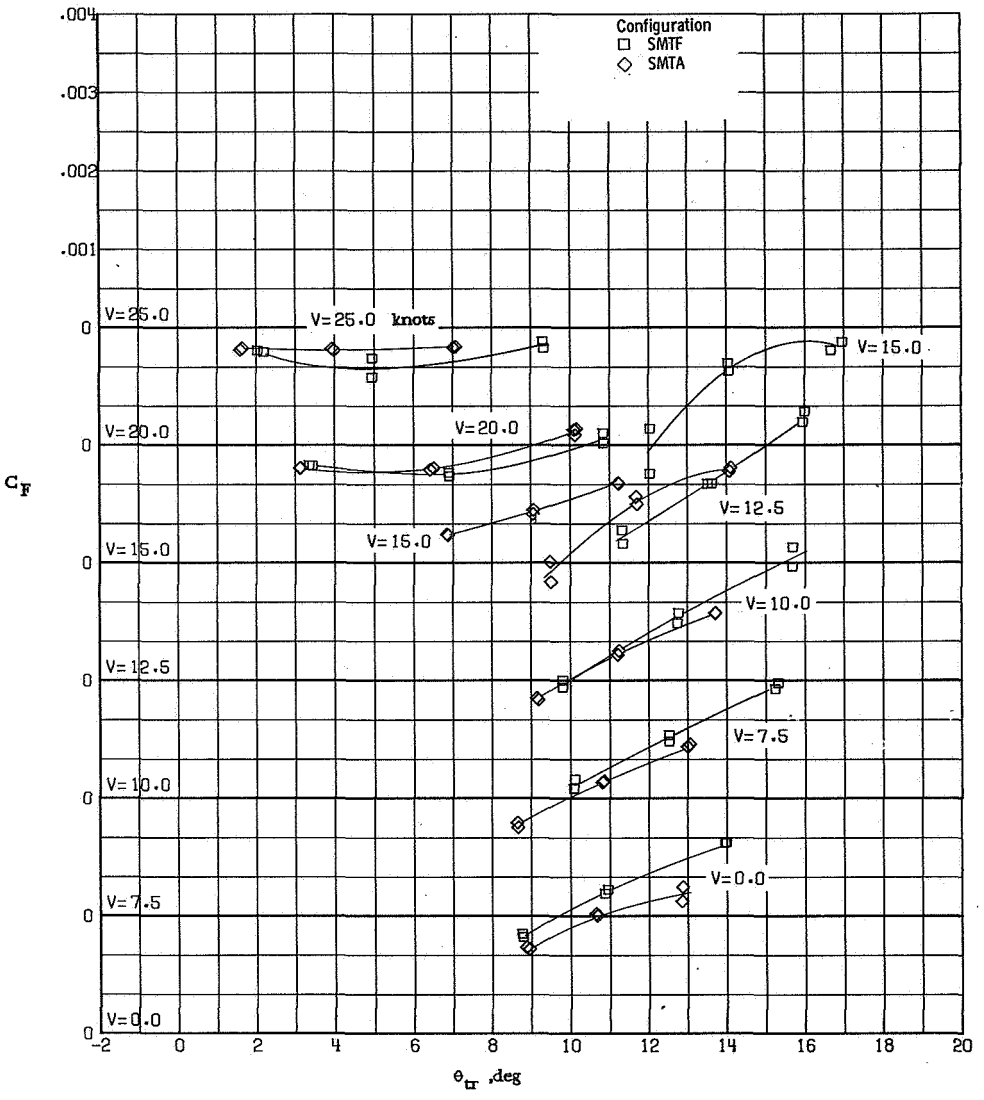

(a) Fin force.

Figure 36.- Aerodynamic characteristics of various configurations with and without the main rotor at $\beta = 210^{o}$.

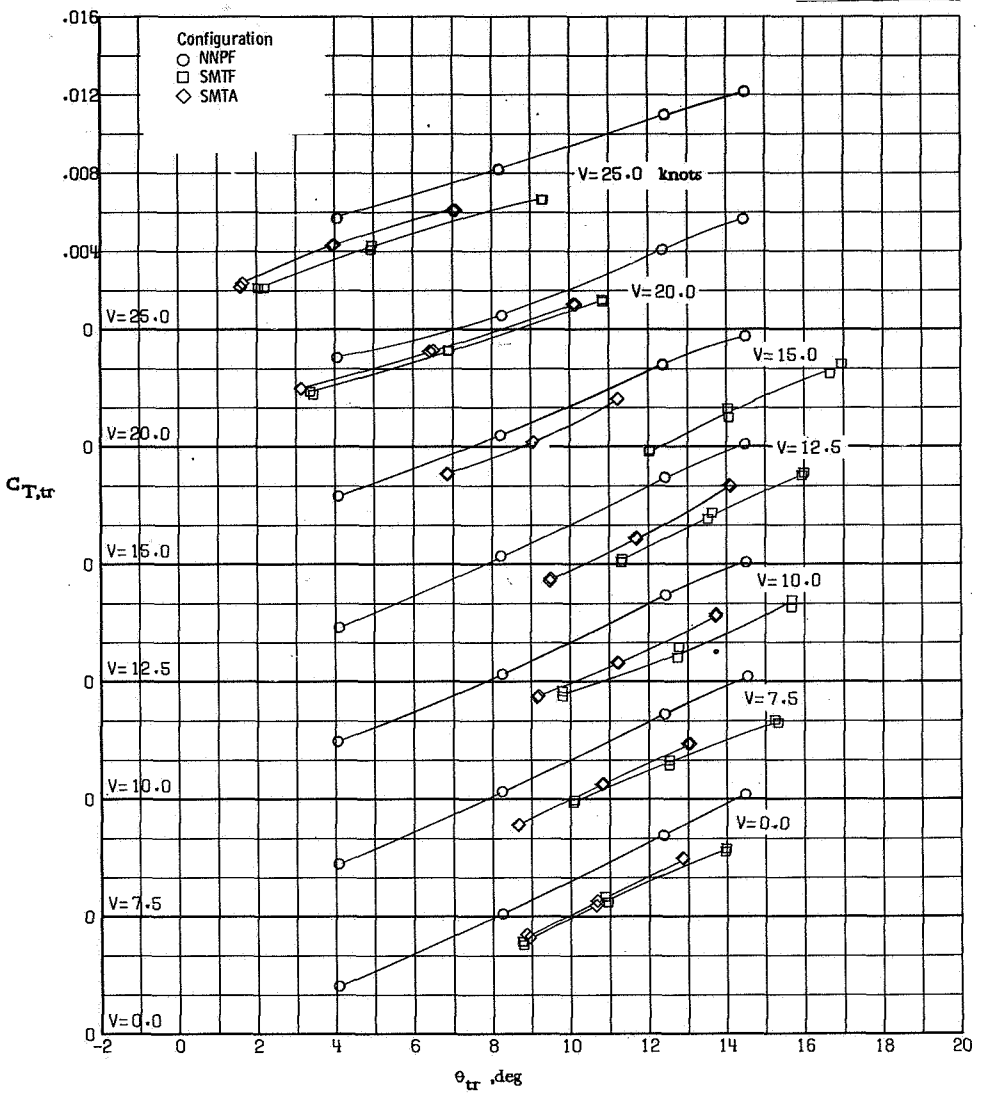

(b) Tail-rotor thrust.

Figure 36.- Continued.

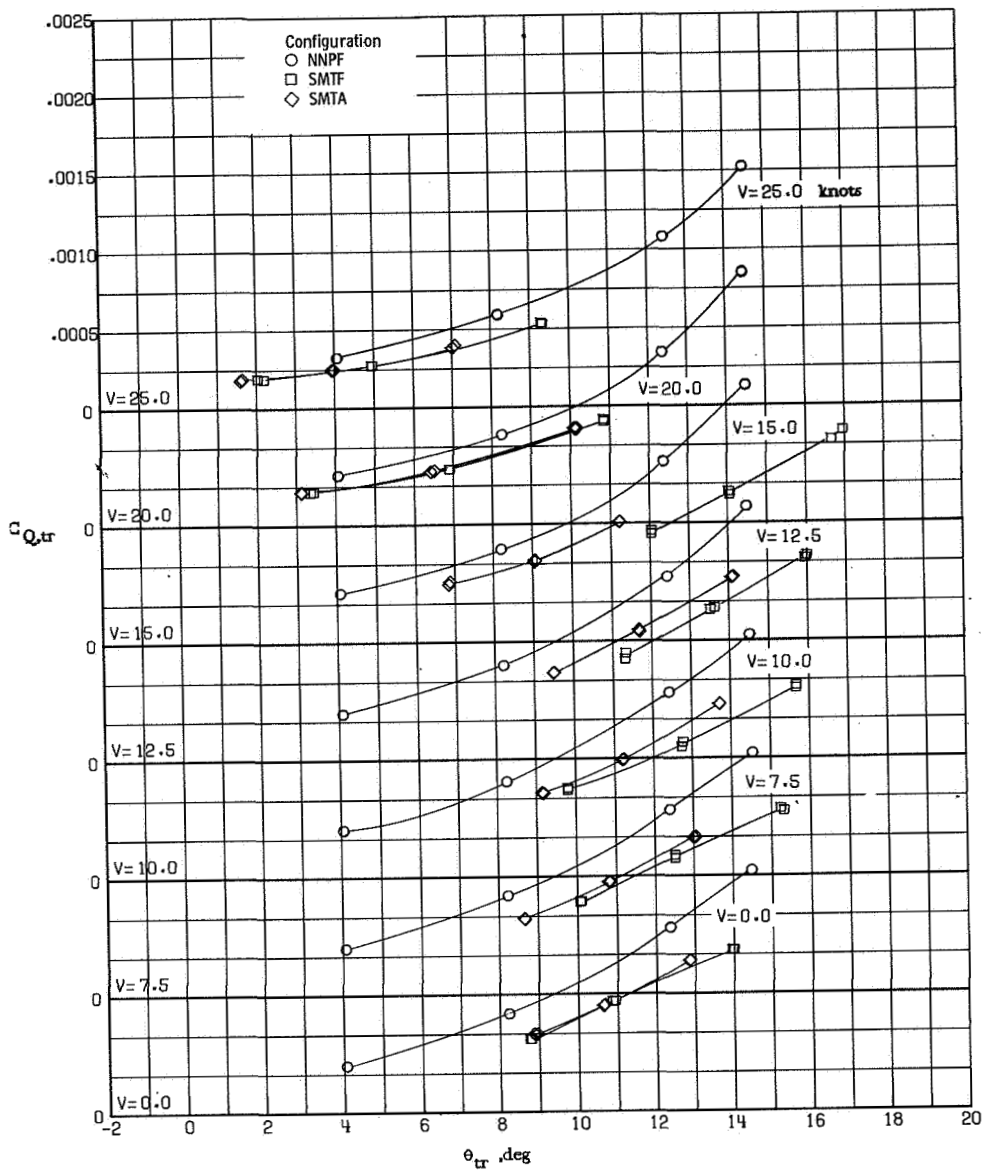

(c) Tail-rotor torque.

Figure 36.- Continued.

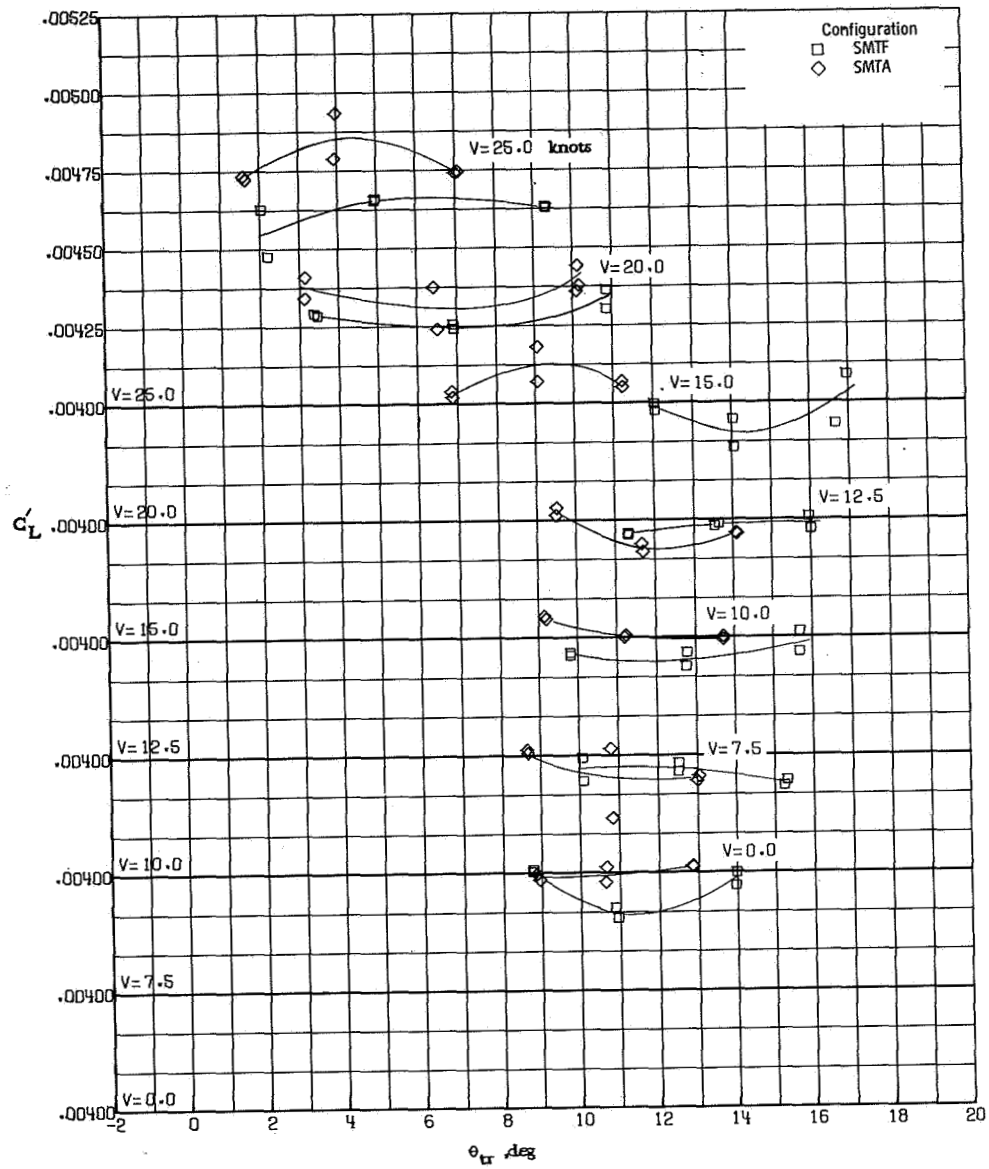

(d) Main-rotor lift.

Figure 36.- Continued.

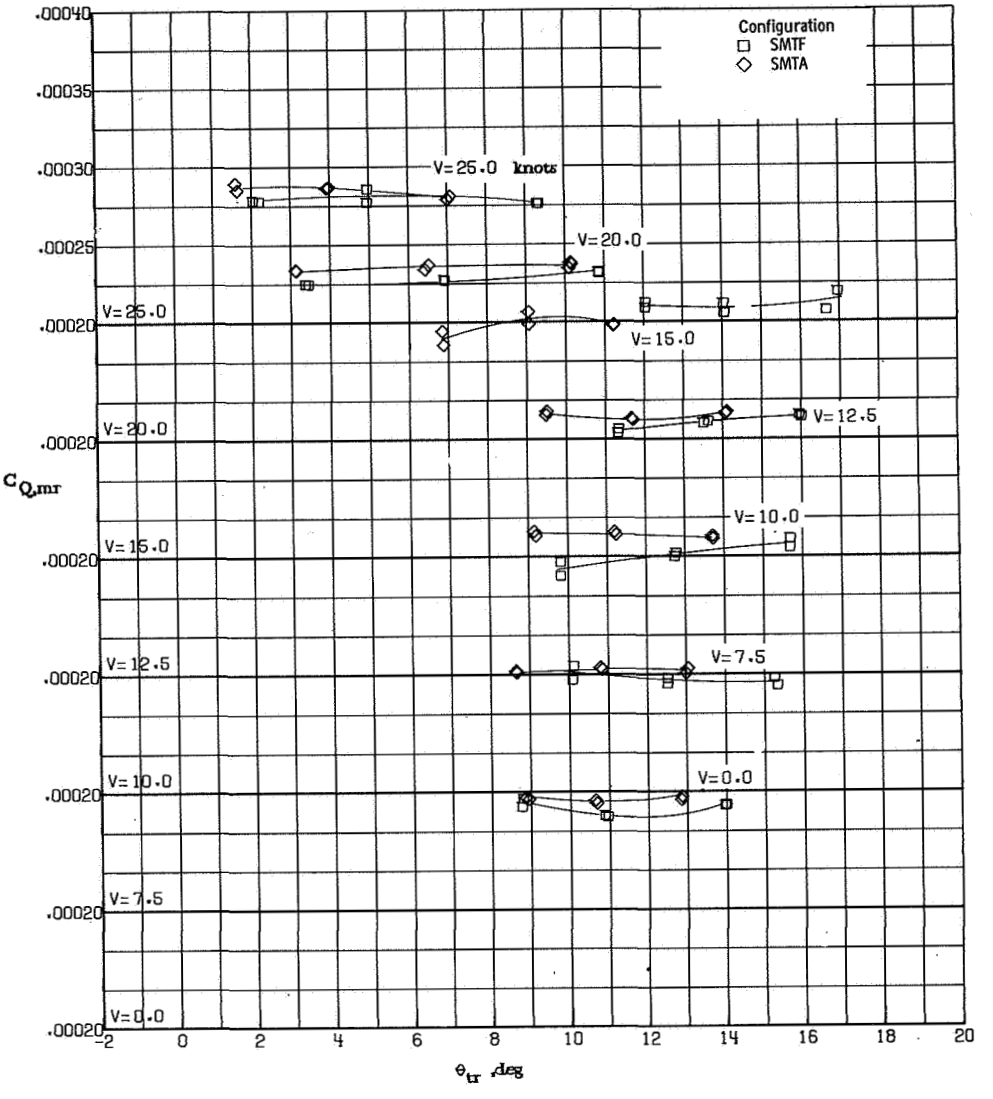

(e) Main-rotor torque.

Figure 36.- Continued.

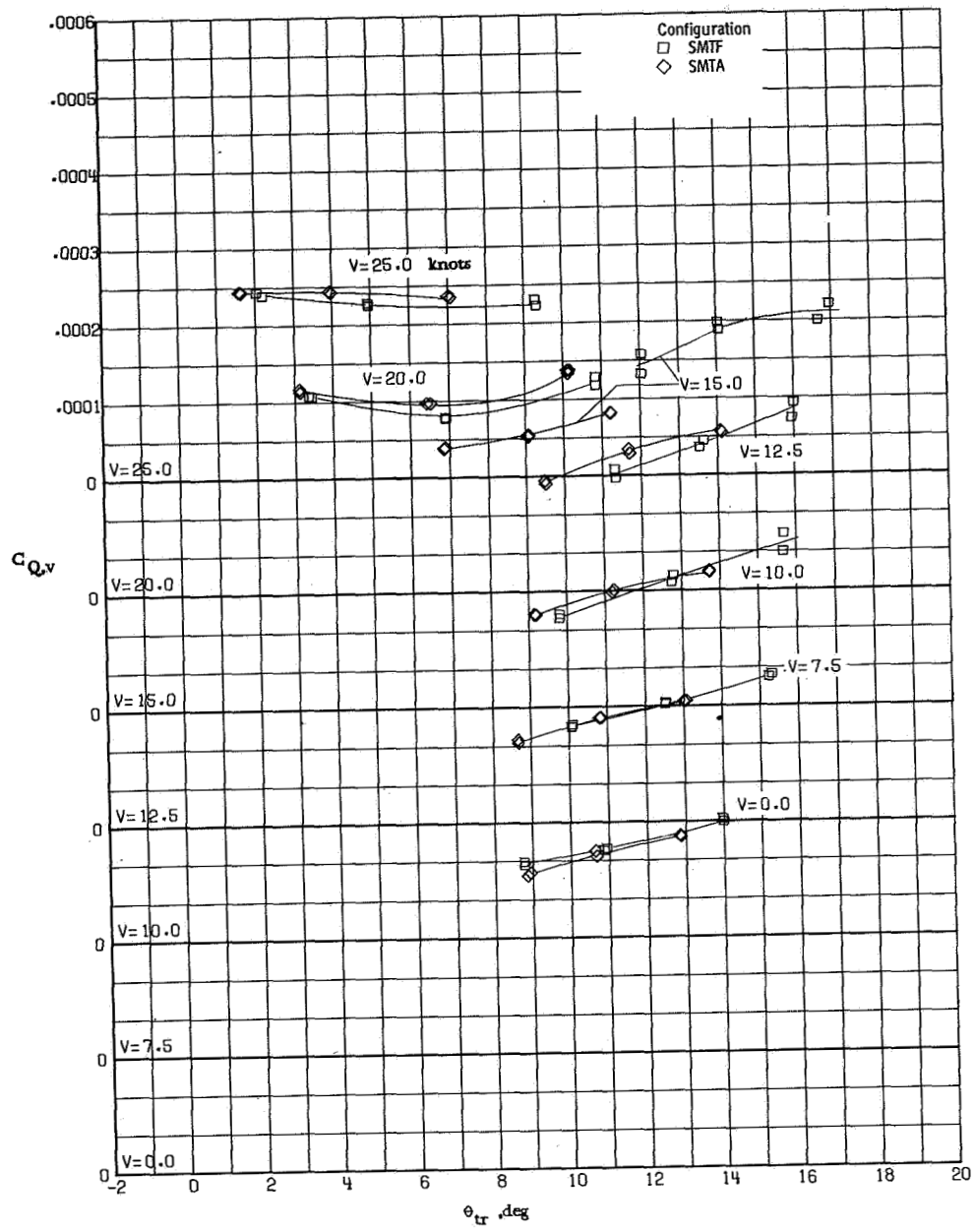

(f) Vehicle torque.

Figure 36.- Continued.

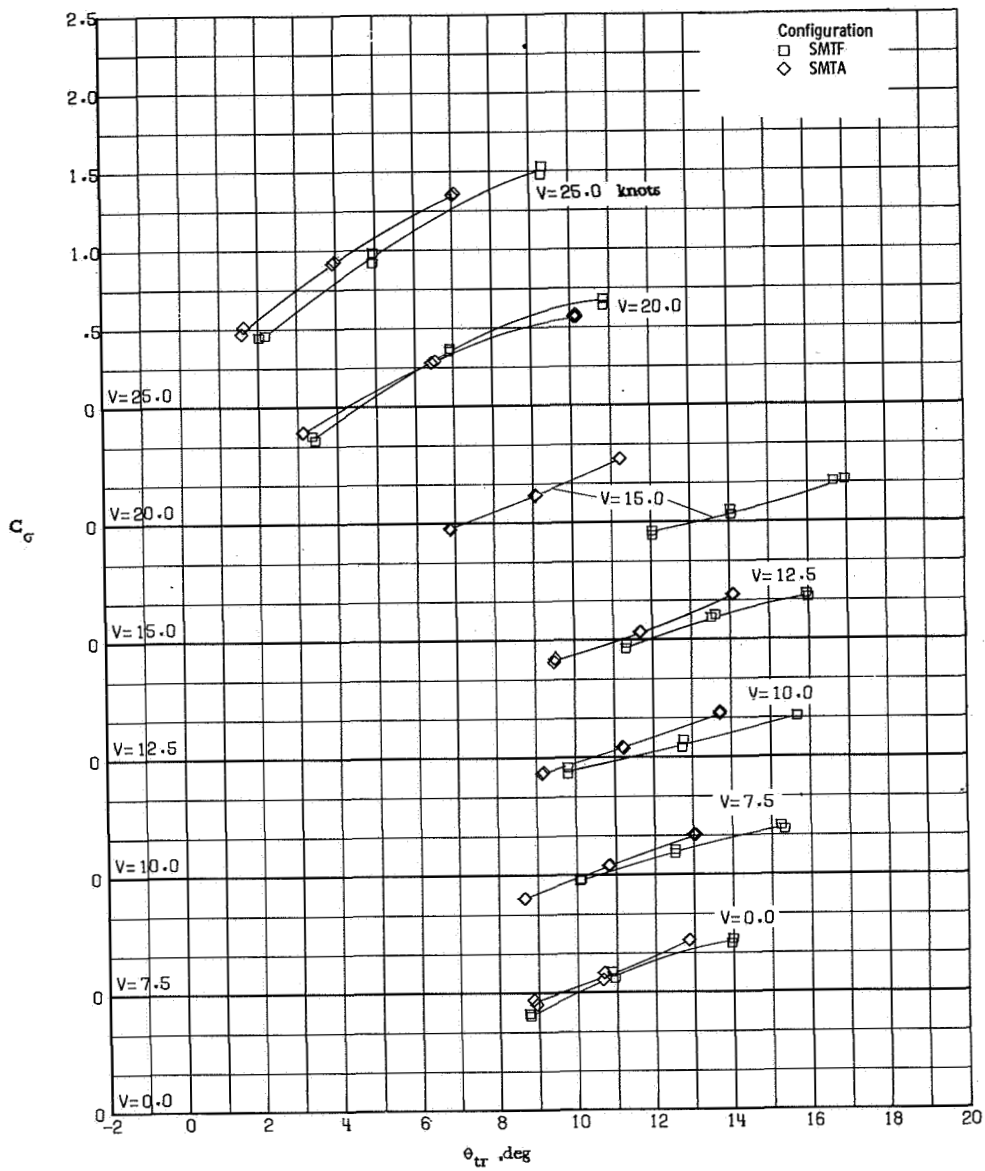

(g) Torque balance factor.

Figure 36.- Concluded.

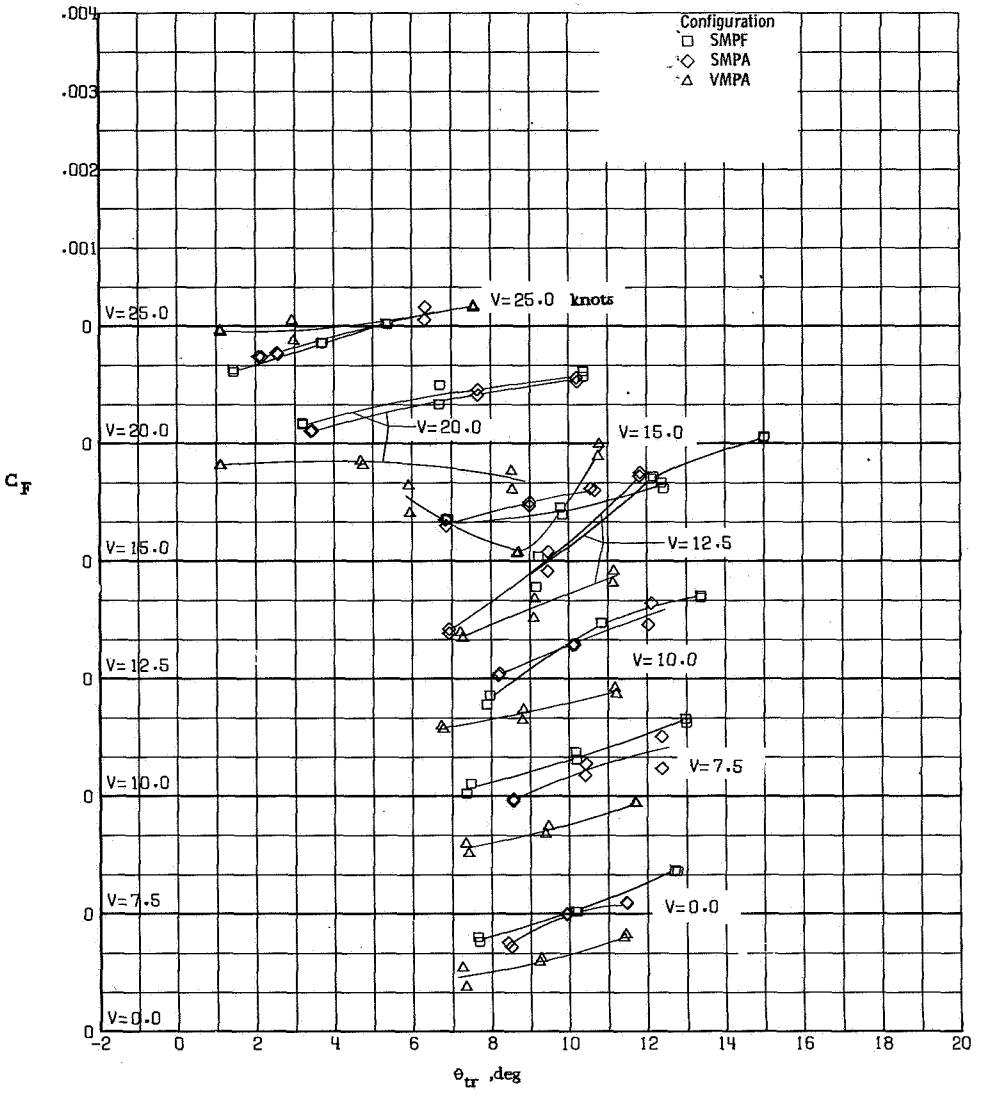

(a) Fin force.

Figure 37.- Aerodynamic characteristics of configurations with a pusher tail rotor at $\beta = 240^{o}$.

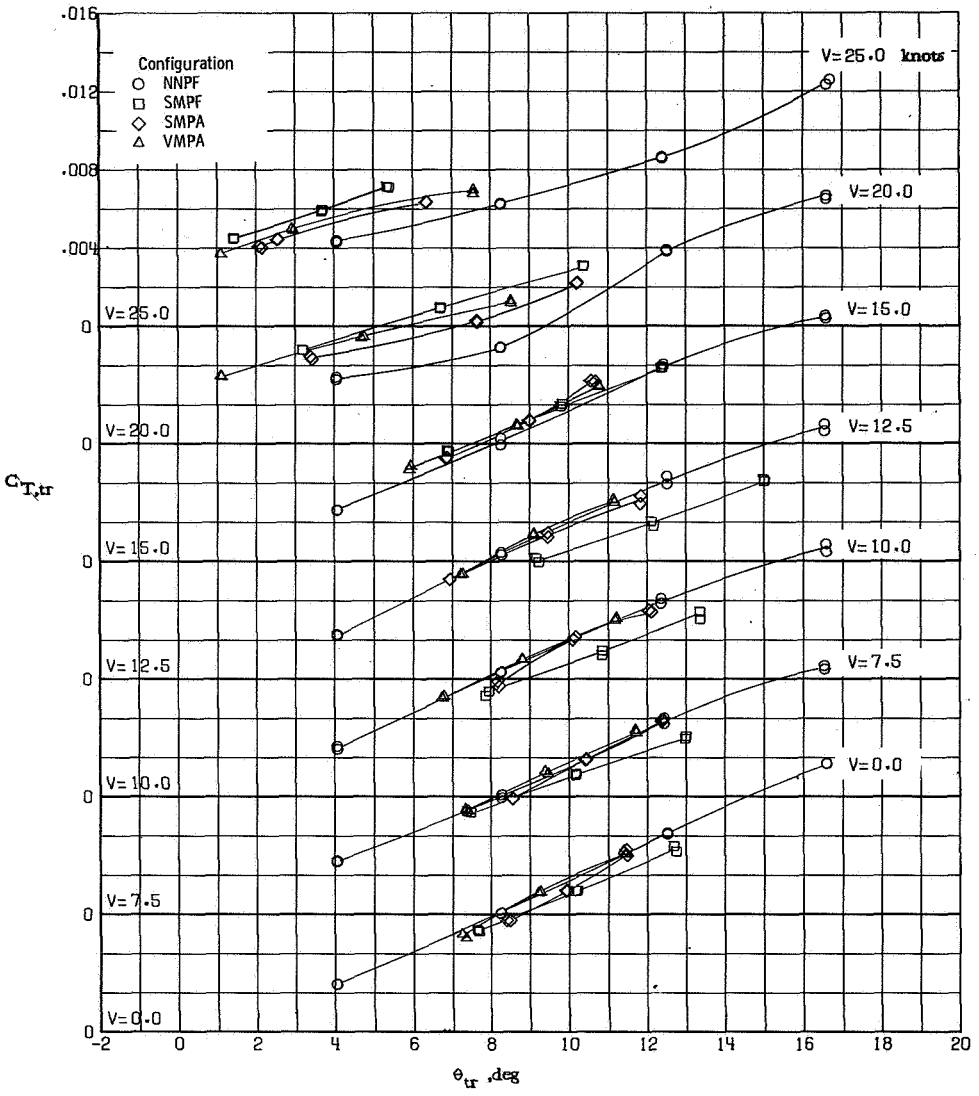

(b) Tail-rotor thrust.

Figure 37.- Continued.

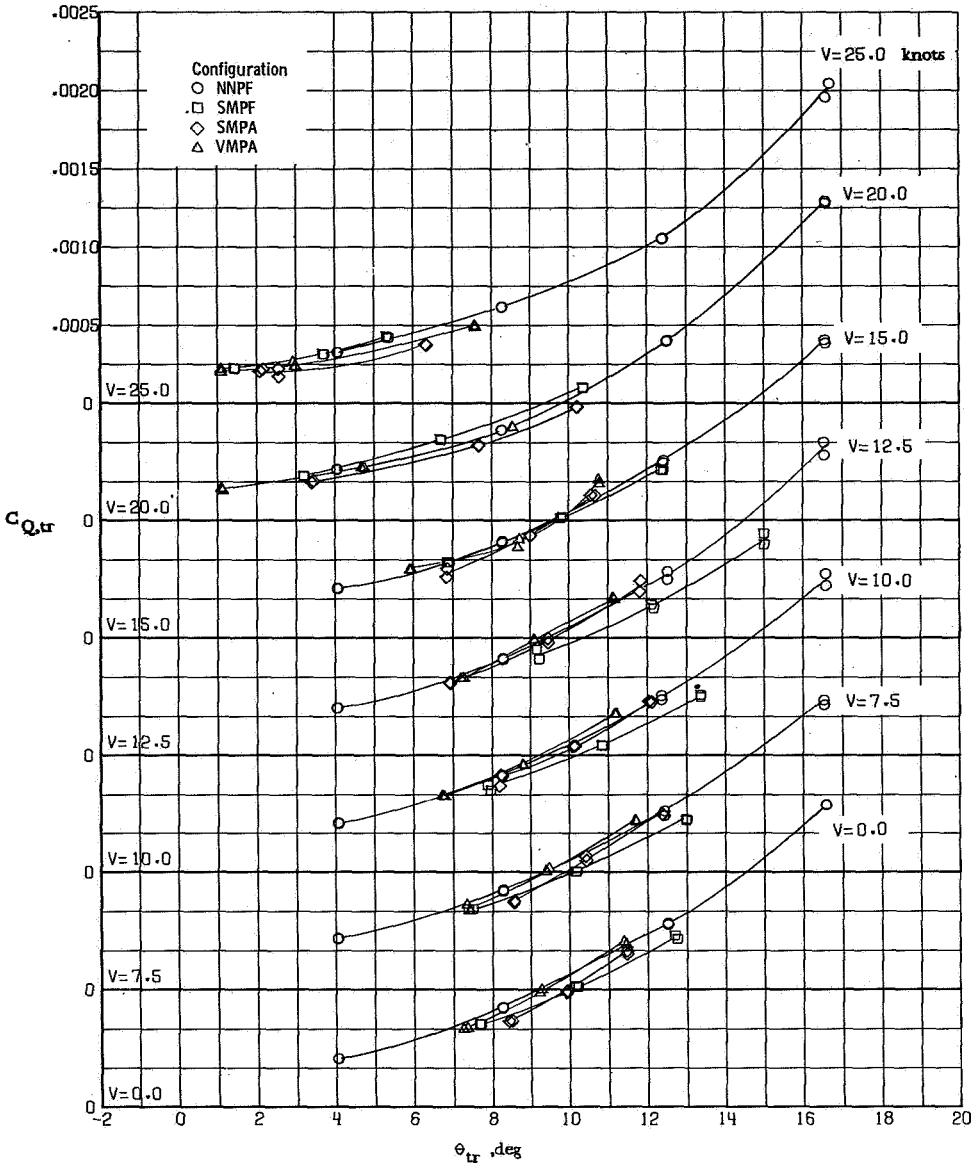

(c) Tail-rotor torque.

Figure 37.- Continued.

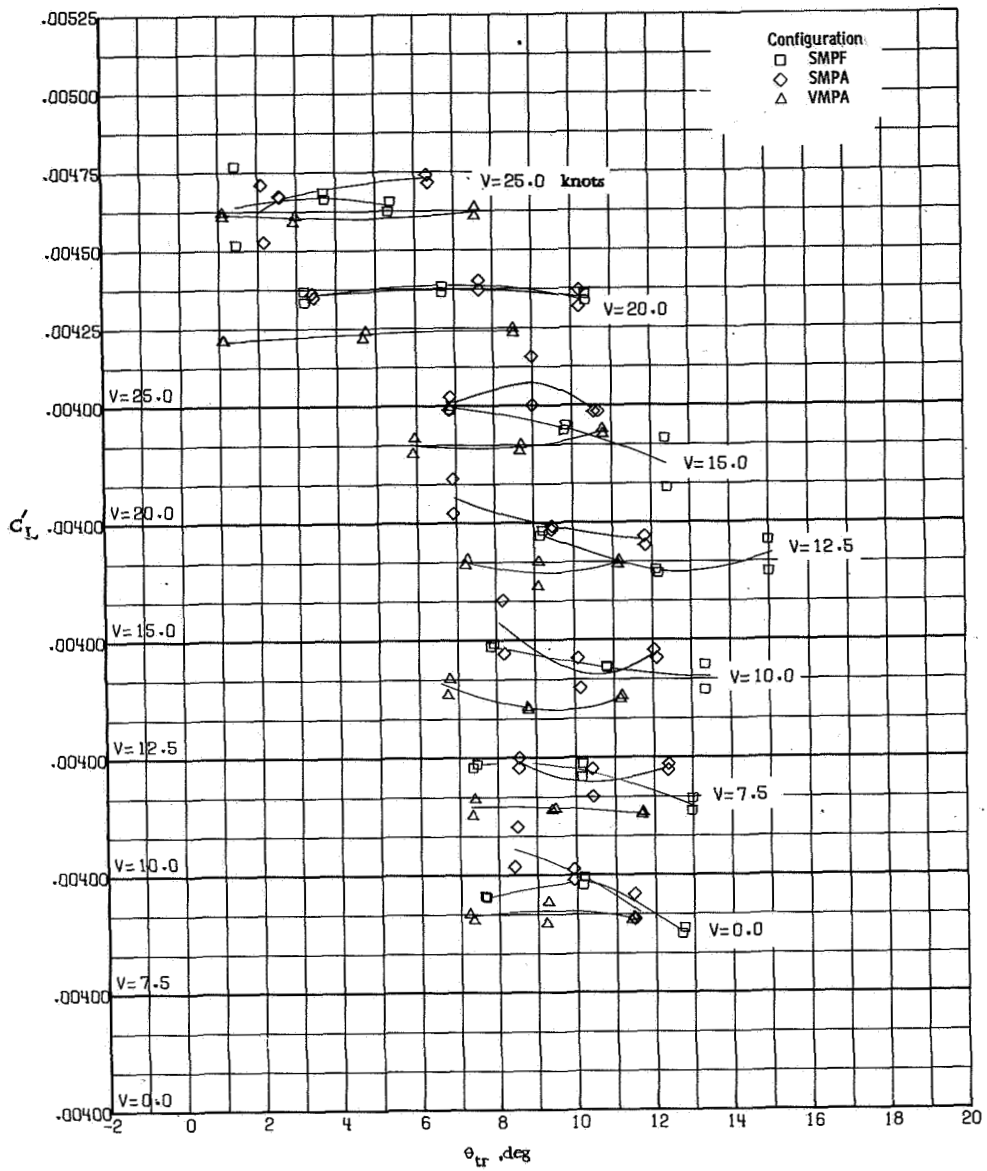

(d) Main-rotor lift.

Figure 37.- Continued.

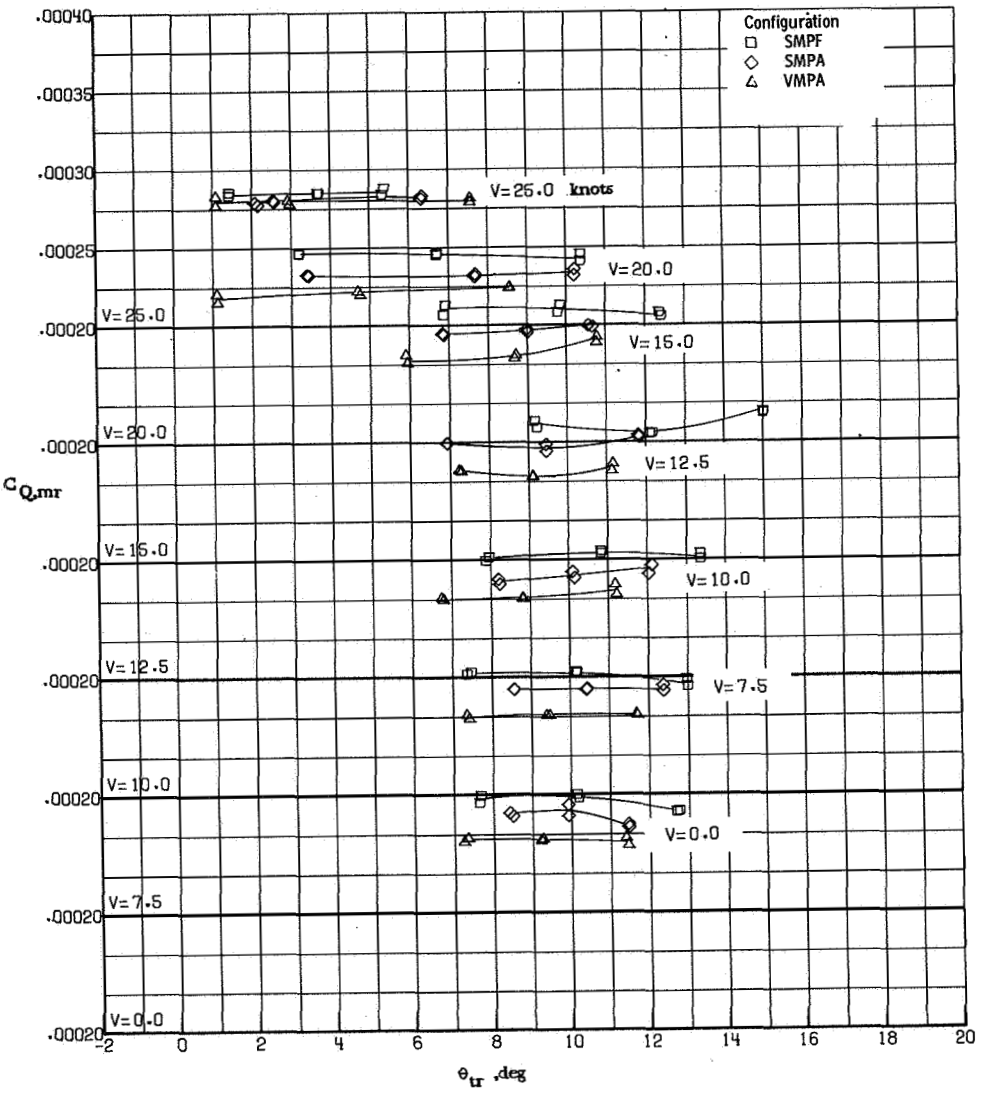

(e) Main-rotor torque.

Figure 37.- Continued.

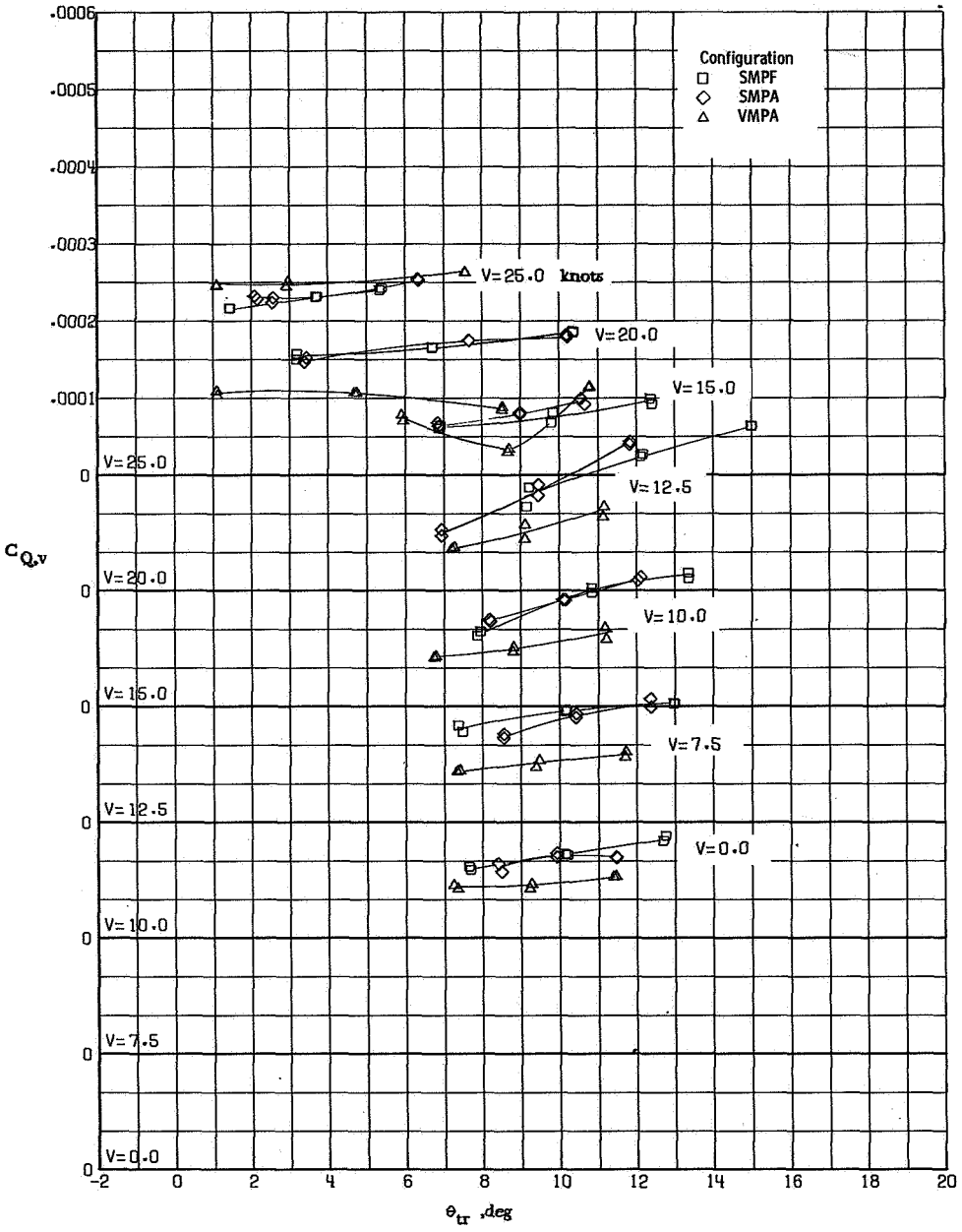

(f) Vehicle torque.

Figure 37.- Continued.

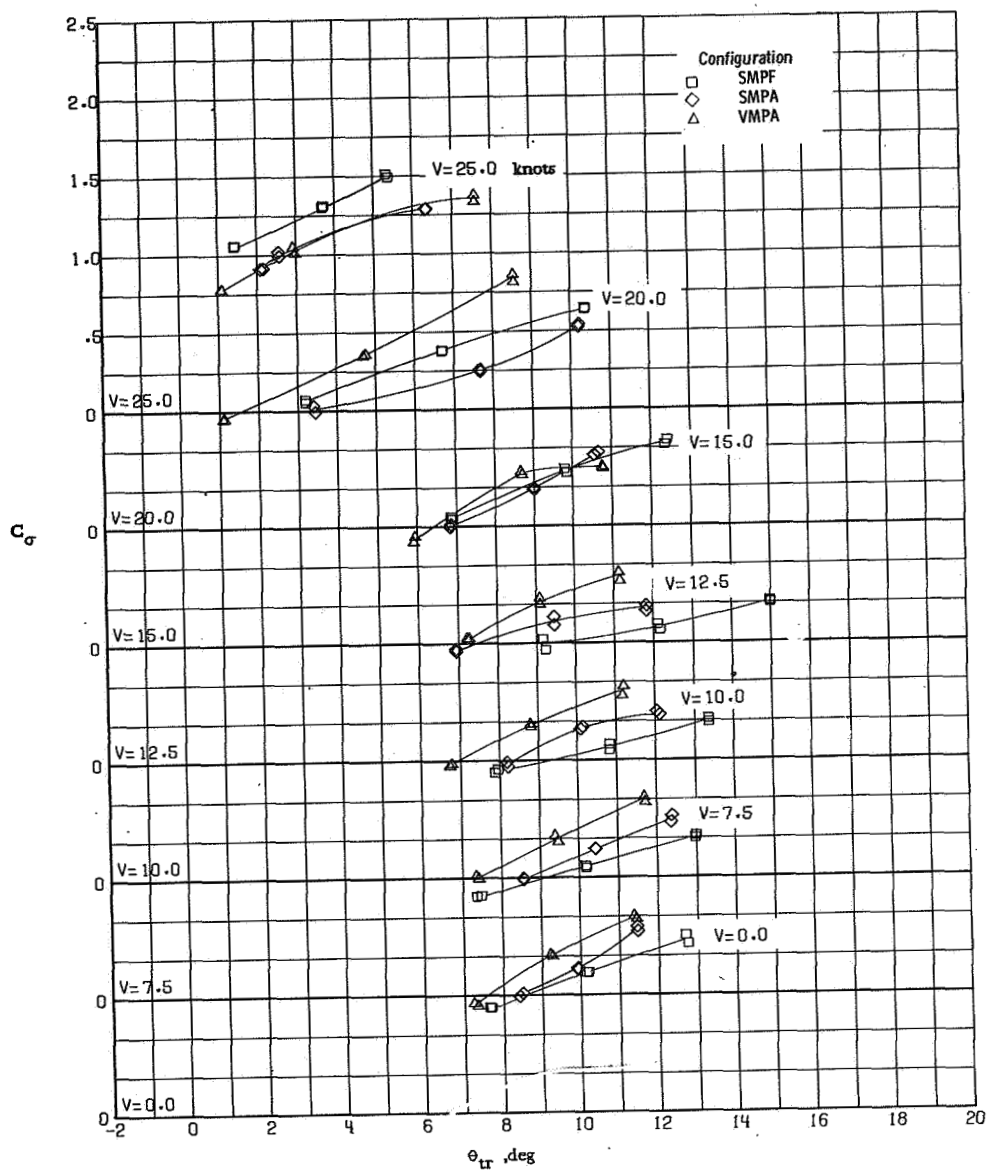

(g) Torque balance factor.

Figure 37.- Concluded.

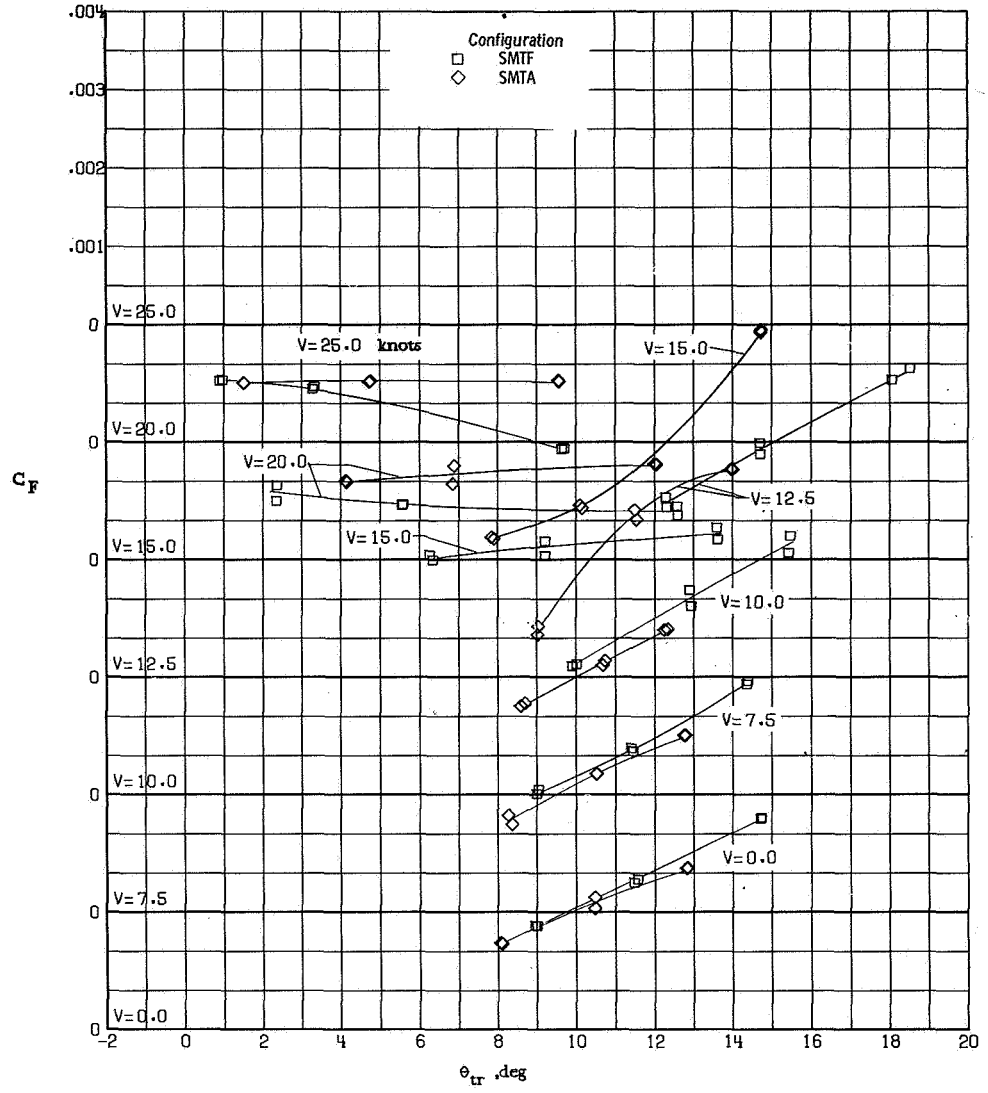

(a) Fin force.

Figure 38.- Aerodynamic characteristics of various configurations with and without the main rotor at $\beta = 240^{o}$.

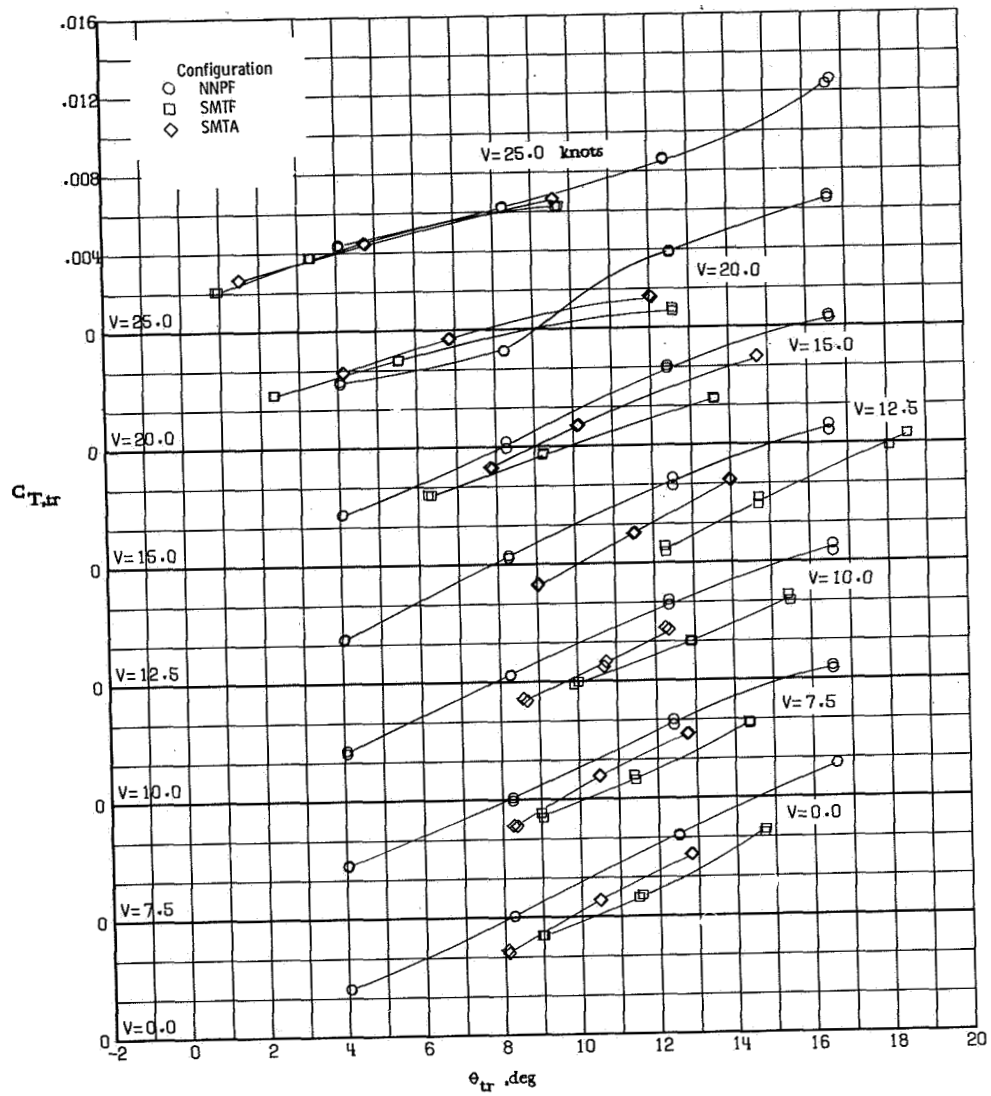

(b) Tail-rotor thrust.

Figure 38.- Continued.

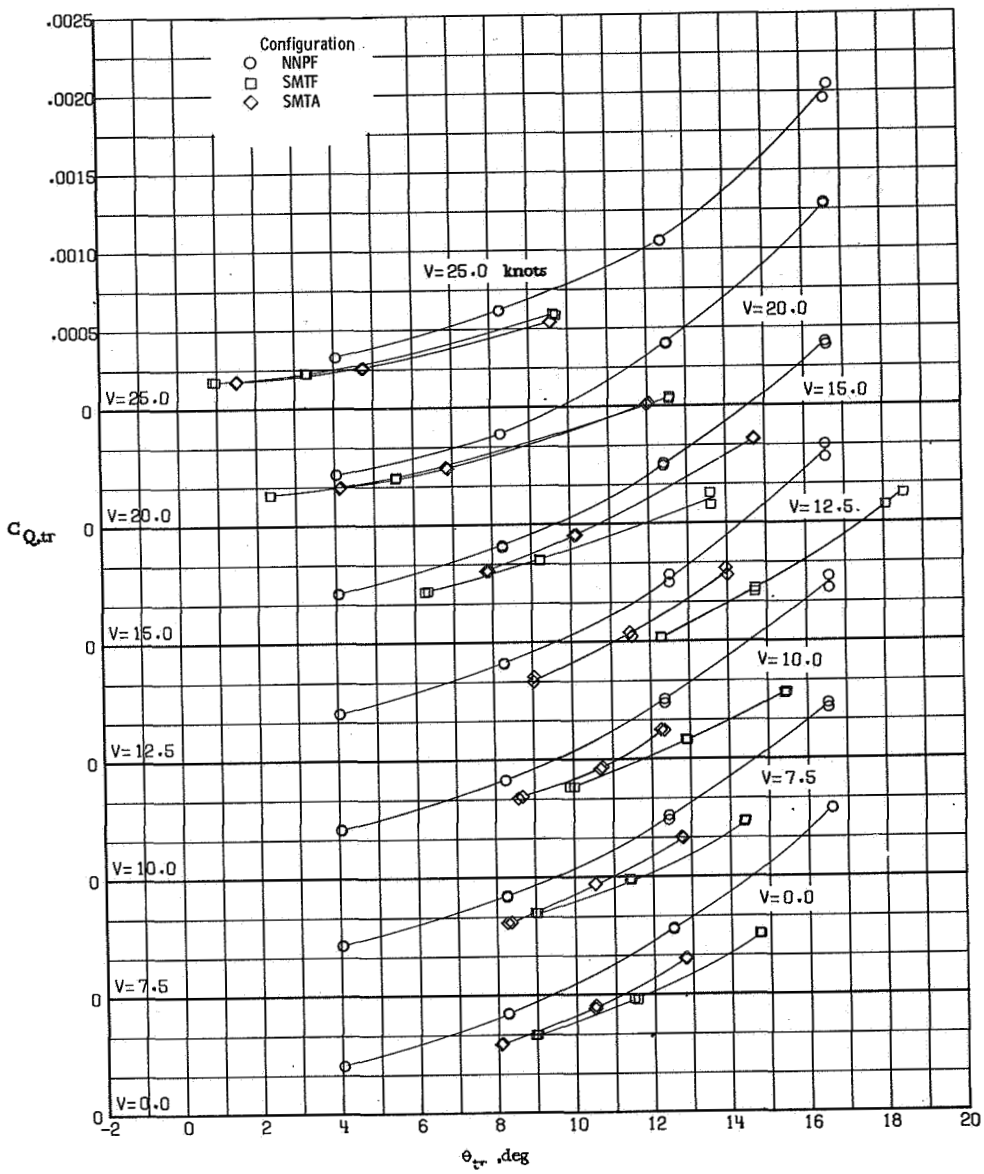

(c) Tail-rotor torque.

Figure 38.- Continued.

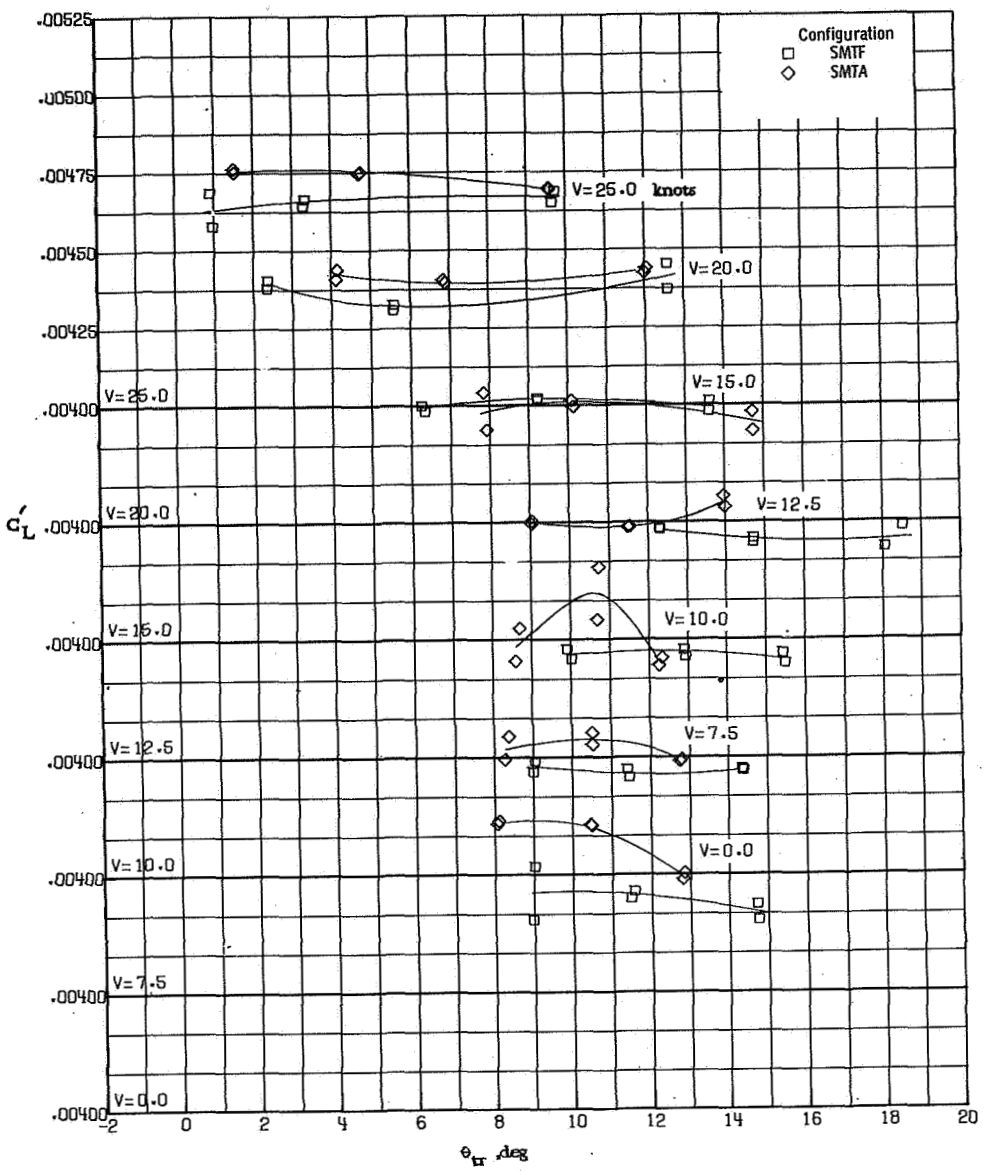

(d) Main-rotor lift.

Figure 38.- Continued.

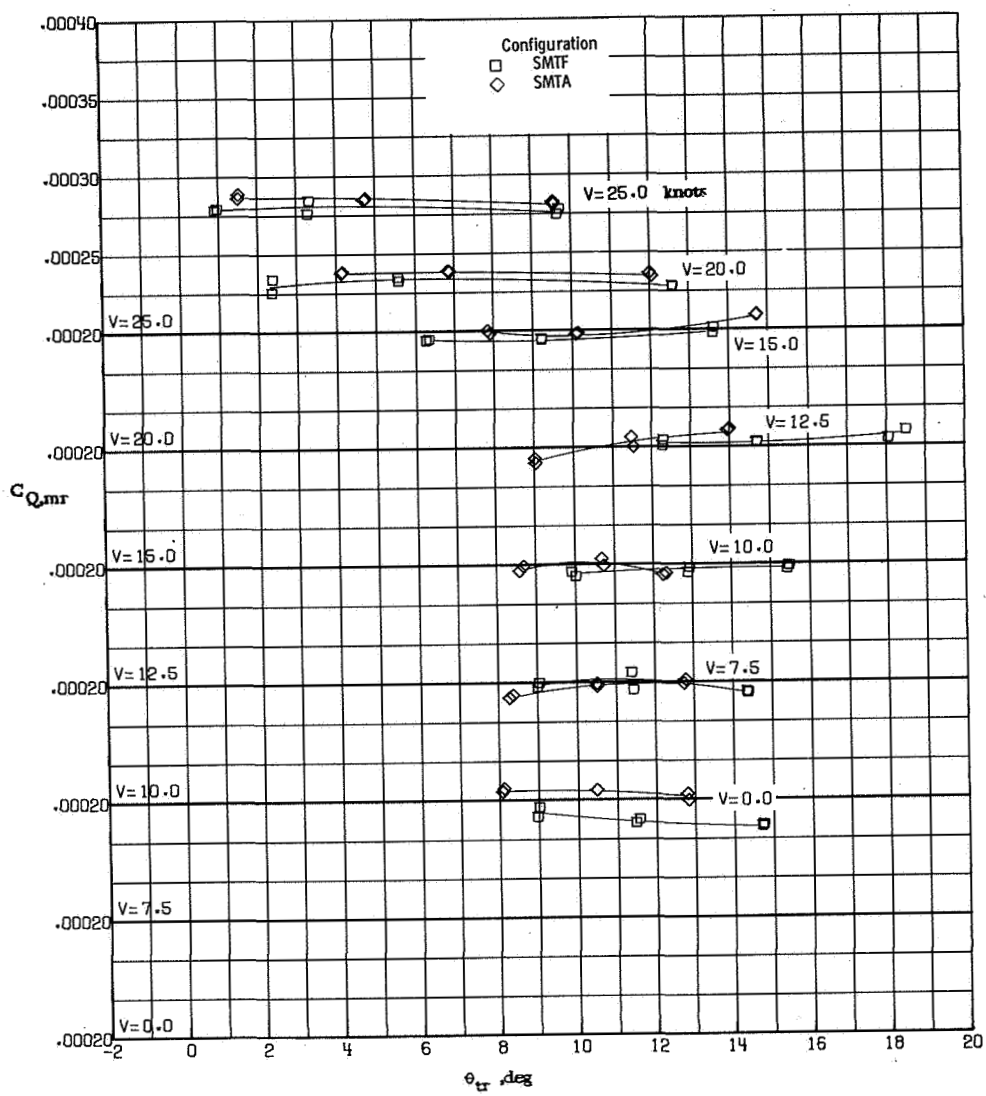

(e) Main-rotor torque.

Figure 38.- Continued.

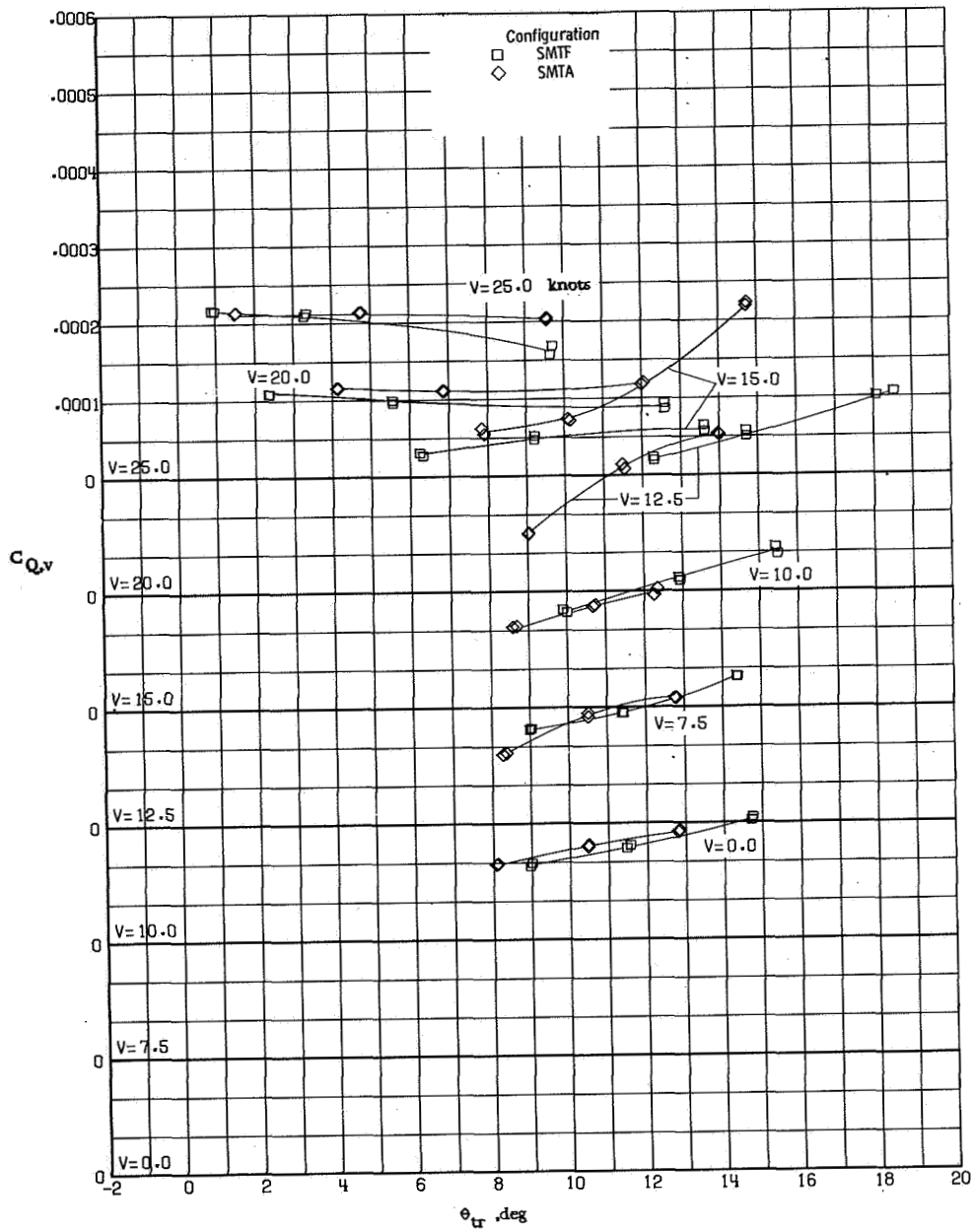

(f) Vehicle torque.

Figure 38.- Continued.

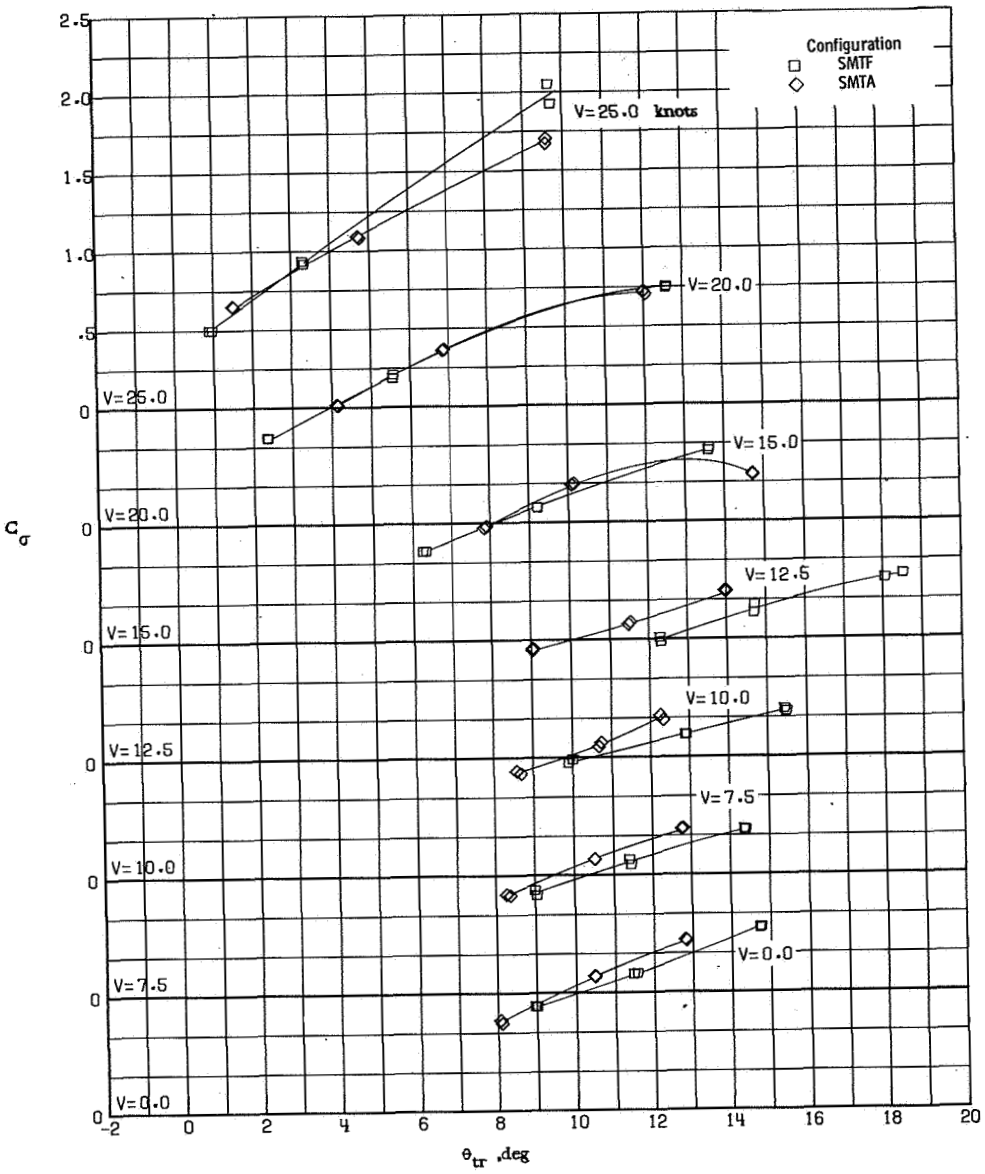

(g) Torque balance factor.

Figure 38.- Concluded.

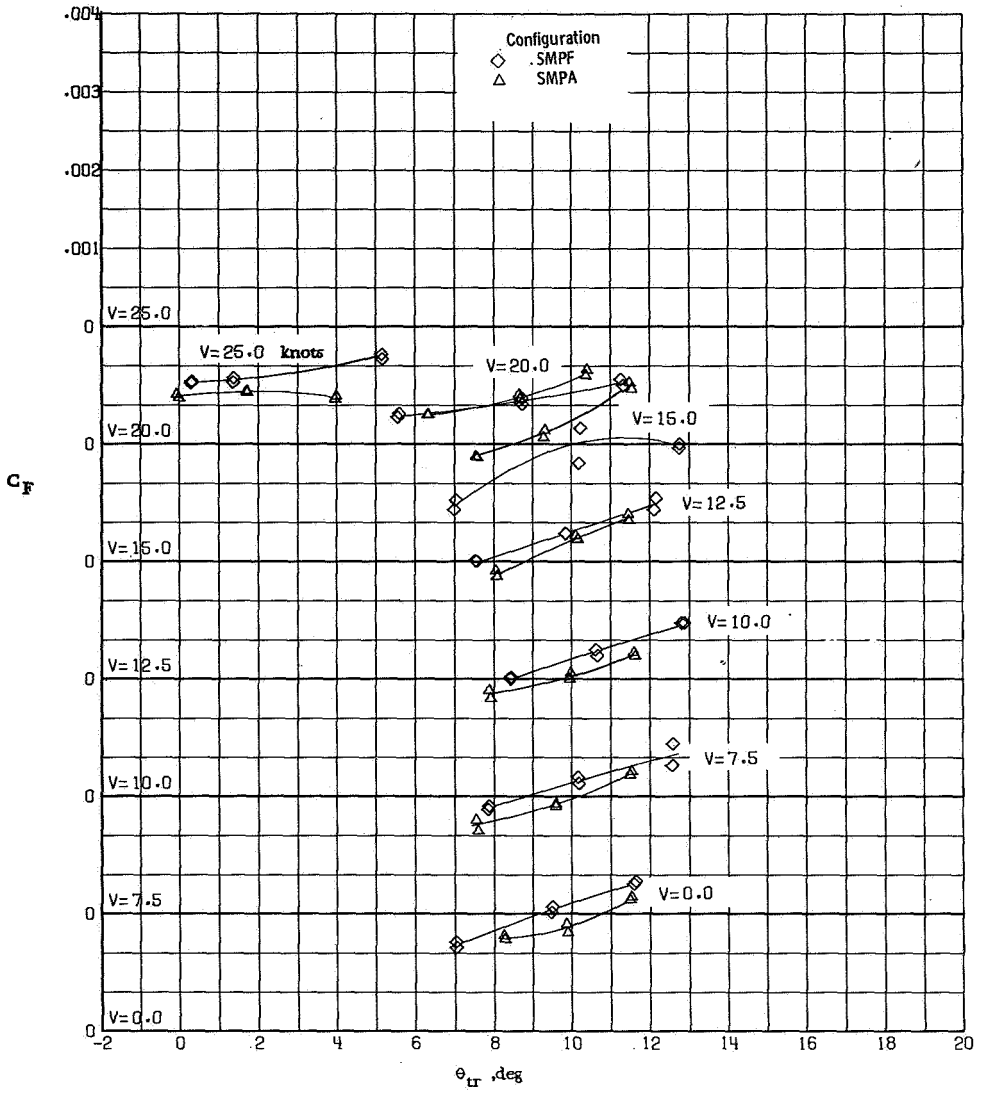

(a) Fin force.

Figure 39.- Aerodynamic characteristics of various configurations at $\beta = 270^{o}$.

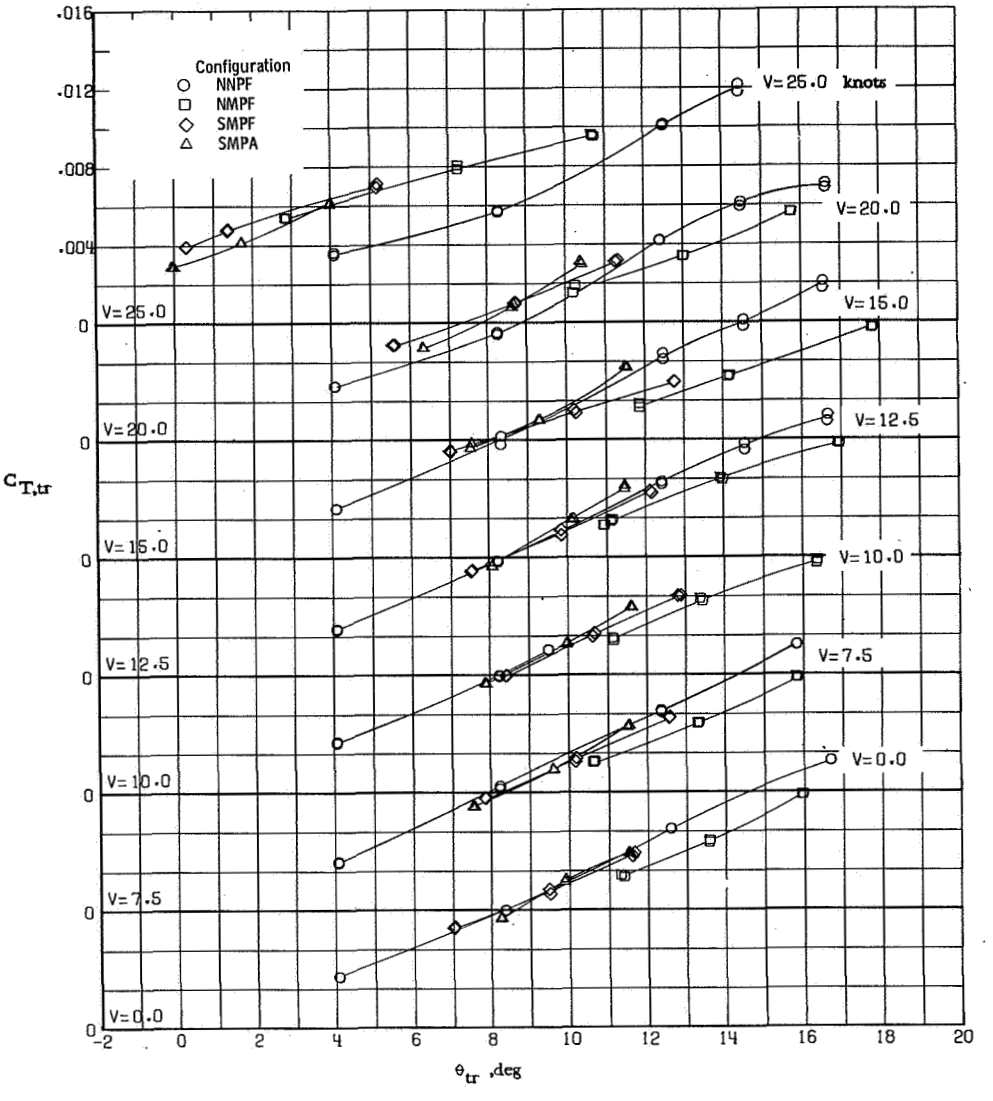

(b) Tail-rotor thrust.

Figure 39.- Continued.

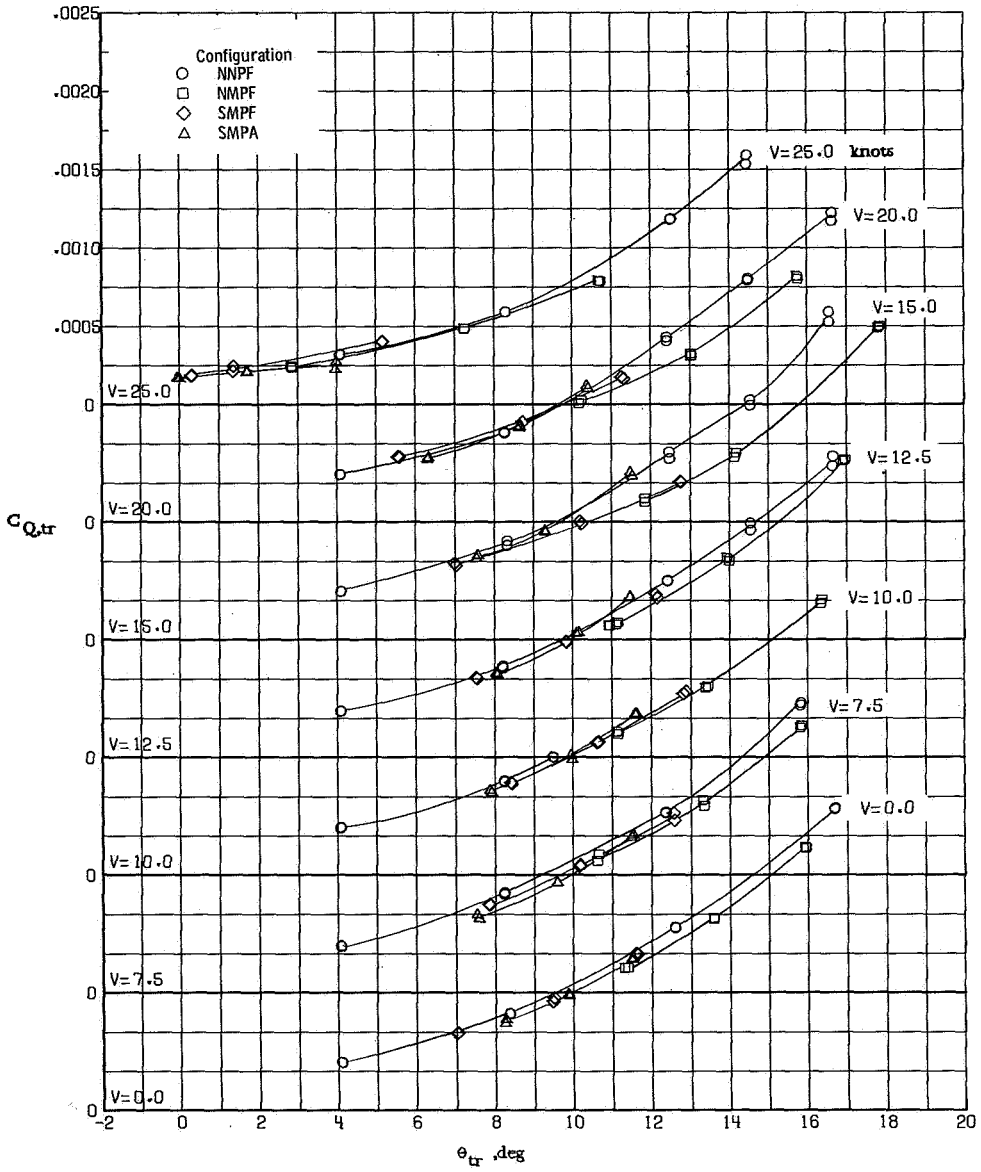

(c) Tail-rotor torque.

Figure 39.- Continued.

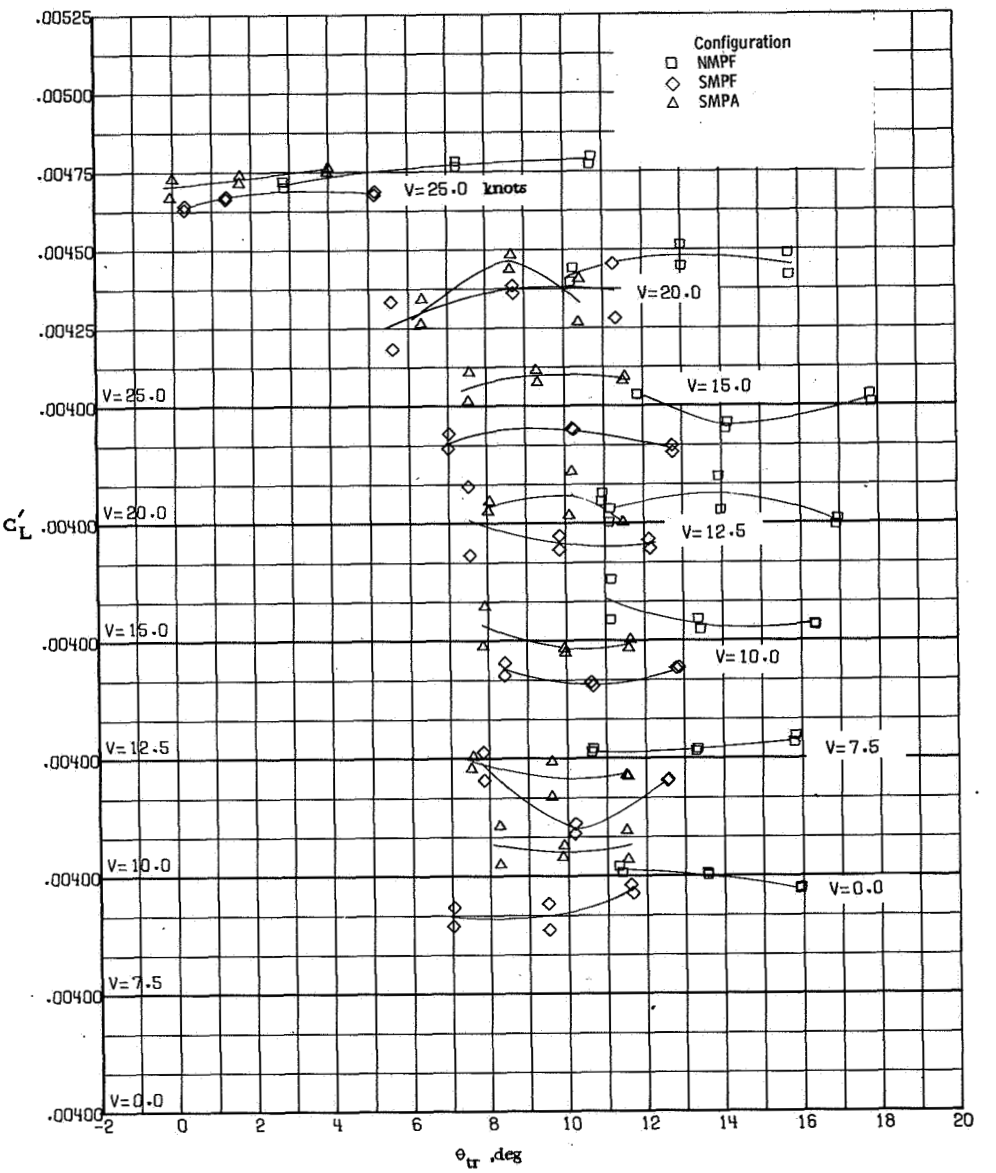

(d) Main-rotor lift.

Figure 39.- Continued.

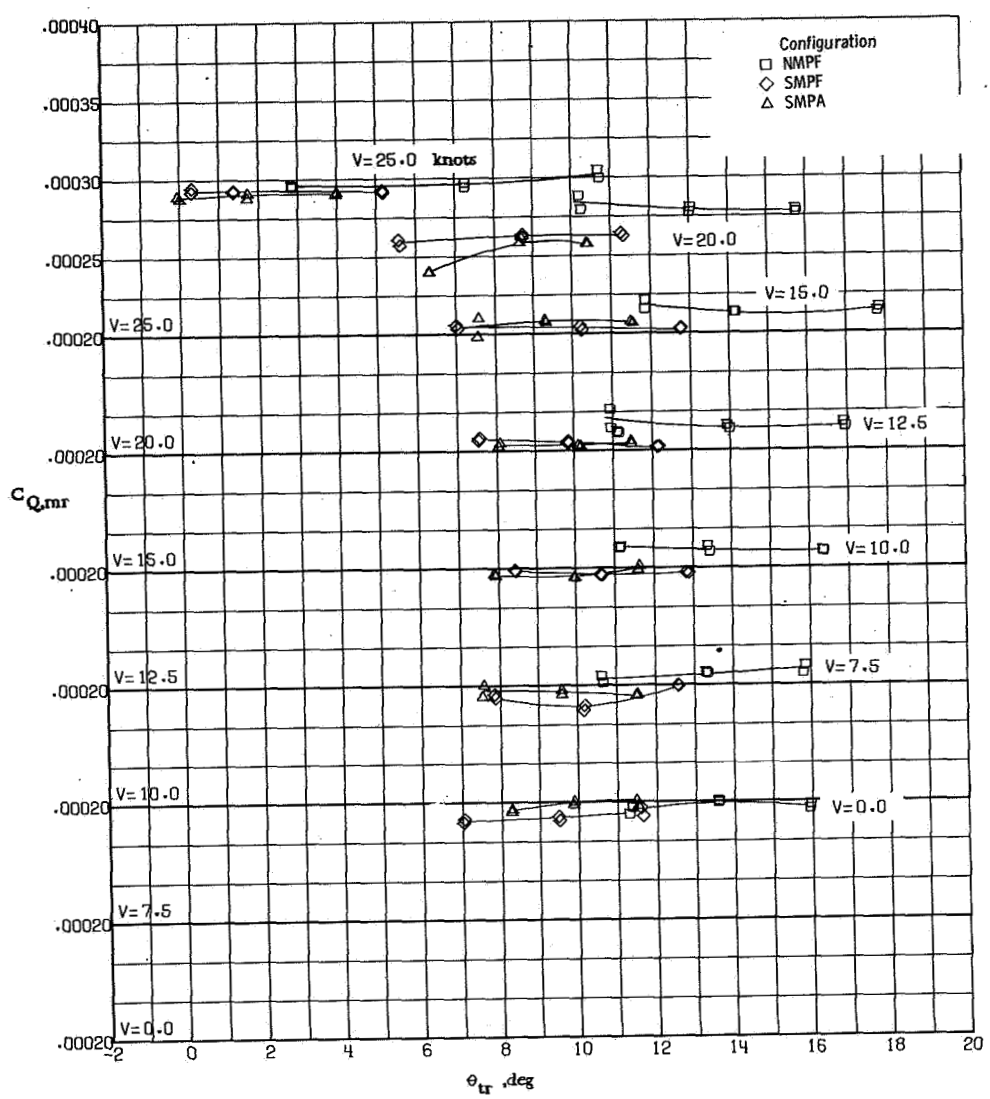

(e) Main-rotor torque.

Figure 39.- Continued.

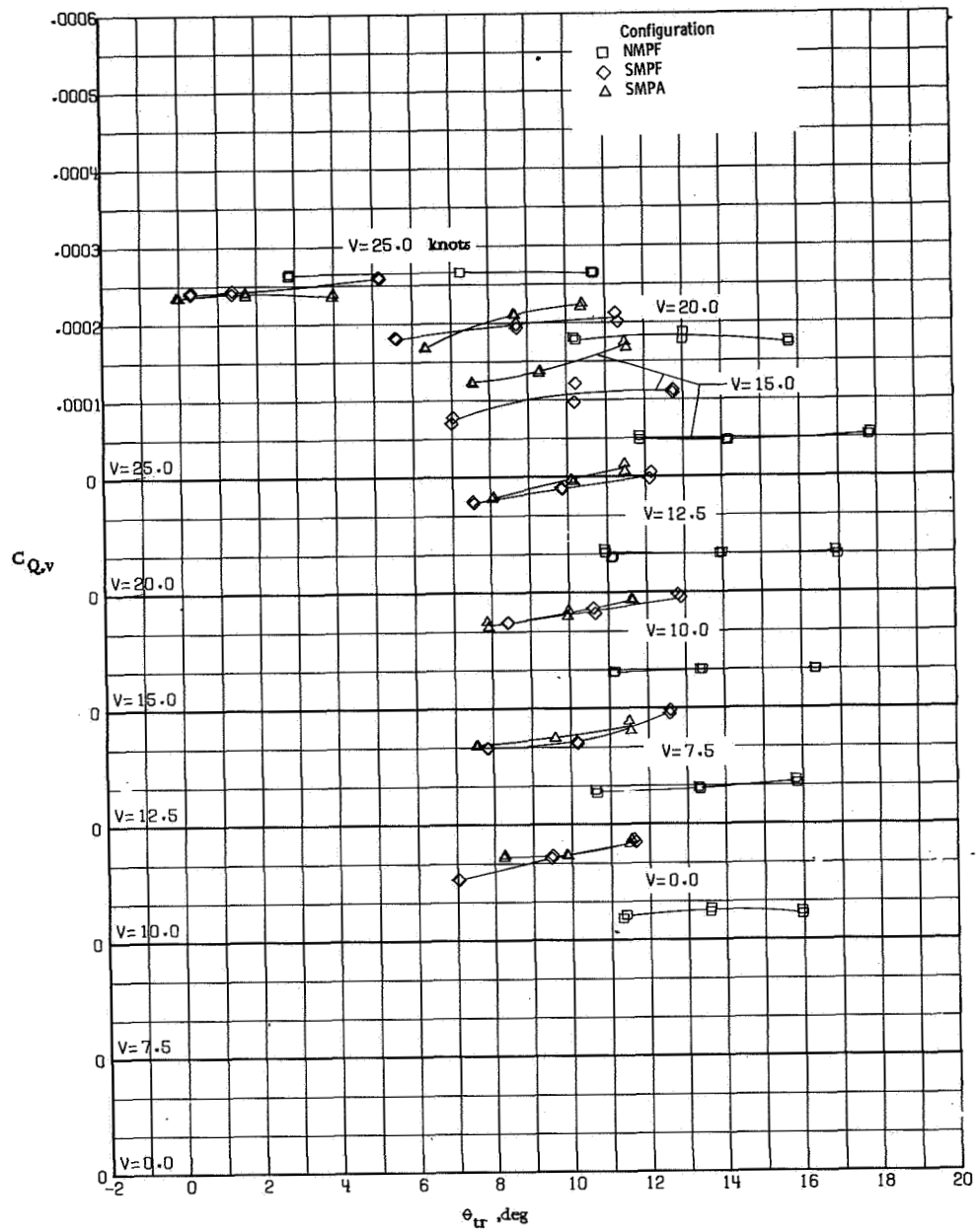

(f) Vehicle torque.

Figure 39.- Continued.

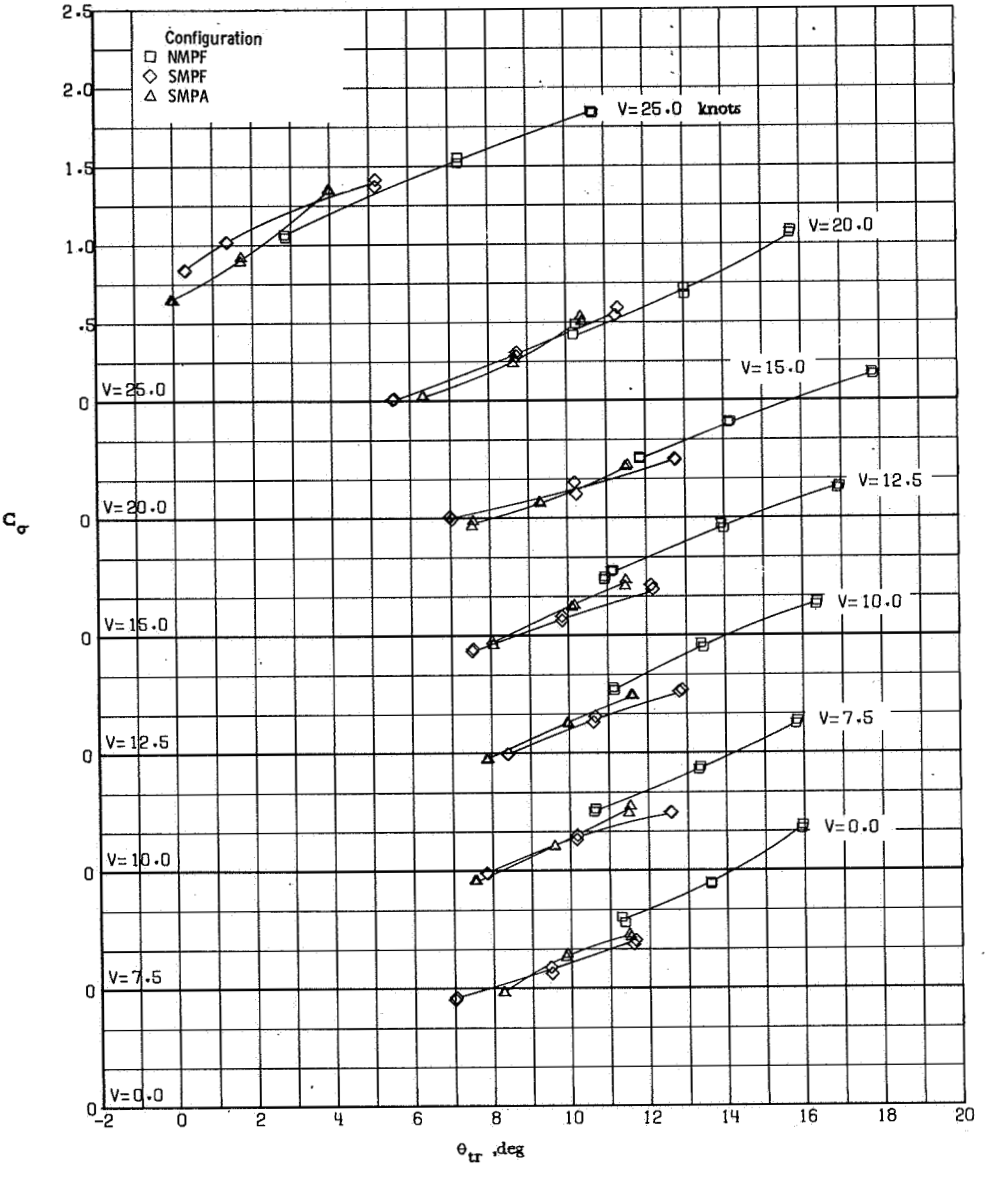

(g) Torque balance factor.

Figure 39.- Concluded.

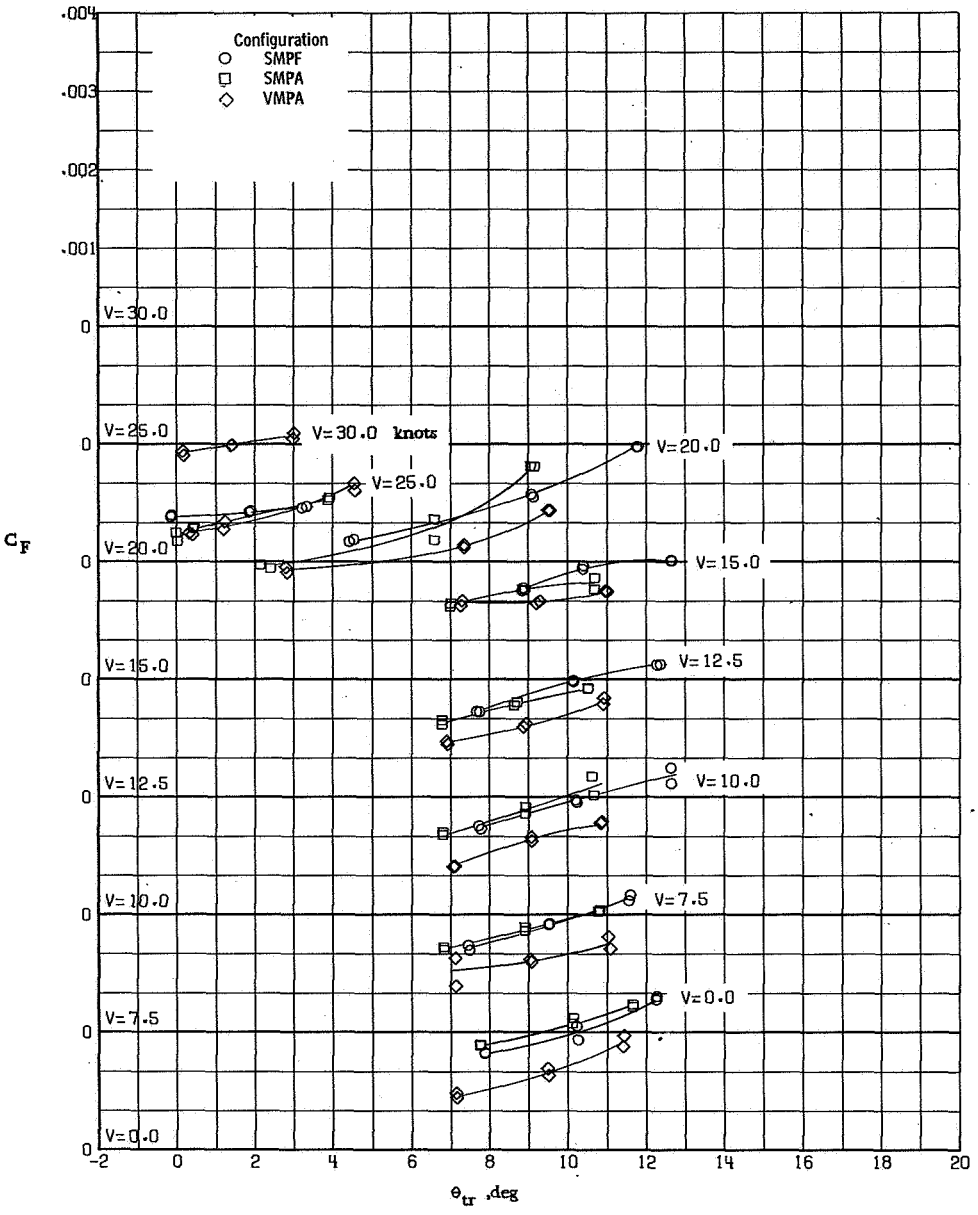

(a) Fin force.

Figure 40.- Aerodynamic characteristics of various configurations at $\beta = 300^{o}$.

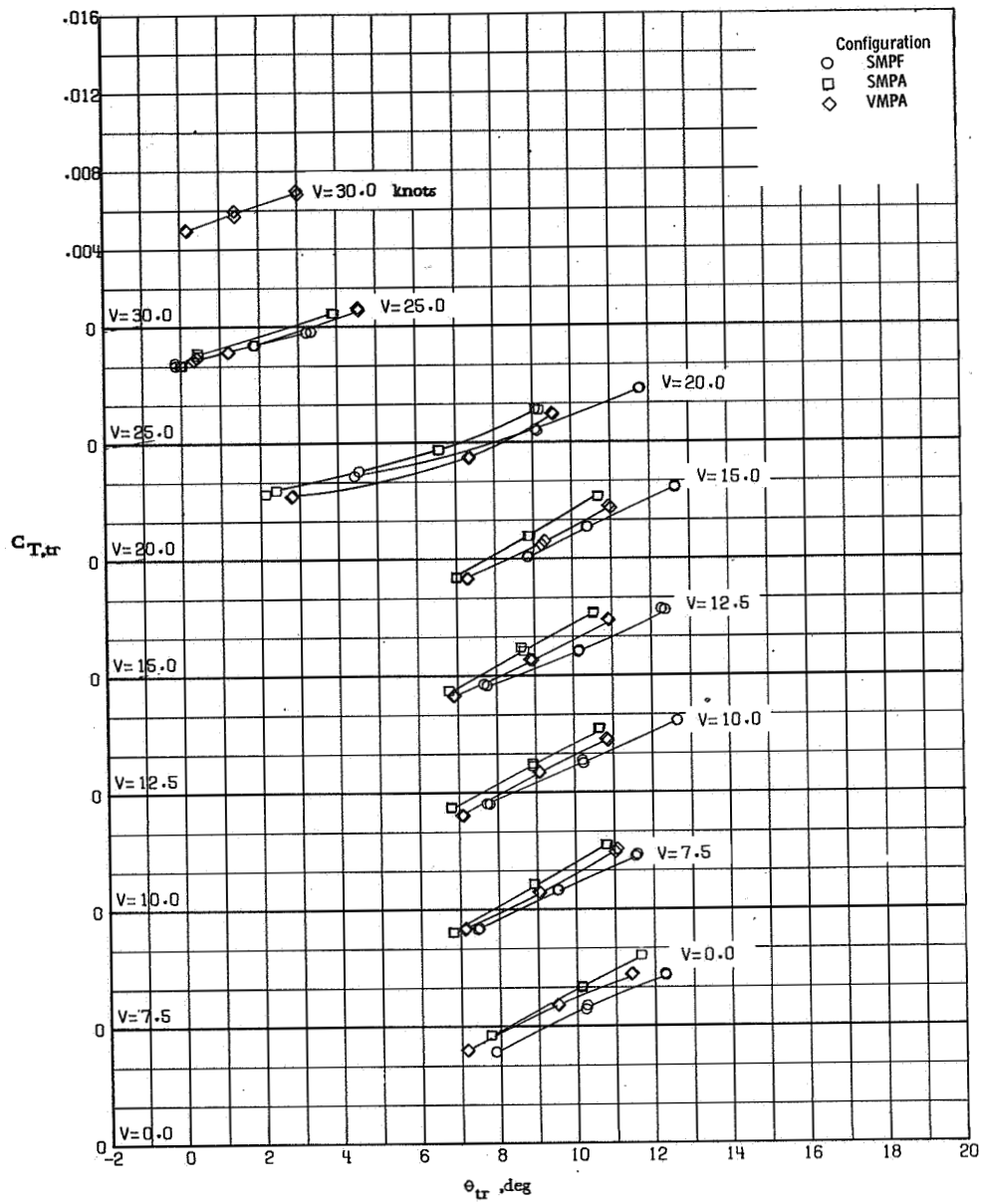

(b) Tail-rotor thrust.

Figure 40.- Continued.

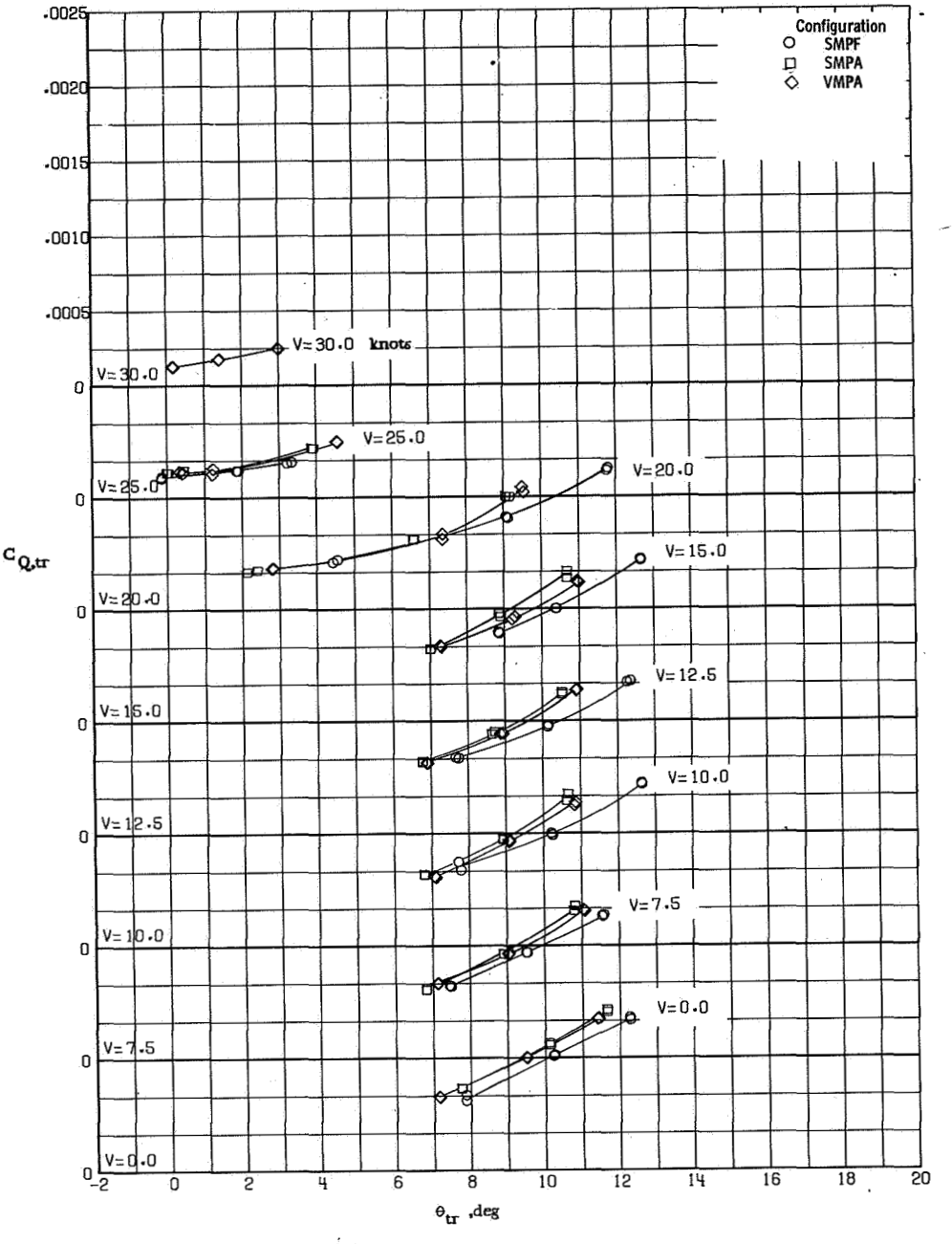

(c) Tail-rotor torque.

Figure 40.- Continued.

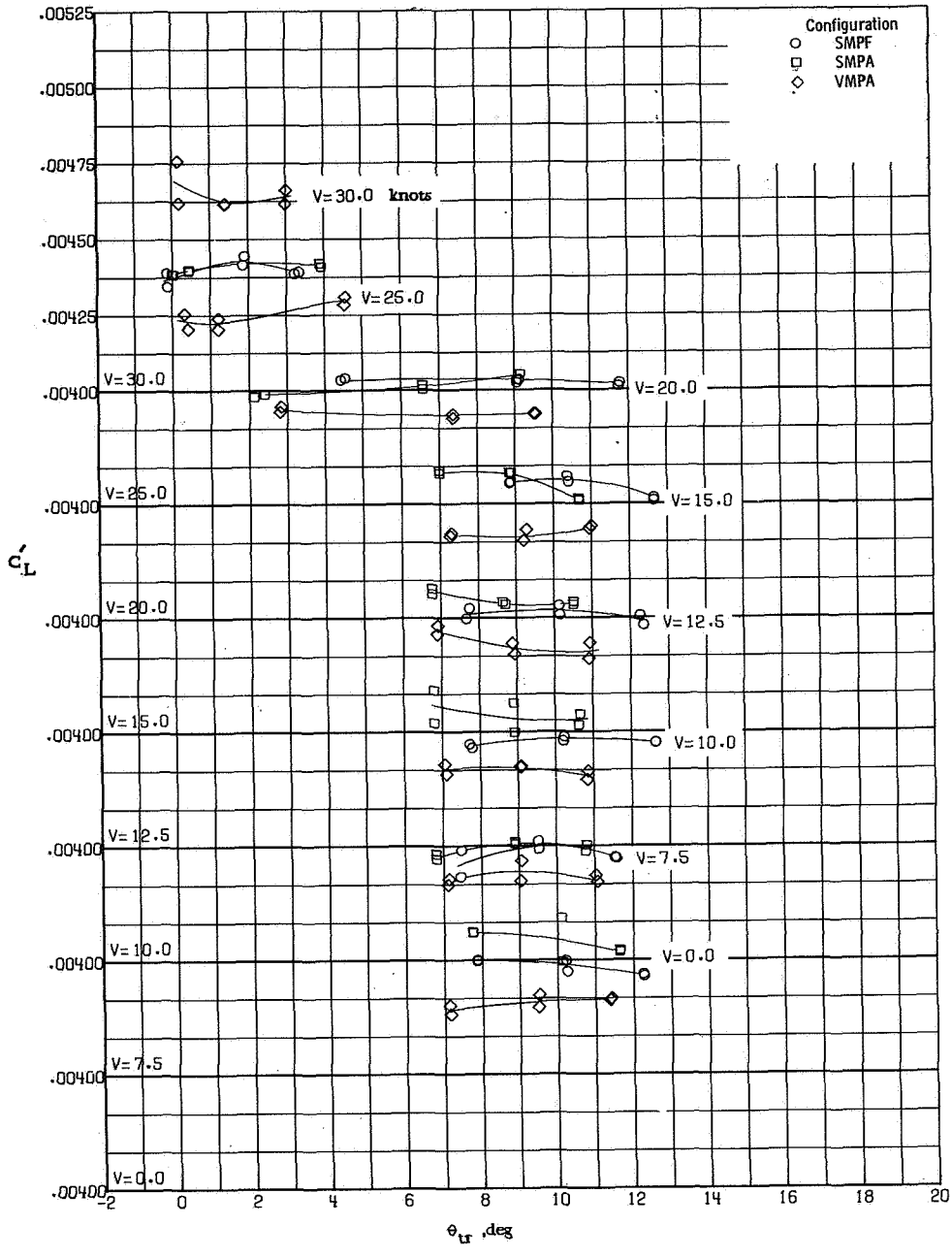

(d) Main-rotor lift.

Figure 40.- Continued.

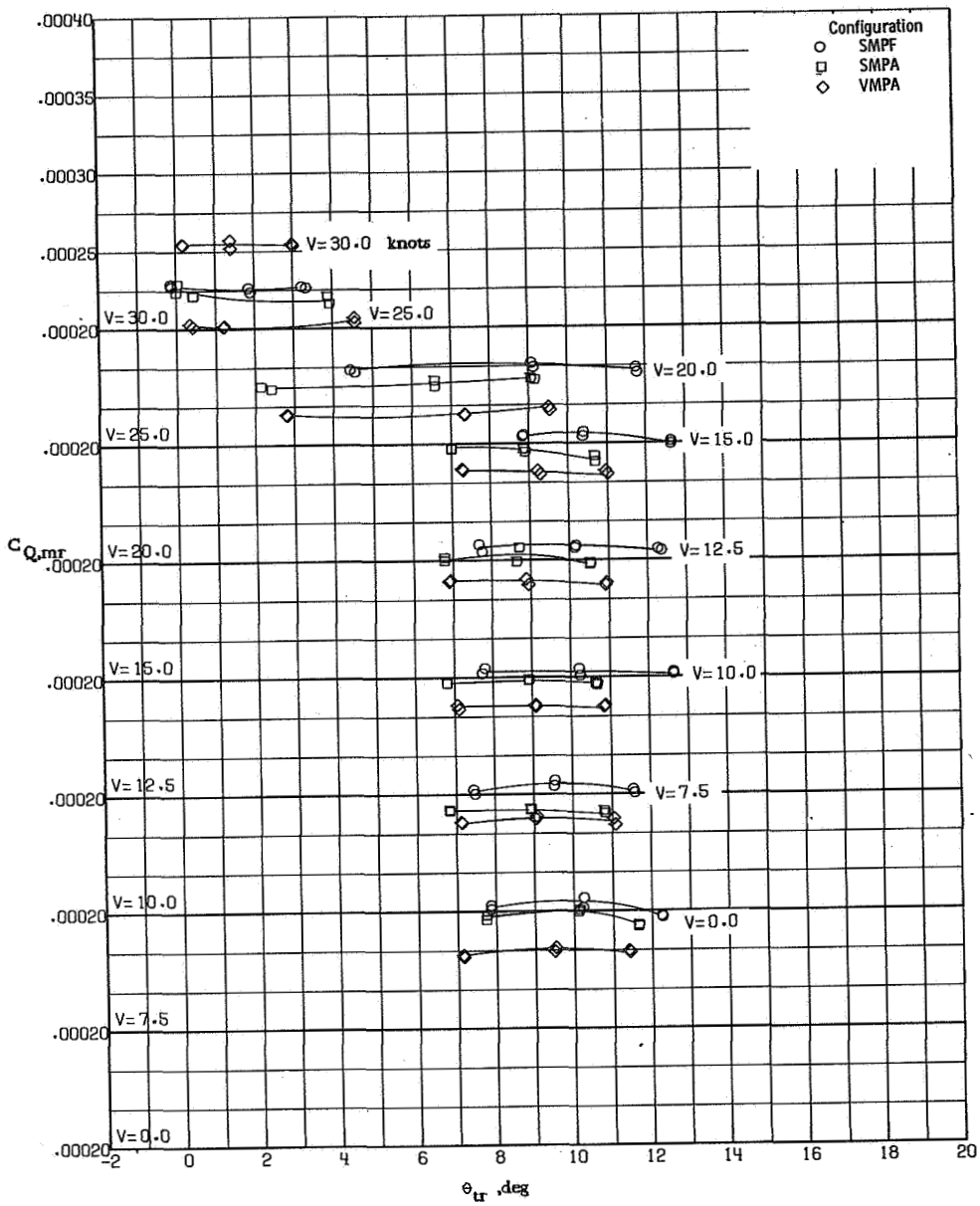

(e) Main-rotor torque.

Figure 40.- Continued.

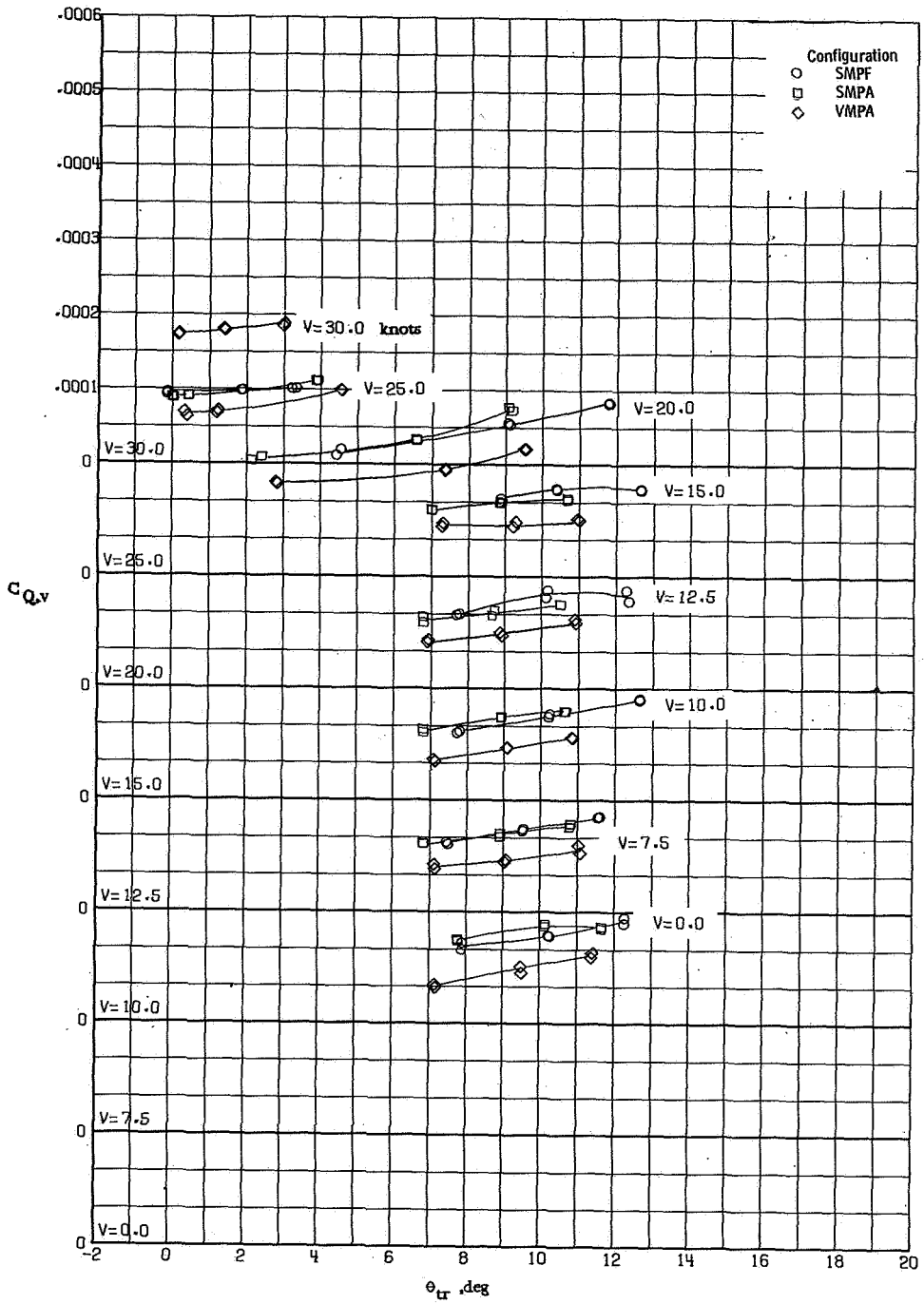

(f) Vehicle torque.

Figure 40.- Continued.

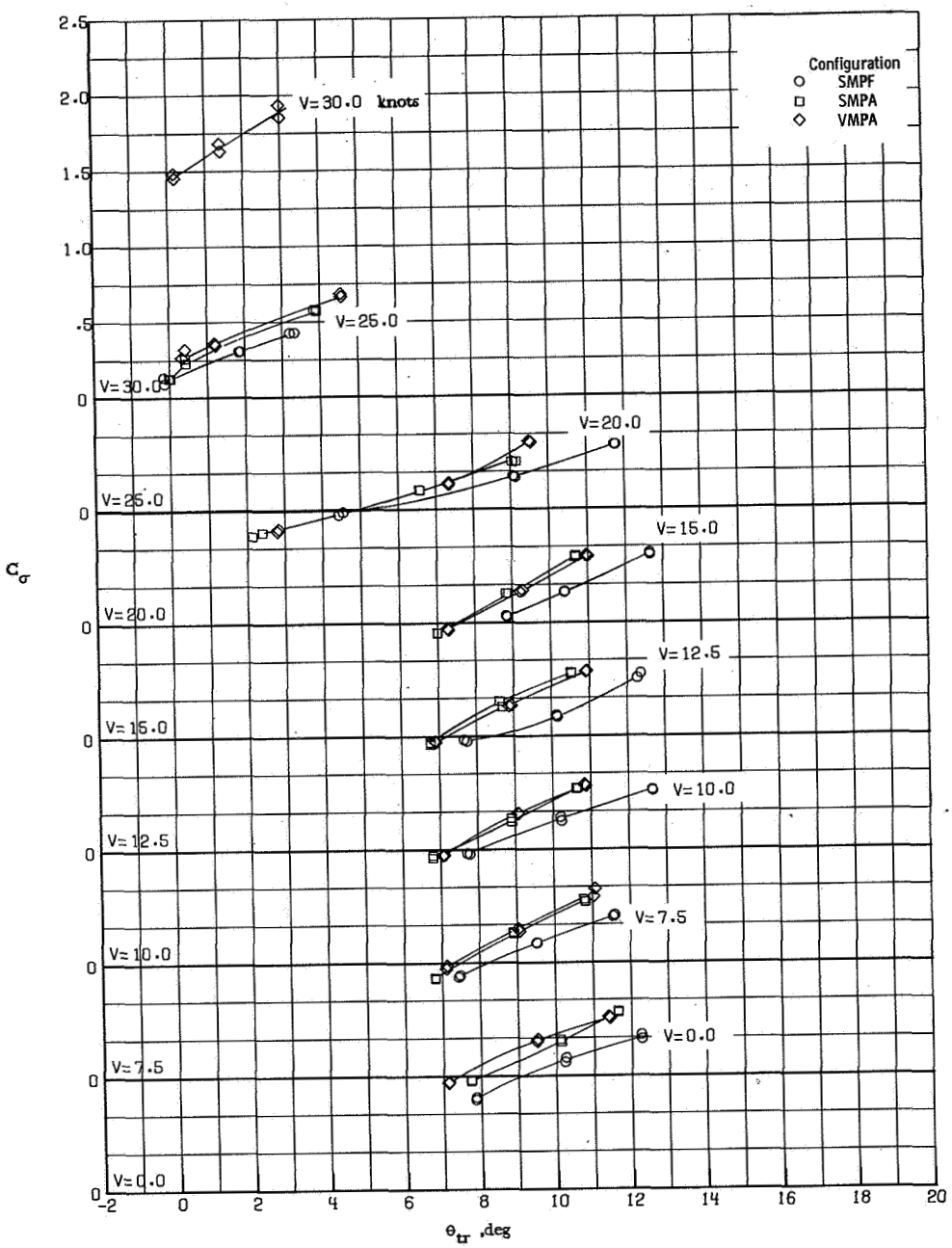

(g) Torque balance factor.

Figure 40.- Concluded.

NATIONAL AERONAUTICS AND SPACE ADMINISTRATION
WASHINGTON, D.C. 20546

OFFICIAL BUSINESS
PENALTY FOR PRIVATE USE $300

SPECIAL FOURTH-CLASS RATE BOOK

POSTAGE AND FEES PAID
NATIONAL AERONAUTICS AND SPACE ADMINISTRATION
451

U.S.MAIL

POSTMASTER: If Undeliverable (Section 158 Postal Manual) Do Not Return

"The aeronautical and space activities of the United States shall be conducted so as to contribute . . . to the expansion of human knowledge of phenomena in the atmosphere and space. The Administration shall provide for the widest practicable and appropriate dissemination of information concerning its activities and the results thereof."

—NATIONAL AERONAUTICS AND SPACE ACT OF 1958

NASA SCIENTIFIC AND TECHNICAL PUBLICATIONS

TECHNICAL REPORTS: Scientific and technical information considered important, complete, and a lasting contribution to existing knowledge.

TECHNICAL NOTES: Information less broad in scope but nevertheless of importance as a contribution to existing knowledge.

TECHNICAL MEMORANDUMS: Information receiving limited distribution because of preliminary data, security classification, or other reasons. Also includes conference proceedings with either limited or unlimited distribution.

CONTRACTOR REPORTS: Scientific and technical information generated under a NASA contract or grant and considered an important contribution to existing knowledge.

TECHNICAL TRANSLATIONS: Information published in a foreign language considered to merit NASA distribution in English.

SPECIAL PUBLICATIONS: Information derived from or of value to NASA activities. Publications include final reports of major projects, monographs, data compilations, handbooks, sourcebooks, and special bibliographies.

TECHNOLOGY UTILIZATION PUBLICATIONS: Information on technology used by NASA that may be of particular interest in commercial and other non-aerospace applications. Publications include Tech Briefs, Technology Utilization Reports and Technology Surveys.

Details on the availability of these publications may be obtained from:

SCIENTIFIC AND TECHNICAL INFORMATION OFFICE

NATIONAL AERONAUTICS AND SPACE ADMINISTRATION

Washington, D.C. 20546